Identification of novel mediators of T cell function in chronic infection and cancer

Leonie Heyden

ORCID:

0009-0001-2018-8747

from Holzminden, Germany

Submitted in total fulfilment of the requirements of the joint degree of Doctor of Philosophy (PhD)

of

The Medical Faculty

The Rheinische Friedrich-Wilhelms-Universität Bonn

and

The Department of Microbiology and Immunology

The University of Melbourne

Bonn/Melbourne, 2025

Performed and approved by The Medical Faculty of The Rheinische Friedrich-Wilhelms-Universität Bonn and The University of Melbourne

1. Supervisor: Prof. Dr. Zeinab Abdullah (Bonn)

2. Supervisor: Prof. Dr. Axel Kallies (Melbourne)

Month and year of the original thesis submission: March 2025

Month and year of the oral examination: October 2025

Institute of Molecular Medicine and Experimental Immunology

Table of Contents

Abbreviation

AKT	protein kinase B
APC	antigen presenting cells
ATAC	Assay for Transposase-Accessible Chromatin
BATF	basic leucine zipper transcription factor
Bcl	B cell lymphoma
BCR	B cell receptor
Blimp1	B lymphocyte-induced maturation protein-1
BRF	Biological Resources Facility
BUR	base-unpairing regions
c-Myc	cellular myelocytomatosis proto-oncogene
CAR	chimeric antigen receptor
CCL	chemokine ligand
CCR	chemokine receptor
CD	cluster of differentiation
CRISPR	clustered regularly interspaced short palindromic repeats
CTLA-4	cytotoxic T-lymphocyte-associated protein 4
Ctrl	control
CTV	cell trace violete
CXCL	CXC-chemokine ligand
CXCR	C-X-C motif chemokine receptor
DAMPS	danger-associated molecular pattern
DC	dendritic cell
DNA	deoxyribonucleic acid
DNMT3A	DNA (Cytosine-5)-Methyltransferase 3 Alpha
DP	double positive
EDTA	ethylenediaminetetraacetic acid
EOMES	eomesodermin
ESL	E-selectin
FDA	Food and Drug Administration
FDC	follicular dendritic cells
Fdw	forward
FOXO1	forkhead box protein O1
FoxP3	forkhead box P3
GFP	Green Fluorescent Protein
GlyCAM-1	glycosylation-dependent cell adhesion molecule-1
GzmB	granzyme B
HBV	hepatitis B virus
HCV	hepatitis C virus
HET	House of Experimental Therapy
HEV	high endothelial venules

HIV	human immunodeficiency virus
Hobit	zinc finger protein 683
hrs	hours
HSC	hematopoietic stem cells
HSV	herpes simplex virus
ICB	immune checkpoint blockade
ID2	inhibitor Of DNA Binding 2
ID3	inhibitor of DNA binding 3 protein
IFN	interferon
IL	interleukin
IR	inhibitory receptors
IRF4	interferon regulatory factor 4
KLF2	krüppel-like factor 2
KLF4	krüppel-like factor 4
KLRG1	killer cell lectin-like receptor G1
Lag-3	lymphocyte activation gene 3
Lck	lymphocyte-specific protein tyrosine kinase
LCMV	lymphocytic choriomeningitis virus
LN	lymph nodes
MAR	matrix attachment regions
MHC-I	major histocompatibility complex class I
min	minutes
miRNAs	micro-RNAs
MPC	memory precursor cells
MYB	myeloblastosis Proto-Oncogene
Myb	myeloblastosis proto-oncogene
MZ	marginal zone
NFAT	Nuclear factor of activated T-cells
NK	natrual killer cells
NR4A	nuclear receptor subfamily 4 group A
NURD	Nucleosome Remodelling and Deacetylase
Oct4	octamer-binding transcription factor 4
p.i.	post infection
PAMP	pathogen-associated molecular pattern
PD-1	programmed cell death protein 1
PD-L	programmed death-ligand
PDI	Peter Doherty Institute
PGC1α	peroxisome proliferator-activated receptor gamma coactivator 1-alpha
PI3K	phosphoinositide 3-kinase
PRR	pattern-recognition receptor

PSL	P-selectin
RBC	red blood cells
RCRB	red cell lysis buffer
Rev	reverse
RNA	ribonucleic acid
RP	red pulp
Rt	room temperature
RunX3	Runt-related transcription factor 3
S1P	sphingosine-1-phosphate
S1PR1	sphingosine-1-phosphate receptor 1
SATB1	special AT-rich sequence binding protein 1
SLEC	short-lived effector cells
SLO	secondary lymphoid organs
Sox2	(sex determining region Y)-box 2
SP	single positive
STAT	signal transducer and activator of transcription
T-bet	T-box transcription factor TBX21
TCF1	T cell factor 1
T_{CM}	central memory T cells
TCR	T cell receptor
TCZ	T cell zone
T_{EM}	effector memory T cells
T_{EX}	exhausted T cells
T_F	transcription factor
T_{FH}	T follicular helper
Tg	transgenic
TGFb	transforming growth factor β
TIGIT	T-cell immunoreceptor with immunoglobulin and ITIM domain
Tim-3	T-cell immunoglobulin and mucin domain 3
TLR	Toll-like receptor
TLS	tertiary lymphoid structures
TNF	tumor necrosis factor
TOX	thymocyte selection-associated high mobility group box protein
T_{PEX}	precuorser of exhuasted T cells
Treg	regulatory T cel
T_{RM}	tissue memory T cells
WP	white pulp
Wt	wild typ
ZAP-70	zeta-associated protein kinase of 70 kDa
Zeb-2	zinc finger E-box binding homeobox 2 protein

List of Tables

List of Figures

Abstract

Cytotoxic $CD8^+$ T cells are critical mediators of immunity against chronic viral infection and cancer. However, when $CD8^+$ T cells are persistently exposed to high amounts of antigen, they lose their functionality and differentiate into 'exhausted' T cells (T_{EX}). Hallmarks of exhaustion are high expression of inhibitory receptors, also called immune checkpoints, like PD-1, increased expression of TCR-responsive transcription factors like TOX, compromised cytokine production and diminished proliferative capacity. Previous studies by our group and others have shown that the pool of exhausted T cells contains functionally important subsets with distinct epigenetically and transcriptional profiles, including precursors of exhausted T cells (T_{PEX}). T_{PEX} display characteristics of both, exhausted and memory T cells. Furthermore, they include a population of stem-like cells, marked by the expression of CD62L and the transcription factor Myb, that mediates long term maintenance of $CD8^+$ T cell immunity and response to PD-1 checkpoint inhibition by a proliferative burst. It was shown that T_{PEX} cells can differentiate into two distinct populations of T_{EX}, including $CX3CR1^+$ effector-like cells and $CD101^+$ terminally exhausted cells. The molecular mechanism that regulates and drive the differentiation of T_{PEX} and T_{EX} and thus giving rise to new targets of cancer therapy, are still not fully understood. In this thesis we identify SATB1 as a critical factor in T_{PEX} and T_{EX} differentiation. SATB1 deficiency accelerates T_{EX} formation in chronic infection and skews acute infection responses toward effector memory. It also regulates cytokine expression and PD-1 levels, making it a potential target for CAR-T therapies. Additionally, we show that migratory molecules (CD62L, CCR7, S1PR1) are crucial for T_{PEX} maintenance and T_{EX} generation. Their disruption primarily affects $CX3CR1^+$ T_{EX} cells, highlighting the role of spatial organization in exhaustion regulation. Finally, we establish KLF2 as a key regulator controlling the development of $CD62L^+$ T_{PEX} cells and their differentiation into $CX3CR1^+$ T_{EX} cells. KLF2 loss enhances effector function but increases exhaustion markers. Notably, statins upregulate KLF2, suggesting a pharmacological approach to modulating exhaustion dynamics. These findings advance our understanding of

$CD8^+$ T cell differentiation and exhaustion, providing insights for improving immunotherapies in chronic infections and cancer.

Declaration

The work presented in this thesis was conducted at The Peter Doherty Institute in Melbourne (University of Melbourne) in the laboratory of Prof. Dr. Axel Kallies and the Institute of Molecular Medicine and Experimental Immunology (IMMEI, The Rheinische Friedrich-Wilhelms-University of Bonn) in the laboratory of Prof. Dr. Zeinab Abdullah. Leonie Heyden was supported by the Melbourne Research Scholarship.

This is to certify that

I. The thesis comprises only my original work towards the joined PhD, except where indicated;
II. due acknowledgement has been made in the text to all other material used; and
III. the thesis is less than 100,000 words in length, exclusive of tables, graphs, bibliographies, and appendices.

Melbourne, March 2025 Leonie Heyden

Preface

The experimental studies of this thesis were designed and performed by me, with contributions from my supervisor and co-supervisors. The contributions of this study to the results are detailed below. My contributions to the experiments described in the Results section of this thesis are as follows:

Chapter 3: 95 %
Chapter 4: 100 %
Chapter 5: 95 %

I gratefully acknowledge the important contributions of other researchers to the experiments presented in this thesis.

Chapter 3:
Analysis of bulk-RNA-sequencing and ATAC-sequencing was conducted by Lachlan Dryburgh and Jan Schröder, who also generated the analysis plots used in this thesis.
I would also like to acknowledge the Beyer Lab and Turner Lab for providing the SATB1 mouse models used in this study.

Chapter 5:
Data presented in Fig 5.1A and B and Fig 5.10 was conducted by Carlson Tsui, Analysis of Single cell-RNA-Sequencing was conducted by Nikita Potemkin and Jan Schröder.

Furthermore, I would like to acknowledge the assistance from Carlson Tsui, Sharanya K. Wijesinghe, Marcela Moreira, Lifen Wen, from the Kallies Lab, Helena Horvatic from the Abdullah Lab and Catarina Graça and Sining Li from the Utzschneider Lab for their help during tissue processing, sequencing and experimental procedures.

Acknowledgements

Completing this PhD has been a rewarding yet challenging journey, made possible by the invaluable support of many individuals and institutions. I am deeply grateful to everyone who has contributed to this chapter of my life.

First and foremost, I would like to express my sincere gratitude to my supervisors, Axel Kallies and Zeinab Abdullah, for their unwavering guidance, insightful discussions, and continuous encouragement. Their expertise and mentorship have been instrumental in shaping my scientific thinking and research approach. I also extend my appreciation to my co-supervisors Daniel Utzschneider and Carlson Tsui and the members of my advisory committee Thomas Gebhart and Laura Mackay for their valuable feedback and support throughout this process.

This PhD would not have been possible without the support of the University of Bonn and the University of Melbourne, and I deeply appreciate the opportunities provided by both institutions. A special gratitude to the support of the IRTG coordination team - Marie Greyer, Annabelle Blum, Lucie Delforge, and Sandra Rathmann. Your exceptional organizational skills and dedication ensured that any challenges were swiftly addressed, and I am truly grateful for your efforts.

I am incredibly thankful to my colleagues and collaborators at both the University of Bonn, the University of Melbourne and the Monash University. Especially my lab members, whose discussions and shared struggles have made this journey both enriching and enjoyable. The stimulating research environment and collective pursuit of knowledge have greatly motivated me over the past four years. A special thanks to my collaborators Marc Beyer and Stephen Turner, that helped shaping the SATB1 project.

I am profoundly grateful to my friends, particularly Sharanya, Darya, Catarina, Lyn, Sharon, Carlson, Caro, Rebecca, Katja and Lara for their unwavering support, encouragement, and the much-needed moments of laughter and

relaxation. Our moments and trips together were the balance and motivation throughout this challenging journey I needed.

Finally, I extend my heartfelt gratitude to my family, whose unconditional love, patience, and belief in me have been my greatest strength. Their encouragement has been the foundation of my determination, and I could not have achieved this milestone without them. Ohne euch hätte ich die letzten vier Jahre nicht geschafft. Ich bin unglaublich dankbar, euch an meiner Seite zu haben und für eure unermüdliche Unterstützung in allen Lebensbereichen. Ihr seid einfach die Besten!

To everyone who has been part of this incredible journey a big thank you.

List of publications

Lymph nodes fuel KLF2-dependent effector CD8+ T cell differentiation during chronic infection and checkpoint blockade

Nature immunology; September 2025; Doi.org/10.1038/s41590-025-02276-7

Carlson Tsui***** and **Leonie Heyden***, Lifen Wen, Catarina Gago da Graça, Nikita Potemkin, Daniel Rawlinson, Lei Qin, Verena C. Wimmer, Marjan Hadian-Jazi, Darya Malko, Helena Horvatic, Sharanya K. Wijesinghe, Marcela Moreira, Lachlan Dryburgh, Sining Li, Dominik Schienstock, Lisa Rausch, Daniel T. Utzschneider, Cornelia Halin, Scott N. Mueller, Sammy Bedoui, Zeinab Abdullah, Jan Schröder, Axel Kallies

(***contributed equally)**

Transcriptional regulator SATB1 limits CD8+ T cell population expansion and effector differentiation in chronic infection and cancer

Nature immunology; October 2025; Doi.org/10.1038/s41590-025-02316-2

Leonie Heyden, Lisa Rausch, Michael H. Shannon, Lachlan Dryburgh, Marcela L. Moreira, Aleksej Frolov, Christina M. Scheffler, Marit J. van Elsas, Junming Tong, Olivia Hidajat, Sharanya K. M. Wijesinghe, Sining Li, Helena Horvatic, Anh Nhat Truong, Catarina Gago da Graça, Carlson Tsui, Maren Köhne, Daniel Sommer, F. Thomas Wunderlich, Bianca von Schiedt, Simone Park, Laura Mackay, Daniel T. Utzschneider, Jan Schröder, Stephen J. Turner, Phillip K. Darcy, Marc D. Beyer, Zeinab Abdullah, Axel Kallies

Aerobic glycolysis but not GLS1-dependent glutamine metabolism is critical for anti-tumor immunity and response to checkpoint inhibition

Cell Reports; August 2024; Doi:10.1016/j.celrep.2024.114632

Patrick M Gubser, Sharanya Wijesinghe, **Leonie Heyden**, Sarah S Gabriel, David P de Souza, Christoph Hess, Malcolm M McConville, Daniel T Utzschneider, Axel Kallies

Chapter 1 - Introduction

1.1 The adaptive immune system

Immune responses are a critical to protect the body against pathogens, including viruses, bacteria, and parasites (Marshall *et al.*, 2018). The immune system consists of a large complex of cells and factors that interact with each other. This includes barrier cells, tissue-resident immune cells, leukocytes, lymphocytes and soluble factors, such as the complement system, antibodies, chemokines, and cytokines (Parkin and Cohen, 2001). The immune system can be divided in two main components: the adaptive immune system and the innate immune. Major components of the innate immune system are mast cells, basophils, eosinophils, natural killer (NK) cells, and phagocytes, including dendritic cells (DC), neutrophils and macrophages. Innate immune cells act as a first line of defence and are antigen nonspecific. They are activated through pattern-recognition receptors (PRRs) like Toll-like receptors (TLRs), expressed on the immune cells, that recognize danger- (DAMPs) or pathogen-associated molecular patterns from damaged tissues (PAMPs) (O'Neill *et al.*, 2013). A prominent example is TLR13 that has been shown to recognize bacterial ribosomal RNA (Oldenburg *et al.*, 2012; Hidmark *et al.*, 2012; Li and Chen, 2012). Components of viruses are also recognized by TLRs. For example, TLR9 binds pathogen-derived DNA (J. Lund *et al.*, 2003) while TLR3 recognises doubled-stranded RNA, a component found in various viruses (Alexopoulou *et al.*, 2001). Activation via TLRs leads to maturation of immune cells like of DCs, macrophages and the secretion of cytokines like Type-I interferon (IFN), that initiate and shape the immune answer (Krutzik *et al.*, 2005; O'Neill *et al.*, 2013).

The activation of innate immunity is crucial for triggering the adaptive immune response (Bonilla and Oettgen, 2010). Adaptive immunity operates through recognition of antigens. Antigens are substances that can be recognized by the adaptive immune system, like peptides, proteins, glycoproteins and polysaccharides of pathogens but also chemical structures like metals, drugs, and organic chemicals (Murphy and Weaver, 2017). These antigens are recognized by specific antigen receptors that are expressed on lymphocytes,

including various B cells (BCR) and T cell receptors (TCR) (Miho *et al.*, 2018). TCRs and BCRs are unique antigen receptors that can recognize up to 10^{13} different peptide sequences. This diversity is achieved through somatic rearrangements, nucleotide deletions and additions of the antigen receptor coding sequences (Greiff *et al.*, 2017). Antigen presenting cells (APC) take up antigens at the site of infection before migrating to secondary lymphoid organs, where they present peptides of the antigens to T cells (Guermonprez *et al.*, 2002). Many T cells can interact with APC, but only cells exhibiting a TCR that can bind the antigen will be activated (Anaya *et al.*, 2013). This triggers the development of specialized killer and helper T cells, which play a crucial role in effectively eliminating pathogen. Furthermore, the adaptive immune system establishes immune memory, enabling a swift response upon repeated antigen exposure which is the principle underlying vaccination (Murphy and Weaver, 2017).
In this thesis, factors that control cytotoxic T cell differentiation and function during chronic infection and cancer will be explored.

1.2 $CD8^+$ T cell immunity during acute viral infection

1.2.1 $CD8^+$ T cell priming and activation

During bacterial and viral infections $CD8^+$ T cells are the cell population that can eradicate infected cells. The $CD8^+$ T cell immune response can be separated into four different stages: 1) the effector phase, 2) the contraction phase, 3) memory maintenance and 4) memory restimulation (Williams and Bevan, 2007). During the effector phase, antigen presenting DCs migrate to secondary lymphoid organs including spleen and lymph nodes (LN), where they activate and prime naïve $CD8^+$ T cells (Murphy and Weaver, 2017). At least three independent signals are required to generate cytotoxic $CD8^+$ T cells. First, APC and naïve $CD8^+$ T cells form an immunological synapse (Heath and Carbone, 2001; Steinman *et al.*, 2003; Germain *et al.*, 2006), where the TCR recognizes and binds to its specific antigen displayed by major histocompatibility complex class I (MHC-I) (Doherty and Zinkernagel, 1984). Activation of the TCR is considered the first and primary signal for T cell activation. As a second signal, costimulatory receptors on the surface of naïve $CD8^+$ T cells must bind to their ligands on the

surface of the APC. This often includes the interaction of CD28 with the B7 ligands B7.1 (CD80) or B7.2 (CD86), expressed on the surface of mature DCs (Mescher *et al.*, 2006). Other co-stimulatory interactions might include CD27/CD70, OX40/OX40L, 41BB/41BB-L, and CD30/CD30L (Watts, 2005; Chen and Flies, 2013). The third signal is provided by cytokines. In particular, IL-2, IL-12, and type-I IFN are critical during activation, population expansion and differentiation of $CD8^+$ T cells (Mescher *et al.*, 2006). Incomplete signals result in $CD8^+$ T cells becoming non-responsive and they lose their ability to eliminate pathogens, a state described as anergy (Crespo *et al.*, 2013). After priming and activation, naïve $CD8^+$ T cells start to rapidly undergo proliferation and differentiation into cytotoxic effector cells that migrate to non-lymphoid tissues (Sarah E Henrickson *et al.*, 2008A; Sarah E. Henrickson *et al.*, 2008B). These cytotoxic effector cells produce high levels of effector cytokines IFN-γ, Tumor Necrosis Factor (TNF), and of cytotoxic molecules, such as granzymes and perforin to kill virus and bacterial infected cells. Thus, recruitment of cytotoxic effector cells leads to elimination of pathogen infected cells, decreasing the antigen load (Kaech and Wherry, 2007; Harty and Badovinac, 2008). With decreasing antigen load, $CD8^+$ T cells enter the contraction stage, where the majority of cytotoxic effector cells die via Bim-dependent apoptosis (Hildeman *et al.*, 2002) while memory $CD8^+$ T cells remain (Kaech, Wherry, *et al.*, 2002; Kaech, Hemby, *et al.*, 2002; Williams and Bevan, 2007). Memory $CD8^+$T cells form a long-lived, quiescent population that remains upon infection clearance and survives in the absence of cognate antigen encounter (Lau *et al.*, 1994; Hammarlund *et al.*, 2003). In case of reinfection, memory $CD8^+$ T cells can mount a potent recall response (Williams and Bevan, 2007) that is faster and more cytotoxic than the original response. Activation of memory T cells leads to rapid expansion of cytotoxic effector cells and maintenance of the memory pool.

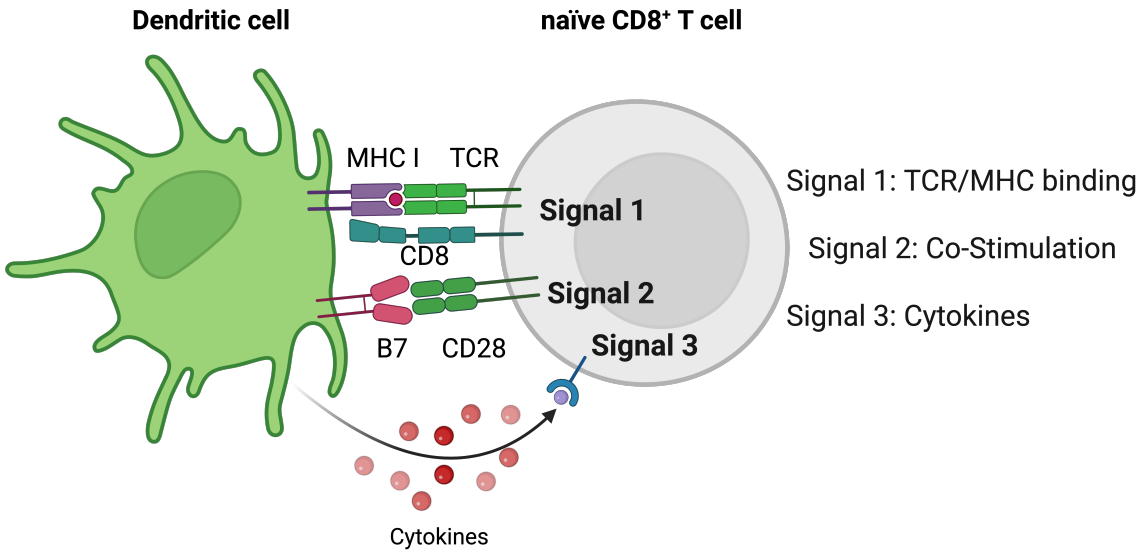

Figure 1.1: Three mandatory signals for CD8⁺ T cell priming by antigen-presenting cells.
Antigen-presenting cells, such as dendritic cells, prime naïve CD8⁺ T cells with three different independent signals: 1) Antigen presentation: CD8+ T cells via the TCR bind their cognate antigen presented by APC via MHC I. 2) Co-stimulatory signals like B7/CD28 binding are also required. 3) Pro-inflammatory cytokines are secreted by APCs to further activate CD8⁺ T cells and guide their differentiation (El-Awady et al., 2022).

1.2.2 CD8⁺ T cell differentiation into effector and memory cells

During the primary immune response, the pool of CD8⁺ T cells is heterogeneous (Figure 1.2). Two distinct cell subsets have been identified: short-lived effector cells (SLECs) and memory precursor cells (MPCs). SLEC are considered to be terminally differentiated, with most of them undergoing apoptosis following antigen clearance, whereas MPC have the potential to develop into long-lived memory cells (Kaech and Wherry, 2007). Both subsets are phenotypically distinct, with SLECs expressing high levels of killer cell lectin-like receptor G1 (KLRG1) while downregulating the expression of IL-7Ra (CD127), C-X-C motif chemokine receptor 3 (CXCR3), CD27, and CD28. MPCs can be classified based on the expression of IL-7Ra, B cell lymphoma (Bcl)-2, CD27, CXCR3, and CD28, while they do not express KLRG1. Therefore SLECs are primarily identified as KLRG1⁺IL-7Ra⁻ cells and MPC as KLRG1⁻IL-7Ra⁺ cells (Ibegbu *et al.*, 2005; Joshi

and Kaech, 2008). The fate decision towards SLECs or MPCs occurs during the early stages of the $CD8^+$ T cell response. Several factors can influence this decision. For example, the TCR/antigen strength as well as the duration of stimulation can modulate differentiation (Badovinac *et al.*, 2004; Obar *et al.*, 2011). Weaker TCR signals favours the differentiation of MPC, while stronger TCR signalling results in increased SLEC differentiation (Smith-Garvin *et al.*, 2010). Additionally, cytokines and costimulatory signals contribute to the fate decision. For example CD27 signalling favours differentiation of MPC while strong 4-1BB can drive effector differentiation (Watts, 2005; Greenwald *et al.*, 2005). Furthermore, inflammatory cytokines like IL-12 and IFN-γ have been shown to play key roles in influencing fate decisions (Badovinac *et al.*, 2005; Kaech and Wherry, 2007; Sarkar *et al.*, 2008). Low inflammatory conditions result in increased differentiation of MPCs, whereas high inflammation promotes the differentiation of SLECs. After the infection is cleared and the amount of antigen is reduced, MPCs can differentiate further into different long-lived memory subsets. Interestingly, a small number of SLECs can also be maintained for a long period and respond to a rechallenge (Olson *et al.*, 2013), indicating that some effector cells are long-lived. Transcription factors T-box transcription factor TBX21 (T-bet) and eomesodermin (EOMES) are essential for $CD8^+$ T cell effector and memory development (Pearce *et al.*, 2003; Intlekofer *et al.*, 2005) During acute infection, T-bet drives terminal $KLRG1^+$ T effector differentiation in response to inflammatory signals, while EOMES promotes IL-15Rβ expression, memory formation, and homeostasis (Pearce *et al.*, 2003; Banerjee *et al.*, 2010; Paley *et al.*, 2012). The loss of either factor has strong effects in the $CD8^+$ T cell immune response to acute infections. T-bet KO reduces $KLRG1^+$ T effector cells but allows memory formation, whereas EOMES loss impairs memory maintenance (Intlekofer *et al.*, 2005; Joshi *et al.*, 2007; Banerjee *et al.*, 2010; Dominguez *et al.*, 2015).

Memory cells are long-lived and require cytokine IL-7 and the IL-15, which promote T cell survival and enable antigen independent proliferation and self-renewal (Williams and Bevan, 2007). Three major subsets of memory $CD8^+$ T

cells that have been described: central memory T cells (T_{CM}), effector memory T cells (T_{EM}) and tissue resident memory T cells (T_{RM}). T_{CM} and T_{EM} cells were defined by distinct surface marker expression and tissue distribution (Sallusto *et al.*, 1999). T_{CM} cells are $CD44^+CCR7^+CD62L^+$, whereas T_{EM} cells are $CD44^+CCR7^-CD62L^-$. T_{CM} and T_{EM} show different characteristics in response to rechallenge with the antigen. T_{CM} cells have to upregulate their effector functions and have a high proliferative capacity, while T_{EM} cells have immediate effector functions and a reduced proliferative capacity. They also reside in different locations. Most T_{EM} cells are found in the blood or spleen; some enter non-lymphoid tissues, whereas T_{CM} cells primarily reside in the LN, spleen, bone marrow and blood (Masopust *et al.*, 2001; Marshall *et al.*, 2001; Wherry, Teichgräber, *et al.*, 2003). The fate decisions of T_{CM} and T_{EM} cell differentiation is driven by various factors, including metabolic controls and transcription factors. Downregulation of krüppel-like factor 2 (KLF2) decreases C-C chemokine receptor (CCR)7 and CD62L expression, thereby promoting the differentiation of T_{EM} cells (Sinclair *et al.*, 2008). Additionally the expression of transcription factors inhibitor of DNA binding 2 protein (ID2), T-bet, Zinc finger E-box binding homeobox 2 protein (Zeb2) and B lymphocyte-induced maturation protein-1 (Blimp1, encoded by *Prdm1*), promote the formation of T_{EM} cells, whereas EOMES, inhibitor of DNA binding 3 protein (ID3), T cell factor 1 (TCF1), and Bcl6 promote T_{CM} cell differentiation (Ichii *et al.*, 2004; Intlekofer *et al.*, 2005; Cannarile *et al.*, 2006; Kallies *et al.*, 2009; Russ *et al.*, 2014; Dominguez *et al.*, 2015; Omilusik *et al.*, 2015).

T_{RM} cells continuously reside in non-lymphoid tissue and make up a significant part of the $CD8^+$ T cell memory pool. They continuously monitor for pathogens and provide a first line of defence thanks of their strong effector functions and strategic positioning near potential sites of reinfection (Masopust and Soerens, 2019). T_{RM} cells are fundamentally distinct from T_{CM} and T_{EM} cells at both transcriptional and epigenetic levels. For example, in contrast to circulating memory T cells, T_{RM} cells consistently express granzyme B (GzmB) (Schenkel *et al.*, 2013; Ariotti *et al.*, 2014; Schenkel *et al.*, 2014). T_{RM} cells usually express

high levels of adhesion and retention molecules, such as CD103, CD69, and CCR9, while they reduce the expression levels of homing molecules, including G-protein-coupled receptor 1 (S1PR1), CCR7, and CD62L (Crowl *et al.*, 2022; Heeg and Goldrath, 2023). These homing markers on lymphocytes enable adhesion to addressins on endothelial cells, guiding migration to lymphoid organs (Jalkantn *et al.*, 1986). The T_{RM} specific molecular expression patterns contribute to lymphoid tissue exit and entry into non-lymphoid tissues (Heeg and Goldrath, 2023). Even through T_{RM} cell in different tissues are heterogenous (Crowl *et al.*, 2022; Lin *et al.*, 2023), comparing cells from various tissues to their circulating counterparts, researchers have identified core gene signatures that define tissue residency (Wakim *et al.*, 2012; Mackay *et al.*, 2016; Kumar *et al.*, 2017; Milner *et al.*, 2017; Crowl *et al.*, 2022). KLF2 expression must be downregulated for acquisition of residency as KLF2 promotes expression of CCR7, CD62L, and S1PR1 that enable circulation and homing. In particular, S1PR1 binds to sphingosine-1-phosphate (S1P), a molecule in the blood that promotes T cells to exit tissues. Thus, reducing S1PR1 is essential for T_{RM} cells to remain in the tissue. In line with this, expression of CD69 also supports T cell residency by blocking S1PR1 from interacting with S1P and preventing T cells from leaving the tissue (Skon *et al.*, 2013). Another factor of T_{RM} formation is the transforming growth factor β (TGFβ) (Li *et al.*, 2022). TGFβ is instrumental in inducing CD103 expression and plays a critical role in the differentiation and function of T_{RM} cells in both murine and human models (Yang and Kallies, 2021). Transcriptomic analyses indicate that more than half of the genes associated with the mouse T_{RM} signature are also induced by TGFβ in $CD8^+$ T cells (Nath *et al.*, 2019; Christo *et al.*, 2021). While T_{RM} cells in the skin require continuous TGFβ signalling for their retention, those located in non-epithelial sites, such as the liver, do not require such signalling (Hirai *et al.*, 2021; Christo *et al.*, 2021). The loss of TGFβ signalling in $CD8^+$ T cells in the skin responding to the herpes simplex virus (HSV), results in restrained development of $CD103^+$ T_{RM} cells (Mackay *et al.*, 2013). Additionally, TGFβ facilitates the expression of CD49a (VLA-1 α1 subunit), a prevalent marker of T_{RM} cells (Yang and Kallies, 2021). During infection, CD49a expression is upregulated on antigen-specific $CD8^+$ T cells (Roberts *et al.*, 1999;

Ray *et al.*, 2004). Although the majority of circulating memory T cells eventually lose CD49a expression, it remains present on many, but not all, T_{RM} cells (Ray *et al.*, 2004; McMaster *et al.*, 2018). Further pre-exposure to TGFβ before TCR stimulation has been found to prime cells for differentiation into the intraepithelial T_{RM} lineage (Mani *et al.*, 2019; Obers *et al.*, 2024). Further mature T_{RM} cells are highly responsive to TGFβ through the down regulation of the transcription factors T-bet and EOMES (Mackay *et al.*, 2013; Laura K. Mackay *et al.*, 2015), which helps T_{RM} cells to stay anchored in tissues, especially in epithelial layers (Zhang and Bevan, 2013; Bergsbaken *et al.*, 2017). Transcription factors such as Blimp1, zinc finger protein 683 (Hobit) (Mackay *et al.*, 2016), and Runt-related transcription factor 3 (Runx3) (Milner *et al.*, 2017) further reinforce T_{RM} identity by enhancing gene expression that supports tissue residency while suppressing those involved in circulation. However, the dependency of cytokines and transcription factors can vary among different tissues (Yang and Kallies, 2021).

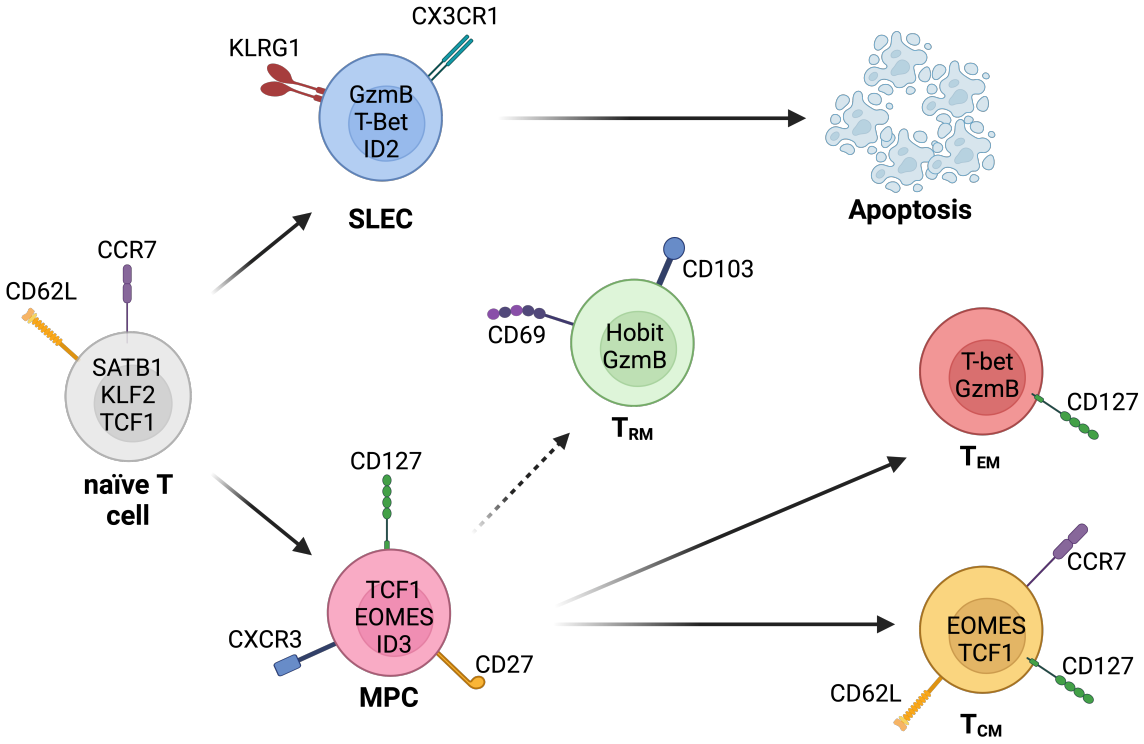

Figure 1.2: Differentiation trajectory of naïve CD8⁺ T cells into effector and memory subsets.
Naïve CD8⁺ T cells get primed and activated and differentiate into short lived effector cells (SLEC) or memory precursor cells (MPCs). After the antigen is cleared, most SLECs die via controlled apoptosis. MPCs can differentiate into

tissue resident memory (T_{RM}) cells in the tissues or effector memory (T_{EM}) or central memory (T_{CM}) cells. Displayed are all cell types with characteristic expression of surface markers and transcription factors. The illustration is adapted from (Chen *et al.*, 2018; Raphael *et al.*, 2020; Verdon *et al.*, 2020)

1.2.3 Localisation and migration of CD8$^+$ T cells

The immune system includes specialised lymphoid organs that support development, activation and differentiation of immune cells. Primary lymphoid organs, including the bone marrow, thymus, and fetal liver, serve as significant sites for lymphocyte development (Ruddle and Akirav, 2009). Secondary lymphoid organs (SLOs), such as lymph nodes, spleen, Peyer's patches, and tonsils, bring immune cells together to detect antigens and activate lymphocytes (Najibi and Mooney, 2020). Additionally, stroma cells of SLOs produce high levels of IL-7, generating an environment that allows naïve and memory T cell survival (Tan *et al.*, 2001). The migration of CD8$^+$ T cells through these organs is tightly regulated. Priming of naïve CD8$^+$ T cells mainly occurs in either the spleen or the LN. T cells enter the LN from the bloodstream through a multistep adhesion process guided by interactions between homing receptors on T cells and their corresponding ligands on blood vessels (Ley *et al.*, 2007). Naïve T cells use CD62L and CCR7 to enter lymph nodes by binding to ligands on high endothelial venules (HEVs) (Girard *et al.*, 2012). In gut-associated tissues, effector and memory T cells rely on integrins α4β7 and CCR9, which recognise MAdCAM-1 and chemokine ligand (CCL)25 in the gut vasculature (Hamann *et al.*, 1994; Kunkel *et al.*, 2000; Johansson-Lindbom *et al.*, 2003; Stenstad *et al.*, 2006). In contrast, homing of effector and memory T cells to the skin is mediated by E-selectin and P-selectin ligands (ESL and PSL), which interact with selectins expressed in inflamed blood vessels (Erdmann *et al.*, 2002). While CCR4 has been suggested to be essential for CD4$^+$ effector T cell entry into inflamed skin (Campbell *et al.*, 2007), other studies have indicated that CCR10, CXCR3, and CCR5 may play a greater role (Reiss *et al.*, 2001; Gregg *et al.*, 2010). Less is known about effector T cell homing to other tissues. Integrin α4β1, which binds VCAM-1, has been linked to T cell infiltration in the brain (Rott *et al.*, 1996), lungs

(Kenyon *et al.*, 2009), and bronchus-associated lymphoid tissue (Kawamata *et al.*, 2009).

Lymphatic vessels and fibroblasts also offer a matrix for immune cell movement and produce chemokines that modulate cellular positioning. T and B cells navigate the node responding to chemical signals that are provided and regulated by distinct stroma cells (Rodda *et al.*, 2018). Thus, stromal cells orchestrate the formation of niches to coordinate different immune functions. T and B cells navigate the node using chemical signals produced by fibroblasts (Rodda *et al.*, 2018). CXC-chemokine ligand (CXCL)13 secreted by follicular dendritic cells (FDCs) guides $CXCR5^+$ B cells to follicles and GCs where they encounter antigens presented by FDCs (Mueller and Germain, 2009). CCL19/CCL21 attracts $CCR7^+$ T cells and DCs to the paracortex (Von Andrian and Mempel, 2003; Eisenbarth, 2019). The lymphatic structure also allows for antigen draining from tissues to LNs during inflammation, by increasing the fluid transport, causing high numbers of immune cells to enter the LN (Schwager and Detmar, 2019). This results in a high number of antigens and APC cells residing in macrophage-enriched subcapsular sinuses (Ruddle and Akirav, 2009), boosting a possible uptake of antigens. Small molecules travel through collagen conduits (Gretz *et al.*, 2000), whereas larger antigens are carried by APCs, such as DCs and macrophages (Phan *et al.*, 2007; Heesters *et al.*, 2014). DCs migrate to the paracortex which can result in T cell priming. Activated effector $CD8^+$ and $CD4^+$ T cells then differentiate, leaving the node to target infection (Najibi and Mooney, 2020), while $CD4^+$ T follicular helper (T_{FH}) cells move to the B cell zone to support germinal center formation and enhance antibody production (De Silva and Klein, 2015).

The spleen functions as a peripheral circulatory organ embedded with lymph node-like structures, the red pulp (RP) and white pulp (WP) (Bronte and Pittet, 2013). The RP plays a dual role in filtering aged, dead, or opsonised cells from circulation, while also detecting pathogens and tissue damage. Blood reaches the marginal zone (MZ) through the terminal arterioles. Aged red blood cells

(RBCs) must pass through narrow venous sinusoids to re-enter circulation. Damaged, infected, or opsonised cells were removed using RP macrophages. (Lewis *et al.*, 2019). In addition, while adaptive immune responses to systemic antigens begin in the WP, many immune effector functions occur in the RP. It houses innate immune cells, such as neutrophils, monocytes, dendritic cells, γδ T cells, and macrophages (Nolte *et al.*, 2000). Unlike the LN, the spleen lacks lymphatic vessels and HEVs, which means that cells enter via the blood (Lewis *et al.*, 2019). In contrast to the LN, the WP lacks a capsule separating it from the RP of the spleen. Instead, the cellular border of innate immune cells defines these boundaries (Lewis *et al.*, 2019). Additionally, the WP lacks afferent lymphatics for direct antigen and cell delivery. Thus, large antigens do not freely enter the WP, but are rather transported by cells from the MZ (Nolte *et al.*, 2003; Lewis *et al.*, 2019). Within the WP, distinct T and B cell compartments resemble those found in LNs. CCL19 and CCL21, produced by fibroblasts and lymphatic endothelial cell concentrate T cells here. Without CCR7, T cells are scattered throughout the spleen as described for the LN. Entry into the WP by T and B cells is facilitated by integrins (αLβ2, α4β1) (Mebius and Kraal, 2005), while fibroblast channels, possibly originating from the MZ, guide T cells through bridging channels into the WP (Nolte *et al.*, 2003; Bajénoff *et al.*, 2008). Fibroblast reticular cells line these channels with CCL21 to direct T cells through the T cell zone (TCZ) and interfollicular zone, while B cells follow a similar path before switching to the CXCL13-lined FDC network within follicles (Lewis *et al.*, 2019).

Another category of structures, where primming of the adaptive immune response might occur are tertiary lymphoid structures (TLS), that share similarities with SLOs but form in non-typical locations (Sautès-Fridman *et al.*, 2019; Sato *et al.*, 2023). When formed in the tumor microenvironment, TLSs recruit several lymphocytes to the tumour by establishing chemokine migration gradients analogous to those present in the LN. Mature TLSs form segregated B and T cell areas that establish interaction *in situ* with APCs (Sautès-Fridman *et al.*, 2019; Wang *et al.*, 2024). In addition, recruitment of B cells along CXCL13 gradients can result in the formation of HEVs upon establishment of LTB-LTBR

interactions with surrounding stromal cells (Johansson-Percival and Ganss, 2021). Formation of HEVs enables direct recruitment of naïve T cells in the tumour site further enhancing the immune response (Blanchard and Girard, 2021).

1.3 $CD8^+$ T cell immunity during chronic viral infection and cancer

1.3.1 T cell exhaustion

T cell responses are essential for protection against infections and cancers. $CD8^+$ T cells produce cytokines that contribute to the elimination of infected or malignant cells; however, excessive $CD8^+$ T cell activity can cause significant tissue damage. In other scenarios, misdirected responses against self-antigens can result in autoimmune disease development, like type 1 diabetes and multiple sclerosis (Collier *et al.*, 2021). To prevent such harmful effects, multiple regulatory mechanisms exist to control T cell activity.

In case of persistent antigen exposure, such as in response to chronic infections or cancer, $CD8^+$ T cells are continuously stimulated, via their TCR, and gradually lose function in a process called 'T cell exhaustion'. Exhaustion serves as a built-in regulatory program to limit T cell activity in chronic settings (Hashimoto *et al.*, 2018; McLane *et al.*, 2019; Blank *et al.*, 2019). Exhausted $CD8^+$ T cells (T_{EX}) share three key features: 1) impaired effector function and reduced proliferation, 2) increased expression of inhibitory receptors (IR), and 3) altered transcriptional, cellular and metabolic programming (McLane *et al.*, 2019).

Exhausted T cells have been identified in mice, for example in response to systemic Lymphocytic Choriomeningitis Virus (LCMV) infection and also in humans, for example during chronic infection with the human immunodeficiency virus (HIV), the hepatitis C virus (HCV), and the hepatitis B virus (HBV) (Day *et al.*, 2006; Urbani *et al.*, 2006; Radziewicz *et al.*, 2007; Fenwick *et al.*, 2019; Utzschneider *et al.*, 2020). Exhausted T cells are also found in murine tumor models and cancer patients (Thommen and Schumacher, 2018; Miller *et al.*, 2019). More recently, exhausted T cells have also been described to form in

response to some autoimmune diseases (Tilstra *et al.*, 2018; Smita *et al.*, 2022; Grebinoski *et al.*, 2022).

The main driver of T cell exhaustion is prolonged antigen exposure, which leads to a gradual loss of function. This includes a decline in cytolytic activity and progressive loss of cytokine production in an hierarchical fashion: first IL-2, then TNF, and finally IFN-γ (Zajac *et al.*, 1998; Wherry, Blattman, *et al.*, 2003). Additionally, exhausted T cells also fail to proliferate effectively (Shin *et al.*, 2007; Blackburn *et al.*, 2008). Exhausted $CD8^+$ T cells produce granzyme B albeit at lower levels compared to acutely stimulated cells (Miller *et al.*, 2019). Thus the cytotoxic function is lower in comparison to T cells responding to acute infections and insufficient to establish full clearance of infections or tumours (McLane *et al.*, 2019). Another key feature of exhaustion is the sustained expression of multiple IRs, such as Programmed cell death protein 1 (PD-1), cytotoxic T-lymphocyte-associated protein 4 (CTLA-4), Lymphocyte activation gene 3 (Lag-3), T-cell immunoglobulin and mucin domain 3 (Tim-3), and T-cell immunoreceptor with immunoglobulin and ITIM domain (TIGIT), which regulate the degree of effector function in T cell responses. Unlike acute infections, where expression of IRs declines as antigen levels drop, chronic stimulation maintains high IR expression in T_{EX} cells (Wherry *et al.*, 2007; Blackburn *et al.*, 2009; Jiang *et al.*, 2015). Both CTLA-4 and PD-1 are key inhibitory receptors that have been shown to play an important role in immune homeostasis. CTLA-4 is a negative regulator of CD28 signalling as it competes with CD28 for the binding of B7-1 and B7-2 on APCs (Linsley *et al.*, 1991; Walunas *et al.*, 1994; Linsley *et al.*, 1994; Esensten *et al.*, 2016; Wei *et al.*, 2018). The binding of these ligands prevents the downstream signalling of phosphoinositide 3-kinase (PI3K) and protein kinase B (AKT), thereby reducing T cell activity (Wei *et al.*, 2018). PD-1 is expressed on all $CD8^+$ T cells upon T cell activation and prevents excessive immune responses (Agata *et al.*, 1996; Sharpe and Pauken, 2018). However, chronic antigen stimulation leads to increased PD-1 expression, which reduces the proliferative capacity and functionality (Barber *et al.*, 2006). PD-1 binds to its ligands, programmed death-ligand (PD-L)1 and PD-L2, which are expressed on the surface of APC but are

also often expressed by tumour cells to evade the immune response (Dong *et al.*, 1999; Latchman *et al.*, 2001). Mechanistically, PD-1 inhibits TCR signalling by recruiting phosphatases (SHP1 and SHP2), which dephosphorylate the key molecules lymphocyte-specific protein tyrosine kinase (Lck) and zeta-associated protein kinase of 70 kDa (ZAP-70), impairing the PI3K-AKT pathway, thereby reducing T cell activation (Chemnitz *et al.*, 2004; Parry *et al.*, 2005; Yokosuka *et al.*, 2012). While PD-1 primarily disrupts TCR signalling, new research suggests its role in the interference of CD28 co-stimulation (Kamphorst *et al.*, 2017; Hui *et al.*, 2017).

Transcriptomic and single-cell analyses have shown that exhausted T cells are distinct from naïve, effector, and memory $CD8^+$ T cells (Crawford *et al.*, 2014). Early studies have revealed that virus-specific $CD8^+$ T cells in chronic infections exhibit distinct transcriptional profiles compared to those in acute infections (Wherry *et al.*, 2007). This includes altered expression of genes related to TCR signalling, migration, and metabolism (Wherry *et al.*, 2007; Doering *et al.*, 2012). Importantly, significant differences were already established early, before the peak of infection, in $CD8^+$ T cells responding to acute vs. chronic infection (Yao *et al.*, 2019; Utzschneider *et al.*, 2020). Importantly, exhausted T cells in chronic infections and tumours share similar gene expression patterns, highlighting exhaustion as a conserved adaptation to prolonged antigen exposure (Miller *et al.*, 2019). Such transcriptomic and epigenetic similarities are also observed in chronically stimulated autoreactive T cells, indicating that activation of the exhausted program is also a feature of autoimmune responses (Grebinoski *et al.*, 2022). More recently, it has become clear that epigenetic modifications play a crucial role in enforcing T cell exhaustion. Changes in chromatin accessibility, DNA methylation, and histone modifications shape the identity of T_{EX} cells and limit their plasticity. Genome-wide studies have shown that T_{EX} cells from chronic infections and tumours have overlapping epigenetic profiles, that actively contribute to the maintenance of exhaustion features and to the restriction of effector function (Scott-Browne *et al.*, 2016; Sen *et al.*, 2016; Mognol *et al.*, 2017). For example, sustained PD-1 expression has been linked to increased chromatin

accessibility at the *Pdcd1* locus (Sen *et al.*, 2016). Additionally, T_{EX} cells acquire DNA methylation at genes critical for effector functions, such as IFN-γ, and memory formation like *Tcf7* (encodes TCF1), restricting their ability to regain functionality even when removed from persistent antigen stimulation (Pauken *et al.*, 2016; Ghoneim *et al.*, 2017; Abdel-Hakeem *et al.*, 2021). These stable epigenetic changes pose a challenge for therapies aimed at reinvigorating exhausted T cells. Indeed, the epigenetic imprinting of T_{EX} cells seems to be quite stable. In HCV patients, cells bearing the epigenetic profile of exhausted T cells could still be found in the blood six months upon therapeutic clearance of the virus (Yates *et al.*, 2021). Complimentary studies in mice showed that exhausted T cells retain the epigenetic landscape of exhausted T cells after transfer into naïve mice and showed, as consequence, low capacity to produce effector cytokines (Abdel-Hakeem *et al.*, 2021).

T_{EX} cells also undergo metabolic dysfunction, shifting away from the efficient energy production observed in normal T cell responses (Scharping and Delgoffe, 2016). In contrast to effector T cells in acute infections, T_{EX} cells in chronic infections and tumours show impaired glucose uptake, reduced mitochondrial mass, and diminished metabolic activity (Bengsch *et al.*, 2016; Gabriel *et al.*, 2021). In cancer, the hypoxic, nutrient-poor tumor microenvironment further impairs the metabolic program of T cells (Scharping *et al.*, 2021). For example, reduced expression of peroxisome proliferator-activated receptor gamma coactivator 1-alpha (PGC1α) in exhausted T cells, a key regulator of cellular bioenergetics, contributes to T cells' metabolic decline in response to tumours (Austin and St-Pierre, 2012). Notably, restoring PGC1α expression has been shown to improve T_{EX} cell function, highlighting metabolism as a potential target for immunotherapy (Bengsch *et al.*, 2016; Scharping *et al.*, 2021).

Even through exhausted T cells are functionally inferior, they are still needed during chronic infection to maintain immune control. Studies in nonhuman primates with HIV showed increased virus loads and worsening of disease with depletion of $CD8^+$ T cells (Schmitz *et al.*, 1999; Jin *et al.*, 1999; Siddiqui *et al.*,

2019). Similarly, in murine tumour models of melanoma removing exhausted T cells led to decreased tumour control, highlighting their role in maintaining immune control despite their dysfunction (Vignali *et al.*, 2023).

1.3.2 Exhausted T cell are heterogenous

The differentiation process underpinning $CD8^+$ T cell exhaustion is distinct from the differentiation of naïve, effector, and memory T cells. Extensive studies have revealed a heterogeneous pool of exhausted T cells that includes precursor and terminally exhausted subsets (Figure 1.3), which differ in their ability to proliferate, in their effector functions and their response upon immunotherapy (Hudson *et al.*, 2019; Zander *et al.*, 2019; Beltra *et al.*, 2020; Utzschneider *et al.*, 2020; Tsui *et al.*, 2022). "Precursors of exhausted T cells" (T_{PEX}) exhibit self-renewal capability, long-term persistence, and the ability to differentiate into more exhausted T_{EX} cells (Utzschneider *et al.*, 2016; Im *et al.*, 2016; Leong *et al.*, 2016; Miller *et al.*, 2019). While all exhausted T cells express PD-1 and the transcription factor TOX, T_{PEX} cells additionally express genes typically associated with naïve and memory-cells, such as TCF1, ID3, and Ly108. In contrast, T_{EX} cells lack these molecules but express the inhibitory receptor Tim-3 (Utzschneider *et al.*, 2016; Im *et al.*, 2016; Wu *et al.*, 2016; Utzschneider *et al.*, 2020).

More recent studies have unravelled further complexity to T_{PEX} and T_{EX} populations. T_{PEX} can be categorised into "stem-like" $CD62L^+$ T_{PEX} that show the highest level of stemness, including self-renewal and developmental capacity, and $CD62L^-$ T_{PEX}, which show reduced stemness. $CD62L^+$ T_{PEX} cells are dependent on the transcription factor myeloblastosis proto-oncogene (Myb) for their development. In $CD8^+$ T cell responding to chronic infection (Tsui *et al.*, 2022) and cancer (Wijesinghe and Rausch, 2025, *in revision*) Myb balances the functional exhaustion to prevent immunopathology, while maintaining self-renewal. Importantly, $CD62L^+$ T_{PEX} are required for response to anti-PD-L1 therapy (Tsui *et al.*, 2022).

T_{EX} cells also consist of, at least, two different populations: effector-like $CX3CR1^+$ T_{EX} cells and terminally differentiated $CD101^+$ T_{EX} cells. $CX3CR1^+$ T_{EX} cells are

functionally superior compared to CD101$^+$ T_{EX} cells, produce higher levels of GzmB and show higher proliferative capacity (Zander *et al.*, 2019; Hudson *et al.*, 2019; Beltra *et al.*, 2020). The precise relationships between these different exhausted T cell populations remain unclear. Two general differentiation models have been proposed. One model suggests a bifurcation where naïve CD8$^+$ T cells give rise to T_{PEX} and T_{EX} cells, and T_{PEX} cells can develop into either CX3CR1$^+$ effector-like T_{EX} cells or CD101$^+$ T_{EX} cells (Zander *et al.*, 2019; Tsui *et al.*, 2022; Giles *et al.*, 2022; Daniel *et al.*, 2022; Kasmani *et al.*, 2023). Another model proposes linear progression from T_{PEX} to CX3CR1$^+$ T_{EX} cells and further into CD101$^+$ T_{EX} cells (Hudson *et al.*, 2019; Beltra *et al.*, 2020). However, which model describes the differentiation of exhausted T cells remains unclear and has to be further investigated.

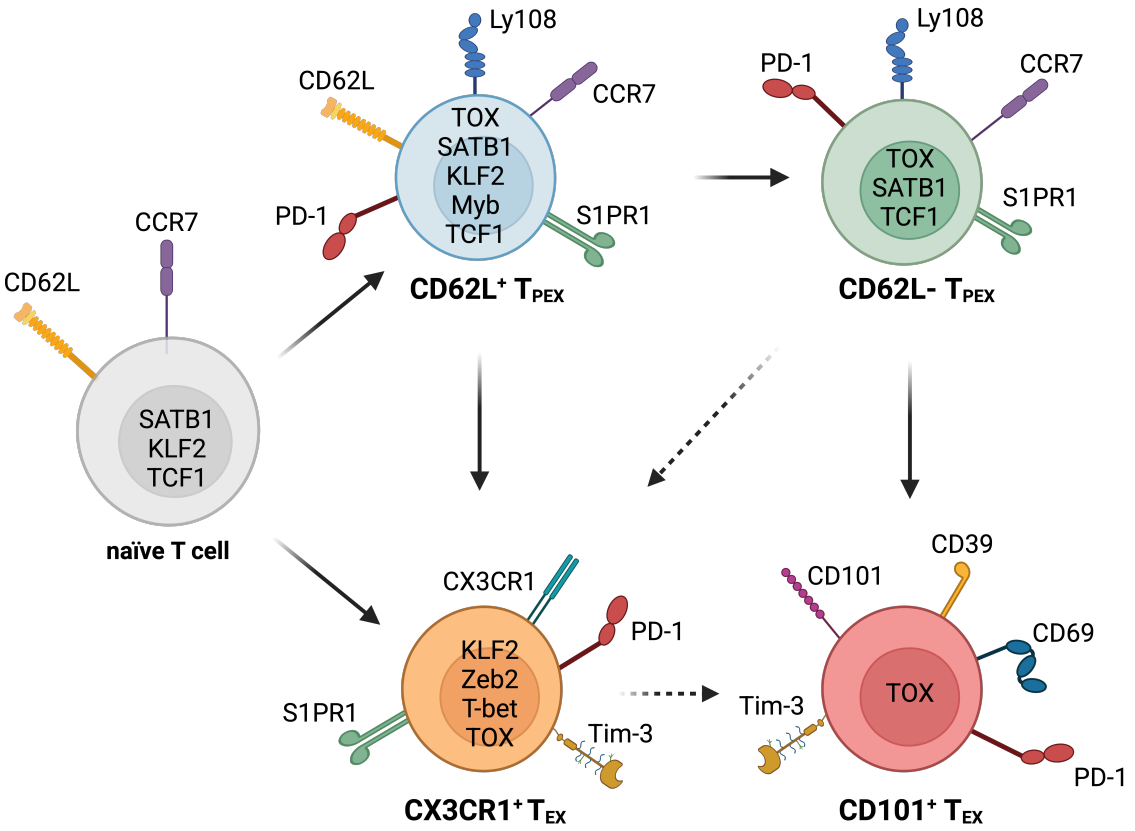

Figure 1.3: Proposed differentiation trajectories of heterogenous exhausted CD8$^+$ T cells.
After priming naïve CD8$^+$ T cells differentiate into T_{PEX} or T_{EX} cells. These populations can be further divided into CD62L$^+$ and CD62L$^-$ T_{PEX} and CX3CR1$^+$ and CD101$^+$ T_{EX} cells. T_{PEX} can differentiate into T_{EX} populations. Cell populations

are displayed with expression of specific population defining surface molecules and transcription factors. Arrows indicate possible differentiation trajectories.

1.3.3 Drivers of T cell exhaustion

Chronic antigen stimulation is the main driver of T cell exhaustion, but persistent TCR activation alone is not enough to fully induce the exhaustion fate (Baessler and Vignali, 2024). Multiple environmental factors contribute to T cell exhaustion. Cytokines are crucial, by influencing expression of inhibitory receptors and supressing effector functions (Baessler and Vignali, 2024). IL-10, an anti-inflammatory cytokine, has been associated with T cell exhaustion by diminishing the $CD8^+$ T cell response (Ejrnaes *et al.*, 2006; Brooks *et al.*, 2006). Blocking of the IL-10 signalling pathway in combination with anti-PD-L1 therapy enhances the T_{EX} functionality, leading to viral clearance (Brooks *et al.*, 2008). Likewise, IL-10 and simultaneously IL-21 production increase STAT3 signalling, leading to enhanced intratumoral terminally exhausted $CD8^+$ T cell differentiation their survival and their effector functions (Sun *et al.*, 2023). IL-35, an anti-inflammatory cytokine that is produced by $CD4^+$ regulatory T (Treg) cells in a tumor microenvironment, limits T cell infiltration and enhances the expression of inhibitory receptors, promoting T cell exhaustion and limiting anti-tumor immunity (Turnis *et al.*, 2016). The combination of IL-10 and IL-35 signalling has been shown to induce signal transducer and activator of transcription (STAT)3 and STAT1/4 signalling, activating Blimp1 and inducing IR expression (Sawant *et al.*, 2019). IL-2 is another cytokine, that has been studied as a diver of T cell exhaustion (Pol *et al.*, 2020). IL-2 is essential for the proliferative capacity and survival of $CD8^+$ T cells and memory formation (Abbas *et al.*, 2018). Studies have suggested that high levels of IL-2 enhance T cell exhaustion in tumor-reactive $CD8^+$ T cells by activating the aryl hydrocarbon receptor. IL-2 binding induces STAT5 signalling, altering the transcriptional and metabolic states of exhausted $CD8^+$ T cells, demonstrated by high expression of various IRs and reduced effector functionality (Y. Liu *et al.*, 2021). However, it has been highlighted that the effects of IL-2 are complex and context-dependent, emphasizing its role in

both sustaining immune responses and driving exhaustion under conditions of persistent antigen exposure (Kwon, 2021). IL-6 is a pleiotropic cytokine produced in response to tissue damage and inflammation. IL-6 bears pro- and anti-inflammatory effects and has been shown to directly promote tumor growth (Kumari *et al.*, 2016). IL-6 can also promote IR expression in T_{EX} cells responding to tumours (Matsuzaki *et al.*, 2010). In line with these studies, in clinical settings, high levels of IL-6 have been associated with enhanced Lag-3 expression - likely through STAT3 signalling - T cell dysfunction, and poor clinical outcomes following anti-PD-L1 treatment (Somasundaram *et al.*, 2022). IL-27, which is primarily an immunoregulatory cytokine (Vignali and Kuchroo, 2012), can also induce the expression of IRs, such as Tim-3, in $CD8^+$ T cells (Hirahara *et al.*, 2012). Further, T cells primed *in vitro* exhibited a transcriptional profile similar to that of T_{EX} cells, and IL-27 receptor deficient tumour-infiltrating $CD8^+$ T cells exhibited decreased expression of multiple IRs (Chihara *et al.*, 2018).

Another heavily investigated cytokine TGFβ. TGFβ is involved in variety of pathways, including cell growth, differentiation, homeostasis and angiogenesis (Li *et al.*, 2006; Ouyang *et al.*, 2010; David and Massagué, 2018). Additionally, recent studies have shown the role of TGFβ in promoting and contributing to the differentiation of exhausted T cells (Gabriel *et al.*, 2021; Ma and Zhang, 2022). In cancer and chronic infection, consistent TCR stimulation of $CD8^+$ T cells in the presence of TGFβ leads to the formation of exhausted T cells (Gabriel *et al.*, 2021; Saadey *et al.*, 2023). Proteomic analysis of urinary bladder cancer revealed high secretion of TGFβ-2 by cancer cells that contributed to the formation of exhausted T cells (Hartana *et al.*, 2018). Furthermore, blocking TGFβ signalling in cancer models, can reverse the exhaustion phenotype, and boost the proliferation and effector functions of anti-tumour $CD8^+$ T cells (Kwon *et al.*, 2020). In chronic lymphocytic choriomeningitis virus (LCMV) infections, TGFβ diminishes the differentiation of T_{PEX} cells into T_{EX} populations (Gabriel *et al.*, 2021; Hu *et al.*, 2022), in part by preserving the metabolic fitness of T_{PEX} cells (Gabriel *et al.*, 2021).

1.3.4 Targeting T cell exhaustion in immunotherapy

In T cells, the strength and quality of the immune response, initiated by antigen recognition through the TCR, are regulated by a balance between co-stimulatory and inhibitory signals, known as immune checkpoints (Pardoll, 2012). Under normal physiological conditions, these checkpoints are crucial for maintaining self-tolerance, preventing autoimmunity, and protecting tissues from damage during immune responses to infections (Sharma *et al.*, 2023). Immune checkpoint blockade (ICB) therapies target these inhibitory signals to enhance T cell activation and promote anti-tumor immune responses (Sharma *et al.*, 2023). Recent advancements in understanding T cell exhaustion have contributed to the success of ICB therapies in cancer treatment. A key strategy in ICB therapy involves blocking immune checkpoint receptors, which can restore some functionality of exhausted T cells and reduce tumor growth (Andrews *et al.*, 2019; Robert, 2020). IRs have become a target of ICB therapy alone and in combination with cytokines because of their unique ability to suppress T cell activity. The most prominent targets are PD-1, CTLA-4, and Lag-3, which have treatments approved by the FDA (Baessler and Vignali, 2024). In tumour models, CTLA-4 blocking enhances $CD8^+$ T-cell responses. Clinically, success has been achieved with the development of ipilimumab, the first Food and Drug Administration (FDA)-approved ICB therapy leading to improved progression free survival in patients (Leach *et al.*, 1996; Wei *et al.*, 2018). Blocking PD-1 signalling reinvigorates T cells in chronic infections and cancers, leading to the development of FDA-approved anti-PD-L1 therapies (Park *et al.*, 2023).

Clinically, ICB treatment has shown great success with long-term remission in the treatment of various cancer types, including melanoma, lung, and head and neck cancers. However, not all patients benefit from ICB therapy (Robert *et al.*, 2018; Robert, 2020). A Dutch study found, that among melanoma patients, only about 35.9 % of patients receiving ICB treatment show lasting benefits with an overall survival of 5 years (Van Not *et al.*, 2024). Across a multitude of cancers, only 12.5 % show successful responses to ICB (Haslam and Prasad, 2019; Haslam *et al.*, 2020). This differences in success can be traced back to the heterogeneity

of exhausted T cells. Different subsets respond differently to the treatment (Baessler and Vignali, 2024). Intense research has uncovered that T_{PEX} are the main population responding to ICB treatment. For instance, an increased proportion of $TCF1^+PD\text{-}1^+CD8^+$ progenitor exhausted $CD8^+$ T cells in biopsies from patients with advanced melanoma, who have been treated with anti-PDL1/anti-CTLA-4 combination therapies, has been correlated with extended progression-free survival and overall survival (Miller *et al.*, 2019). In studies of non-small cell lung cancer, an increase in precursor exhausted T cells was observed in tumours that responded to combination therapies involving anti-PD-1 and chemotherapy. In contrast, nonresponsive tumours did not exhibit an accumulation of precursor exhausted T cells (B. Liu *et al.*, 2021). The level of precursor in patients is therefore a clinical indicator if a patient responds or does not respond to ICB therapy (Kallies *et al.*, 2020).

Recent studies in chronic infection have shown that Myb-dpendent $CD62L^+$ T_{PEX} are the main population responding to ICB treatment (Tsui *et al.*, 2022). This highlights the importance of further understanding heterogeneity and molecular regulation of exhausted T cells to further improve efficacy of ICB-induced tumor control.

1.4 Transcriptional regulation of exhausted T cells

Signalling pathways, transcriptional regulation, and epigenetic programming that drive and maintain T cell exhaustion have been extensively studied. A better understanding of these mechanisms may lead to the development of better therapies. Several transcription factors, including thymocyte selection-associated high mobility group box protein (TOX), TCF1, interferon regulatory factor 4 (IRF4), T-bet, EOMES, Blimp1, nuclear receptor subfamily 4 group A (NR4A), and forkhead box protein O1 (FOXO1), have been discovered to play key roles in T cell exhaustion (McLane *et al.*, 2019; Kallies *et al.*, 2020). TOX is a transcription factor that was originally identified in the thymus, where it plays a key role in T cell development (Aliahmad *et al.*, 2012). It was first linked to exhaustion when gene network analysis showed that TOX was highly expressed in $CD8^+$ T cells in response to chronic but not acute LCMV infection (Doering *et al.*, 2012).

Following studies showed that TOX is a central regulator of exhaustion, revealing that it is rapidly induced and highly expressed in chronically stimulated $CD8^+$ T cells. Expression of TOX is required for high inhibitory receptor expression and reduced cytokine production (Yao *et al.*, 2019; Khan *et al.*, 2019; Alfei *et al.*, 2019). This pattern extends beyond chronic viral infections to tumor models and human melanoma, breast and lung cancers. Indeed, in cancer patients, TOX expression has also been associated with PD-1 upregulation and functional exhaustion (Seo *et al.*, 2019; Scott *et al.*, 2019). TOX-deficient mouse models have demonstrated that TOX is indispensable for T cell exhaustion. TOX knockout $CD8^+$ T cells exhibit lower expression of inhibitory receptors, enhanced cytokine production, and enhanced terminal effector differentiation. Although these cells showed an early proliferative advantage and increased cytotoxic function in response to chronic infection, they failed to persist (Seo *et al.*, 2019; Khan *et al.*, 2019; Scott *et al.*, 2019). TOX-deficient T cells also displayed improved tumor control and viral clearance but at the cost of increased immune-mediated pathology (Seo *et al.*, 2019; Alfei *et al.*, 2019). Importantly, this was specific to chronic antigen stimulation, as TOX was not required for responses to acute infections. This shows that TOX helps T cells adapt to continuous stimulation in chronic infection or cancer, preventing excessive activation and potential death. At the epigenetic level, TOX alters chromatin accessibility and DNA methylation, thereby reinforcing exhaustion. TOX specifically promotes PD-1 expression by increasing enhancer accessibility and interaction with chromatin-remodelling proteins (Khan *et al.*, 2019; Alfei *et al.*, 2019).

Other transcription factors and pathways regulate T cell exhaustion by balancing effector functions and exhaustion-specific gene expression (McLane *et al.*, 2019). Blimp1 (Shin *et al.*, 2009), basic leucine zipper transcription factor (BATF) (Quigley *et al.*, 2010; Man *et al.*, 2017) and IRF4 (Man *et al.*, 2017; Hirsch *et al.*, 2024), can either promote or counteract exhaustion, depending on their expression levels and cellular context.

T-bet and EOMES play important but complex roles (Paley *et al.*, 2012). T-bet repressed expression of inhibitory receptors, like PD-1 (Kao *et al.*, 2011), and is needed for the differentiation of CX3CR1$^+$ T_{EX} cells (Raju *et al.*, 2021). That study identified a T-bet–dependent CX3CR1$^+$Tim-3$^-$PD-1^{low} subpopulation, which was distinct from the Tim-3$^+$CX3CR1$^+$PD-1$^+$ proliferative effector subset (Raju *et al.*, 2021). T-bet downregulation marks the irreversible loss of effector potential. This is at least in part mediated by TOX, which suppresses T-bet activity, promoting terminal differentiation and cell cycle exit (Beltra *et al.*, 2020). The dynamic regulation of T-bet within T_{EX} cells highlights its importance in shaping exhaustion trajectories. and suggests that modulating this transcription factor could be a strategy to enhance T cell responses in chronic infections and cancer immunotherapy. EOMES is expressed in both T_{PEX} cells and terminally exhausted T cells (Li *et al.*, 2018), but its precise roles need to be further elucidated.

Tcf7 (which encodes TCF1) is a transcription factor that is essential for T cell development and differentiation. In CD8$^+$ T cells, TCF1 is crucial for generating memory precursor cells (Kim *et al.*, 2020) and for the development of the T_{PEX} population (Utzschneider *et al.*, 2016; Im *et al.*, 2016; Leong *et al.*, 2016). In CD8$^+$ T cells during chronic LCMV infections TCF1 promotes Bcl6 expression (Wu *et al.*, 2016) while repressing genes expressed in T_{EX} cells, such as *Prdm1* and *Havcr2* (encoding Tim-3) (Utzschneider *et al.*, 2016; Im *et al.*, 2016; Leong *et al.*, 2016). FOXO1, a key regulator of *Tcf7*, is required for T_{PEX} maintenance (Utzschneider *et al.*, 2018). It is inhibited by AKT signalling downstream of TCR activation, which suggests a direct link between TCR signalling and the limitation of *Tcf7* gene expression (Hedrick *et al.*, 2012; Baessler and Vignali, 2024). As T_{PEX} differentiate, they lose *Tcf7* expression due to epigenetic repression via DNA (Cytosine-5)-Methyltransferase 3 Alpha (DNMT3A)-mediated methylation (Ghoneim *et al.*, 2017).

In chronic infection and murine tumour models, special AT-rich sequence binding protein 1 (SATB1) and KLF2 have been shown to be highly expressed in T_{PEX}

cells (Miller *et al.*, 2019; Tsui *et al.*, 2022). Thus, both SATB1 and KLF2 could play central roles in T_{PEX} maintenance or differentiation. However, their role in T cell exhaustion has not been examined in detail.

1.4.1 The genome organizer SATB1

SATB1, described in the literature as a chromatin organiser and transcription factor, has been shown to be crucial in T cell development and the function of both $CD4^+$ and $CD8^+$ T cells (Alvarez *et al.*, 2000). On a structural basis, the SATB1 protein contains multiple compartments, the nuclear matrix-binding domain, a ubiquitin-like domain, multiple DNA-binding domains and the nuclear localisation signal (Dickinson *et al.*, 1997; Seo *et al.*, 2005; Yamasaki *et al.*, 2007; Z. Wang *et al.*, 2012; Wang *et al.*, 2014). The DNA-binding domain can be further separated into different subunits, the homeodomain, a CUT repeat-like domain, a CUT1 and a CUT2 domains. Together, these facilitate the binding of SATB1 to specific base-unpairing regions (BURs). These BURs are often discovered in AT-rich matrix attachment regions (MAR) (Dickinson *et al.*, 1997; Wang *et al.*, 2014). Additionally, the ubiquitin-like domain enables DNA binding through the tetramerization of SATB1 (Z. Wang *et al.*, 2012; Wang *et al.*, 2014). Mechanistic regulation of genes by SATB1 has been well studied and several mechanisms have been identified (Shannon, 2003). SATB1 organises the DNA in a three-dimensional fashion by attaching BURs to the nuclear matrix. This leads to the development of highly ordered chromatin loops which comprise chromatin network (Cai *et al.*, 2003). Thus, distant gene elements are brought together in close proximity, allowing them to bind and interact, which can lead to chromatin reorganisation (Gong *et al.*, 2011; Yang *et al.*, 2015). In addition, SATB1 functions as a transcriptional regulator of gene expression. This is primarily achieved at an epigenetic level. SATB1 recruits various chromatin remodelling enzymes, acting as a docking station for interaction partners, thereby regulating gene expression (Yasui *et al.*, 2002). The quality of these interactions is regulated through post-translational modifications of SATB1. Phosphorylated SATB1 results primarily in the transcriptional downregulation of genes, whereas acetylation of SATB1 leads to the upregulation of gene expression. Additionally, SATB1 has also been shown

to be sumoylated, specifically in relation to caspase-6-induced cleavage of SATB1 during Jurkat T cell apoptosis (Galande *et al.*, 2001; Tan *et al.*, 2008; Tan *et al.*, 2010). Not only SATB1 itself is regulated through various post-translational modifications, but also the epigenetic DNA modifications of SATB1 binding sites are regulated through these mechanisms. Depending on SATB1s post-translational modifications, it can bind to either histone acetyltransferases or deacetylases, leading to epigenetic changes in the target DNA (Pavan Kumar *et al.*, 2006; Purbey *et al.*, 2009).

SATB1's role across various disease models has been widely investigated. In addition to its involvement in brain development, it also plays a significant role in multiple cancers, such as colorectal and breast cancer, among others (Alvarez *et al.*, 2000; Naik and Galande, 2019). Studies using SATB1-deficient cell and mouse models have demonstrated its critical role in development. Mice lacking SATB1 entirely do not survive beyond three weeks following birth, succumbing to severe neurological abnormalities. (Alvarez *et al.*, 2000). Additionally, SATB1 is an important mediator of neuronal plasticity during postnatal brain development (Balamotis *et al.*, 2012). Interestingly, SATB1 has also been identified as a risk factor for Parkinson's disease, with a strong correlation of the disease and the expression levels in dopaminergic neurones that prevent cellular aging and inflammatory responses in the brain (International Parkinson's Disease Genomics Consortium *et al.*, 2017; Riessland *et al.*, 2019). Further, SATB1 is also important in the growth of the epidermis and early phase erythropoiesis (Wen *et al.*, 2005; Fessing *et al.*, 2011). During embryogenesis, SATB1 is a crucial contributor to X-chromosome inactivation and facilitating base excision repair processes. (Agrelo *et al.*, 2009; Kaur *et al.*, 2016).

SATB1 has been shown to have dual effects in cancer. High SATB1 expression positively correlates with tumor progression in several cancer types, including liver, lung, and breast cancers, and is therefore associated to poor prognosis. Mechanistically, cancer cells use SATB1 to transcriptionally activate tumour oncogenes and deactivate tumour suppressor genes, leading to aggressive and fast-growing tumour cells. Conversely, in pancreatic adenocarcinoma and cutaneous skin melanoma, low SATB1 levels are associated with reduced

prognosis, indicating the importance of tight regulation of SATB1 expression (Naik and Galande, 2019).

The most important role of SATB1 in lymphocytes has been described thus far in T cell development, with SATB1 regulating about 2% of the verified genes required for T cell development (Alvarez *et al.*, 2000). Not only is SATB1 required for lymphopoiesis, but also for lymphoid lineage decisions of hematopoietic stem cells (HSC). This was exhibited in SATB1-null mice, that displayed smaller thymi due to low cell numbers (Alvarez *et al.*, 2000). HSC can be divided into two populations, SATB1 expressing and non-expressing HSC. While $SATB1^-$ HSC mainly give rise to the progenitors of myeloid cells, $SATB1^+$ HSC develop into lymphocytes (Doi *et al.*, 2018). During thymic maturation, SATB1 is highly expressed in the double positive (DP) T cells and the $CD4^+$ single positive (SP) stages. Experiments using SATB1-deficient mouse models showed a complete stop of thymic T cell development at the DP stage, with cell being incapable to further differentiate into single positive $CD4^+$ and $CD8^+$ T cells (Alvarez *et al.*, 2000; Satoh *et al.*, 2013; Kondo *et al.*, 2016). One of the most important functions of SATB1 in the DP stage is the TCRα rearrangement, through enabling expression of *Rag1* and *Rag2* (Hao *et al.*, 2015). During the SP stage, SATB1 plays a crucial role in guiding lineage decisions by regulating key genes such as *Runx*, *CD4*, *CD8*, and *Thpok*, which determine CD4/CD8 lineage commitment (Kakugawa *et al.*, 2017). For instance, *Runx* coordinates differentiation of DP cells into SP $CD4^+$ T_H cells (Taniuchi, 2009) and SATB1 heterozygous knock out mice, displayed reduced ability to differentiate into SP $CD8^+$ T cells (Nie *et al.*, 2005) due to prevention of long-distance interaction of the distal *Runx* enhancer with its promoter (Seo *et al.*, 2020). Interestingly Treg precursor cells also express high levels of SATB1 for the upregulation of Treg-specific super-enhancers (Kondo *et al.*, 2016; Gottimukkala *et al.*, 2016; Kitagawa *et al.*, 2017). Consequently, thymocytes deficient for SATB1 fail to develop from $CD4^+$ SPs into precursor Treg cells and later mature Treg cells resulting in autoimmune disorders (Kondo *et al.*, 2016; Kitagawa *et al.*, 2017; Tanaka *et al.*, 2017).

The role of SATB1 in peripheral $CD4^+$ T cells has been studied extensively, whereas its role in $CD8^+$ T cells needs further characterization. Indeed, multiple studies have shown a critical role of SATB1 in homeostasis and activation of T cells (Kondo *et al.*, 2016; Yasuda *et al.*, 2019; Nüssing *et al.*, 2019). SATB1 expression is up-regulated after TCR stimulation, downstream of the transcription factor nuclear factor of activated T-cells (NFAT) (Beyer *et al.*, 2011; Gottimukkala *et al.*, 2016; Stephen *et al.*, 2017; Akiba *et al.*, 2018) (Gabriel *et al.*, 2016). In accordance with that notion, *Nfat* mediated regulation of IL-2 signalling has been connected to SATB1, silencing the *Il-2* gene as well as suppressing gene expression of IL-2 receptor (Kumar *et al.*, 2005; Pavan Kumar *et al.*, 2006; Liao *et al.*, 2013). Additionally, SATB1 is essential for the differentiation of various T_H subsets. SATB1 is upregulated by IL-4 signalling and promotes T_{H2} differentiation (R. Lund *et al.*, 2003; Lund *et al.*, 2005). Consistent with this finding, STAT6 and Gata3 signalling upregulate SATB1 (Ahlfors *et al.*, 2010; Jargosch *et al.*, 2016; Gottimukkala *et al.*, 2016). Moreover, SATB1 contributes to the regulation of cytokine production, including IL-4, IL-14 and IL-5, in T_H2 cells (Cai *et al.*, 2006; Notani *et al.*, 2010; Ahlfors *et al.*, 2010). Tight expression control of SATB1 is needed for peripheral Treg. Downregulation of SATB1 is necessary for Treg formation, differentiation and maintenance as shown in over-expression experiments where overexpression of SATB1 led to the loss of suppressive functions, establishment of transcriptional T effector cell programs and induction of T effector cell cytokines (Beyer *et al.*, 2011; Kitagawa *et al.*, 2017; Wang *et al.*, 2017). Upregulation of forkhead box P3 (FoxP3), the Treg master transcription factor, and Foxp3-related micro-RNAs (miRNAs) coordinate downregulation of SATB1 and thereby promote Treg differentiation (Beyer *et al.*, 2011). Further, IL-2/STAT5 signalling increases miRNA155, which in turn contribute to downregulation of SATB1 in T cell lymphomas (Fredholm *et al.*, 2018). Similarly, TGFβ has also been shown to downregulate SATB1 (Stephen *et al.*, 2017).

In $CD8^+$ T cells, SATB1 has been primarily studied in naïve cells where it is essential to maintain the naïve transcriptional state by repressing effector genes like *Ifng*, *Zeb2*, and *Prdm1* and promoting the expression of genes, associated

with naïve T cells, such as *Bcl6*, *Bcl11b*, *Foxo1*, *Lef1* and *Tcf7*. Furthermore, SATB1 recruits the nucleosome remodelling and deacetylase (NURD) complex to the *Pdcd1* locus, resulting in restriction of PD-1 expression (Stephen *et al.*, 2017; Nüssing *et al.*, 2019).

1.4.2 The transcription factor Krüppel-factor 2 (KLF2)

KLF2 is part of the Krüppel-like factor family, a group of 17 transcription factors (McConnell and Yang, 2010). KLF transcription factors contain three zinc finger domains at the carboxyl terminus. These domains are able to bind to GC-rich DNA sequences (Mizuguchi *et al.*, 2021), regulating gene expression (Preiss *et al.*, 1985). KLF2, first found in 1995, is highly expressed in the lung (Anderson *et al.*, 1995) but has also been found in various immune cells and endothelial cells. KLF2 regulates gene expression in lymphocytes $CD8^+$ and $CD4^+$ T cells and B cells, along with NK cells, monocytes, macrophages and neutrophils. It has been demonstrated to play a role in various regulatory pathways, including immune cell quiescence, activation, proliferation, adhesion and migration (Hart *et al.*, 2012). Expression levels in different cell types can differ based on their differentiation and activation status (Hart *et al.*, 2012). Importantly, germline deletion of KLF2 leads to embryonic death due to systemic haemorrhaging, caused by defective blood vessels (Kuo *et al.*, 1997).

KLF2 is expressed in naïve $CD8^+$ T cells and involved in the regulation of T cell quiescence and survival. $KLF2^{-/-}$ T cells exhibit spontaneous T cell activation, and increased expression of activation markers, including CD69 and CD44 and increased FAS-mediated cell apoptosis (Kuo *et al.*, 1997; Wittner and Schuh, 2021). In contrast, over-expression of KLF2 leads to reduced proliferation, and diminished protein synthesis, accompanied by decreased cell size. KLF2 overexpression also decreased expression of CD71 and other activation markers while increasing markers of quiescence. KLF2 is rapidly downregulated upon TCR engagement (Hart *et al.*, 2012). Interestingly, KLF2 expression correlates with reduced cellular myelocytomatosis proto-oncogene (c-Myc) expression (Buckley *et al.*, 2001). Thus, c-Myc is likely a key downstream target of KLF2, as

the phenotypic effects KLF2 expression can largely be replicated by a forced expression of c-Myc and reversed by wild-type c-Myc expression in Jurkat cells (Berns *et al.*, 1997; Buckley *et al.*, 2001). c-Myc is important for clonal expansion by promoting T cell growth and proliferation through the suppression of cell-cycle inhibitors and growth arrest genes while minimizing DNA damage (Gnanaprakasam and Wang, 2017). This suggests a pathway whereby KLF2 suppresses T cell proliferation by repressing c-Myc, thereby maintaining quiescence. Further, doxycycline treatment of Jurkat cells led to increased KLF2 expression and reduced proliferation and DNA synthesis (Wu and Lingrel, 2004).

One of KLF2 unique functions is the control of T cell migration. Mature naïve $CD4^+$ and $CD8^+$ T cells leave the thymus after selection, migrating to secondary lymphoid organs (Matloubian *et al.*, 2004; Allende *et al.*, 2004). This thymic egress is regulated by the bioactive metabolite Sphingosine-1-phosphate (S1P), that is highly secreted in the thymus and abundant in the blood. T cells express S1PR receptors 1-5 that sense S1P, leading to exit of the thymus via a concentration gradient (O'Sullivan and Dev, 2013). KLF2 directly regulates this process by promoting S1PR1 gene expression (Carlson *et al.*, 2006). Indeed, in KLF2 deficient mice, $CD4^+$ and $CD8^+$ T cells fail to egress from the thymus due to lack of S1PR1 expression (Carlson *et al.*, 2006). KLF2 also regulates $CD8^+$ T cell migration to secondary lymphoid organs through the expression of lymphoid homing markers CCR7 and CD62L (Kuo *et al.*, 1997; Takada *et al.*, 2011; Preston *et al.*, 2013). In mature $CD4^+$ T cells, dysregulation of KLF2 expression has been linked with abnormal cell migration and preferential accumulation in non-lymphoid tissue instead of homing towards the SLOs. This was largely due to dysregulated expression of chemokine receptors, including CCR5, CXCR3 and CXCR5 (Sebzda *et al.*, 2008). Notably, KLF2 negatively regulates the expression of CXCR3 in $CD8^+$ T cells and therefore pro-inflammatory responses to chemokine CXCL10 (Preston *et al.*, 2013). However, this phenotype, in particular dysregulation of CXCR3 has to be fully confirmed, as other studies (Weinreich *et al.*, 2009) reported non-T-cell intrinsic cell effects in KLF2-deficient T cells. Indeed, wild-type T cells in mixed bone marrow chimeric mice containing KLF2

deficient T cells also exhibited upregulation of CXCR3, and effect of increased IL-4 produced by KLF2 deficient T cells (Weinreich *et al.*, 2009). Since CXCR3 is critical in the migration and homing to inflamed tissues, this shows the importance of downregulation of KLF2 to ensure migration to non-lymphoid tissues. Further CXCR3 has been associated with T cell fate decisions particularly in T_H1 cells (Groom and Luster, 2011), reinforcing the involvement of KLF2 in shaping T cell fate.

Peripheral $CD4^+$ and $CD8^+$ T cells express high levels of KLF2, that is rapidly downregulated upon TCR engagement (Kuo *et al.*, 1997). This downregulation results in reduced expression of CCR7, CD62L, S1PR1, CCR2, tgα4, F2rt1, Itgβ2, CD44, Itgβ7, and Itgα1, and the upregulation of CXCR3, Fut4 and CCR4, enabling the migration into inflamed tissues. $CD4^+$ T cells that express high levels of KLF2 differentiate into classical $CD4^+$ T_{FH} cells, whereas low KLF2 expression skews cells towards Treg differentiation (Pabbisetty *et al.*, 2014). In T_{FH} cells, KLF2 controls migratory functions akin to its role on naïve T cells. For instance, ICOS/ICOSL interactions downregulate KLF2 and in return promote the expression of CCR7 and downregulation of Blimp1, which, in turn, leads to upregulation of CXCR5 and the positioning of T_{FH} cells in the B cell zone (Weber *et al.*, 2015). *Prdm1* has been shown to be a target gene, which is directly repressed by KLF2 (Weinreich *et al.*, 2009). While KLF2 is thought to be largely absent in effector T cells, it is re-expressed in circulating memory T cells where it regulates homing (Weber *et al.*, 2015). T_{RM} cells on the other hand downregulate KLF2 as they differentiate, as discussed previously (Chapter 1.2.2). Thus, KLF2 can act as a master regulator of T cell migration, influencing both developmental egress and peripheral trafficking while integrating signals that shape T cell fate and immune responses. Recently, it was found in murine tumour models that KLF2 promoted the differentiation of effector $CD8^+$ T cells and inhibited terminal exhaustion in chimeric antigen receptor (CAR) T cells (Z. Zhu *et al.*, 2024). Indeed, gene network analysis revealed KLF2 as a key transcription factor that regulated the differentiation of stem-like $CD8^+$ CAR T cells into either effector or exhausted $CD8^+$ CAR T cells (Z. Zhu *et al.*, 2024). These results are in stark

contrast to previous work which had suggested that KLF2 is not expressed in effector cells (Weber *et al.*, 2015).

1.5 Aim of the study

$CD8^+$ T cells in response to chronic infection form a precursor-progeny relationship that allows for differentiation of effector cells, while maintaining self-renewal of the antigen-specific T cell compartment, thus enabling a prolonged immune response. However, the molecular pathways governing precursor cell development and maintenance or their differentiation towards effector fate remain incompletely understood. Fine-tuning our understanding of such pathways will contribute to the development of improved immunotherapies.

In this study, we explored the role molecular regulators that may shape the quality of precursor cells and effector differentiation.

Firstly, we aimed to evaluate the contribution of SATB1 to exhausted T cell differentiation and function. To this end we used both knock out and overexpression models to clearly delineate SATB1's role in response to both acute, chronic virus infections. We further dissected SATB1's function using epigenetic and transcriptomic profiling and investigated possible molecular pathways by which SATB1 operates.

Secondly, we aimed to evaluate the contribution of KLF2 to exhausted T cell differentiation and function in response to chronic infection. Furthermore, we explored the impact of T cell homing in shaping the exhausted T cell response. Specifically, using the CRISPR-Cas9 system, we evaluated how deletion of KLF2, and downstream homing molecules CCR7, CD62L and S1PR1 affects T cell location and positioning and its subsequent impact on T cell differentiation and function.

Aims of this study:

(1) Characterizing the role of SATB1 on T cell differentiation in acute and chronic infection

(2) Characterizing the impact of $CD8^+$ T cell localization in lymphoid organs on T_{PEX} and T_{EX} differentiation in chronic viral infection

(3) Characterizing the role of KLF2 on exhausted T cell differentiation in chronic viral infection

Chapter 2 - Materials and methods

2.1 Materials

2.1.1 Consumables

Table 1: Consumables used

Product	Manufacturer
0.5 mL Tube with Frosted Flat Cap	Scientific Specialties Inc., Lodi, CA, AU
1 mL Luer-Lok syringe	Becton Dickinson GmbH
25 mL Divided Reagent Reservoir	INTEGRA Biosciences GmbH, Bbiebertal, DE
Axygen® 0.2 mL Polypropylene PCR Tube Strips	Corning Inc., Corning, NY, US
Axygen® 1.7 mL MaxyClear Snaplock Microcentrifuge	Corning Inc.
Axygen® PCR Strip Caps	Corning Inc.
Cell Strainer, 40/70/100 µm	Sarstedt AG & Co. KG
Cell Strainer, 40/70 µm	Miltenyi Biotec
Corning® Costar® TC-Treated Multiple Well Plates, 96-well	Corning Inc.
Cutfix stainless scalpel #10	B. Braun Melsungen AG, Melsungen, DE
DNA low bind tube	Eppendorf
FACS tube 5 mL	Sarstedt AG & Co. KG
Falcon™ Round-Bottom Polystyrene Test Tubes with Cell Strainer Snap Cap, 5mL	Corning Inc.
Filter Tips, Barrier Tip, Low Retention (10/200/1,000 µL)	Neptune Scientific, San Diego, CA, US
Greiner CELLSTAR® centrifuge tubes, 50 mL	Greiner Bio-One GmbH, Kremsmuenster, AT
Greiner CELLSTAR® dish (H 100 mm × 20 mm, vented)	Sigma-Aldrich
Glass pippets	Volac
High Sensitivity D5000 ScreenTape	Agilent Technologies
Injekt® Solo Syringe 5/10 mL	B. Braun Melsungen AG
Insulin Syringe With Needle - 1mL	Terumo Australia Pty Ltd., Macquarie Park , NSW, AU
LS columns	Miltenyi, Bergisch Gladbach, Germany
Micro Centrifuge Tube, 2 mL	Wuxi NEST Biotechnology Co. Ltd, Wuxi, JS, CN
Micro tube 0.5/1.5/2 mL SafeSeal	Sarstedt AG & Co. KG
Micro tube 1.5 mL SafeSeal	Sarstedt AG & Co. KG
MICROFLEX® 93-833 nitrile gloves	Ansell Europe, Brussels, BE
Microplate, 96 well, PS, V-bottom, clear	Greiner-Bio-One GmbH
Microvette® 500 K3 EDTA	Sarstedt AG & Co. KG
Multiply®-µStrip Pro 8-strip	Sarstedt AG & Co. KG
Nisense Powder Free Nitrile Gloves	Mediflex Industries, Kingsgrove, NSW, AU

Nunc™ 15 mL Conical Sterile Polypropylene Centrifuge Tubes	Thermo Fisher Scientific, Waltham, MA, US
Pipette Tip Refill, Eclipse (200/1,000 µL)	Edwards Group, Narellan, NSW, AU
QPCR plates (384 wells)	Thermo Scientific
Scalpel blades #23	Swann-Morton, Sheffield, UK
Serological pipette 5/10/25/50 mL	Sarstedt AG & Co. KG
Thin Wall Glass Capillaries, 4 in, OD 1.0 mm, No Filament	World Precision Instruments, Sarasota, FL, US
TipOne® RPT Filter Tips 10/200/1,000 µL	Starlab Innternational GmbH, Hamburg, DE
Tube 15/50 mL	Sarstedt AG & Co. KG
Tube 5 mL	Eppendorf AG

2.1.2 Chemical reagents and kits

Table 2: List of reagents, chemicals and kits

Reagent/Kit	**Provider**
2-Mercaptoethanol (55 mM)	Thermo Fisher Scientific
50 bp DNA Ladder	Thermo Fisher Scientific
AccuCount fluorescent flow cytometry particles, 10^6/ml, 7.0-7.9um	ProSciTech Pty Ltd
Agarose	Carl Roth GmbH + Co. KG
Alt-R® S.p. Cas9 Nuclease V3, 500 µg	Integrated DNA Technology
Anti-CD28	WEHI Mab Lab
Anti-CD3	WEHI Mab Lab
Antibiotin microbeads	Miltenyi Biotec
Bovine Serum Albumin (BSA)	Sigma-Aldrich
Brefeldin A	Sigma-Aldrich
CD4 (L3T4) MicroBeads, mouse	Miltenyi Biotec
CD8 microbeads, mouse	Miltenyi Biotec
CELLTRACE VIOLET 1 KIT (CellTrace Violet Cell Proliferation Kit, for flow cytometry)	Invitrogen
Chromium Single Cell 5’ Library	10X Genomics
Collagenase type III	Scimar (Worthington)
Compensation beads	Thermo Fisher Scientific
Cytofix/Cytoperm Solution Kit	Becton Dickinson Pty Ltd
digitonin	Promega
Dimethyl sulphoxide (DMSO)	Sigma Aldrich
Dispase	Thermo Scientific
DNA Clean & Concentrator-5 Kit	Zymo Research
DnaseI, 100mg	Sigma-Aldrich
DreamTaq DNA	Thermo Fisher Scientific
DreamTaq DNA Polymerase (5 U/µL)	Thermo Fisher Scientific
DreamTaq Green Buffer	Thermo Fisher Scientific
Dulbecco's Modified Eagle Medium (DMEM)	Gibco™ or in house at Media Preparation Unit (MPU)
Dulbecco’s phosphate-buffered saline	Sigma-Aldrich

Dynabeads mouse T activation CD3/CD28 2mL	Thermo Fisher Scientific
Ebioscience Fixation Diluent	Thermo Fisher Scientific
Ebioscience Fixation/Permeabilization Concentrate	Thermo Fisher Scientific
eBioscience Foxp3 fixation kit	Thermo Fisher Scientificaust Pty Ltd
eBioscience™ Foxp3 / Transcription Factor Staining Buffer Set	Thermo Fisher Scientific
EDTA, (Ethylenediaminetetraacetic acid disodium salt dihydrate or solution; 0.5 M, pH 8.0, RNase-free)	Thermo Fisher Scientific
Ethanol	ChemSupply Australia,
FBS QUALIFIED AUSTRALIA ORIGIN 500ML (Fetal Bovine Serum, qualified, Australia)	Thermo Fisher Scientific
Fixable Viability dye, eF506, 5 x 100T	Thermo Fisher Scientific
Fixable Viability dye, eF780, 5 x 100T	Thermo Fisher Scientific
Fluvastatin sodium salt	Thermo Fisher Scientific
Formaldehyde 16% vials	Thermo Fisher Scientific
Gel Bead Kit v2	10X Genomics
Glutamax, 100X 100mL	Thermo Fisher Scientific
Green Taq + Nuclease Free Water (GoTaq® Master Mixes)	Promega
Gsk-Inhibitor	n.a.
H-2Db gp33-41 (KAVYNFATC) Peptide for *ex vivo* stimulation	Xaia Custom Peptides, Göteborg, Sweden
H-2Db gp33-41 (KAVYNFATC) Tetramer staining	National Institutes of Health Tetramer Facility
Hanks' Balanced Salt solution (HBSS), without or with Ca_2^+/Mg_2^+	in house at MPU
HEPES (2-[4-(2-hydroxyethyl)piperazin-1-yl]ethanesulfonic acid, 1 M)	Thermo Fisher Scientific
High Sensitivity D5000	Agilent Technologies
Ladder	Agilent Technologies
Hyperladder 100bp	Bioline aust Pty Ltd
Ionomycin from Streptomyces conglobatus	Sigma-Aldrich
IL15	Peprotech
IL2	Lonza Australia Pty Ltd
IL2 (rhIL2)	Peprotech
iScriptt^M Reverse Transcription Supermix, 100 x 20 ul rxns, 400 ul	Bio-Rad Laboratories Pty Ltd
Live/Dead Fixable Blue Dead Cell Stain Kit, for UV excitation	Thermo Fisher Scientific
Methyl cellulose 2 %	Sigma-Aldrich
Magnesium-Chloride ($MgCl_2$)	Sigma-Aldrich
Naïve $CD8^+$ T cell isolation kit, mouse	Miltenyi Biotec
NEBNext Libary Quant Master Mix Kit	New England Biolabs

NEBNext Ultra II Q5 2x Master Mix	New England Biolabs
Neomycin trisulfate salt hydrate	Sigma-Aldrich
NP40	Millipore-Sigma
P3 Primary Cell 4D X Kit S (32 RCT)	Lonza Australia Pty Ltd
Pen-strep	Thermo Fisher Scientificaust Pty Ltd
Percoll	Bio-Strategy Pty Ltd
Perm/Wash Buffer 100ml	Becton Dickinson Pty Ltd
POWRUP SYBR MASTER MIX,1 ML 1 ML (PowerUp SYBR Green Master Mix)	Thermo Fisher Scientific
Proteinase K Solution 5ml	Millenium Science Pty Ltd
Read cell removal buffer	in house at MPU
Rneasy Plus micro kit (50)	Qiagen Pty Ltd
RNeasy Plus Mini Kit (50)	Qiagen Pty Ltd
RPMI	Iin house at MPU
SMART-Seq mRNA LP (with UMIs) (24 Rxns)	Scientifix
Sodium chloride (NaCl)	Sigma-Aldrich
Sodium pyruvate 100mL	Thermo Fisher Scientific
Sybr Safe	Thermo Fisher Scientific
SYTOX™ Blue Dead Cell Stain, for flow cytometry	Thermo Fisher Scientific
Tagment DNA buffer	Illumina
TGFb1 (recombinant human)	Thermo Fisher Scientific
Tn5 Tagment DNA TDE1 Enzyme	Illumina
Total-Seq™- anti-mouse Hashtags	Biolegend
Tris–HCl	Sigma-Aldrich
TruSeq® RNA Sample Preparation v2 kit	Illumina
Trypan Blue, 100mL	Sigma
Trypsin Versane	in house at MPU
Tween-20	Millipore-Sigma
Unique Dual Index Kit (1–24) (24 Rxns)	Scientifix
UltraPure™ DNase/RNase-Free Distilled Water	Invitrogen™
Virkon tablets	Merck Pty Ltd

2.1.3 Buffer and media compositions

In the following table, buffers that were used are listed, with their compositions.

Table 3: List of buffers used and their compositions

Buffer	**Ingredients**
50x TAE buffer	40 mM Tris base,1 mM EDTA pH 8.0, 20 mM glacial acetic acid in deionized water
ACK lysis buffer	Deionized water, 8.26 % ammonium chloride, 1 % potassium bicarbonate, 0.037 % EDTA; pH=7.2

ATAC buffer	10 mM Tris–HCl (pH 7.5), 10 mM NaCl and 3 mM $MgCl_2$ in UltraPure DNase/RNase-free distilled water
ATAC-Lysis buffer	ATAC buffer comprising of NP40 (0.1 %), Tween-20 (0.1 %) and digitonin (0.01 %)
Digestion buffer - ear samples	50 mM Tris pH 8.0, 50 mL KCl, 2.5 mM EDTA pH 8.0 0.45 % NP40 or Igepal 0.45 % Tween20 in deionized water
Digestion buffer - organs	RPMI, 10 % FCS, 1 µg/mL DNAse, 200 µg/mL Dispase and 1 mg/mL Collagenase III
FACS/MACS buffer	0.2 % (w/v) BSA, 2 mM EDTA, in PBS
PCR master mix	1x GoTaq Green Master Mix 0.2 µM Primer Mix in dH_2O
T cell medium	10 % FCS, 2 mM Glutamax, 1 % penstrep, 1 % Sodium pyruvat, 1 % MEM non-essential amino acids, 25 mM HEPES in RPMI
Vero cell medium	10 % FCS and 5 mL P/S in 500 mL DMEM
BHK cell medium	10% FCS, 1 % penstrep in RPMI
L929 cell medium	200 mM glutamine (2%), 10% FCS, 1 % penstrep in DMEM
DMEM methylcellulose	265 mL 2x DMEM (10 % FCS, 2 % penstrep, 1.1 g Bi-carbonat in 235 mL deionized water) and 265 mL methylcellulose
OPD substrate	12.5 ml of solution C, 12.5 ml of solution D, 25 mL milli Q water, 1 tablet of OPD, 50 µL of H_2O_2
Solution A	0.2 M of Na_3PO_4 pH 7.4, 77.4 mL of 1 M Na_2HPO_4, 22.6 mL 1 M NaH_2PO_4 pH 7.4, H_2O to 500 mL
Solution B	40 g PFA in deionized water (8 %), 5 M NaOH, pH 7.4

2.1.4 Equipment

Table 4: List of equipment used

Equipment	**Manufacturer**
10-/15-/20-/30-Well Comb, Fixed Height, 1.5 mm Thickness	Bio-Rad Laboratories, Hercules, CA, US
4 Block Digital Dry Block Heater	Ratek Instruments Pty. Ltd., Boronia, VIC, AU
4200 TapeStation System	Agilent Technologies
Analysis Scale MS104S and EL2001	Mettler-Toledo Ltd., Port Melbourne, VIC, AU
Biological Safety Cabinet, TOPSAFE 1.8 ABC	Euroclone S.p.A., Pero, MI, IT
Centrifuges: 5424 R, 5810 R	Eppendorf AG
Centrifuges: Allegra® X-12R, Microfuge® 20R	Beckman Coulter, Brea, CA, US
Cytek® Aurora, 5L, 5 laser	Cytek Biosciences
CytoFLEX SRT Benchtop Cell Sorter	Beckman Coulter life science
DynaMag-2 Magnet	Thermo Fisher Scientific
Electrophoresis Power Supplies EPS 301	Global Life Sciences Solutions USA LLC, Marlborough, MA, US

LSRFortessa™ II Flow Cytometer / FACSAria™ III Cell Sorter	BD Biosciences
Force Mini Microcentrifuge (Labnet)	Fisher Biotec Australia, Wembley, WA, AU
G:BOX Imager	Syngene by SDI Group plc, Cambridge, UK
Gel casting system compact	Analytik Jena AG
Heraeus Megafuge 40R	Thermo Fisher Scientific
Inverted Laboratory Microscope Leica DM IL LED	Leica Microsystems GmbH, Wetzlar, DE
MCO-230AICUV-PE CO2 Incubator	Panasonic, Osaka, JP
Mline® Mechanical Pipettes (1/20/200/1,000 µL)	Sartorius AG, Goettingen, DE
Neubauer improved, bright-line BOECO blood counting chamber	Boeckel + Co (GmbH + Co), Hamburg, DE
NextSeq 500	Illumina, San Diego, CA, US
4D-Nucleofactor™ Core Unit	Lonza
Orbital Shaking Incubator SI500	Cole-Parmer (Stuart Equipment), Staffordshire, OSA, UK
Personal Vortex Mixer	Ratek Instruments Pty. Ltd., Boronia, VIC, AU
PowerPac™ Basic/HC High-Current Power Supply	Bio-Rad Laboratories
Quintix® Milligram Balance (QUINTIX613-1S)	Sartorius AG, Goettingen, DE
Research® plus pipette 100/300 µL 12-channel	Eppendorf AG
Research® plus pipettes 2.5/10/200/1,000 µL	Eppendorf AG
Scissors ES18/100/101	Everhards GmbH, Meckenheim, DE
SIL 06 - Infrared lamp, with continuous function	Hans Dinslage GmbH, Uttenweiler, DE
T100 Thermal Cycler	Bio-Rad Laboratories
ThermoMixer® C, F1.5	Eppendorf AG
ZEISS Axioscan 7 Microscope Slide Scanner	Carl Zeiss AG, Oberkochen, DE

2.1.5 Mice

All mice were housed under specific pathogen free (SPF) conditions in compliance with federal and regional regulations at the animal facilities of the Biological Resources Facility (BRF) at The Peter Doherty Institute for Infection and Immunity (PDI) in Melbourne, Australia or the House of Experimental Therapy (HET) at the University of Bonn, Germany. All experimental procedures involving animals were approved by the Local Animal Care Commission of

Nordrhein-Westfalen (NRW) in Bonn, Germany and the Animal Ethics Committee of the University of Melbourne, Australia. Mice were housed at both animal facilities on a 12-hour light-dark cycle at a temperature of 19-24 °C. All mice lines were maintained on a C57BL/6J background. At start of the experiment, mice were aged 6-20 weeks old. Both females and males were used in an age and sex matched manner.

Table 5: Mouse lines

Mouse line	Details
C57BL/6J (CD45.2 or CD45.1)	Wild type C57BL/6J mice on a congenic CD45.2 or CD45.1 background are non-transgenic mice that were used for all wildtype experiments. For experiments conducted in Bonn, mice were purchased from either Janvier (Le Genest-Saint Isle, France) or Charles River (France). For experiments conducted in Melbourne, mice were purchased from the inhouse Biological Resources Facility (PDI), Animal Resources Centre/Ozgene (ARC) or from The Australian BioResources (ABR).
Rag1$^{-/-}$	Rag-1 KO mice (B6.129S7-*Rag1*^{tm1Mom}/J) (Mombaerts *et al.*, 1992) were sourced from the WHEI in Melbourne. Mice have a 1356 base pair deletion in the recombinase activation gene 1, resulting in an immune deficiency in which mice produce no B or T cells.
P14 CD45.1	P14 CD45.1 mice were generated by crossing P14 mice (B6;D2-Tg(TcrLCMV)327Sdz/JDvsJ) (Pircher *et al.*, 1989) (Jackson Laboratories, USA) and CD45.1 mice (B6.SJL-*Ptprc*^{a} *Pepc*^{b}/BoyJ) (Jackson Laboratories, USA). Mice were used for experiments conducted in Germany. CD8^{+} T cells of these mice develop with the transgenic TCR, specific against the epitope 33-41 of the LCMV glycoprotein. Offspring of these mice are either CD45.2^{+}, CD45.1.2^{+} or CD45.1^{+}.
P14 tdTomato	P14 tdTomato mice were generated by crossing P14 mice (B6;D2-Tg(TcrLCMV)327Sdz/JDvsJ) (Jackson Laboratories, USA) with CD45.1 mice (B6.SJL-*Ptprc*^{a} *Pepc*^{b}/BoyJ) (Jackson Laboratories, USA) and tdTomato mice (B6.Cg-*Gt(ROSA)26Sor*^{tm14}*(CAG-tdTomato)Hze*/J) (Madisen *et al.*, 2010) (Jackson Laboratories, USA). Mice were used for experiments conducted in Germany. CD8^{+} T cells of these mice develop with the transgenic TCR, specific against the epitope 33-41 of the LCMV glycoprotein. Offspring of these mice are either CD45.2^{+}, CD45.1.2^{+} or CD45.1^{+}. Additionally, CD8 T cells express the red fluorescent protein (tdTomato)
P14-F1/*Cd4*^{Cre}	P14 F1 CD4Cre mice were generated by crossing P14 mice (B6;D2-Tg(TcrLCMV)327Sdz/JDvsJ) with *Cd4*^{Cre} mice (B6.Cg-Tg(Cd4-cre)1Cwi/BfluJ) (Miyazaki *et al.*, 2011) and CD45.1 mice (B6.SJL-*Ptprc*^{a} *Pepc*^{b}/BoyJ). Mice were used for experiments conducted in Australia. CD8^{+} T cells of these mice

	have the transgene TCR specific for LCMV gp33-41 of the LCMV glycoprotein. Offspring of these mice are either CD45.2$^+$, CD45.1.2$^+$ or CD45.1$^+$. Cre recombinase is inserted downstream of the CD4 promoter and will be expressed in all mature T cells.
Id3^{GFP}/P14	*Id3*^{GFP}/P14 mice (*Id3*^{GFP} x *Ptprc*^{a} x Tg(H2-K-TcrbP14)128Mak) were generated by crossing P14 mice (B6;D2-Tg(TcrLCMV)327Sdz/JDvsJ) with with *Id3*^{GFP} (B6;129S-*Id3*^{tm1Pzg}/J) mice (Miyazaki *et al.*, 2011) and CD45.1 mice (B6.SJL-*Ptprc*^{a} *Pepc*^{b}/BoyJ). Mice were used for experiments conducted in Australia. CD8$^+$ T cells of these mice have the transgene TCR specific for LCMV gp33-41 of the LCMV glycoprotein. Offspring of these mice are either CD45.2$^+$, CD45.1.2$^+$ or CD45.1$^+$. A GFP encoding sequence has been inserted into exon 1 of *Id3* (mouse chromosome 4) resulting in GFP expression in place of *Id3*, as such this mouse is used as a reporter in heterozygote.
Myb^{GFP}/P14	*Myb*^{GFP}/P14mice (*Myb*^{GFP} x *Ptprc*^{a} x Tg(H2-K-TcrbP14)128Mak) were generated by crossing P14 mice (B6;D2-Tg(TcrLCMV)327Sdz/JDvsJ) with *Myb*^{GFP} mice (Dias *et al.*, 2017) and CD45.1 mice (B6.SJL-*Ptprc*^{a} *Pepc*^{b}/BoyJ). Mice were used for experiments conducted in Australia. CD8$^+$ T cells of these mice have the transgene TCR specific for LCMV gp33-41 of the LCMV glycoprotein. Offspring of these mice are either CD45.2$^+$, CD45.1.2$^+$ or CD45.1$^+$. An internal ribosome entry site (IRES)-eGFP cassette is in the *Myb* 3′ UTR, leaving the *Myb* coding region and the mRNA binding site intact to get a functional Myb protein. Cells expressing *Myb*, also express the green fluorescent protein (GFP).
Satb1^{flex}/*Cd8*^{Cre}/P14	*Satb1*^{flex}/*Cd8*^{Cre}/P14 mice were generated crossing *Satb1*^{flex} mice (C57BL/6JRcc-*SatB1*-flex) (Sommer *et al.*, 2014), kindly provided by Marc Beyer (DZNE, Germany) with *Cd8*^{Cre} mice (C57BL/6-Tg(Cd8a-cre)1Itan/J) (Maekawa *et al.*, 2008), P14 mice (B6;D2-Tg(TcrLCMV)327Sdz/JDvsJ) and CD45.1 mice (B6.SJL-*Ptprc*^{a} *Pepc*^{b}/BoyJ). Mice were used for experiments conducted in Australia. CD8$^+$ T cells of these mice have the transgene TCR specific for LCMV gp33-41 of the LCMV glycoprotein. Offspring of these mice are either CD45.2$^+$, CD45.1.2$^+$ or CD45.1$^+$. The *Satb1* allele is reverted upon Cre-mediated recombination, acting as a reporter, where GFP is expressed instead of SATB1. *Cd8*^{Cre} recombinase is expressed downstream of the CD8a promoter in CD8a$^+$ T cells, leading to SATB1 deletion only in CD8$^+$ T cell in the periphery.
Satb1$^{Amnu1/Amnu1}$	Bone marrow was kindly provided by Stephen Turner (Monash University Clayton, Australia). Bone marrow was used for experiments conducted in Australia. Using *N*-ethyl-*N*-nitrosourea mutant mice were created exhibiting a point mutation in the SATB1 DNA-binding domain, leading to reduced DNA-binding activity, creating a functional knock out (Nüssing *et al.*, 2022).
Rosa26^{Satb1}/*Lck*^{Cre}	Bone marrow was kindly provided by Stephen Turner (Monash University Clayton, Australia). Bone marrow was used for

	experiments conducted in Australia. In this transgenic mouse model, a floxed STOP-codon following *Satb1*-GFP is inserted in the *Rosa26* locus leading to *Lck*^{Cre} mediated deletion of the STOP. CD4^{+} and CD8^{+} T cells conditionally over express SATB1-GFP (unpublished)

2.1.6 Primer

2.1.6.1 Genotyping

To confirm the transgenic constructs of the mouse lines used in Table 5, polymerase chain reaction (PCR) genotyping was performed. Genotyping primers were sourced from Integrated DNA Technologies, Inc. (Coralville, IA, USA) and used at a stock concentration of 10 µM. The sequences for the forward (Fwd) and reverse (Rev) primers are listed below. *Id3*^{GFP}, *Myb*^{GFP}, tdTomato, P14, CD45.1 and CD45.2 were genotyped using FACS analysis.

Table 6: Genotyping Primer (wild typ=Wt/transgenic=Tg)

Gene	**Sequence (5'-3")**
Cd4^{Cre}	WT Fwd: CTAGGCCACAGAATTGAAAGATCT WT Rev: GCGGTCTGGCAGTAAAAACTATC Tg Fwd: GCGGTCTGGCAGTAAAAACTATC Tg Rev: GTGAAACAGCATTGCTGTCACTT
Cd8^{Cre}	WT Fwd: CACACATGCAAGTCTAAATCAGG WT/Tg Rev: TGGGATTTACAGGGCATACTG Tg Fwd: CAATGGAAGGAAGTCGTGGT
Lck^{Cre}	Tg Fwd: TGTGAACTTGGTGCTTGAGG Tg Rev: CAGGTTCTTGCGAACCTCAT
Satb1^{flex}	Fwd: TGCTGAGGTTTCCGTCCATAAC Rev: TGTGCTCCCAAGCCTTCCTC

2.1.6.2 CRISPR-guide-RNA

CRISPR-guides were used construct gene specific knock out cells. Guides were designed using the online platforms BENCHLNG, CRISPOR and CHOPCHOP. Protein coding exons that played a role in protein functionality were specifically targeted. Guide RNAs were sourced from Synthego and used at a stock concentration of 3 nM or 10 nM. Gene targets and primer sequences are listed in the following table.

Table 7: CRISPR-Guide RNA Primer sequences

Target gene (Protein)	Exon targeted	Sequence
Klf2 (KLF2)	Exon 2	CUGGCCGCGAAAUGAACCCG
		CGGCGUGAGGAGACCGCGCG
		GCCGCCCTACAGCATCCCCG
	Exon 1	CGGGCTGGCGAAAGTGGCAA
Ccr7 (CCR7)	Exon 3	CAUCGGCGAGAAUACCACGG
		CCUGGACGAUGGCUACGUAG
		GAAGCACACCGACUCGUACA
Sell (CD62L)	Exon 3	CCAUGGUGUAUCAGGAAGUC
	Exon 2	AGGGTACTTACTGGGGCTCG
S1pr1 (S1PR1)	Exon 2	AGGCAAGTTGAACATCGGGG
		GGTGTCCACTAGCATCCCGG
		AGCTCCTTCCCTGAGTGGCA
Prdm1 (Blimp-1)	Exon 2	CGUCAGCGCCGGAAUCCCAG
	Exon 3	UAGUGUAGACUUCACCGAUG
	Exon 5	UUGGAACUAAUGCCGUACGG

2.1.6.3 QPCR Primer

qPCR-primers were used to determine change in gene expression of genes listed below. Primers were designed and sourced from Integrated DNA Technologies, Inc. (Coralville, IA, USA). Primers were reconstituted at a concentration of 100 µM and used at a final concentration of 1 µM. Below, sequences of the primers for each gene and their melt temperature are listed.

Table 8: List of qPCR primers and their melt temperature

Target	Sequence	T_M
Klf2	Fwd: AGCCTATCTTGCCGTCCTTT	56.4 °C
	Rev: CGCCTCGGGTTCATTTC	53.8 °C
Cd69	Fwd: CCCTTGGGCTGTGTTAATAGTG	55.7 °C
	Rev: AACTTCTCGTACAAGCCTGGG	57.0 °C
Actin	Fwd: TGGCACCCAGATCGAGAAC	57.1 °C
	Rev: GTGGAACCGCATTTTTCCCC	57.2 °C

2.1.6.4 Barcode sequences for RNA-Sequencing

To identify each sample during the bulk-RNA-Sequencing, DNA of each sample was labelled with unique DNA-Barcode-Adapters. Adapters were sourced from Illumina. Below the sequences of the adapters are listed.

Table 9: Sequences of Unique Barcodes used for bulk-RNA sequencing

Adapter_ Reverse Barcode	Adapter-Sequence
Ad1	GATCGGAAGAGCACACGTCTGAACTCCAGTCACATCACGATCTCGTATGCCGTCTTCTGCTTG
Ad2	GATCGGAAGAGCACACGTCTGAACTCCAGTCACCGATGTATCTCGTATGCCGTCTTCTGCTTG
Ad3	GATCGGAAGAGCACACGTCTGAACTCCAGTCACTTAGGCATCTCGTATGCCGTCTTCTGCTTG
Ad4	GATCGGAAGAGCACACGTCTGAACTCCAGTCACTGACCAATCTCGTATGCCGTCTTCTGCTTG
Ad5	GATCGGAAGAGCACACGTCTGAACTCCAGTCACACAGTGATCTCGTATGCCGTCTTCTGCTTG
Ad6	GATCGGAAGAGCACACGTCTGAACTCCAGTCACGCCAATATCTCGTATGCCGTCTTCTGCTTG
Ad7	GATCGGAAGAGCACACGTCTGAACTCCAGTCACCAGATCATCTCGTATGCCGTCTTCTGCTTG
Ad8	GATCGGAAGAGCACACGTCTGAACTCCAGTCACACTTGAATCTCGTATGCCGTCTTCTGCTTG
Ad9	GATCGGAAGAGCACACGTCTGAACTCCAGTCACGATCAGATCTCGTATGCCGTCTTCTGCTTG
Ad10	GATCGGAAGAGCACACGTCTGAACTCCAGTCACTAGCTTATCTCGTATGCCGTCTTCTGCTTG
Ad11	GATCGGAAGAGCACACGTCTGAACTCCAGTCACGGCTACATCTCGTATGCCGTCTTCTGCTTG
Ad12	GATCGGAAGAGCACACGTCTGAACTCCAGTCACCTTGTAATCTCGTATGCCGTCTTCTGCTTG
Ad13	GATCGGAAGAGCACACGTCTGAACTCCAGTCACAGTCAACAATCTCGTATGCCGTCTTCTGCTTG
Ad14	GATCGGAAGAGCACACGTCTGAACTCCAGTCACAGTTCCGTATCTCGTATGCCGTCTTCTGCTTG
Ad15	GATCGGAAGAGCACACGTCTGAACTCCAGTCACATGTCAGAATCTCGTATGCCGTCTTCTGCTTG
Ad16	GATCGGAAGAGCACACGTCTGAACTCCAGTCACCCGTCCCGATCTCGTATGCCGTCTTCTGCTTG

2.1.6.5 Barcode sequences for ATAC-Sequencing

To identify each sample during the ATAC-Sequencing, DNA of each sample was labelled with unique DNA-Barcode-Adapters. Adapters were sourced from either Geneworks (Thebarton, SA, Australia) or Integrated DNA Technologies, Inc. (Coralville, IA, USA) and used at a stock concentration of 100 µM. Below the sequences of the adapters are listed.

Table 10: Sequences of Unique Barcodes used for ATAC sequencing

Adapter_ Reverse Barcode	Adapter-Sequence
Ad1.1_ GCGATCTA	AATGATACGGCGACCACCGAGATCTACACTAGATCGCTCGTCGGCAGCGTCAGATGTGTAT
Ad2.1_TAAGGCGA	CAAGCAGAAGACGGCATACGAGATTCGCCTTAGTCTCGTGGGCTCGGAGATGT
Ad2.2_CGTACTAG	CAAGCAGAAGACGGCATACGAGATCTAGTACGGTCTCGTGGGCTCGGAGATGT
Ad2.3_AGGCAGAA	CAAGCAGAAGACGGCATACGAGATTTCTGCCTGTCTCGTGGGCTCGGAGATGT
Ad2.4_TCCTGAGC	CAAGCAGAAGACGGCATACGAGATGCTCAGGAGTCTCGTGGGCTCGGAGATGT
Ad2.5_GGACTCCT	CAAGCAGAAGACGGCATACGAGATAGGAGTCCGTCTCGTGGGCTCGGAGATGT
Ad2.6_TAGGCATG	CAAGCAGAAGACGGCATACGAGATCATGCCTAGTCTCGTGGGCTCGGAGATGT
Ad2.7_CTCTCTAC	CAAGCAGAAGACGGCATACGAGATGTAGAGAGGTCTCGTGGGCTCGGAGATGT
Ad2.8_CAGAGAGG	CAAGCAGAAGACGGCATACGAGATCCTCTCTGGTCTCGTGGGCTCGGAGATGT

Ad2.9_GCTACGCT	CAAGCAGAAGACGGCATACGAGATAGCGTAGCGTCTCGTGGGCTCGGAGATGT
Ad2.10_CGAGGCTG	CAAGCAGAAGACGGCATACGAGATCAGCCTCGGTCTCGTGGGCTCGGAGATGT
Ad2.11_AAGAGGCA	CAAGCAGAAGACGGCATACGAGATTGCCTCTTGTCTCGTGGGCTCGGAGATGT
Ad2.12_GTAGAGGA	CAAGCAGAAGACGGCATACGAGATTCCTCTACGTCTCGTGGGCTCGGAGATGT
Ad2.13_GTCGTGAT	CAAGCAGAAGACGGCATACGAGATATCACGACGTCTCGTGGGCTCGGAGATGT
Ad2.14_ACCACTGT	CAAGCAGAAGACGGCATACGAGATACAGTGGTGTCTCGTGGGCTCGGAGATGT
Ad2.15_TGGATCTG	CAAGCAGAAGACGGCATACGAGATCAGATCCAGTCTCGTGGGCTCGGAGATGT
Ad2.16_CCGTTTGT	CAAGCAGAAGACGGCATACGAGATACAAACGGGTCTCGTGGGCTCGGAGATGT

2.1.7 Cell lines

Cells were cultured cell line specific medium at 37 °C in a humidified incubator at 37 °C with 5 % CO_2. Cells were split every 2-3 days, once they reached a confluency of 70-80 %. To detach the cells a trypsin versane was used.

Table 11: Cell lines used for LCMV propagation and titration.

Cell line	Description
L929	Mouse fibroblast cell line, ATCC # CCL-1 CCL-1 is NCTC clone 929 of strain L, derived in 1948 from a C3H/An male mouse
Baby hamster kidney cells (BHK)	The BHK21 fibroblast cell line was established in 1961 by Macpherson and Stoker from the kidneys of 5 Syrian hamsters (Hernandez and Brown, 2010)
Vero	Vero cells are a mammalian cell line derived from the kidney of an African green monkey (Cercopithecus aethiops) in 1962 by Yasumura and Kawakita (Ammerman *et al.*, 2008)

2.1.8 Antibodies used for flow cytometry

In the following table all antibodies that were used for flow cytometry analysis, Sorting and genotyping are listed.

Table 12: FACS antibodies

Antigen	**Clone**	**Fluorophore**	**Manufacturer**
Anti-GFP	FM264G	AF488	BioLegend
B220	RA3-6B2	FITC/eF450	eBioscience
CCR7 (CD197)	4B12	APC	BioLegend

CD101(Igsf2)	Moushi101/307707	PE-Cy7/ AF647	eBioscience/ BD
CD103 (Integrin aE, ITGAE)	2E7	BUV661/eF450/ PE-Cy7	BD/eBioscience/BioLegend
CD127 (IL7Ra)	A7R34	Biotin/BV421	eBioscience/BioLegend
CD19	6D5/1D3/eBio 1D3	Biotin/BUV395/ PE-Cy7	BioLegend/BD/eBioscience
CD183 (CXCR3)	CXCR3-173	BV421	BioLegend
CXCR6 (CD186)	DANID2	PE	eBioscience
CD223 (Lag3)	eBio C9B7W (C9B7W)	PerCP-eF710	eBioscience
CD244.2 (2B4) (B6 Alloantigen)	eBio244F4	FITC/PE/PE-Cy7	eBioscience
CD25	PC61/3C7/PC 61.5	BV605/PE/PE-Cy7	BioLegend/eBioscience
CD27	LG.3A10	PerCP-Cy5.5	BioLegend
CD279 (PD-1)	J43/29F.1A12/ RMP1-30	PE/BV711/PE-Cy7	eBioscience/BioLegend
CD39	24DMS1	PECy7	eBioscience
CD4	GK1.5	BUV496	BD
CD44	IM7	BUV395	Thermo Fisher
CD45.1 (Ly5.1)	A20	Biotinylated/APC/ FITC/PerCP-Cy5.5/ eF450	ThermoFisher/BD/Invitrogen
CD45.2 (Ly5.2)	104	PB/Biotin/APC/ BUV805/ BV605/FITC/eF450/ PerCP-Cy5.5	WEHI/BD/ThermoFisher/ BioLegend
CD49a	Ha31/8	BUV661	BD
CD62L	MEL-14	BV650	BD
CD69	H1.2F3	FITC/PE/PE-Cy7	Invitrogen (ThermoFisher)/BD /eBioscience
CD73	TY/11.8	PE	BioLegend
CD8a	53-6.7	BV510/BUV737/PB	eBioscience/ BioLegend/WHEI
CX3CR1	SA011F11	BV711/BV785/PE	BioLegend
CXCR5	SPRCL5	Biotin	ThermoFisher
Foxp3	FJK-16s	PE-eF610	eBioscience
GzmB	GB12	APC/PE/PB	Invitrogen/Biolegend
IFN-g	XMG1.2	PE-Cy7	eBioscience
Ki-67	SolA15/B56	eFl660/PECy7/ AF488/PerCP-Cy5.5	eBioscience/Invitrogen/BD /BioLegend
KLF2	E7K8Y	-	Cell Signaling
KLRG1	2F1	BV711/PE	BD/eBioscience
Lef1	C12A5	PE	CST
Ly108 (Slamf6)	13G3/eBio13 G3-18D	BV421/BUV615/ APC	BD/eBioscience
SATB1	14/SATB1	AF647	BD

Streptavidin	n/a	APC/BUV395/ BUV805/ BV421	BioLegend/BD
T-bet	4B10	FITC	Santa Cruz
TCF1	C63D9	AF647/AF488/PB	Cell Signalling Technologies
TCRβ	H57-597	BUV563	BD
Tim3 (CD366)	RMT3-23	BV605/PE/BV785	BioLegend
TNF	MP6-XT22	APC/PE	ThermoFisher
TOX	TXRX10	PE	eBioscience
Va2 TCR	B20.1	PE/eF450	WHEI

2.1.9 Software

Below are all Software's listed, including provider and version, that were used to generate, analyze and present data.

Table 13: List of Software's used

Software	**Provider**
Affinity Publisher	Serif, West Bridgford, UK
Animal Management software (AMS) Versiom 2024.2	Walter and Eliza Hall Institute of Medical Research, Melbourne, AU
BD FACSDivaTM 9.0	BD Biosciences, San Jose, CA, USA
BENCHLING	BENCHLING, San Fransisco, USA
BioRender	BioRender, Toronto, CA
CHOPCHOP version 3.0	University of Bergen, Norway
CRISPOR Version 5.2	UC, Santa Cruz, USA
FlowJoTM 10.8.0	FlowJo LLC, Ashland, USA
GraphPad Prism 9	GraphPad Software, Inc., La Jolla, USA
Infonetica, 2022 Version 2.6.0.1	Infonetica Ltd, Esher, UK
Microsoft office Version 16.92	Microsoft, Redmond, USA
PyRAT animal facility software	University of Bonn, Germany

2.2 Methods

2.2.1 Genotyping

DNA was extracted from animal ear notches, by incubating samples at 55 °C in digestion buffer (Table 3) supplemented with 400 µg/mL Proteinase K, overnight. Enzymes were inactivated through incubation at 85 °C for one hour. The extracted DNA was added to individual PCR Master Mixes and amplified afterwards. PCR products were analyzed on 2-3 % agarose gel, that was pre-stained with SYBR^{TM} Safe DNA Gel Stain. As controls, a HyperLadder100 bp marker and water controls were included for size comparison. The gel was visualized using a transilluminator.

2.2.2 Bone marrow chimeras

Experiments using mixed bone marrow chimeras, were conducted in accordance with the approval of the University of Melbourne ethics committee. Naïve, wild-type C57BL/6J mice, that expressed the congenic protein CD45.1 or Rag$^{-/-}$, were used as host mice. C57BL/6J mice were irradiated twice with a dose of 2x550 Rad and Rag$^{-/-}$ mice with a dose of 2x350 Rad. After irradiation, mice were reconstituted with a minimum of 2x10^6 donor bone marrow cells that were either CD45.1/2$^+$ or CD45.2$^+$. Mice were subjected to Neomycin infused water (20 µg/mL) for four weeks post irradiation. Chimerism efficacy was assessed 6 weeks post irradiation, by blood, before mice were used for experiments.

2.2.3 Experimental treatments

2.2.3.1 Immune checkpoint blockage (ICB)

Mice were treated with checkpoint blockade (ICB) during the chronic phase of infection after day 18. Mice received 200 µg of monoclonal anti-PD-L1 antibodies (clone B7-H1) or Atezolizumab (Roche) in 200 µL PBS intraperitoneally every two days for a maximum of 3 treatments.

2.2.3.2 Statin treatment

Fluvastatin was dose dependent on the average mouse weight. Mice were treated intraperitoneally at the chronic phase of infection after day 21 with 25 µg Fluvastatin sodium slat (Thermo Fisher Scientific) per mouse weight dissolved in 200 µL PBS. Mice received injections every 2 days for a maximum of 3 shots.

2.2.4 Preparation of single cell suspension from organs

2.2.4.1 Lymphoid organs spleen and LN

Spleens and LN were collected from animals in T cell medium. Using the flat end of a 3 mL syringe plunger, spleens were homogenized through a 70 µm nylon-filter and LN through a 40 µm nylon-filter in 2 mL red cell lysis buffer (RCRB). Samples were washed with T cell medium and centrifuged at 1500 rpm at 4 °C, for 5 min. Samples were re-suspended in T cell media, and concentration was determined by counting the cells, and adjusted to a single cell suspension with a concentration of $2x10^7$ cell/mL.

2.2.4.2 Blood

Blood was either collected from living animals by submandibular vein bleeding, or tail vein bleeding, and from recently euthanized mice by cardiac bleeding. Blood was collected in EDTA coated tubes. Red blood cells were excluded through RCLB treatment for 5 minutes. After centrifugation for 5 min at 500xg, remaining cell pellets were washed with MACS buffer and resuspended for further experimental use.

2.2.4.3 Liver

Livers were harvested in T cell medium and processed by smashing through 70 µm nylon cell strainers. After washing with liver buffer and centrifugation for 5 min at 1500 rpm and 4 °C. To remove the fat, cells were resuspended in 44 % Percoll. Through centrifugation at 2000 rpm for 20 min at room temperature fat cells separated from other cells and was suctioned of. Red blood cells in the remaining cells pellet were lysed using RCRB for 3 min at room temperature. After washing and centrifugation for 5 min at 1500 rpm and 4 °C, cells were resuspended in T cell medium.

2.2.4.4 Salivary gland and lung

Salivary glands and lungs were minced into pieces in a petri dish using scalpel blades and digested indigestion buffer (RPMI, 10 % FCS, 1 µg/mL DNAse, 200 µg/mL Dispase, 1 mg/mL Collagenase III) for 40 minutes in a shaker at 37 °C. After 20 min mixes were shortly vortex for 1 minute each. The digestion was stopped with cold MACS buffer and the digestion mix was mashed through a 70 µM nylon cell strainer before washing with a HANKS buffer supplemented with 2 % FCS. Suspensions were centrifuged for 7 min at 1700 rpm and room temperature and resuspended in 40 % Percoll. To create a 40 % to 80 % Percoll gradient, 80 % Percoll were underlaid and the gradient centrifuged 20 min at 2200 rpm and room temperature. Lymphocytes were collected from the interface and washed with T cell medium.

2.2.4.5 Bone marrow

The bones of Tibia, femur and the pelvis were isolated and flushed with 3 mL of cold T cell media. Bone marrow cells were washed using T cell medium and filtered through 70-µm nylon cell strainer before resuspension in pure RPMI. The cell concentration was determined and readjusted for experimental use.

2.2.5 Naïve $CD8^+$ T cells isolation

Single cell suspension from spleen and LN were prepared according to 2.2.4. CD8 T cells were isolating using positive or negative selection. Cell suspensions were incubated 20 min on ice with magnetic CD8-targeting microbeads (Miltenyi) in MACS buffer, according to the manufacturer's instructions. Incubation mix was washed twice and cell suspension transferred onto LS-columns to isolate magnetically labeled $CD8^+$ T cells. Isolated $CD8^+$ T cells were counted and resuspended in PBS for injections. Aliquots of the suspension were checked by FACS analysis for purity and ratios for co-transfers, before injections.

2.2.6 Adoptive P14 T cell transfer

P14 cells of mouse lines listed in Table 5 were harvested from lymphoid organs spleen and LN. Naïve $CD8^+$ T cells were isolated as described in 2.2.5. T cells were counted and resuspended in sterile PBS. For chronic and acute LCMV infections with Docile, Clone13 or Armstrong, 5000 naïve $CD8^+$ T cells were adoptively transferred intravenous (i.v.) into recipient mice. For Co-transfer experiments, 2500 P14 cells of either cell type, was infected together into recipient mice. For KLF2 *in vivo* migration assays a minimum of $1x10^6$ cells were transferred.

2.2.7 CRISPR of naïve $CD8^+$ T cells

Naïve $CD8^+$ T cells were isolated in a single cell suspension according to 2.2.4. T cells were washed twice with PBS. CRISPR reactions were performed as previous described (Nüssing *et al.*, 2020). In an Eppendorf tube 1 µL of each guide-RNA, specific for the target, were mixed with nuclease free water to archive a total volume of 4.4 µL. 0.6 µL Cas9 Nuclease was added to the reaction mix and incubated for 10 minutes at room temperature to form the complex of guide-RNA and Cas9. P3 buffer was prepared by adding 3.6 µL of Supplement 1 to 16.4 µl P3 Primary Cell Solution (Lonza 4D Nucleofector kit). Within 15 min cells were centrifuged and resuspended in with 20 µL of P3 buffer. These 20 µL were added to the guide-RNA/Cas9 complex and transferred into the to the bottom hole of a well of the Lonza nucleofector strip. Cells were electroporated in the Lonza nucleofector once. 130 µL of warm T cell medium was added and cells were rested for 10 min at 37 °C and 5 % CO_2. Afterwards cells were counted and prepared for further use.

2.2.8 Viral infections with LCMV

2.2.8.1 LCMV propagation

Different LCMV-strains, listed below were propagated in cell cultures. LCMV-Armstrong and -Clone13 are propagated in BHK cells, while LCMV-Docile was propagated in L929 cells. Cells were thawed from liquid nitrogen and grown for at least 3 passages in cell culture. Before viral infection BHK cells were plated in

175 cm^2 flask and L929 cells in 75 cm^2 flasks. Once cells reached a confluency of 70-80 % one flask was used to determine the number of cells per flask. LCMV-Docile was propagated using 0.001 Plaque forming units (PFU), whereas LCMV-Armstrong and -Clone13 was made using 0.05 PFU. Cells were incubated in as little volume as possible (BHK 3 mL, L929 1.5 mL) for 3 hours at 37 °C and 5 % CO_2. Flasks were lightly shaken every 30 min. After the incubation, the monolayer of BHK cells was carefully overlaid with 7 mL of BHK-media and L929 cells with 6.5 mL and incubated at 37 °C and 5 % CO_2. The supernatant containing the virus was collected after 48 and 72 hours.

Table 14: Viral LCMV strains

Infectious strain	Description
Lymphocytic choriomeningitis virus (LCMV)-Armstrong	The Armstrong strain was isolated from a monkey undergoing a lymphocytic choriomeningitis
Lymphocytic choriomeningitis virus (LCMV)-Docile	Is a derivative of the WE strain
Lymphocytic choriomeningitis virus (LCMV)-Clone13	Is a derivative of the Armstrong strain The virus was originally provided by the university of Basel (Switzerland)

2.2.8.2 Virus titration of propagated virus protocol 1 (Melbourne)

For quantitation of LCMV titers two different staining methods were used. Vero or L929 cells were cultured until a confluency of 75 – 90 % before usage. Virus was thawed from -80 °C on ice. Serial 10-fold dilutions were prepared until a dilution of $1x10^{10}$. Cells were harvested and 1.6×10^5 were plated in a 24 well plates together with 200 µL of virus dilutions $10^5 – 10^{10}$ and incubated for 3 hrs at 37 % and 5 % CO_2. Monolayers were overlaid with 400uL of DMEM-methylcellulose and incubated 60-72 hrs at 37 °C and 5 % CO_2. The supernatant was removed, and the cells were fixed with 4 % PFA for 30 min at RT. The fixation solution was removed, and a TritonX (FLUKA 93418) solution was added to the monolayer and incubated exactly 20 min at RT. The solution was removed, and cells were incubated 20 min RT with 400µl of 5 % FCS in PBS. Afterwards monolayers were stained a VL-4 antibody (BioXcell) for 60 min at. After washing

cells were stained with a secondary antibody (Peroxydase AffiniPure Goat Anti Rat IgG, Jackson ImmunoResearch Laboratories, Inc) for 60 min at RT. Monolayers were washed and OPD substrate was added and incubated for 15-20 min, until a good colour was produced. The staining was wash twice with PBS and dried overnight. The concentration was calculated by counting of the stained plaques: number of plaques x 5 (dilution factor)

2.2.8.3 Virus titration of propagated virus protocol 2 (Bonn)

Vero or L929 cells were seeded in 6 well plates 24 hours before virus incubation at 37 % and 5 % CO_2, to archive a confluency of 75 – 90 % before usage. Virus was thawed from -80 °C on ice. Serial 10-fold dilutions were prepared until a dilution of $1x10^{10}$. 100 µL of dilutions were added to monolayers of cells and incubated for 60-90 min at 37 °C and 5 % CO_2, rocking the plates every 20 min. Afterwards monolayers were covered with a 1.8 % methyl cellulose solution and incubated for 3 days at 37 °C and 5 %. The solutions were removed, and cells fixed using a crystal violet solution followed by plaque enumeration. Counterstained plaques could be counted and viral titers determined.

2.2.8.4 LCMV infection

Different LCMV-strains were propagated as described in **LCMV propagation**. Vials of the virus were thawed from -80 °C at room temperature and dilutions adjusted with sterile PBS to $1x10^7$ cells/mL for LCMV-Docile and Clone13 or $1x10^6$ cells/mL for LCMV-Armstrong. Mice were infected intravenous or intraperitoneally with 200 µL of $2x10^5$ PFU LCMV-Armstrong, for acute viral infections, or intravenous $2x10^6$ PFU of LCMV-Docile or LCMV-Clone13, for chronic viral. Mice on infection were monitored according to monitoring guidelines approved by the Animal Ethics Committee Melbourne, one day prior to injection, daily from day 6 to day 10 p.i and twice a week then after. If body conditions decreased, monitoring, including weighting of the mice, was adapted.

2.2.9 Cell trace violet staining (CTV)

Naïve CD8 T cells were isolates as described in chapter 2.2.5. Cells were washed twice with sterile PBS by centrifugation at 1500 rpm, 4 °C for 5 min. Pelleted cells were resuspended in the cell trace violet mix (CTV, end concentration 5 µM) and incubated 10 min at 37 °C. The CTV mix was vortexed for 30 seconds before again being incubated for 10 min at 37 °C. The staining was stopped and remaining CTV clenched with 5 times the volume of warm T cells medium for 5 min at 37 °C. The viability was assessed with the microscope and the CTV staining tested at the flow cytometry.

2.2.10 Cell culture

2.2.10.1 *In vitro* experiments

For antigen unspecific activation, 96-well plates are pre-incubated with 100 µL anti-CD3 (3 µg/mL) in PBS over night at 4 °C. The coted plate was washed twice with war T cell medium. $2x10^4$ – $5x10^4$ naïve CD8 T cells were added to the coated plates. anti-CD28 (4 µg/mL) was added to all conditions. Further cytokines were added as indicated. TGFβ was added 24 hours after activation in indicated concentrations. For antigen specific experiments, $2x10^4$ – $5x10^4$ naïve P14 cells were put into 96-well plates and activated using Gp33 (5 µM) and anti-CD28 (4 µg/mL). T cells were activated for 24-96 hrs at 37 °C and 5 % CO_2.

2.2.10.2 *Ex vivo* cytokine stimulation

Single cell suspensions were prepared as descripted in chapter 2.2.4. Cells were resuspended in T cell medium, counted and the concentration adjusted. $3x10^6$ cells were put into U-bottom 96-well plates in 150 µL. For antigen specific P14 stimulation 50 µL of 20 µM Gp33 solutions were added to a final concentration of 5 µM and stimulated for 5 hrs at 37 °C and 5 % CO_2. For polyclonal *ex vivo* stimulation Ionomycin was added at a final concentration of 0.5 µg/mL and PMA at a final concentration of 50 ng/mL. The mix was stimulated for 4 hrs at 37 °C and 5 % CO_2. For both 50µL of 1x Brefeldin A was added after 30 min of initial incubation.

2.2.11 RNA isolation for sequencing and qPCR experiments

RNA of was isolated using the RNeasy Plus Mini ($5x10^5$-10^7 cells) or Micro (<$5x10^5$ cells) Kit (Qiagen), according to manufactures instructions. Cells were lysed using RLT-buffer supplemented with 2-Mercaptoethanol. Genomic DNA was separated by column specific centrifugation, before isolating RNA with RNA-binding columns. Concentrations of the RNA was determined and depending on the following steps adjusted for each sample.

2.2.12 Real time quantitative Polymerase-chain-reaction (RT-qPCR)

Isolated RNA was adjusted to a concentration of 0.2 pg/uL – 0.2 µg/µL. RNA was reverse translated into DNA using iScript^M Reverse Transcription Supermix (Bio-Rad). qPCR reactions were prepared using DNA templates, and primers listed in chapter 2.1.6.3 at an end concentration of 1 µM. For the reaction the PowerUp SYBR Green Master Mix (2X) was used. Using a Thermocycler the reaction mix was activated at 50 °C for 2 minutes, before DNA-polymerase was activated at 95 °C for 2 minutes. Afterward DNA double strands were denatured at 95 °C for 15 second, followed by primer annealing 60 °C for 15 second and Polymerase extension at 72 °C for 1 min. These steps were repeated at least >30 cycles, depending on input cDNA concentration.

2.2.13 Flow cytometry

2.2.13.1 Viability, surface and tetramer staining

$4x10^6$ cells were stained in a round-bottom 96-well plate, unless indicated differently. Cells were stained with 50 µL surface staining mix using antibodies listed in Table 12, including surface markers, LD and Fc-block on ice for 20 min in MACS buffer. Staining solutions was washed twice with 200 µL ice cold MACS buffer by centrifugation at 1900 rpm for 2 min at 4°C. Stained cells were analyzed using flow cytometry or processed further as described below. Antigen specific Gp33-tetramers, staining the Gp33 specific TCR, were added into the surface mix and stained as described.

2.2.13.2 Cytokine and intracellular staining

After surface marker staining (chapter 2.2.13.1), samples were fixed using a Cytofix/Cytoperm kit from eBioscience. Membranes of the cells were fixed in 100 µL for 30 min at 4 °C or on ice. Afterwards the fixation solutions were washed twice with 200 µL MACS buffer by centrifugation at 1900 rpm, for 2 min at 4 °C. Cytokines were intra cellular stained for 1 hour, at 4 °C or on ice in 50 µL permeabilization buffer. The staining was stopped by washing the cells twice with 200 µL ice cold MACS buffer by centrifugation at 1900 rpm for 2 min at 4°C, before cells were analyzed by flow cytometry.

2.2.13.3 Intra-nuclear staining

After surface marker staining (2.2.13.1), samples were fixed using the Foxp3 Transcription Factor Staining Buffer Set. Membranes and nuclei of the cells were fixed in 50 µL for 30 min at 4 °C or on ice. Afterwards fixation solutions were washed twice with 200 µL MACS buffer by centrifugation at 1900 rpm, for 2 min at 4 °C. Transcription factors and intra-nuclear proteins were stained intra nuclear for 2-3 hours, at 4 °C or on ice in 50 µL permeabilization buffer. The staining was stopped by washing the cells twice with 200 µL ice cold MACS buffer by centrifugation at 1900 rpm for 2 min at 4°C, before cells were analyzed by flow cytometry.

2.2.14 Transcriptomic analysis (Sequencing)

2.2.14.1 Preparation and purification for Sequencing of infected mice

Single-cells suspension from spleens were prepared as descripted in chapter 2.2.4 and enriched for CD8 cells using negative selection. Cells were incubated with anti-CD4 beads (L3T4, Miltenyi Biotec) and anti-CD19-Biotin (6D5, Biolegend) for 20 min on ice succeeding an incubation with anti-Biotin-microbeads (Miltenyi Biotec) for 20 min on ice. Cells were isolated unsing magnetic separation with LS-MACS columns (Miltenyi Biotec). Isolated CD8 T cells were stained, and cell populations sorted according to experiment.

2.2.14.2 Bulk-RNA sequencing and analysis

RNA was isolated from sorted populations using the RNeasy Plus Micro Kit according to the manufacturer's instructions (QIAGEN) as descripted in chapter 2.2.11. Each sample group consisted of two experimental replicates. DNA libraries were constructed using the TruSeq® RNA Sample Preparation v2 kit (Illumina). Libraries were sequenced using NovaSeq X (Illumina) 10B flow cell, paired-end reads. Paired-end FASTQ files were aligned and sorted with STAR (Dobin *et al.*, 2013) (rusing the GRCm39 reference genome). A counts matrix was calculated with featureCounts using ensembl gene annotation (GRCm39 release 105). The counts matrix was loaded into R (4.2.1) and analyzed with the edgeR pipeline (Ritchie *et al.*, 2015). FilterByExpr was used (min.count = 200, min.totalcount = 300). Normalization factors were calculated with 'TMM' method. Dispersion estimates were calculated and used to fit the edgeR genewise negative binomial generalized linear model (glmFit), with batch included as an additional covariate to control for batch effects. Batch effects and clustering was assessed using PCA plots. Differentially expressed genes were calculated using edgeR log likelihood ratio test. Results were filtered to only include genes with count-per-million (CPM) > 15 in at least 2 of the samples in each comparison. Comparisons were made between KO and WT for each of the 4 sorted cell types. Genes with FDR <0.1 and absolute logFC >0.5 were cross referenced with ATAC and ChIP annotated gene lists. Intersections between ATAC and ChIP peaks were found with bedtools. Gene expression heatmaps were generated with pheatmap and MA plots were generated with ggplot2. A gene set enrichment analysis was performed using clusterProfiler (Yu *et al.*, 2012) using the Gene Ontology (GO), Kyoto Encycloedia of Genes and Genomes (KEGG) and MSigDB Hallmarks mouse gene sets. We considered genes expressed in the cell type (CPM > 15 in at least 2 samples) with enrichment calculated by KO vs WT logFC. Highly enriched pathways were selected for functional relevance and to remove duplication.

2.2.14.3 Single cell-RNA-Sequencing and analysis

Sorted cells were labelled with unique Total-Seq antibody-oligonucleotide cocktails (Biolegend) and processed following the manufacturer's specifications.

Chromium Single Cell 5' Library and Gel Bead Kit v2 was used to generate cDNA libraries (10X Genomics) following the manufacturers protocol. Approximately 56,000 cells were loaded into Chromium Next GEM Chip with reverse transcription (RT) master mix and single cell 5' gel beads for a gel bead-in-emulsion (GEM). Reverse transcription from poly-adenylated mRNA to cDNA in every single GEM containing an Ilumina R1 primer sequence, Unique Molecular Identifier (UMI), the 10x Barcode and template switch oligo was performed. Simultaneously Barcoded DNA from cell surface protein feature barcode conjugated to the hashtag antibody were constructed in the same single cell within GEM. For gene expression and surface protein feature library, pooled barcoded cDNA products were purified using Silane Dyna Beads and further amplified by PCR and sheared to fragments. Appropriate-sized (200 – 9000bp) fragments were selected using SPRIselect reagent for subsequent library construction. Sequencing libraries were generated with unique Sample indexes. Libraries quality was assessed using Agilent Tape station D5000. Sequencing data was aligned to mouse genome mm10 and to hashtag oligonucleotide (HTO) feature barcodes using CellRanger v7.0.0. to generate feature-barcode matrices. Succeeding data analysis was completed using the Seurat R package v4.4.0 (Hao *et al.*, 2021). HTOs for demultiplexing were normalised with Centred-Log-Ratio. For T cells, gene expression data were normalized using SCTransform v0.4.183 (Choudhary and Satija, 2022), regressing for Interferon response signals (Howe *et al.*, 2018; Castanza *et al.*, 2023) and cell cycle score (from R package gprofiler2 v0.2.3 (Kolberg *et al.*, 2020) to avoid these variables dominating the data. From the principal components reductions, UMAPs were generated and clusters identified. Transcriptional diversity was calculated using the CytoTRACE package (Gulati *et al.*, 2020). Cluster-specific genes were identified using FindMarkers from Seurat with minimum
percentage expression set to 10%, and in some instances, clusters were merged manually and annotated. Signature enrichment analysis was performed using AddModuleScore from Seurat, and barcode plots generated using the barcodeplot function from limma v3.58.1 (Ritchie *et al.*, 2015).

2.2.14.4 ATAC-Sequencing and analysis

ATAC-seq was performed as previously described (Grandi *et al.*, 2022). 50,0000 cells from sorted P14 populations were lysed using cold ATAC buffer (10 mM Tris–HCl pH 7.5, 10 mM NaCl and 3 mM MgCl2 in UltraPure DNase/RNase-free distilled water (Thermo Fisher Scientific) comprising NP40 (Millipore-Sigma, 0.1 %), Tween-20 (Millipore-Sigma, 0.1 %) and digitonin (Promega, 0.01 %) for 3 min. Nuclei were pelleted at 500 g for 10 min 4 °C and resuspended in Transposition Mix (Tagment DNA buffer and Tn5 Tagment DNA TDE1 Enzyme from Illumina, PBS, UltraPure DNase/RNase-free distilled water, 0.001 % digitonin, 0.1 % Tween-20). Enzymatic transposition of DNA was achieved by incubation at 37 °C for 30 min at 1000 rpm. DNA was purified using the DNA Clean and Concentrator-5 Kit (Zymo Research). Fragments were barcoded in a PCR reaction with unique Adapter sequences using the NEBNext Ultra II Q5 2x Master Mix (New England Biolabs). Libraries were quantified using the NEBNext Libary Quant Master Mix Kit (New England Biolabs) by qPCR. Individual samples were further amplified to obtain unified library concentrations. Final libraries were purified using the DNA Clean and Concentrator-5 Kit (Zymo Research). Final library concentration was

determined using Agilent Tape station D5000 (Agilent Technologies). Libaries were pooled and sequenced on NovaSeq X (Illumina) 10B flow cell, paired-end reads. Paired-end FASTQ files had adapter sequences trimmed with cutadapt 65. Alignment was performed with BWA-mem2. to reference GRCm39. BAM files were sorted and index with SAMTools (Danecek *et al.*, 2021), bigwig files were generated with deepTools bamCoverage (Ramírez *et al.*, 2016) with RPKM normalization. Peaks were called for each with MACS2 (Zhang *et al.*, 2008) with shifting model disabled, peak regions were merged for all samples. A Peaks Counts matrix was generated for the merged peaks and all samples, using Subreads featureCounts (Liao *et al.*, 2014). Peaks were annotated with nearest gene Transcription start site (TSS) (Ensmbl/havana GRCm39). The counts Matrix was loaded in R(4.2.1) and analysed with the limma pipeline 62 Peaks where all samples logCPM < -1 were filtered. Nomalization factors were calculated using the ‘TMM’ method. Variance was estimated with the voom transformation and

fitted with a limma linear model (lmFit) with batch used as an additional covariate for batch correction, clustering and batch correction was assessed with PCA plots. Differentially accessible peaks were calculated using ebayes empirical bayes method. False discovery rate (FDR) was controlled with Benjamini-Hochberg procedure. Comparisons were made between KO and WT for each cell type as well as between wildtype CD62L$^{+/-}$, CD101^{+}/CX3CR1^{+}, T_{PEX}/T_{EX} cell groups. Heatmaps of differentially accessible regions were generated using deeptools, replicates were merged into single coverage bigwig file for each cell type. Profiles of knockout and wild type were plotted at the same regions for all samples from each condition.

2.2.14.5 ChIP-Sequencing analysis

Satb1 ChIP-seq data was downloaded from ncbi (accession no. SRR5385297, SRR5385298) (Kitagawa *et al.*, 2017). Alignment was done using BWA-mem2 and sorted and indexed with SAMtools, bigwig files were generated with deepTools. Peaks were called using MACS2 with shifting model. Low confidence peaks were filtered at q-value < 10 and, with the remaining from each dataset, merged. Each of these peaks was annotated with the nearest gene TSS. Intersecting ATAC and Chip peaks were found using bedtools.

2.2.15 Statistics

Statistical analysis were conducted using the software GraphPad Prism. Two groups were compared using the Student's t-test. If groups had the same variables (within one sample) a paired t-test was used. For groups of different samples, the unpaired student t-test was used. For comparison of more than two groups an Analysis of Variance (ANOVA) with at Tukey's multiple comparisons test was performed. If multiple conditions were compared a multiple paired (same sample) or unpaired (different samples) t-test was used. A p-value of <0.05 was considered as statistically significant. Details of the used test, the number of mice and replicates are provided within each individual figure legend.

Chapter 3 – Molecular regulation of T cell differentiation by the transcription regulator SATB1

3.1 Introduction

Genomic DNA functions as a blueprint for protein synthesis, which is essential for the regulation of cellular processes, directing activities such as RNA production (Sherwood *et al.*, 2014; Miyamoto *et al.*, 2018) and the repair of DNA (Ball and Yokomori, 2011). While certain genomic sequences are universally employed across all cell types (Cairns, 2009; Klemm *et al.*, 2019), others are exclusive in specific cell types (J. Wang *et al.*, 2012; Liu *et al.*, 2019). During T cell differentiation, epigenetic changes play a critical role. Particularly when naïve $CD8^+$ T cells differentiate into effector T cells, effector genes are activated and naïve-associated genes are suppressed (Frias *et al.*, 2021). A prime example is the *Ifng* locus. Expression of IFN-γ has been correlated with the level of DNA methylation (Fukunaga *et al.*, 1986). In chronic infection, epigenetic changes have also been observed. T_{PEX} and T_{EX} cells exhibit highly distinct chromatin landscapes that are associated with different gene expression signatures (Utzschneider *et al.*, 2020; Abdel-Hakeem *et al.*, 2021). This led us to investigate which possible mechanisms could regulate these epigenetic changes. A critical part of regulating the activity of specific regulatory regions involves controlling the physical accessibility of chromatin by Transcription factors (TF) (Hammelman *et al.*, 2020). There are two types of TF: the first interacts with closed chromatin to enhance the accessibility of cell type–specific regions, thereby initiating cell state transitions such as differentiation (Sherwood *et al.*, 2014; Soufi *et al.*, 2015); the second type of TF binds to open regions and activates or inactivates gene expression (Hammelman *et al.*, 2020). Examples of the first category are octamer-binding transcription factor 4 (Oct4), (sex determining region Y)-box 2 (Sox2), Krüppel-like factor 4 (Klf4) (Soufi *et al.*, 2015) and special AT-rich binding protein 1 (SATB1) (Cai *et al.*, 2003). SATB1 has been studied extensively in T cells in thymic development (Feng *et al.*, 2022). However, its role in mature T cells and specifically $CD8^+$ T cells in the periphery is less clear. In homeostatic settings, SATB1 has been shown to repress effector genes and facilitating accessibility to genes associated with the naïve T cell phenotype (Nüssing *et al.*,

2022). This includes immune receptors such as *Ccr7, Ccr5, Cxcr3, Cxcr5, Xcr1*; costimulatory and inhibitory checkpoint molecules such as *Bcl2, Cd28, Havcr2, Icos, Pdcd1, and Tigit;* effector molecules such as *Gzmb, Gzmm, Ifng, Il7, Il12, Il15*; cytokine receptors such as *Il2ra, Il2rb, Il4ra, Il7r, Il15ra, Il17ra;* key naïve transcription factors, *Bcl6, Foxo1, Lef1, and Tcf7*; and effector transcription factors such as *Irf4, Prdm1, Runx3, Stat5a, Stat5b, Tox, Zeb1, and Zeb2* (Nüssing *et al.*, 2022). Some of these genes, such as *Prdm1* and *TOX*, as well as effector molecules like *GzmB* and *Ifng*, have been associated with altered gene expression in chronic infection, suggesting that SATB1 might regulate these genes during differentiation of exhausted T cells. Further, SATB1 has been shown to repress PD-1 expression in $CD8^+$ T cells (Stephen *et al.*, 2017). Based on our analysis of published RNA-seq data (Utzschneider *et al.*, 2020), SATB1 itself is expressed in T_{PEX} cells, but downregulated during the differentiation of T_{EX} cells.

Given its role as a chromatin organiser and taking into consideration that SATB1 regulates key effector and naïve-associated genes, we sought to understand how SATB1 may impact effector and exhausted CD8 T cell differentiation. To this end, we utilised various knock-out and overexpression mouse models to investigate the effect of SATB1 depletion in $CD8^+$ T cells in acute and chronic LCMV-infection.

3.2 Results

3.2.1 SATB1 regulates effector differentiation and function of CD8⁺ T cells during acute viral infection.

To start our investigation into how SATB1 impacts CD8⁺ T cell differentiation, we first analysed SATB1 expression in effector and memory cells after acute infection. For this purpose, we transferred CD45.1⁺ P14 cells adoptively into naïve CD45.2⁺ recipient mice that were subsequently infected with LCMV-Armstrong and analysed the expression of SATB1 using flow cytometry (Figure 3.1A). On day 7 p.i. we observed increased SATB1 expression in MPC and SLEC compared to naïve CD8⁺ T cells, with MPC exhibiting higher levels than SLEC (Figure 3.1B). Later, SATB1 was downregulated in CD8⁺ T cells during virus clearance and memory formation. T_{CM} cells exhibited similar SATB1 expression levels as naïve CD8⁺ T cells, whereas T_{EM} cells demonstrated reduced expression (Figure 3.1C and D). Thus, SATB1 is upregulated during the effector phase and downregulated in the memory phase.

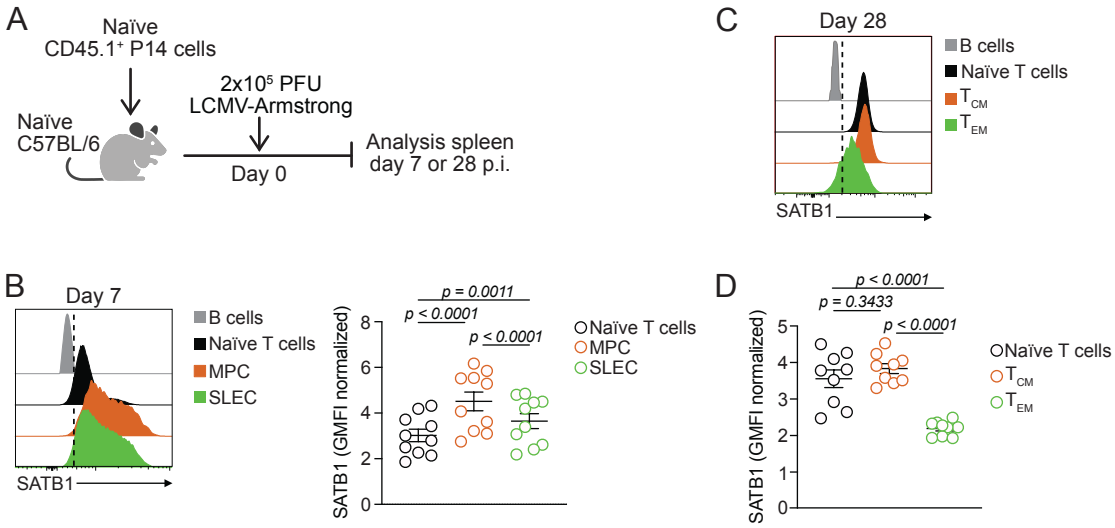

Figure 3.1: SATB1 is upregulated during the effector phase and downregulated in the memory phase.
(A-D) Naïve CD45.1⁺ P14 cells were adoptively transferred into naïve wildtype CD45.2⁺ mice and infected with LCMV-Armstrong. spleens were harvested on days 7 (B) or 28 p.i. (C-D) and analysed using flow cytometry. (A) Schematic of experimental setup. (B) Representative histogram and quantification showing the expression of SATB1 in MPC and SLEC cells compared to naïve CD8 T cells and B cells. (C) Representative histogram and (D) quantification showing the expression of SATB1 in T_{CM} and T_{EM} cells compared to naïve CD8 T cells and B

cells. Dots in graphs represent individual mice; horizontal lines and error bars of bar graphs indicate means ± SEM, respectively. Data is pooled from two independent experiments. P values are from unpaired student's t test (A-D).

To investigate the effect of SATB1 loss on T cell differentiation in acute viral infection, we utilised a mouse model with a conditional *Satb1*^{flex} allele, provided by Dr. Marc Beyer (Sommer *et al.*, 2014). These mice were crossed with *Cd8*^{Cre} mice, in which Cre recombinase is specifically activated in CD8$^+$ T cells in the periphery following thymic development (Maekawa *et al.*, 2008). Upon Cre expression, the *Satb1* gene is inverted and a GFP reporter is expressed in its place (Figure 3.2A). To validate the model and assess its suitability as our targeting approach, we characterised naïve *Satb1*$^{flex/flex}$/*Cd8*^{Cre} (SATB1-KO) mice and compared them to *Satb1*$^{flex/flex}$ (Ctrl) mice using flow cytometry. We observed that in SATB1-KO mice, peripheral CD8$^+$ T cells, but not CD4$^+$ T cells, expressed GFP (Figure 3.2B). Furthermore, compared to Ctrl mice, SATB1 expression in SATB1-KO CD8$^+$ was greatly reduced, while CD4$^+$ T cells in both SATB1-KO and Ctrl mice exhibited similar expression levels (Figure 3.2C). The overall numbers of T cells per spleen were not altered by deletion of SATB1 (Figure 3.2D). The frequencies of CD62L$^+$ CD8$^+$ T cells were marginally increased in the SATB1-KO mice compared to Ctrl mice (Figure 3.2E). SATB1-KO mice showed a reduction in the number of CD62L$^+$CD44$^+$ T_{CM} cells but similar numbers of naïve CD62L$^+$CD44$^+$ CD8$^+$ T cells compared to Ctrl mice (Figure 3.2F), suggesting that the development of naïve CD8$^+$ T cells in SATB1-KO mice is not impaired. Overall, the data indicate that the *Satb1*$^{flex/flex}$/*Cd8*^{Cre} mouse model is as an efficient system for investigating the consequences of SATB1 deletion in CD8$^+$ T cells.

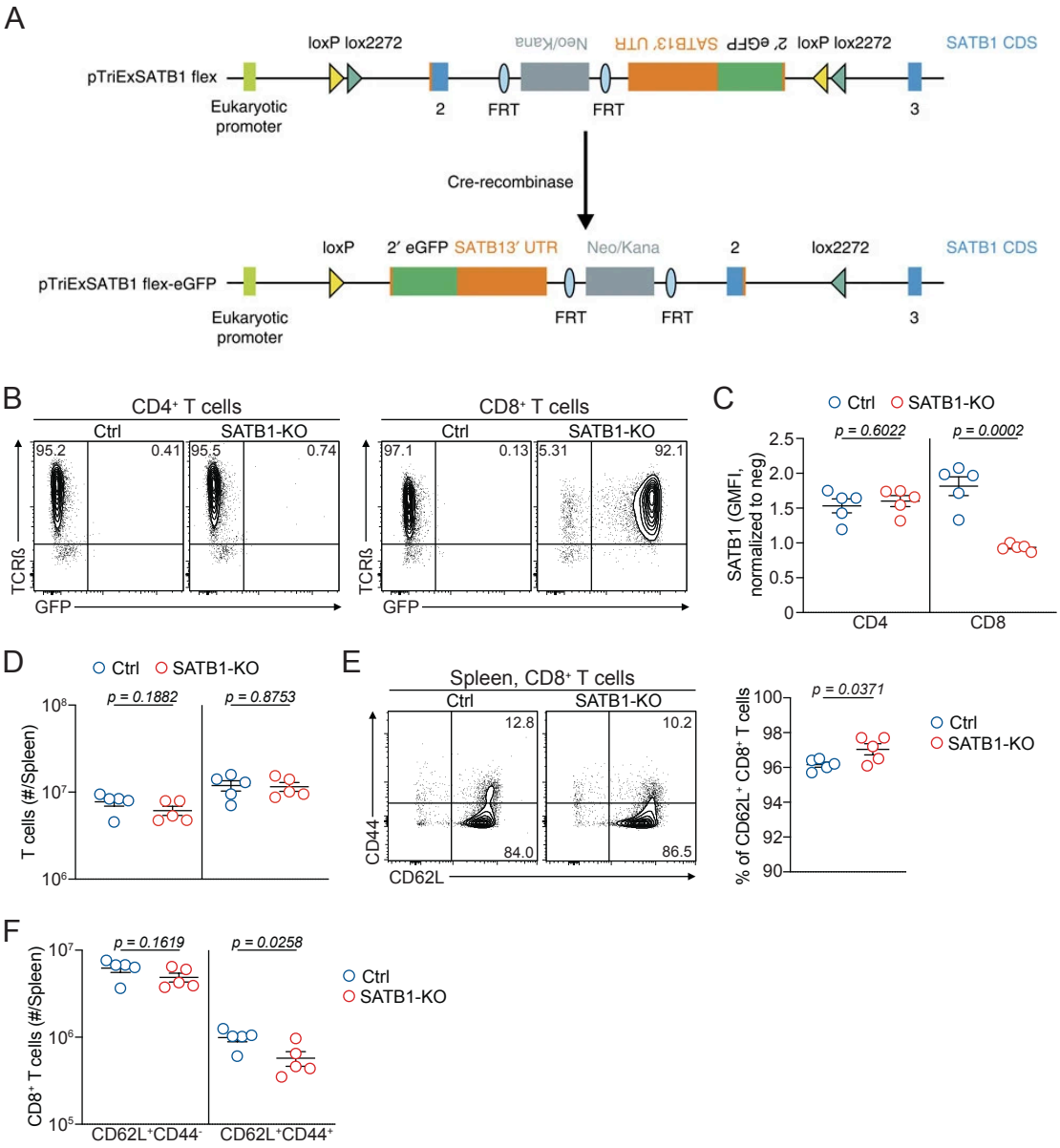

Figure 3.2: Validation of the SATB1-KO mouse model (*Satb1*$^{flex/flex}$/*Cd8*^{Cre})
(A) Schematic description of the Satb1 gene locus in SATB1-KO (*Satb1*$^{flex/flex}$/*Cd8*^{Cre}) or Ctrl (*Satb1*$^{flex/flex}$) mice and Cre mediated gene flip (Sommer et al., 2014). (B) Representative flow cytometry plots displaying GFP expression upon Cre-mediated *Satb1* gene flip in CD8$^+$ T cells of KO mice compared to Ctrl mice. (C) Quantification of SATB1 expression in CD4$^+$ and CD8$^+$ T cells. (D) Numbers of splenic CD4$^+$ and CD8$^+$ T cells in SATB1-KO and Ctrl mice. (E) Representative flow cytometry plots and quantification showing CD44 vs CD62L expression in SATB1-KO and Ctrl mice and quantification of naïve and memory phenotype CD8$^+$ T cells. Dots in graphs represent individual mice; horizontal lines and error bars of bar graphs indicate means ± SEM, respectively. Data is representative of one experiment. P values are from unpaired student's t test.

We next generated SATB-KO or Ctrl mice on a P14 TCR transgenic background and adoptively transferred P14 cells into naïve congenically marked ($CD45.1^+$) recipient mice that were subsequently infected with LCMV-Armstrong. SATB1-KO and Ctrl P14 cells from the spleen were analysed on day 7 post infection using flow cytometry (Figure 3.3A). We observed no difference in the population expansion of SATB1-KO P14 compared to Ctrl P14, with both exhibiting similar frequencies and numbers of P14 cells per spleen (Figure 3.3B). However, SATB1-KO P14 cells exhibited a significant increase in the expression levels of the inhibitory receptor PD-1 and a decrease in Tim-3 expression compared to Ctrl P14 cells (Figure 3.3C and D). Furthermore, SATB1-KO P14 cells demonstrated increased frequencies of $KLRG1^+$ SLEC and decreased frequencies of $KLRG1^-$ MPC compared to Ctrl P14 cells (Figure 3.3E). Numbers of SATB1-KO SLEC were increased compared to Ctrl SLEC, while no differences in the MPC population were observed between SATB1-KO and Ctrl cells (Figure 3.3E). SATB1-KO and Ctrl MPC expressed similar levels of TCF1 (Figure 3.3F). Further, SATB1-KO and Ctrl P14 cells expressed similar levels of T-bet (Figure 3.3G). Among SATB1-KO P14 cells, the effector population expressing both KLRG1 and CX3CR1 was significantly increased compared to those in Ctrl P14 cells (Figure 3.3H).

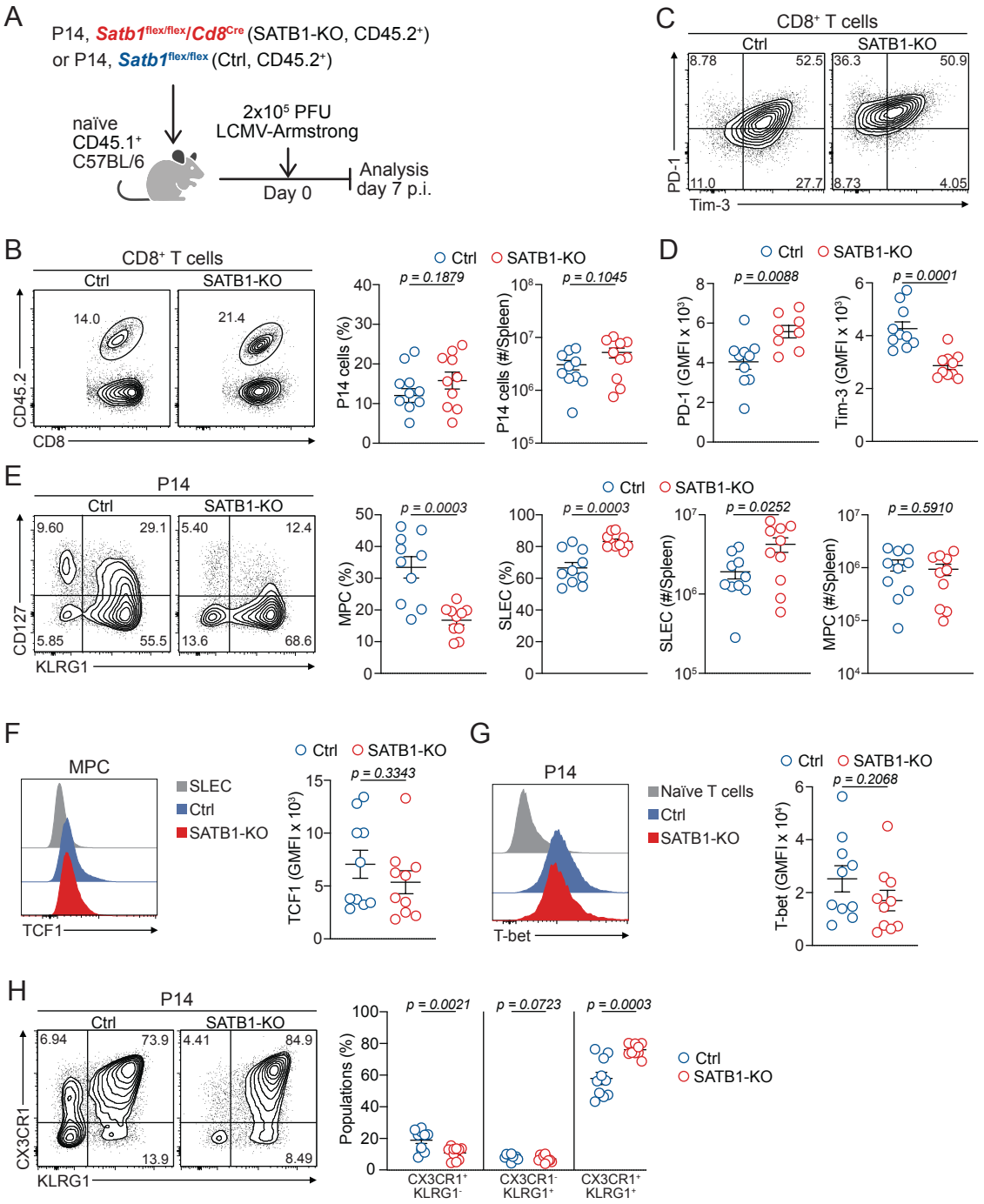

Figure 3.3: Loss of SATB1 increases SLEC differentiation during acute viral infection

(A-H) Naïve CD45.2+ SATB1-KO P14 cells (*Satb1*$^{flex/flex}$/*Cd8*^{Cre}) or Ctrl P14 cells (*Satb1*$^{flex/flex}$) were adoptively transferred into naïve wildtype CD45.1+ mice and subsequently infected with LCMV-Armstrong. spleens were harvested on day 7 p.i. during the acute phase and analysed using flow cytometry. (A) Schematic of experimental setup. (B) Representative flow cytometry plots and quantification showing frequencies among CD8+ T cells and numbers per spleen of SATB1-KO and Ctrl P14 cells. (C) Representative flow cytometry plots showing PD-1 and Tim-3 expression in SATB1-KO and Ctrl P14 cells. (D) Quantification of PD-1 and

Tim-3 expression in SATB1-KO and Ctrl P14 cells. (E) Representative flow cytometry plots and quantification showing frequencies and numbers per spleen MPC ($KLRG1^-$) and SLEC ($KLRG1^+$) SATB1-KO and Ctrl P14 cells. (F) Representative histogram and quantification of TCF1 expression in SATB1-KO and Ctrl MPC. (G) Representative histogram and quantification of T-bet expression in SATB1-KO and Ctrl P14 cells. (H) Representative flow cytometry plots and quantification showing frequencies of $CX3CR1^+$ and $KLRG1^+$ SATB1-KO and Ctrl P14 cells. Dots in graphs represent individual mice; horizontal lines and error bars of bar graphs indicate means ± SEM, respectively. Data is pooled from two independent experiments. P values are from unpaired student's t test.

Next, we assessed, if the loss of SATB1 impaired effector functions. SATB1-KO P14 cells exhibited impaired cytokine production compared to Ctrl P14 cells, with reduced frequencies of IFN-γ^+ cells and IFN-γ^+/TNF^+ co-producing cells (Figure 3.4A). Consistent with these findings, the production of IFN-γ and TNF at the single cell level was significantly reduced in SATB1-KO P14 cells compared to that in Ctrl P14 cells (Figure 3.4B). Similar to the overall population, SATB1-KO SLEC exhibited decreased IFN-γ^+ and IFN-γ^+TNF^+ cells and reduced cytokine expression levels compared to Ctrl SLEC (Figure 3.4C-E). Frequencies of cytokine producing MPC were also reduced (Figure 3.4C-E). Expression levels of IFN-γ were lower in SATB1-KO MPC compared to Ctrl MPC, while the expression of TNF was similar in both (Figure 3.4E). In contrast, SATB1-KO and Ctrl SLEC produced similar levels of GzmB (Figure 3.4F). Thus, SATB1 depletion impairs the capacity to produce effector cytokines IFN-γ and TNF, but not the ability to produce GzmB.

Taken together this data shows that SATB1 restrains $CD8^+$ effector T cell differentiation and inhibitory receptor expression during acute viral infection. Furthermore, SATB1 is required for efficient cytokine production.

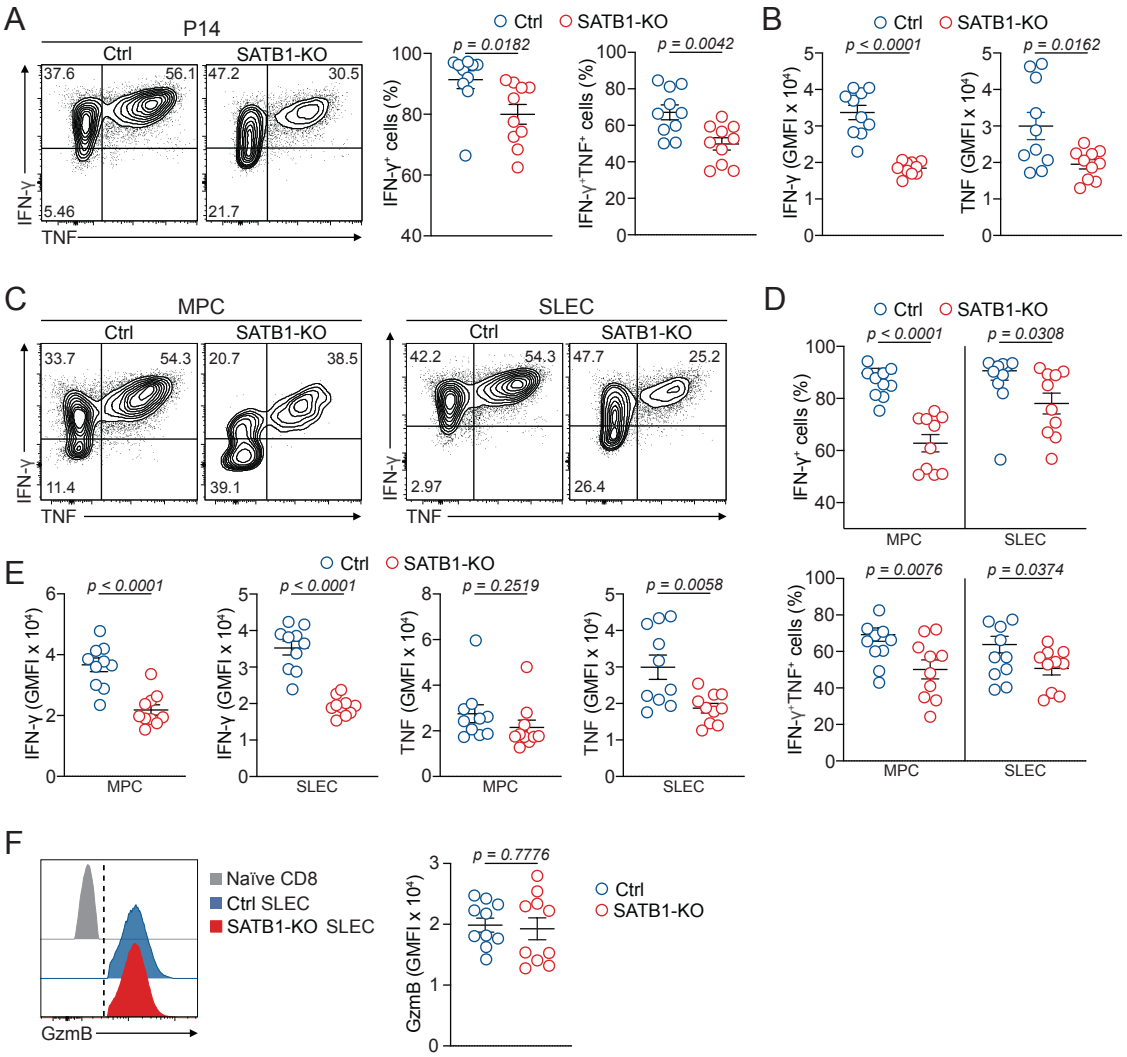

Figure 3.4: SATB1-KO cells show impaired IFN-γ and TNF production in MPC and SLEC in an acute infection.

(A-F) Naïve CD45.2⁺ SATB1-KO P14 cells (*Satb1*$^{flex/flex}$/*Cd8*^{Cre}) or Ctrl P14 cells (*Satb1*$^{flex/flex}$) were adoptively transferred into naïve wildtype CD45.1⁺ mice and subsequently infected with LCMV-Armstrong. spleens were harvested on day 7 p.i. during the acute phase and analysed using flow cytometry. (A) Representative flow cytometry plots and quantifications of frequencies of IFN-γ and TNF producing SATB1-KO or Ctrl P14 cells after incubation with Gp33 peptide *ex vivo*. (B) Quantifications of IFN-γ and TNF expression on a single cell level in SATB1-KO or Ctrl P14 cells after incubation with Gp33 peptide *ex vivo*. (C) Representative flow cytometry plots and (D) quantifications of frequencies of IFN-γ and TNF producing SATB1-KO or Ctrl MPC and SLEC after incubation with Gp33 peptide *ex vivo*. (E) Quantifications of IFN-γ and TNF expression on a single cell level in SATB1-KO or Ctrl MPC and SLEC after incubation with Gp33 peptide *ex vivo*. (F) Representative histogram and quantification of GzmB producing SATB1-KO or control SLEC. Dots in graphs represent individual mice; horizontal lines and error bars of bar graphs indicate means ± SEM, respectively. Data is

pooled from two independent experiments. P values are from unpaired student's t test.

3.2.2 SATB1 promotes differentiation of MPC during acute viral infection

Our data suggests that SATB1 actively suppresses SLEC differentiation and maintains effector function during acute viral infection. To further test these findings, we investigated the effects of enforced SATB1 expression in $CD8^+$ T cells during acute viral infections. To this end, we utilised a transgenic mouse model in which SATB1 is conditionally overexpressed from the *Rosa26* locus in T cells (*Rosa26*^{Satb1}/*Lck*^{Cre}, henceforth referred to as *Satb1*^{Tg}). These mice were produced in the Beyer lab. To this end, *Satb1* fused to an IRES site and sequence encoding thr green gluorescent protein (GFP) was inserted into the *Rosa26* locus downstream of the CAG promoter. The promoter sequence precedes a STOP codon flanked by two loxP sites (Figure 3.5A). Upon *Lck* expression, Cre excises the stop codon, resulting in constitutive expression of SATB1-GFP. To validate this model, we analysed mixed bone marrow chimeric mice harbouring Ctrl and *Satb1*^{Tg} cells. Within *Satb1*^{Tg} cells, only 60 % expressed GFP, demonstrating a partial knock-in of the *Satb1* gene (Figure 3.5B). For all subsequent analyses, *Satb1*^{Tg} cells were gated on GFP^+ cells. In *Satb1*^{Tg} and Ctrl $CD8^+$ T cells exhibiting similar frequencies of naïve $CD62L^+CD44^-$ CD8 T cells (Figure 3.5C and D), indicating that enforced SATB1 expression does not impair the development of naïve *Satb1*^{Tg} $CD8^+$ T cells. The same was observed for $CD62L^+CD44^+$ T_{CM} cells, while of *Satb1*^{Tg} T_{EM} cells were reduced compared to Ctrl cells (Figure 3.5C and D). SATB1 expression was significantly elevated in *Satb1*^{Tg} naïve $CD8^+$ T cells and T_{CM} cells compared to Ctrl cells (Figure 3.5E). *atb1*^{Tg} T_{EM} cells, which normally express low levels of SATB1 (Chapter 3.2), exhibited expression levels of SATB1 as high as those in naïve $CD8^+$ T cells (Figure 3.5E). Notably, the expression of key naïve markers, CD127 and CD62L, were altered by SATB1 overexpression. CD127 expression was lower in *Satb1*^{Tg} naïve $CD8^+$ T cells and higher in *Satb1*^{Tg} T_{CM} and T_{EM} cells than in Ctrl cells (Figure 3.5F). CD62L expression was similar in naïve *Satb1*^{Tg} and Ctrl cells but increased in *Satb1*^{Tg} T_{CM} cells (Figure 3.5G). Overall, the data demonstrate that

the model of SATB1-overexpression is functional and thus suitable for further investigation.

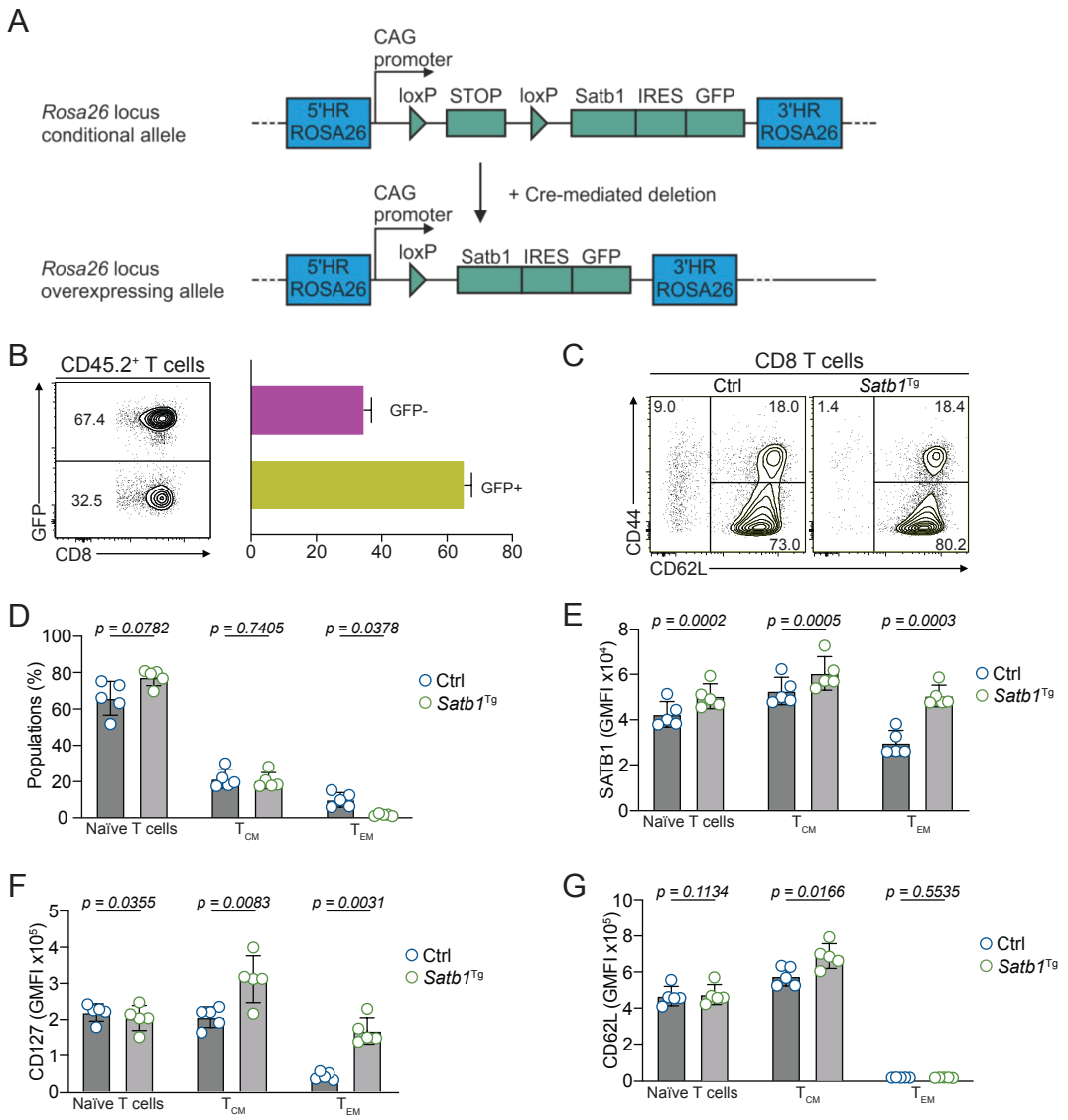

Figure 3.5: The *Rosa26*^{Satb1}/*Lck*^{Cre} (*Satb1*^{Tg}) mouse model
(A-J) Mixed bone marrow chimeric mice containing *Satb1*^{Tg} (CD45.2^{+}) and Ctrl T cells (CD45.1/2^{+}) used. spleens were harvested and analysed using flow cytometry. (A) Schemata of gene construct of Satb1tg mice. *Satb1-Ires-Gfp* is knocked into the *Rosa26* locus after a loxP-STOP-loxP sequence. Upon Cre expression, the STOP is deleted and SATB1-GFP is expressed. (B) Representative flow cytometry plot and quantification, showing GFP^{+} cells in *Satb1*^{Tg} cells. (C) Representative flow cytometry plots showing *Satb1*^{Tg} and Ctrl naïve CD62L^{+}CD44^{-} CD8^{+} T cells, CD62L^{+}CD44^{+} T_{CM} cells and CD62L^{-}CD44^{+} T_{EM} cells. (D) Quantification of *Satb1*^{Tg} and Ctrl naïve CD62L^{+}CD44^{-} CD8^{+} T cells, CD62L^{+}CD44^{+} T_{CM} cells and CD62L^{-}CD44^{+} T_{EM} cells. (E) Quantification of SATB1 expression in *Satb1*^{Tg} and Ctrl naïve CD62L^{+}CD44^{-} CD8^{+} T cells,

CD62L^{+}CD44^{+} T_{CM} cells and CD62L^{-}CD44^{+} T_{EM} cells. (F) Quantification of CD127 expression in *Satb1*^{Tg} and Ctrl naïve CD62L^{+}CD44^{-} CD8^{+} T cells, CD62L^{+}CD44^{+} T_{CM} cells and CD62L^{-}CD44^{+} T_{EM} cells. (G) Quantification of CD62L expression in *Satb1*^{Tg} and Ctrl naïve CD62L^{+}CD44^{-} CD8^{+} T cells, CD62L^{+}CD44^{+} T_{CM} cells and CD62L^{-}CD44^{+} T_{EM} cells. Dots in graphs represent individual mice; horizontal lines and error bars of bar graphs indicate means ± SEM, respectively. Data is representative of one independent experiment. P values are from unpaired student's t test.

Next, we tested how STAB1 overexpression impacts CD8 T cell differentiation during acute viral infection. To this end, we generated mixed bone marrow chimeric mice containing congenically marked *Satb1*^{Tg} and wild-type control (Ctrl) cells as described in the method section. Following reconstitution, the mice were infected with acute LCMV-Armstrong, and the effect of constant SATB1 expression was analysed in the spleen using flow cytometry (Figure 3.6A). We observed similar frequencies of antigen-specific gp33–H-2D^{b} tetramers+ cells (referred to as Gp33^{+} cells) in the *Satb1*^{Tg} cells and Ctrl cells compartments (Figure 3.6B). Consistent with this finding, no differences between the frequencies of activated CD44^{+} *Satb1*^{Tg} and Ctrl cells were observed (Figure 3.6C). Both CD44^{+} and Gp33^{+} *Satb1*^{Tg} cells expressed significantly less PD-1 at a single-cell level than Ctrl cells (Figure 3.6D). On the other hand, CD44^{+} *Satb1*^{Tg} cells displayed elevated levels of Tim-3 and reduced T-bet compared to Ctrl cells (Figure 3.6E and F). Additionally, *Satb1*^{Tg} cells exhibited increased frequencies of MPC and a corresponding decrease in SLEC compared to Ctrl cells (Figure 3.6G and H). This was evident in both the CD44^{+} and Gp33^{+} *Satb1*^{Tg} cells compartments (Figure 3.6G and H). Notably, CX3CR1^{+} cells were substantially reduced in *Satb1*^{Tg} cells among activated CD44^{+} and Gp33^{+} *Satb1*^{Tg} cells compared to Ctrl cells (Figure 3.6I and J). Overall, these data indicate that enforced SATB1 expression impairs effector differentiation but promotes accumulation of MPC.

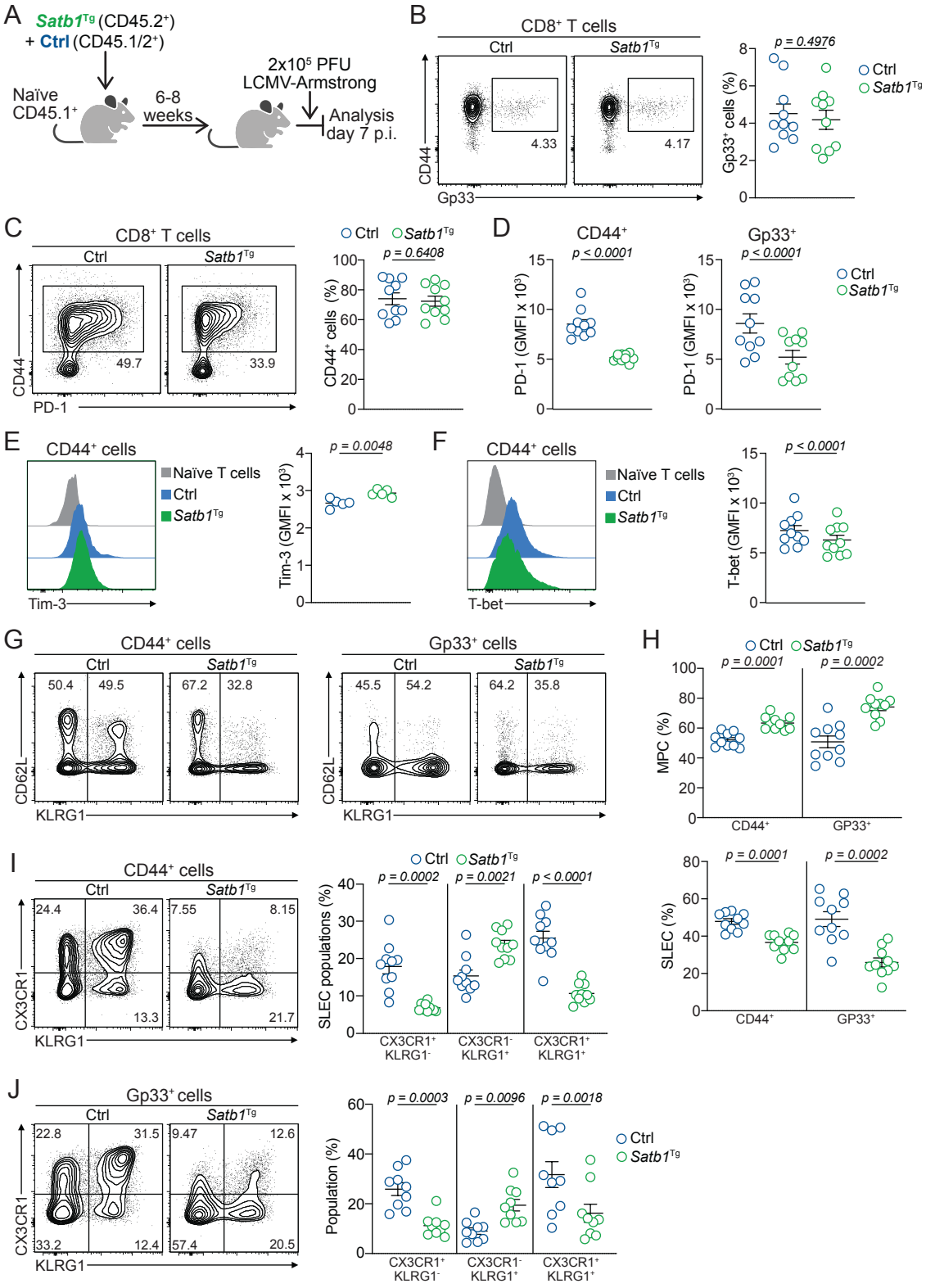

Figure 3.6: Overexpression of SATB1 promotes accumulation of MPC and reduces accumulation of SLEC, particular CX3CR1⁺ SLEC.
(A-J) Mixed bone marrow chimeric mice containing *Satb1*^{Tg} (CD45.2⁺) and Ctrl T cells (CD45.1/2⁺) were infected with LCMV-Armstrong. spleens were harvested

on day 7 p.i. and analysed using flow cytometry. (A) Schematic of experimental setup. (B) Representative flow cytometry plots and quantification of antigen specific Gp33^{+} *Satb1*^{Tg} and Ctrl cells. (C) Representative flow cytometry plots and quantification of activated CD44^{+} *Satb1*^{Tg} and Ctrl cells. (D) Quantification of PD-1 expression in CD44^{+} and Gp33^{+} *Satb1*^{Tg} and control cells. (E) Representative histogram showing Tim-3 expression in CD44^{+} *Satb1*^{Tg} or control cells. r (G) Representative flow cytometry plots showing frequencies of MPC (KLRG1^{+}) and SLEC (KLRG1^{-}) in CD44^{+} and Gp33^{+} *Satb1*^{Tg} or control cells. (H) Quantification of MPC (KLRG1^{+}) and SLEC (KLRG1^{-}) frequencies in CD44^{+} and Gp33^{+} *Satb1*^{Tg} or control cells. (I) Representative flow cytometry plots and quantification showing frequencies of CX3CR1^{+} and KLRG1^{+} CD44^{+} *Satb1*^{Tg} or control cells. (J) Representative flow cytometry plots and quantification showing frequencies of CX3CR1^{+} and KLRG1^{+} Gp33^{+} *Satb1*^{Tg} or control cells. Dots in graphs represent individual mice; horizontal lines and error bars of bar graphs indicate means ± SEM, respectively. Data is pooled or from two independent experiments. P values are from paired student's t test.

Lastly, we investigated whether enforced SATB1 expression affects the functionality of CD8 T cells by measuring their ability to produce GzmB and effector cytokines IFN-γ and TNF in response to Gp33 peptide restimulation. Overall, we observed no differences in the frequencies of IFN-γ and IFN-γ/TNF double-producing cells between CD44^{+} *Satb1*^{Tg} and Ctrl cells (Figure 3.7A). Additionally, both CD44^{+} Satb1^{Tg} and Ctrl cells expressed similar levels of IFN-γ and TNF on a single cell level (Figure 3.7A). Satb1^{Tg} SLEC cells exhibited a modest increase in the frequencies of IFN-γ^{+} cells compared to Ctrl cells, while we did not observe differences in the frequency of IFN-γ^{+} MPC (Figure 3.7B and C). In both SLEC and MPC populations, similar frequencies of IFN-γ/TNF double-producing cells were observed (Figure 3.7B-D). At the single cell level, the expression level of IFN-γ in MPC was increased in the Satb1^{Tg} cells compared to Ctrl cells but similar in SLEC (Figure 3.7D). The level of TNF per cell was similar in both Satb1^{Tg} and Ctrl MPC or SLEC (Figure 3.7D). Further Satb1^{Tg} cells displayed similar GzmB expression compared to Ctrl cells (Figure 3.7E).

In summary, we observed that SATB1 overexpression promotes differentiation of MPC and restrains differentiation of SLEC. Furthermore, the enforced SATB1 enhances IFN-γ cytokine production in SLEC.

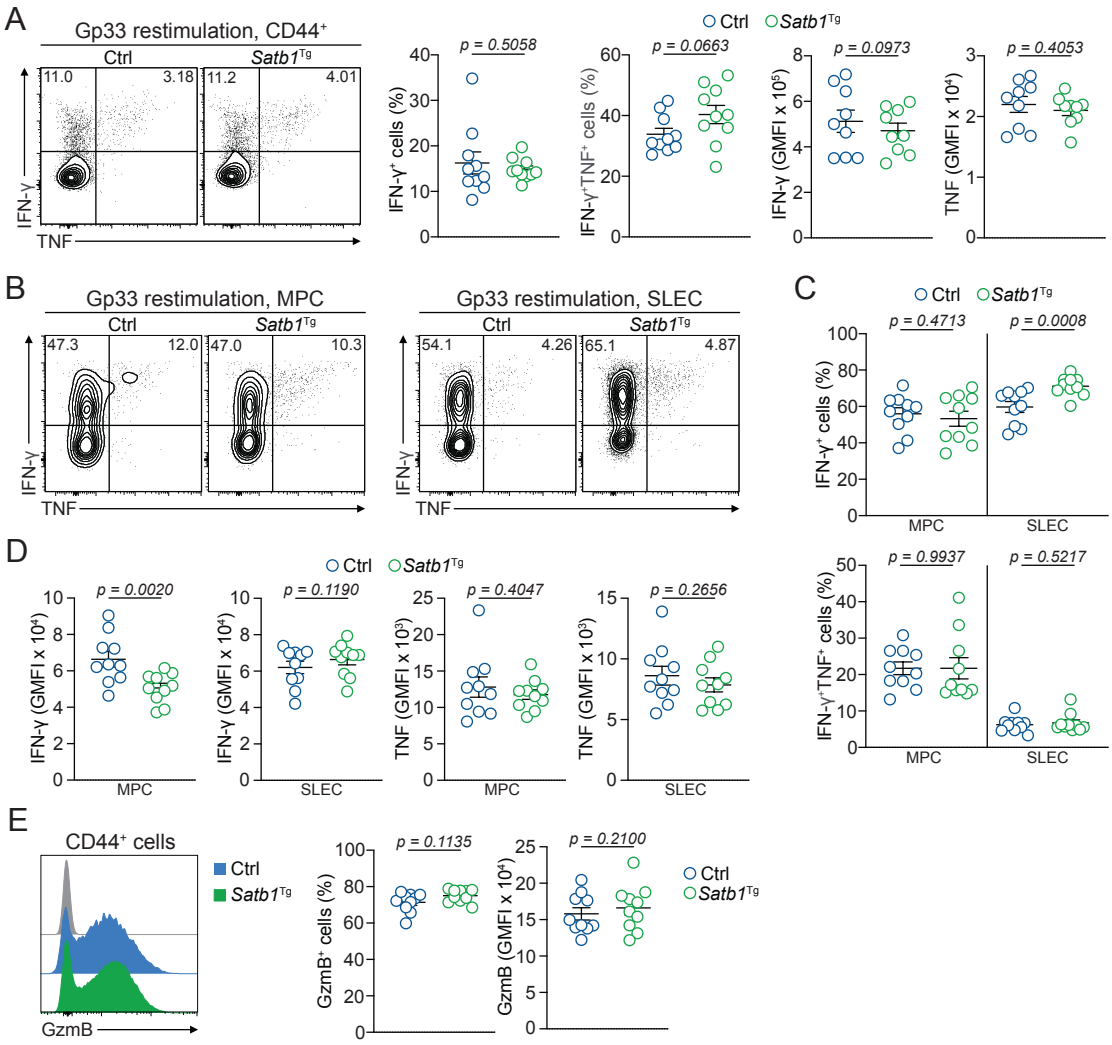

Figure 3.7: Enforced SATB1 expression enhances IFN-γ cytokine production in SLEC.

(A-E) Mixed bone marrow chimeric mice containing *Satb1*^{Tg} (CD45.2^{+}) and Ctrl T cells (CD45.1/2^{+}) were infected with LCMV-Armstrong. spleens were harvested on day 7 p.i. and analysed using flow cytometry. (A) Representative flow cytometry plots and quantification showing frequencies of CD44^{+} *Satb1*^{Tg} or Ctrl cells producing IFN-γ and TNF and quantification of IFN-γ and TNF expression on a single cell level after incubation with Gp33 peptide ex vivo. (B) Representative flow cytometry plots showing frequencies of *Satb1*^{Tg} or Ctrl MPC (KLRG1^{-}) and SLEC (KLRG1^{+}) producing IFN-γ and TNF after incubation with Gp33 peptide ex vivo. (C) Quantification of *Satb1*^{Tg} or Ctrl MPC and SLEC frequencies producing IFN-γ and TNF after incubation with Gp33 peptide ex vivo. (D) Quantification of IFN-γ and TNF expression in *Satb1*^{Tg} or Ctrl MPC and SLEC after incubation with Gp33 peptide ex vivo. (E) Representative histogram and quantification showing production of GzmB in CD44^{+} *Satb1*^{Tg} or Ctrl cells. Dots in graphs represent individual mice; horizontal lines and error bars of bar graphs indicate means ± SEM, respectively. Data is pooled from two independent experiments. P values are from paired student's t test.

3.2.3 Depletion of SATB1 impairs T_{CM} and T_{RM} formation and impairs functionality of memory $CD8^+$ T cells

To investigate whether the loss of SATB1 impacts the formation of $CD8^+$ T cell memory subsets, we adoptively transferred $CD45.2^+$ SATB-KO or Ctrl P14 cells into naïve $CD45.1^+$ recipients and infected the mice with LCMV-Armstrong. During the memory phase on day 26 post infection, spleens, liver and salivary glands were analysed using flow cytometry (Figure 3.8A) We observed reduced frequencies of SATB1-KO P14 cells compared to Ctrl P14 cells in the liver and salivary gland, while the frequencies of SATB1-KO P14 and Ctrl P14 cells were similar in the spleen (Figure 3.8B and C) Analysis of the spleen revealed a significant increase in frequencies of $CD62L^-$ T_{EM} cells with a concurrent decrease in $CD62L^+$ T_{CM} cells frequencies among SATB1-KO P14 cells compared to Ctrl P14 cells (Figure 3.8D and E). Numerically, SATB1-KO T_{CM} cells were reduced compared to Ctrl P14 cells (Figure 3.8E), while SATB1-KO T_{EM} cells numbers were similar to Ctrl P14 cells numbers (Figure 3.8E). In liver and salivary gland, we observed a substantial reduction of $CD69^+$ T_{RM} cells (Figure 3.8F and G), while the $CD103^+$ T_{RM} cells in the salivary glands were similar in frequencies between SATB1-KO and Ctrl P14 cells (Figure 3.8F and G).

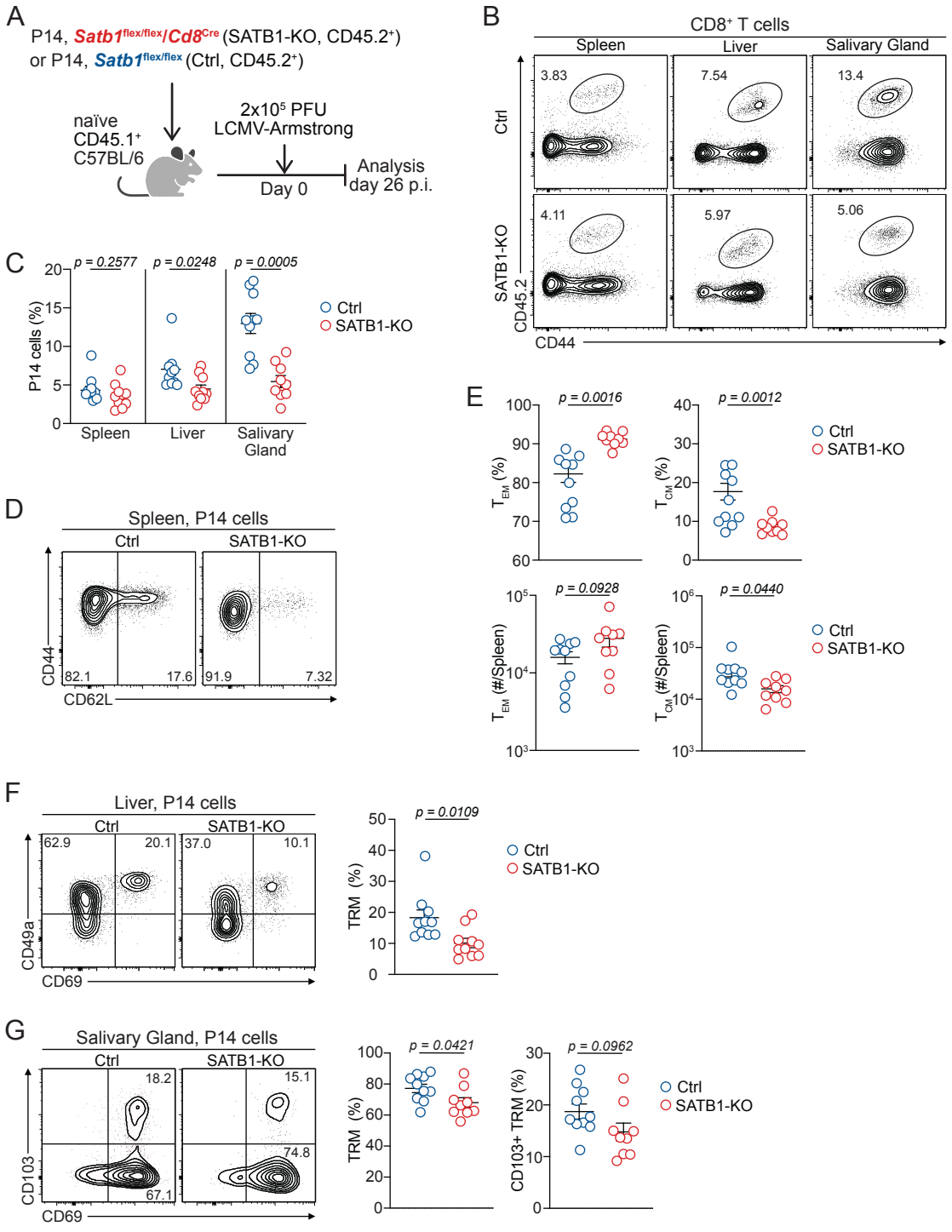

Figure 3.8: Depletion of SATB1 during memory formation impairs formation of T_{CM} and T_{RM} cells.

(A-G) Naïve CD45.2+ SATB1-KO P14 cells (*Satb1*$^{flex/flex}$/*Cd8*^{Cre}) or Ctrl P14 cells (*Satb1*$^{flex/flex}$) were adoptively transferred into naïve wildtype CD45.1+ mice and subsequently infected with LCMV-Armstrong. spleen, liver and salivary gland were harvested on day 26 p.i. during the memory phase and analysed using flow

cytometry. (A) Schematic of experimental setup. (B) Representative flow cytometry plots and (C) quantification showing frequencies of SATB1-KO and Ctrl P14 cells among CD8 T cells in different organs. (D) Representative flow cytometry plots and (E) quantification showing frequencies and numbers per spleen of SATB1-KO and Ctrl T_{CM} and T_{EM} cells. (F) Representative flow cytometry plots and quantification showing frequencies of SATB1-KO and Ctrl $CD69^+$ TRM cells in the liver. (G) Representative flow cytometry plots and quantification showing frequencies of SATB1-KO and Ctrl $CD69^+$ and $CD103^+$ TRM cells in the salivary gland. Dots in graphs represent individual mice; horizontal lines and error bars of bar graphs indicate means ± SEM, respectively. Data is pooled from two independent experiments. P values are from unpaired student's t test.

Consistent with our findings during the acute infection phase, memory $CD8^+$ T cells exhibited diminished capabilities to produce effector cytokines. We observed reduced frequencies of IFN-γ^+ cells and IFN-γ/TNF co-producing SATB1-KO P14 cells compared to Ctrl P14 cells (Figure 3.9A). This was further evidenced by decreased expression levels of IFN-γ and TNF at a single cell level (Figure 3.9A). Both SATB1-KO T_{CM} and T_{EM} cells exhibited reduced frequencies of IFN-γ^+ cells and IFN-γ^+TNF^+ co-producing cells as well reduced expression levels of IFN-γ and TNF compared to Ctrl cells (Figure 3.9B and C).

In summary, we observed that the loss of SATB1 impaired the formation of T_{CM} and T_{RM} cells while it had less impact on T_{EM} cells. Further the absence of SATB1 impaired cytokine production in T_{CM} and T_{EM} cells.

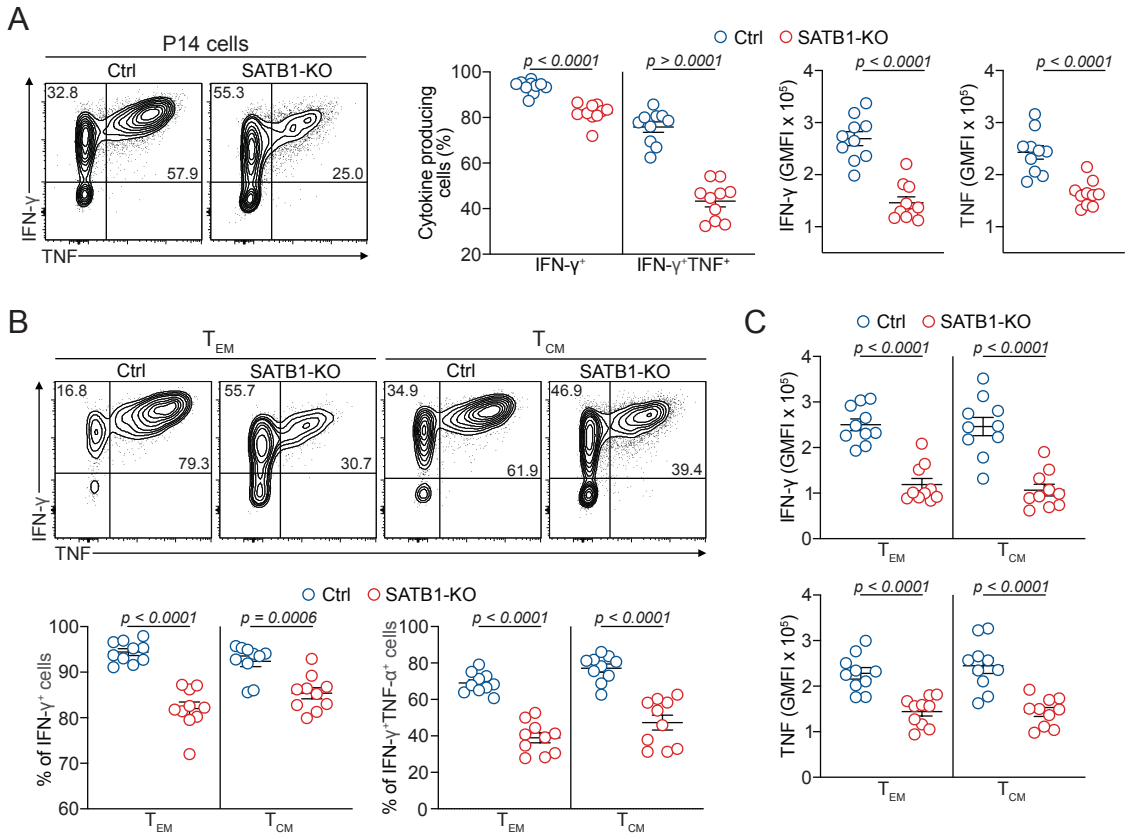

Figure 3.9: Depletion of SATB1 impairs cytokine production in memory CD8⁺ T cells.

(A-C) Naïve CD45.2⁺ SATB1-KO P14 cells (*Satb1*$^{flex/flex}$/*Cd8*^{Cre}) or Ctrl P14 cells (*Satb1*$^{flex/flex}$) were adoptively transferred into naïve wildtype CD45.1⁺ mice and subsequently infected with LCMV-Armstrong. spleens were harvested on day 26 p.i. during the memory phase and analysed using flow cytometry. (A) Representative flow cytometry plots and quantifications of frequencies of IFN-γ and TNF producing SATB1-KO or Ctrl P14 cells and IFN-γ and TNF expression on a single cell level after incubation with Gp33 peptide *ex vivo*. (B) Representative flow cytometry plots and quantifications of frequencies of IFN-γ and TNF producing SATB1-KO or Ctrl T_{EM} and T_{CM} cells after incubation with Gp33 peptide *ex vivo*. (D) Quantification of IFN-γ and TNF expression on a single cell level in SATB1-KO or Ctrl T_{EM} and T_{CM} cells after incubation with Gp33 peptide *ex vivo*. Dots in graphs represent individual mice; horizontal lines and error bars of bar graphs indicate means ± SEM, respectively. Data is pooled from two independent experiments. P values are from unpaired student's t test.

3.2.4 Enforced SATB1 expression promotes formation of T_{CM} and T_{RM} cells and enhances effector cytokine production in T_{EM} cells

We next investigated how enforced SATB1 expression impacted T_{RM} and T_{CM} formation and function. To this end, we used the *Satb1*^{Tg} mouse model and generated mixed bone marrow chimeric mice with *Satb1*^{Tg} and Ctrl cells that were infected with acute LCMV-Armstrong after reconstitution. Spleens, livers and salivary glands were analysed on day 28 post infection during the memory phase using flow cytometry (Figure 3.10A). We observed a decrease of *Satb1*^{Tg} CD62L^{-} T_{EM} cells in the spleen, by approximately 30 % compared to Ctrl T_{EM} cells and an increase of approximately 30 % in *Satb1*^{Tg} CD62L^{+} T_{CM} cells (Figure 3.10C). The CD69^{+} T_{RM} population in the liver was significantly increased among *Satb1*^{Tg} cells compared to Ctrl cells (Figure 3.10D). In the salivary gland, however, no differences were observed between *Satb1*^{Tg} and Ctrl CD69^{+} T_{RM} cells (Figure 3.10E), while the frequencies of CD103^{+}CD69^{+} *Satb1*^{Tg} T_{RM} cells were reduced compared to Ctrl cells (Figure 3.10E). These results indicate that enforced SATB1 promotes formation of T_{CM} and T_{RM} cells while impairing the formation of T_{EM} cells.

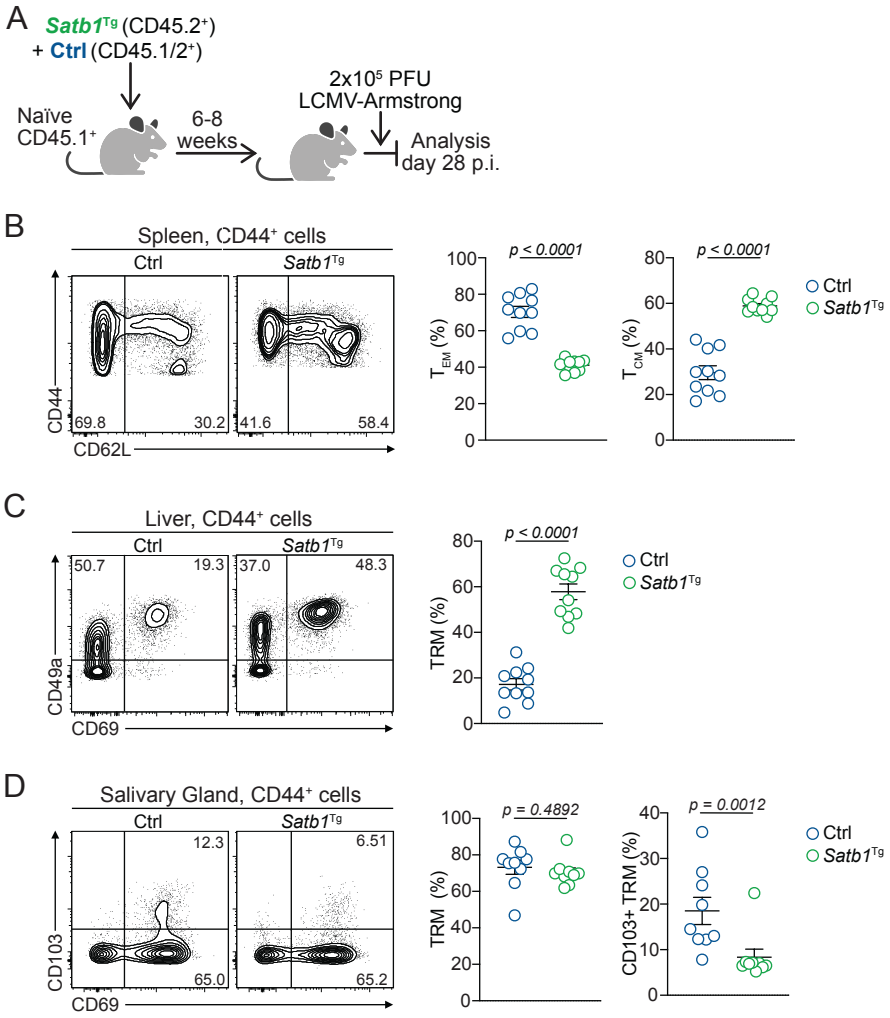

Figure 3.10: Enforced SATB1 expression promotes formation of T_{CM} and T_{RM} cells.

(A-D) Mixed bone marrow chimeric mice containing *Satb1*^{Tg} (CD45.2$^+$) and Ctrl T cells (CD45.1/2$^+$) were infected with LCMV-Armstrong. spleens were harvested on day 28 p.i. and analysed using flow cytometry. (A) Schematic of experimental setup. (B) Representative flow cytometry plots and quantification showing frequencies of *Satb1*^{Tg} and Ctrl T_{CM} and T_{EM} cells in the spleen. (C) Representative flow cytometry plots and quantification showing frequencies of *Satb1*^{Tg} and Ctrl CD69$^+$ TRM cells in the liver. (D) Representative flow cytometry plots and quantification showing frequencies of *Satb1*^{Tg} and Ctrl CD69$^+$ and CD103$^+$ TRM cells in the salivary gland. Dots in graphs represent individual mice; horizontal lines and error bars of bar graphs indicate means ± SEM, respectively. Data is pooled from two independent experiments. P values are from paired student's t test.

Lastly, we examined whether the enforced SATB1 expression affects effector functions in T_{CM} and T_{EM} cells by assessing the capacity to produce effector cytokines IFN-γ and TNF upon restimulation *ex vivo* in the spleen. We therefore stimulated the cells with Gp33 peptide or Ionomycin and PMA. Overall, we observed in $CD44^+$ cells stimulated with Gp33 an increase in frequencies of IFN-γ^+ cells in the *Satb1*^{Tg} cells compartment compared to the Ctrl cells (Figure 3.11A). Furthermore, *Satb1*^{Tg} cells exhibited increased frequencies of IFN-γ^+TNF$^+$ co-producing cells compared to Ctrl cells. The levels of TNF were higher in $CD44^+$ *Satb1*^{Tg} cells than in $CD44^+$ Ctrl cells on a single cell level, while expression of IFN-γ^+ was similar in both (Figure 3.11A). Similar results were observed, when cells were stimulated with Ionomycin and PMA. The frequencies of both IFN-γ^+ and IFN-γ^+TNF$^+$ *Satb1*^{Tg} cells were increased compared to Ctrl cells (Figure 3.11B). Expression levels of both IFN-γ and TNF were increased in the *Satb1*^{Tg} cells compared to Ctrl cells (Figure 3.11B). We further sought to assess the capability of T_{CM} and T_{EM} to produce cytokines. *Satb1*^{Tg} T_{CM} cells exhibited similar frequencies of IFN-γ^+ and IFN-γ^+TNF$^+$ co-producing cells compared to Ctrl cells (Figure 3.11D). The expression levels of IFN-γ were reduced in *Satb1*^{Tg} T_{CM}, whereas TNF levels were increased compared to Ctrl cells (Figure 3.11D). On the contrary, *Satb1*^{Tg} T_{EM} cells exhibited increased frequencies of IFN-γ^+ and IFN-γ^+TNF$^+$ co-producing cells compared to Ctrl cells, which was accompanied by increased expression levels of TNF but not IFN-γ (Figure 3.11D).

Thus, overall, during acute viral infection, SATB1 limits differentiation of SLEC and T_{EM} cells, while promoting the differentiation of MPC, T_{CM} and T_{RM} cells. Furthermore, SATB1 promotes production of effector cytokines IFN-γ and TNF. Thus, precise regulation of SATB1 expression is crucial in $CD8^+$ T cells during acute viral infection.

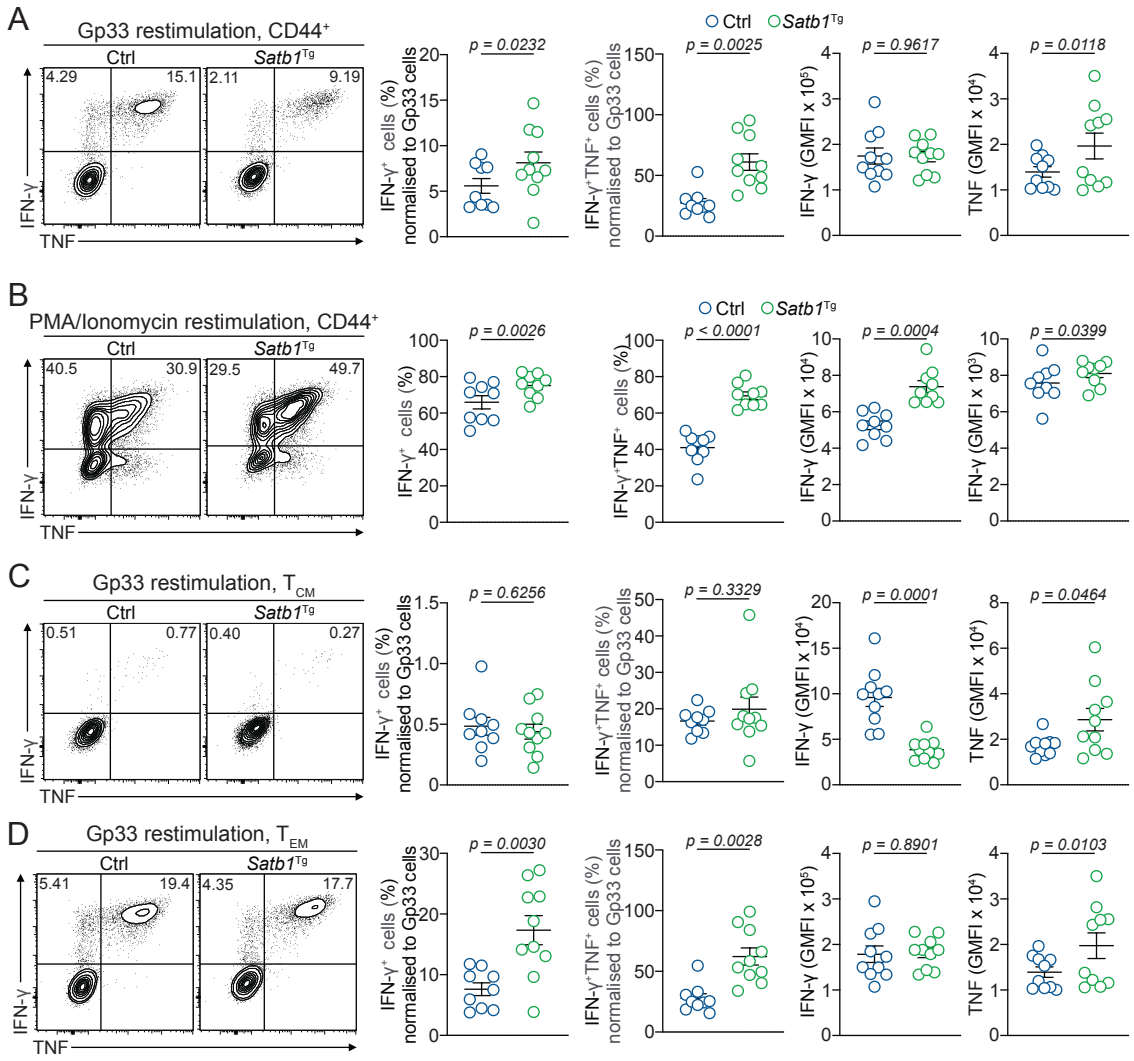

Figure 3.11: Enforced SATB1 expression enhances the capacity to produce effector cytokines in T_{EM} cells.

(A-D) Mixed bone marrow chimeric mice containing *Satb1*^{Tg} (CD45.2$^+$) and Ctrl T cells (CD45.1/2$^+$) were infected with LCMV-Armstrong. spleens were harvested on day 28 p.i. and analysed using flow cytometry. Cells were stimulated *ex vivo* with either Gp33 peptide (A, C and D) or with PMA/Ionomycin (B). (A) Representative flow cytometry plots and quantification showing frequencies of CD44$^+$ *Satb1*^{Tg} or Ctrl cells producing IFN-γ and TNF and quantification of IFN-γ and TNF expression on a single cell level. (B) Representative flow cytometry plots and quantification showing frequencies of CD44$^+$ *Satb1*^{Tg} or Ctrl cells producing IFN-γ and TNF and quantification of IFN-γ and TNF expression on a single cell level. (C) Representative flow cytometry plots and quantification showing frequencies of *Satb1*^{Tg} or Ctrl T_{CM} cells producing IFN-γ and TNF and quantification of IFN-γ and TNF expression on a single cell level. (D) Representative flow cytometry plots and quantification showing frequencies of *Satb1*^{Tg} or Ctrl T_{EM} cells producing IFN-γ and TNF and quantification of IFN-γ and TNF expression on a single cell level. Dots in graphs represent individual mice; horizontal lines and error bars of bar graphs indicate means ± SEM,

respectively. Data is pooled from two independent experiments. P values are from paired student's t test.

3.2.5 Deletion of SATB1 enhances T_{EX} differentiation and impairs cytokine production in exhausted T cells during chronic infection.

We next investigated the role of SATB1 CD8 T cells responding to chronic infection. Previously published RNA sequencing datasets revealed that SATB1 RNA levels were upregulated in T_{PEX} but largely absent in T_{EX} cells (Tsui *et al.*, 2022). To test this observation on a protein level, CD45.1$^+$ P14 cells were adoptively transferred into naïve CD45.2$^+$ recipients and infected with LCMV-Docile, and the expression of SATB1 in T_{PEX} and T_{EX} cell was assessed on day 21 post infection using flow cytometry (Figure 3.12A). T_{PEX} cells expressed SATB1 albeit at a reduced level compared to naïve CD8$^+$ T cells. Among T_{PEX} cells, CD62L$^+$ cells expressed the highest levels of SATB1 (Figure 3.12B). Effector-like CX3CR1$^+$ T_{EX} cells on the other hand, and terminally exhausted CD101$^+$ T_{EX} cells exhibited low to no SATB1 expression (Figure 3.12B). The same expression patterns were observed in the polyclonal exhausted PD-1$^+$ CD8$^+$ T cells (Figure 3.12C).

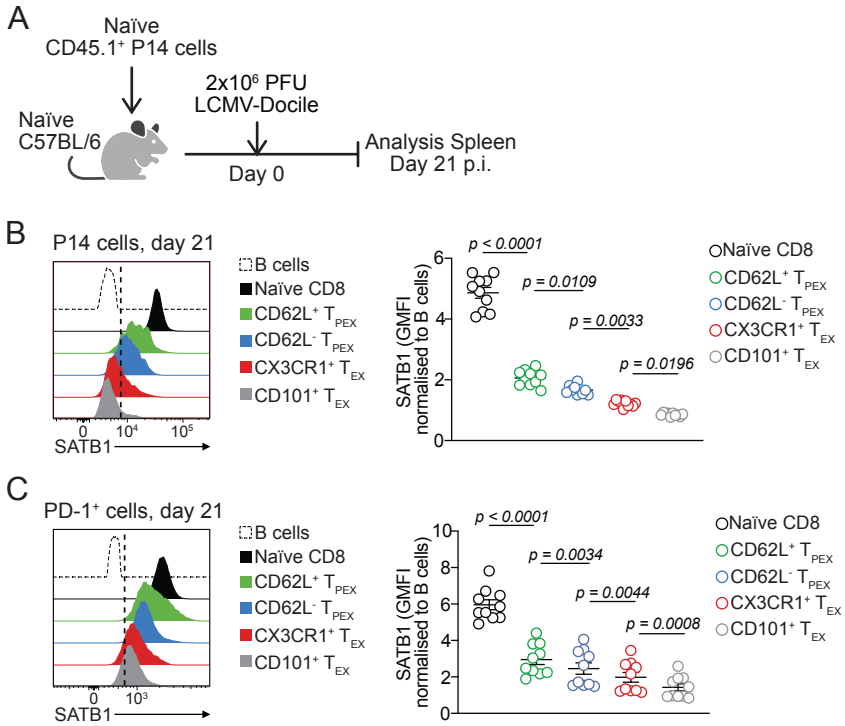

Figure 3.12: SATB1 is expressed in T_{PEX} cells and downregulated in during the differentiation of T_{EX} cells.
(A-C) Naïve CD45.1$^+$ P14 cells were adoptively transferred into naïve wildtype CD45.2$^+$ mice and infected with LCMV-Docile. spleens were harvested on day 21 p.i. and analysed using flow cytometry. (A) Schematic of experimental setup. (B) Representative histogram and quantification showing the expression of SATB1 in CD62L$^+$ and CD62L$^-$ T_{PEX}, CX3CR1$^+$ T_{EX} and CD101$^+$ T_{EX} P14 cells compared to naïve CD8 T cells and B cells. (C) Representative histogram and quantification showing the expression of SATB1 in polyclonal PD-1$^+$ CD62L$^+$ and CD62L$^-$ T_{PEX}, CX3CR1$^+$ T_{EX} and CD101$^+$ T_{EX} cells compared to naïve CD8 T cells and B cells. Dots in graphs represent individual mice; horizontal lines and error bars of bar graphs indicate means ± SEM, respectively. Data is pooled from two independent experiments. P values are from two-way ANOVA test.

To test the role of SATB1 in the differentiation and functionality of T_{PEX} and T_{EX} cells, we adoptively transferred SATB1-KO or Ctrl P14 cells into congenically marked recipient mice, which were subsequently infected with chronic LCMV-Docile. P14 cells in the spleen were analysed on day 12 and day 21 post infection using flow cytometry (Figure 3.13A). We observed increased frequencies and numbers of SATB1-KO P14 cells compared to Ctrl cells on both days (Figure 3.13B and C). In contrast to acute infection, loss of SATB1 did not alter the expression of PD-1 in the spleen on either day, with both SATB1-KO and Ctrl P14 cells exhibiting similar expression levels of PD-1 (Figure 3.13D). Similarly, no changes in the expression of TOX were observed between the SATB1-KO and Ctrl P14 cells (Figure 3.13E).

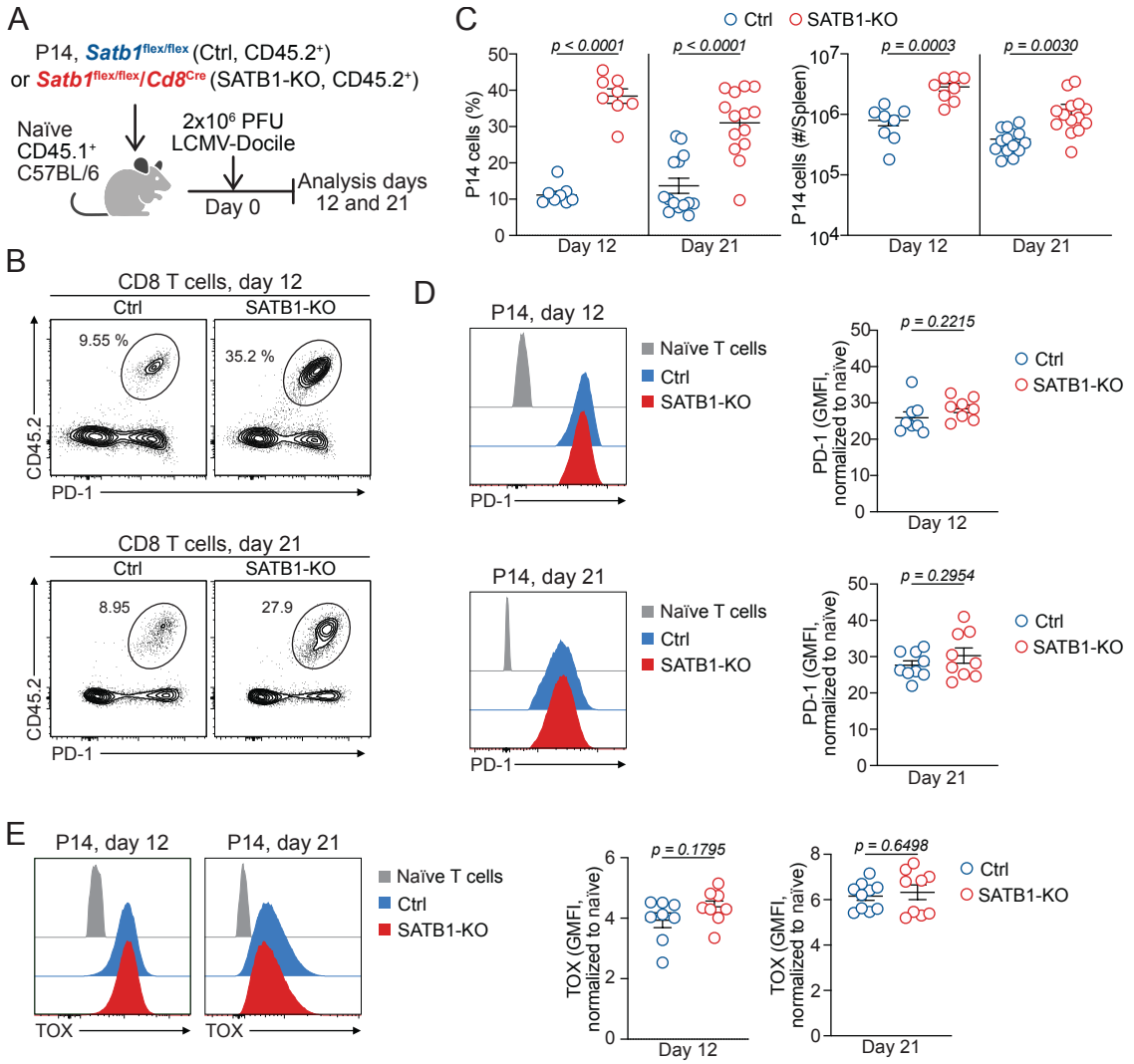

Figure 3.13: Depletion of SATB1 enhances exhausted T cell accumulation during chronic infection.

(A-E) Naïve CD45.2$^+$ SATB1-KO P14 cells (*Satb1*$^{flex/flex}$/*Cd8*^{Cre}) or Ctrl cells (*Satb1*$^{flex/flex}$) P14 cells were adoptively transferred into naïve wildtype CD45.1$^+$ mice and subsequently infected with LCMV-Docile. On days 12 and 21 p.i., spleens were analysed using flow cytometry. (A) Schematic of experimental setup. (B) Representative flow cytometry plots showing frequencies of SATB1-KO or Ctrl P14 (CD45.2$^+$) cells. (C) Quantification showing frequencies and numbers of SATB1-KO or Ctrl cells per spleen. (D) Representative histogram and quantification showing expression of PD-1 in SATB1-KO or Ctrl P14 cells compared to naïve cells. (E) Representative histogram and quantification showing expression of TOX in SATB1-KO or Ctrl P14 cells compared to naïve cells. Dots in graphs represent individual mice; horizontal lines and error bars of bar graphs indicate means ± SEM, respectively. Data is pooled or from two (C for day 12; D and E) or three (C for day 21) independent experiments. P values are from unpaired student's t test.

We next compared the frequency of both T_{PEX} and T_{EX} cells between Ctrl and SATB1-KO in the spleen. We observed reduced frequencies of SATB1-KO T_{PEX} cells compared to Ctrl T_{PEX} cells on both days with a corresponding increase in T_{EX} cells (Figure 3.14A). Numerically, however, SATB1-KO T_{PEX} cells on day 12 p.i. were increased while there were no differences on day 21 p.i. compared to Ctrl cells (Figure 3.14A), indicating that the accumulation of T_{PEX} cells was not impaired by the loss of SATB1. The total number of T_{EX} per spleen was considerably increased for SATB1-KO T_{EX} cells compared to Ctrl T_{EX} cells on both days (Figure 3.14A). We next examined expression of the T_{PEX} associated molecules TCF1 and Ly108. We observed no differences in the expression of TCF1 in SATB1-KO T_{PEX} cells, but decreased levels of Ly108 compared to Ctrl T_{PEX} cells (Figure 3.14B). While there were decreased frequencies of SATB1-KO CD62L$^+$ T_{PEX} compared to Ctrl cells, the total number of SATB1-KO CD62L$^+$ T_{PEX} cells was similar in both (Figure 3.14C and D).

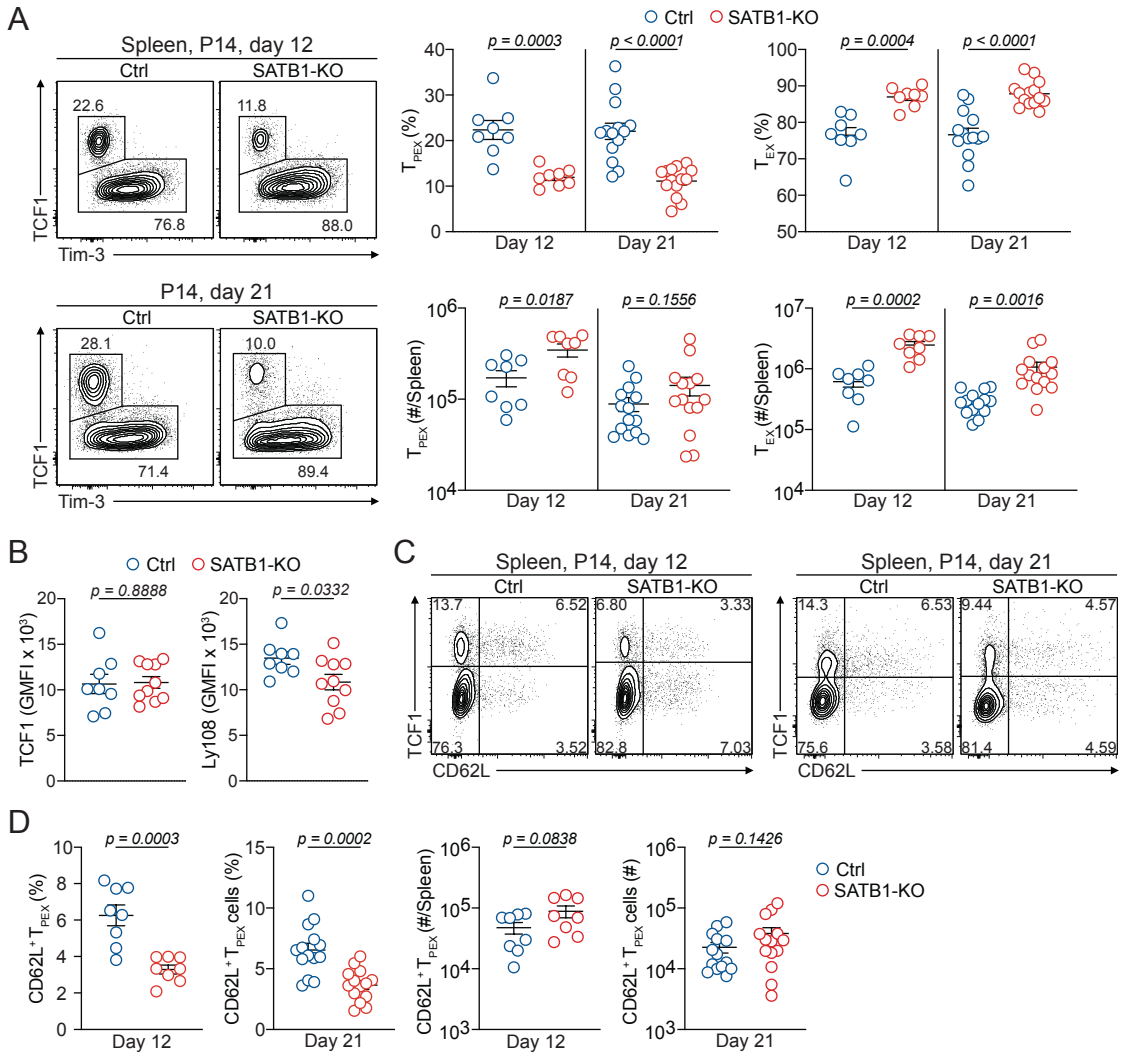

Figure 3.14: The loss of SATB1 enhances T_{EX} accumulation but has no major impact on T_{PEX} cells.

(A-D) Naïve CD45.2⁺ SATB1-KO P14 cells (*Satb1*$^{flex/flex}$/*Cd8*^{Cre}) or Ctrl cells (*Satb1*$^{flex/flex}$) P14 cells were adoptively transferred into naïve wildtype CD45.1⁺ mice and subsequently infected with LCMV-Docile. On days 12 and 21 p.i. spleens were analysed using flow cytometry. (A) Representative flow cytometry plots and quantification showing frequencies and numbers of SATB1-KO or Ctrl T_{PEX} (TCF1⁺Tim-3⁻) or T_{EX} (TCF1⁻Tim-3⁺) cells. (B) Quantification of TCF1 and Ly108 expression in SATB1-KO or Ctrl T_{PEX} on day 21. (C) Representative flow cytometry plots showing frequencies of SATB1-KO or Ctrl CD62L⁺ T_{PEX} (TCF1⁺CD62L⁺) or CD62L⁻ T_{PEX} (TCF1⁺CD62L⁻) cells. (D) Quantification showing frequencies and numbers of SATB1-KO or Ctrl CD62L⁺ T_{PEX} cells. Dots in graphs represent individual mice; horizontal lines and error bars of bar graphs indicate means ± SEM, respectively. Data is pooled or from two (day 12) or three (day 21) independent experiments. P values are from unpaired student's t test.

To evaluate whether the enhanced accumulation of SATB1-KO T_{EX} cells was attributable to a specific T_{EX} population, we compared the frequencies of CX3CR1$^+$ and CD101$^+$ T_{EX} subsets between Ctrl and SATB1-KO cells in the spleen. On day 12, frequencies of CX3CR1$^+$ and CD101$^+$ T_{EX} cells similar in KO and Ctrl cells (Figure 3.15A and B). Numerically, however, both CX3CR1$^+$ and CD101$^+$ SATB1-KO T_{EX} cells were increased in the spleen compared to Ctrl cells (Figure 3.15B). On day 21 p.i., similar results were observed (Figure 3.15A and C). We did not observe significant changes in the expression of the inhibitory receptors 2B4, CD39 and Tim-3 among Ctrl and SATB1-KO T_{EX} cells on day 21 p.i., while expression levels of Lag-3 were reduced in the SATB1-KO T_{EX} cells (Figure 3.15D). Collectively, our data indicate that the loss of SATB1 enhanced the differentiation or expansion of both CX3CR1$^+$ and CD101$^+$ T_{EX} cells. Furthermore, SATB1 did not alter expression of most inhibitory receptors, but Lag-3 expression was impaired by the loss of SATB1.

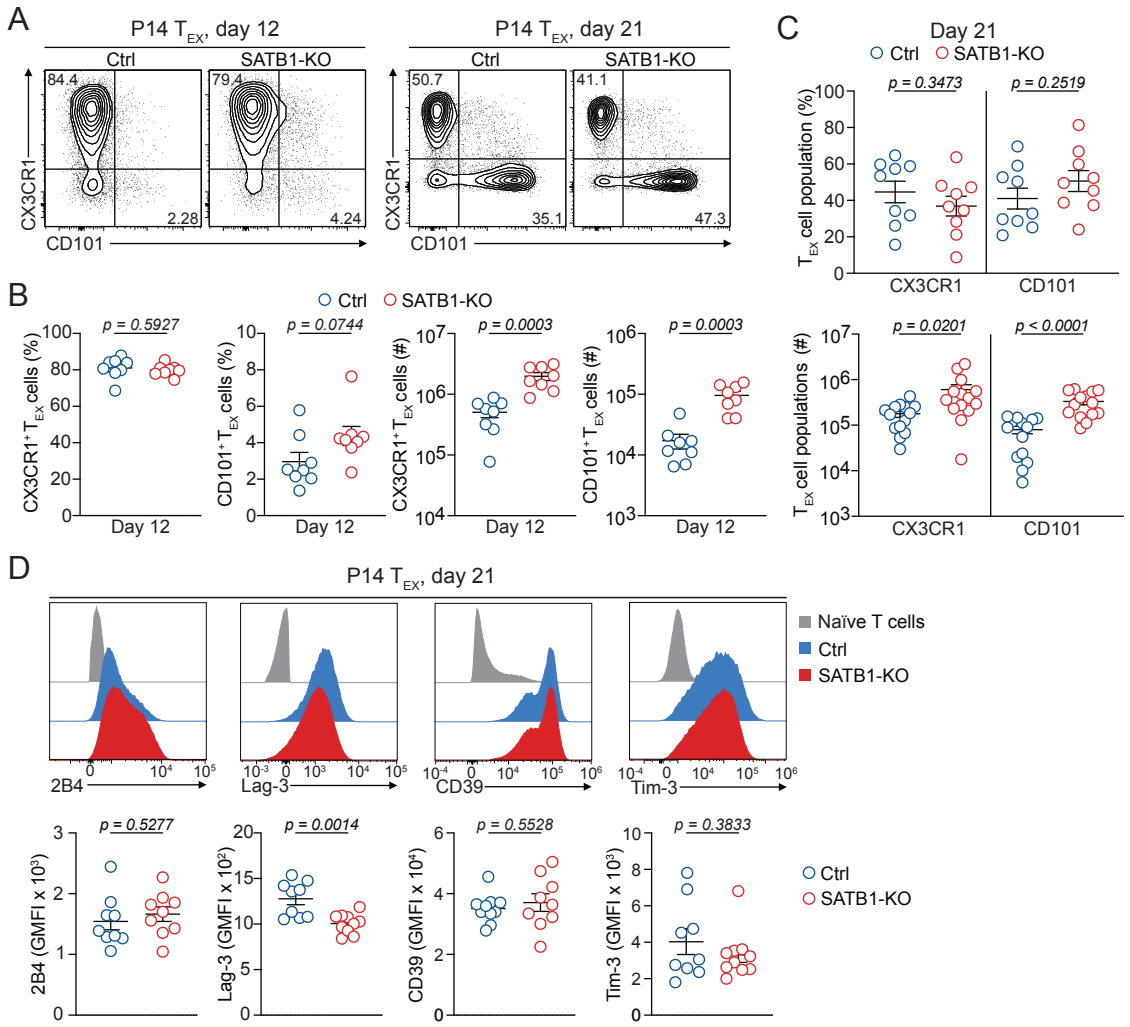

Figure 3.15: Depletion of SATB1 enhance accumulation of both CX3CR1⁺ and CD101⁺ T_{EX} cells.

(A-D) Naïve CD45.2⁺ SATB1-KO P14 cells (*Satb1*$^{flex/flex}$/*Cd8*^{Cre}) or Ctrl cells (*Satb1*$^{flex/flex}$) P14 cells were adoptively transferred into naïve wildtype CD45.1⁺ mice and subsequently infected with LCMV-Docile. On days 12 and 21 p.i. spleens were analysed using flow cytometry. (A) Representative flow cytometry plots showing frequencies of SATB1-KO or Ctrl CX3CR1⁺ T_{EX} or CD101⁺ T_{EX} cells. (B) Quantification showing frequencies and numbers of SATB1-KO or Ctrl CX3CR1⁺ T_{EX} or CD101⁺ T_{EX} cells on day 12. (C) Quantification showing frequencies and numbers of SATB1-KO or Ctrl CX3CR1⁺ T_{EX} or CD101⁺ T_{EX} cells on day 21. (D) Representative histograms and quantification showing expression of inhibitory receptors Lag-3, 2B4 (CD244), CD39 and Tim-3 in SATB1-KO or Ctrl T_{EX} cells compared to naïve CD8 T cells. Dots in graphs represent individual mice; horizontal lines and error bars of bar graphs indicate means ± SEM, respectively. Data is pooled or from two (day 12; D) or three (day 21) independent experiments. P values are from unpaired student's t test.

We next assessed the capacity to produce effector cytokines IFN-γ and TNF upon restimulation *ex vivo* in the spleen as well as the capacity to produce GzmB. In general, SATB1-KO P14 cells exhibited a reduced capacity to produce effector cytokines. The frequencies of SATB1-KO IFN-γ^+ cells on days 12 and 21 were decreased compared to Ctrl P14 cells (Figure 3.16A and B). Furthermore, the frequencies of polyfunctional IFN-γ/TNF double-producing cells were reduced in SATB1-KO P14 cells on day 21 but were similar on day 12 compared to Ctrl P14 cells (Figure 3.16A and B). At the single-cell level, the amount of IFN-γ and TNF expression in SATB1-KO P14 cells was also decreased on day 12 p.i. compared to that in Ctrl P14 cells (Figure 3.16A). SATB1-KO P14 cells expressed lower levels of IFN-γ on day 21 p.i. compared to Ctrl P14 cells, while expression levels of TNF were similar between both groups (Figure 3.16B). On day 12, SATB1-KO T_{PEX}, but not T_{EX} cells, displayed reduced frequencies of IFN-γ producing cells compared to Ctrl T_{PEX} cells (Figure 3.16C and D). Both SATB1-KO and Ctrl T_{PEX} and T_{EX} cells had similar frequencies of polyfunctional IFN-γ/TNF double-producing cells (Figure 3.16C and D). On day 21 p.i., SATB1-KO T_{PEX} and T_{EX} cells exhibited increased frequencies of IFN-γ^+ cells, but no major differences were observed in the frequencies of polyfunctional IFN-γ/TNF double-producing cells compared to the Ctrl T_{PEX} and T_{EX} cells (Figure 3.16E and F). Furthermore, it was observed that SATB1-KO T_{EX} cells produced reduced levels of GzmB on both days compared to Ctrl T_{EX} cells (Figure 3.16G).

In summary, SATB1 is expressed in T_{PEX} cells but lost during T_{EX} differentiation. It regulates P14 cell accumulation in the spleen and specifically impairs T_{EX} differentiation while sparing T_{PEX} cells. Additionally, SATB1 is essential for efficient cytokine production.

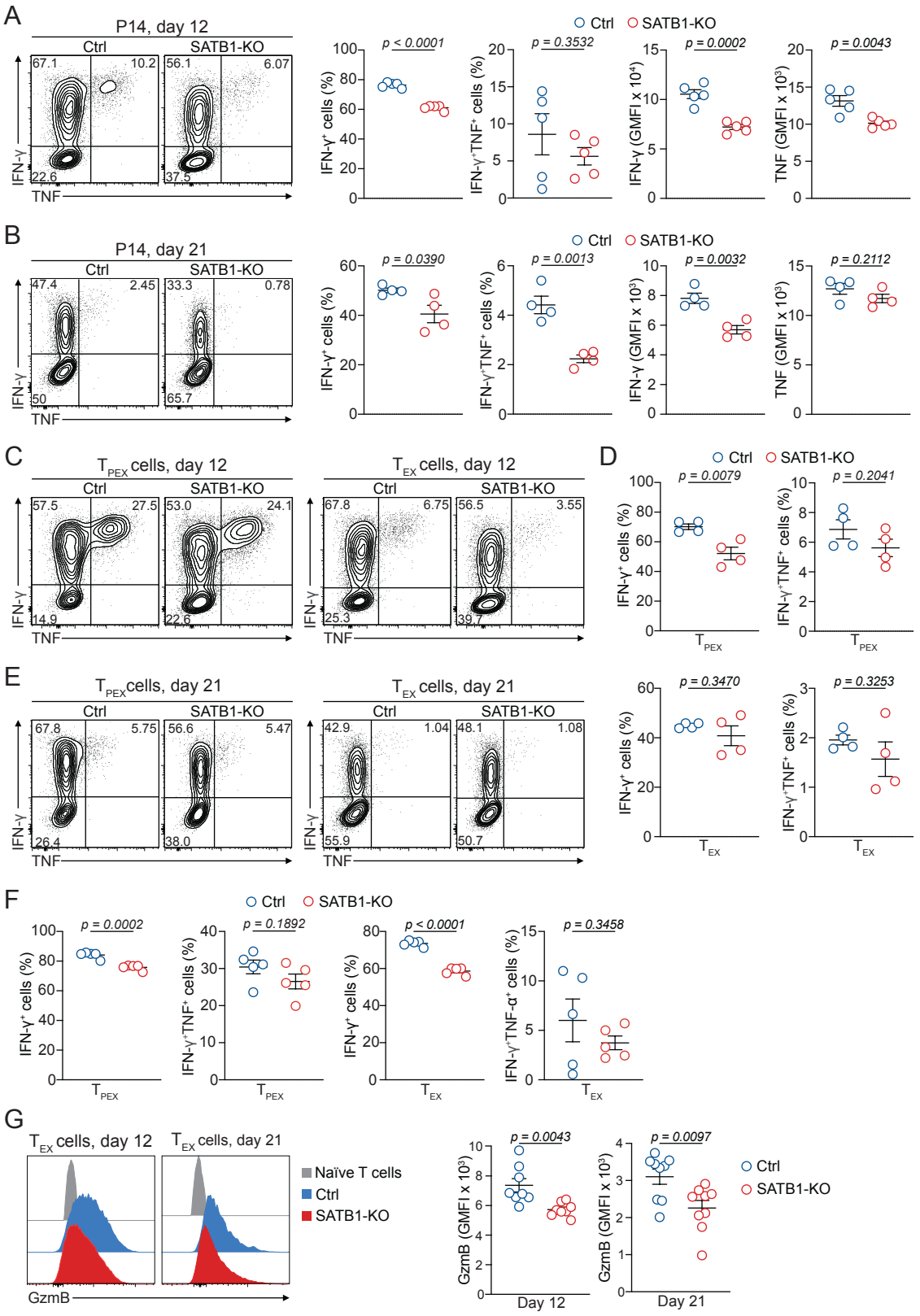

Figure 3.16: Loss of SATB1 impairs effector function in T_{PEX} and T_{EX} cells during chronic viral infection.

(A-G) Naïve CD45.2$^+$ SATB1-KO P14 cells (*Satb1*$^{flex/flex}$/*Cd8*^{Cre}) or Ctrl cells (*Satb1*$^{flex/flex}$) P14 cells were adoptively transferred into naïve wildtype CD45.1$^+$ mice and subsequently infected with LCMV-Docile. On days 12 and 21 p.i. spleens were analysed using flow cytometry. Splenocytes were stimulated with Gp33 peptide *ex vivo.* (A) Representative flow cytometry plots and quantifications of frequencies of IFN-γ and TNF producing SATB1-KO or Ctrl P14 cells and IFN-γ and TNF expression on a single cell level on day 12 and (B) day 21. (C) Representative flow cytometry plots showing frequencies of IFN-γ and TNF producing SATB1-KO or Ctrl T_{PEX} and T_{EX} cells on day 12. (D) Quantification of frequencies of IFN-γ and TNF producing SATB1-KO or Ctrl T_{PEX} and T_{EX} cells and IFN-γ and TNF expression on a single cell level on day 12. (E) Representative flow cytometry plots showing frequencies of IFN-γ and TNF producing SATB1-KO or Ctrl T_{PEX} and T_{EX} cells on day 21. (F) Quantification of frequencies of IFN-γ and TNF producing SATB1-KO or Ctrl T_{PEX} and T_{EX} cells and IFN-γ and TNF expression on a single cell level on day 21. (G) Representative histograms and quantification showing GzmB production in SATB1-KO or Ctrl T_{EX} cells. Dots in graphs represent individual mice; horizontal lines and error bars of bar graphs indicate means ± SEM, respectively. Data is representative of one (A-F) experiment or pooled from two independent experiments (G). P values are from unpaired student's t test.

3.2.6 Downregulation of SATB1 is required for T_{EX} differentiation

SATB1 is expressed in T_{PEX} cells but downregulated in T_{EX} cells. To determine whether SATB1 downregulation is required for T_{EX} differentiation, we made use of the *Satb1*^{Tg} model, in which SATB1 expression was enforced in CD8$^+$ T cells (Figure 3.5). To examine intrinsic effects on CD8$^+$ T cells, mixed bone marrow chimeric mice with *Satb1*^{Tg} and Ctrl cells were generated, infected with chronic LCMV-Docile and analysed 12 and 21 days post-immunization (Figure 3.17A). Enforced expression of SATB1 resulted in reduced frequencies of antigen-specific Gp33$^+$ CD8$^+$ T cells in *Satb1*^{Tg} cells compared to Ctrl cells on day 12 (Figure 3.17B) and day 21 of infection, with approximately eight times more Gp33$^+$ Ctrl CD8$^+$ T cells than *Satb1*^{Tg} cells (Figure 3.17C). This was also shown numerically, with decreased *Satb1*^{Tg} Gp33$^+$ cells compared to Ctrl cells on both days (Figure 3.17C). The frequencies of CD44$^+$ CD8$^+$ T cells was also lower in *Satb1*^{Tg} cells than in Ctrl cells on days 12 and 21 (Figure 3.17E-G). This was accompanied by a noticeable increase in CD44 expression on a single cells level in *Satb1*^{Tg} cells compared to Ctrl cells (Figure 3.17E-G). In addition to activation,

the accumulation of PD-1$^+$ exhausted CD8$^+$ T cells was significantly impaired. Only about 18 % of *Satb1*^{Tg} cells expressed PD-1 compared to 50 % of Ctrl cells on day 12, and 10 % of *Satb1*^{Tg} cells expressed PD-1 compared to 58 % of Ctrl cells on day 21 (Figure 3.17E-G). Furthermore, on both days *Satb1*^{Tg} PD-1$^+$ cells exhibited downregulation of the inhibitory receptor PD-1 compared to Ctrl cells (Figure 3.17E-G). Numerically, CD44$^+$ *Satb1*^{Tg} cells and PD-1$^+$ *Satb1*^{Tg} cells were reduced in comparison to Ctrl cells on both days (Figure 3.17H). Additionally, polyclonal PD-1$^+$ *Satb1*^{Tg} cells exhibited decreased levels of TOX expression on day 21 p.i. compared to Ctrl cells (Figure 3.17I). Antigen-specific Gp33$^+$ *Satb1*^{Tg} cells also downregulated PD-1 on both days (Figure 3.17J), as well as TOX on day 21 p.i. compared to Ctrl cells (Figure 3.17K). Overall, these data indicate that enforced SATB1 expression impairs the differentiation of exhausted CD8$^+$ T cells and show that SATB1 must be downregulated for TOX and PD-1 to be fully expressed.

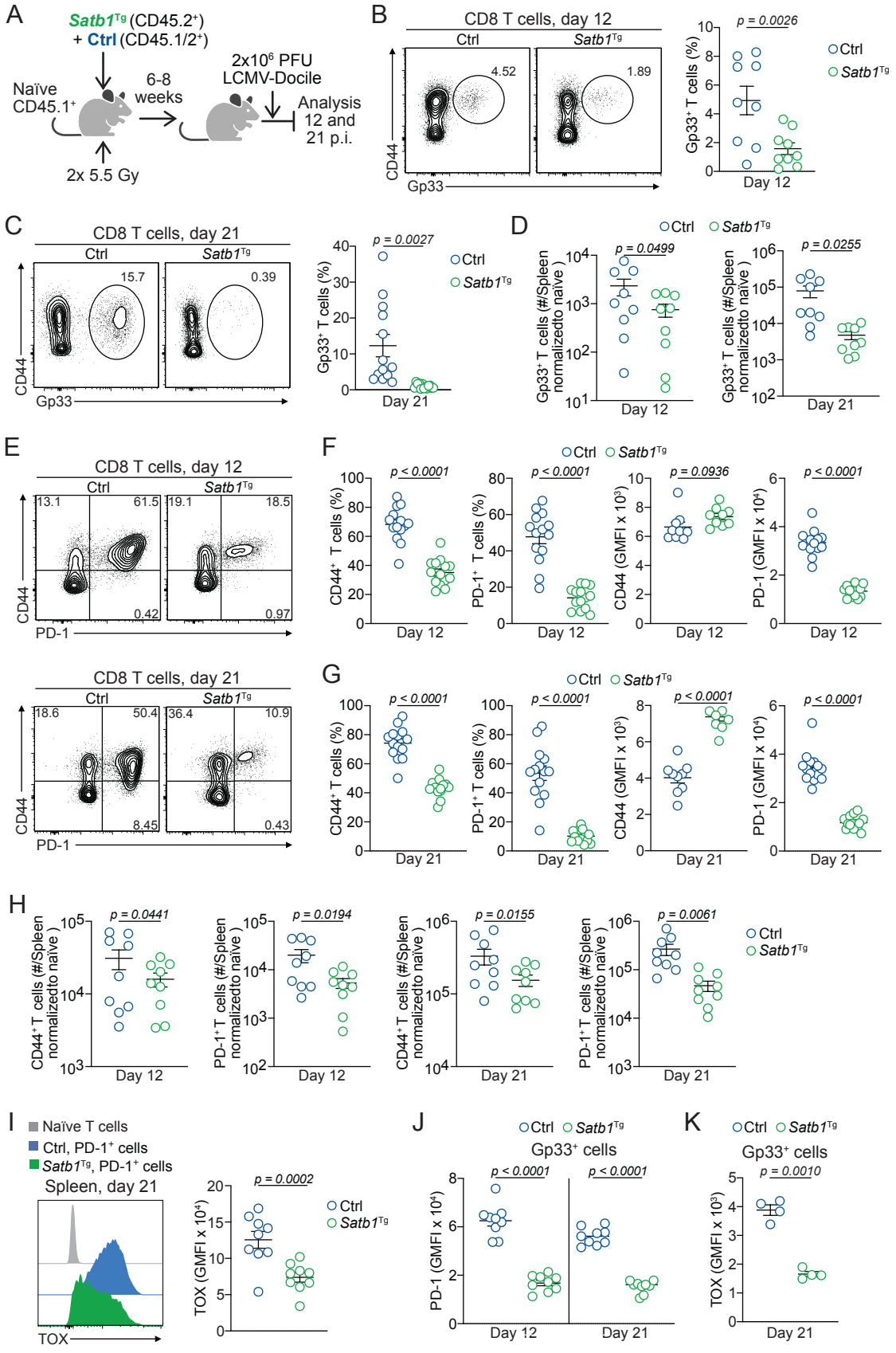
A
Satb1Tg (CD45.2+)
+ Ctrl (CD45.1/2+)
Naïve CD45.1+
6-8 weeks
2x10^6 PFU LCMV-Docile
Analysis 12 and 21 p.i.
2x 5.5 Gy
B
CD8 T cells, day 12
Ctrl
Satb1Tg
4.52
1.89
CD44
Gp33
p = 0.0026
Gp33+ T cells (%)
Day 12
C
CD8 T cells, day 21
15.7
0.39
p = 0.0027
D
p = 0.0499
p = 0.0255
Gp33+ T cells (#/Spleen normalizedto naïve)
E
CD8 T cells, day 12
13.1
61.5
19.1
18.5
0.42
0.97
PD-1
CD8 T cells, day 21
18.6
50.4
36.4
10.9
8.45
0.43
F
p < 0.0001
p < 0.0001
p = 0.0936
p < 0.0001
CD44+ T cells (%)
PD-1+ T cells (%)
CD44 (GMFI x 10^3)
PD-1 (GMFI x 10^4)
G
p < 0.0001
p < 0.0001
p < 0.0001
p < 0.0001
H
p = 0.0441
p = 0.0194
p = 0.0155
p = 0.0061
CD44+ T cells (#/Spleen normalizedto naïve)
PD-1+ T cells (#/Spleen normalizedto naïve)
I
Naïve T cells
Ctrl, PD-1+ cells
Satb1Tg, PD-1+ cells
Spleen, day 21
TOX
p = 0.0002
TOX (GMFI x 10^4)
J
Gp33+ cells
p < 0.0001
p < 0.0001
PD-1 (GMFI x 10^4)
K
Gp33+ cells
p = 0.0010
TOX (GMFI x 10^3)

Figure 3.17: Enforced SATB1 expression impairs exhausted T cell differentiation.
(A-K) Mixed bone marrow chimeric mice containing *Satb1*^{Tg} (CD45.2^{+}) and Ctrl T cells (CD45.1/2^{+}) were infected with LCMV-Docile. Spleens were harvested on day 12 and 21 p.i. and analysed using flow cytometry. (A) Schematic of experimental setup. (B) Representative flow cytometry plots and quantification showing frequencies of antigen specific Gp33^{+} *Satb1*^{Tg} and Ctrl cells on day 12. (C) Representative flow cytometry plots and quantification showing frequencies of antigen specific Gp33^{+} *Satb1*^{Tg} and Ctrl cells on day 21. (D) Quantification of numbers of activated Gp33^{+} *Satb1*^{Tg} and Ctrl cells per spleen. (E) Representative flow cytometry plots showing activated CD44^{+} and exhausted PD-1^{+} *Satb1*^{Tg} and Ctrl cells on day 12 and 21. (F) Quantification of activated CD44^{+} and polyclonal exhausted PD-1^{+} *Satb1*^{Tg} and Ctrl cells frequencies and CD44 and PD-1 expression levels on day 12. (G) Quantification of activated CD44^{+} and polyclonal exhausted PD-1^{+} *Satb1*^{Tg} and Ctrl cells frequencies and CD44 and PD-1 expression levels on day 21. (H) Quantification of numbers of activated polyclonal CD44^{+} and exhausted PD-1^{+} *Satb1*^{Tg} and Ctrl cells per spleen. (I) Representative histogram and quantification showing TOX expression in polyclonal PD-1^{+} *Satb1*^{Tg} and Ctrl cells compared to naïve CD8^{+} T cells on day 21. (J) Quantification of PD-1 expression on the single cell level in Gp33^{+} *Satb1*^{Tg} and Ctrl cells on day 12 and 21. (K) Quantification of TOX expression in Gp33^{+} *Satb1*^{Tg} and Ctrl cells on day 21. Dots in graphs represent individual mice; horizontal lines and error bars of bar graphs indicate means ± SEM, respectively. Data is pooled from two or three independent experiments or representative of two (I) independent experiments. P values are from paired student's t test.

Next, the frequencies of both T_{PEX} and T_{EX} subsets were compared between Ctrl and *Satb1*^{Tg} cells in the spleen on days 12 and 21 post-infection. T_{PEX} cell frequencies were significantly increased in *Satb1*^{Tg} cells compared to Ctrl cells on both days (Figure 3.18A and B). Conversely, T_{EX} cell frequencies were massively reduced in the *Satb1*^{Tg} cells compared to Ctrl cells on both days (Figure 3.18A and B). No differences in the numbers of *Satb1*^{Tg} and Ctrl T_{PEX} cells were observed on either day, while the number of *Satb1*^{Tg} T_{EX} cells were reduced by more than tenfold compared to Ctrl cells (Figure 3.18A and B). Further investigation into whether enforced SATB1 expression impacted the quality of T_{PEX} cells was conducted by assessing the expression of TCF1 and Ly108 on day 21 post infection. *Satb1*^{Tg} T_{PEX} cells expressed similar levels of TCF1, while the expression of Ly108 was increased compared to Ctrl T_{PEX} cells (Figure 3.18C). *Satb1*^{Tg} T_{PEX} cells displayed reduced expression levels of PD-1 and TOX

compared to Ctrl T_{PEX} cells (Figure 3.18D); however, the expression of CD44 was unchanged. Furthermore, although the frequencies of CD62L^{+} T_{PEX} cells were reduced in *Satb1*^{Tg} cells on both days (Figure 3.18E and F), no significant numerical differences between *Satb1*^{Tg} and Ctrl CD62L^{+} T_{PEX} cells were observed (Figure 3.18F).

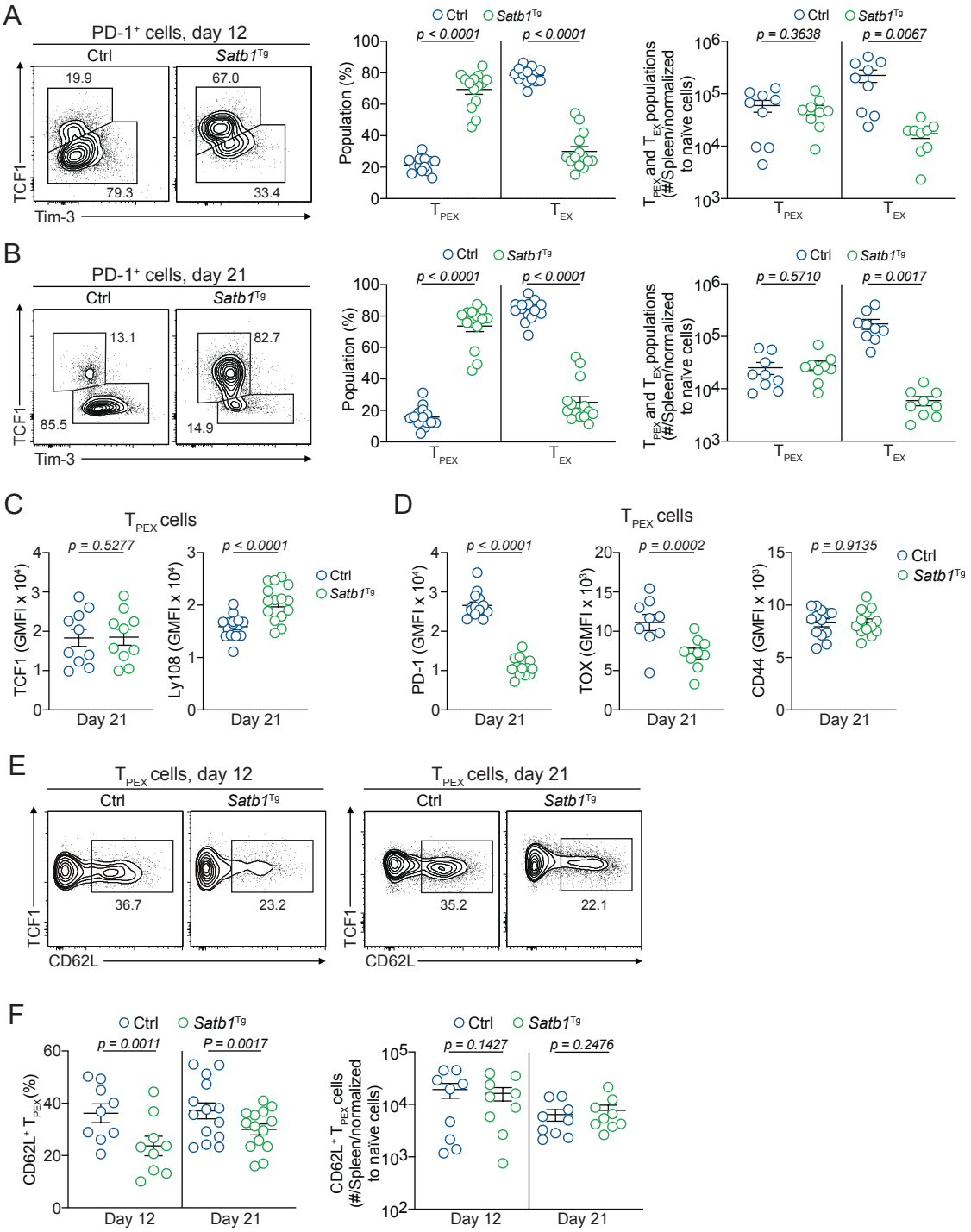

Figure 3.18: Enforced SATB1 expression impairs T_{EX} cell differentiation but does not impact differentiation of T_{PEX} cells.
(A-F) Mixed bone marrow chimeric mice containing *Satb1*^{Tg} (CD45.2$^+$) and Ctrl T cells (CD45.1/2$^+$) were infected with LCMV-Docile. spleens were harvested on day 12 and 21 p.i. and analysed using flow cytometry. (A) Representative flow cytometry plots and quantification showing frequencies and numbers of T_{PEX} (TCF1$^+$Tim-3$^-$) and T_{EX} (TCF1$^-$Tim-3$^+$) *Satb1*^{Tg} and Ctrl cells on day 12. (B) Representative flow cytometry plots and quantification showing frequencies and numbers of T_{PEX} (TCF1$^+$Tim-3$^-$) and T_{EX} (TCF1$^-$Tim-3$^+$) *Satb1*^{Tg} and Ctrl cells on day 21. (C) Quantification of TCF1 and Ly108 expression levels in *Satb1*^{Tg} and Ctrl cells on day 21. (D) Quantification of PD-1, TOX and CD44 expression levels in *Satb1*^{Tg} and Ctrl T_{PEX} cells on day 21. (E) Representative flow cytometry plots *Satb1*^{Tg} and Ctrl CD62L$^+$ T_{PEX} cells on day 12 and 21. (F) Quantification of frequencies and cell numbers of *Satb1*^{Tg} and Ctrl CD62L$^+$ T_{PEX} cells on day 12 and 21. Dots in graphs represent individual mice; horizontal lines and error bars of bar graphs indicate means ± SEM, respectively. Data is pooled from two or three independent experiments. P values are from paired student's t test.

We observed reduced frequencies and numbers of CX3CR1$^+$ and CD101$^+$ T_{EX} cells on both days (Figure 3.19A). Furthermore, on a single cells level, compared to Ctrl T_{EX} cells, *Satb1*^{Tg} T_{EX} cells expressed reduced levels of inhibitory receptors Tim-3, 2B4, and Lag-3, whereas CD39 expression was not altered (Figure 3.19B). In summary, these data indicate that enforced SATB1 expression hinders the differentiation of T_{EX} cells. Additionally, SATB1 overexpression impairs the expression of TOX and PD-1 in T_{PEX} cells as well as the expression of inhibitory receptors Tim-3, Lag-3 and 2B4.

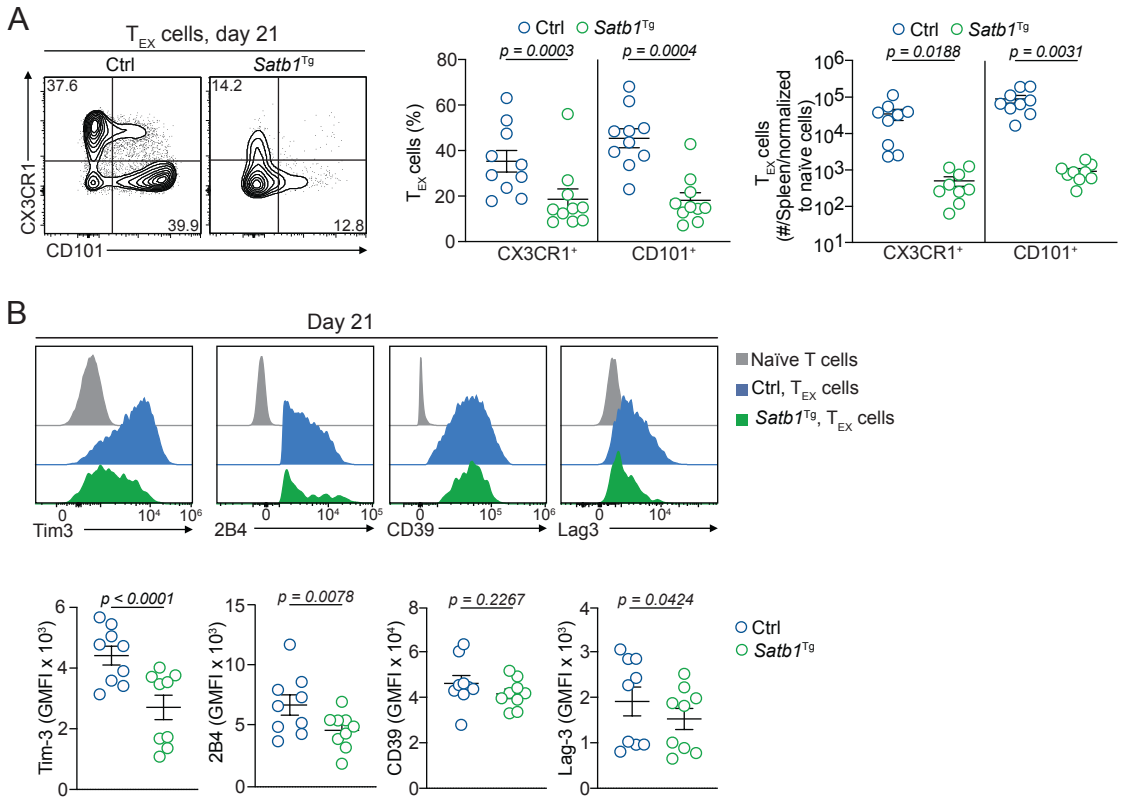

Figure 3.19: Enforced SATB1 expression impairs differentiation of CX3CR1$^+$ and CD101$^+$ T_{EX} cells and the expression of Lag-3, Tim-3 and 2B4.
(A-B) Mixed bone marrow chimeric mice containing *Satb1*^{Tg} (CD45.2$^+$) and Ctrl T cells (CD45.1/2$^+$) were infected with LCMV-Docile. spleens were harvested on day 12 and 21 p.i. and analysed using flow cytometry. (A) Representative flow cytometry plots and quantification showing frequencies and numbers of *Satb1*^{Tg} and Ctrl CX3CR1$^+$ and CD101$^+$ T_{EX} cells on day 21. (B) Representative histogram and quantification of Tim-3, 2B4, CD39 and Lag-3 expression in *Satb1*^{Tg} and Ctrl T_{EX} cells on day 21. Dots in graphs represent individual mice; horizontal lines and error bars of bar graphs indicate means ± SEM, respectively. Data is pooled from two independent experiments. P values are from paired student's t test.

We next tested whether the changes in T_{PEX} and T_{EX} cell development in *Satb1*^{Tg} cells were accompanied by changes in functionality. Higher frequencies of Gp33$^+$ *Satb1*^{Tg} cells produced IFN-γ, and co-produced IFN-γ and TNF compared to Ctrl cells (Figure 3.20A). Moreover, the expression levels on a single cell level were increased for TNF but not IFN-γ (Figure 3.20A). In accordance with this, polyclonal PD-1$^+$ *Satb1*^{Tg} cells exhibited increased IFN-γ$^+$ and polyfunctional IFN-γ$^+$TNF$^+$ cells compared to Ctrl cells (Figure 3.20B). In contrast to Gp33$^+$ cells, IFN-γ expression in polyclonal PD-1$^+$ *Satb1*^{Tg} cells was increased compared to

Ctrl cells, while expression of TNF was unchanged (Figure 3.20B). Further, we observed increased frequencies of IFN-γ single and IFN-γ/TNF double producing cells in *Satb1*^{Tg} T_{PEX} and T_{EX} cells compared to Ctrl cells (Figure 3.20C). The level of IFN-γ in *Satb1*^{Tg} T_{PEX} cells was decreased compared to Ctrl T_{PEX} cells, while TNF expression was similar between both (Figure 3.20C and D). In T_{EX} cells, the expression of IFN-γ and TNF was increased in the *Satb1*^{Tg} compared to Ctrl cells (Figure 3.20C and D). Lastly, we observed reduced GzmB production in *Satb1*^{Tg} T_{EX} cells compared to Ctrl T_{EX} cells (Figure 3.20E). Overall, these data indicate that the overexpression of SATB1 enhances the capacity to produce IFN-γ and TNF, while impairing the capacity to produce GzmB.

In summary, in this sub-chapter we characterized the effect of enforced SATB1 expression on the differentiation, maintenance, and functionality of T_{PEX} and T_{EX} cells during chronic LCMV infection. We observed that SATB1 impairs CD8$^+$ T cell activation as well as differentiation of T_{EX} cells. Specifically, the differentiation CX3CR1$^+$ and CD101$^+$ T_{EX} cells populations, is impaired, supporting a model where SATB1 regulates the switch of T_{PEX} to T_{EX} differentiation. Furthermore, we observed that SATB1 promotes production of effector cytokines IFN-γ and TNF.

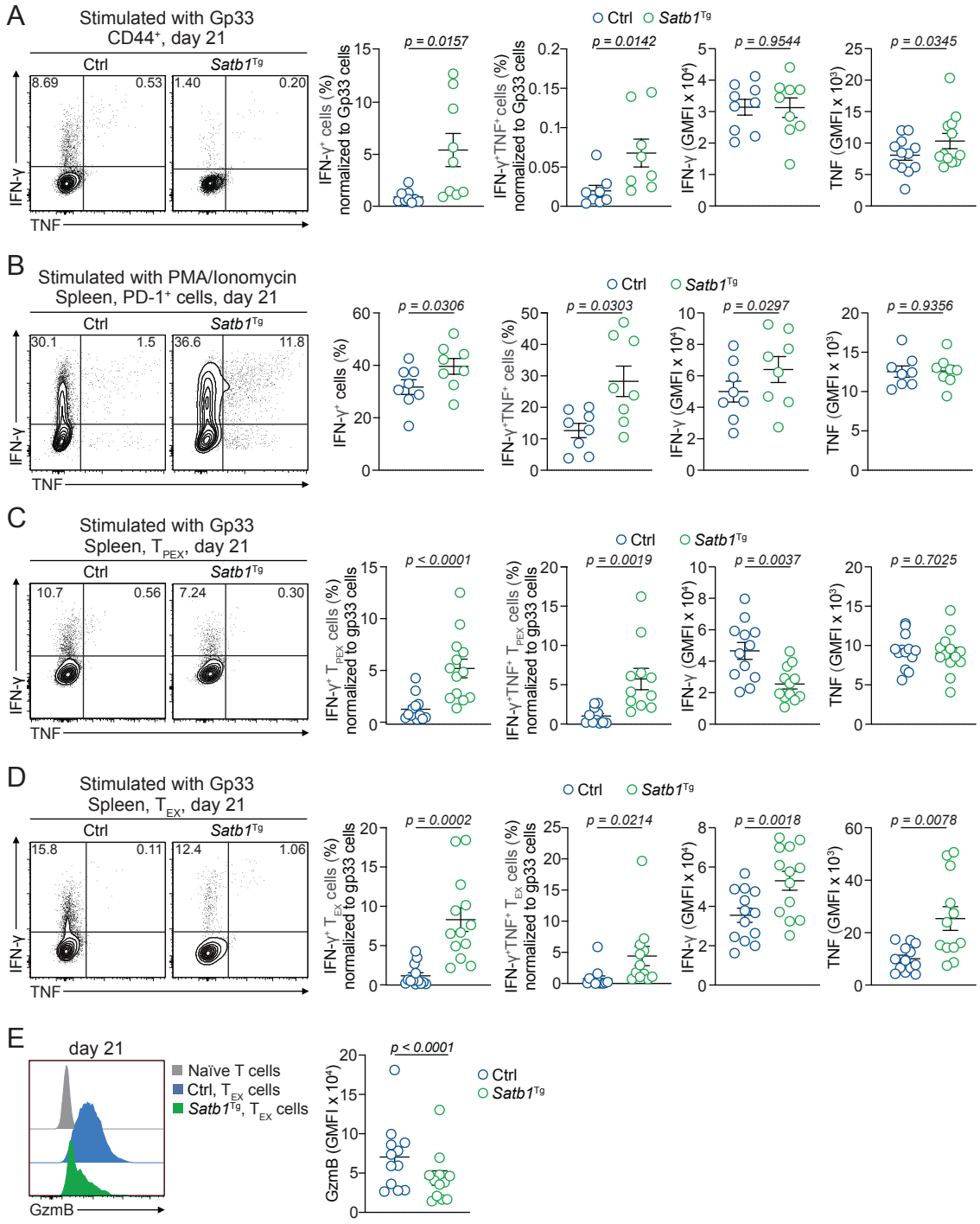

Figure 3.20: Enforced SATB1 expression enhances the effector capacity of T_{PEX} and T_{EX} cells to produce IFN-γ and TNF.

(A-D) Mixed bone marrow chimeric mice containing *Satb1*^{Tg} (CD45.2$^+$) and Ctrl T cells (CD45.1/2$^+$) were infected with LCMV-Docile. spleens were harvested on day 21 p.i. and analysed using flow cytometry. Cells were stimulated *ex vivo* with either Gp33 peptide (A, C and D) or with PMA/Ionomycin (B). (A) Representative flow cytometry plots and quantification showing frequencies of CD44$^+$ *Satb1*^{Tg} or Ctrl cells producing IFN-γ and TNF and quantification of IFN-γ and TNF

expression on a single cell level. (B) Representative flow cytometry plots and quantification showing frequencies of polyclonal PD-1$^+$ *Satb1*^{Tg} or Ctrl cells producing IFN-γ and TNF and quantification of IFN-γ and TNF expression on a single cell level. (C) Representative flow cytometry plots and quantification showing frequencies of *Satb1*^{Tg} or Ctrl T_{PEX} cells producing IFN-γ and TNF and quantification of IFN-γ and TNF expression on a single cell level. (D) Representative flow cytometry plots and quantification showing frequencies of *Satb1*^{Tg} or Ctrl T_{EX} cells producing IFN-γ and TNF and quantification of IFN-γ and TNF expression on a single cell level. (E) Representative histogram and quantification showing production of GzmB in *Satb1*^{Tg} or Ctrl T_{EX} cells. Dots in graphs represent individual mice; horizontal lines and error bars of bar graphs indicate means ± SEM, respectively. Data is pooled from two (A;B) or three (C-E) independent experiments. P values are from paired student's t test.

3.2.7 The role of SATB1 in regulating transcription and chromatin accessibility in exhausted T cells

Our data indicated that SATB1 represses the differentiation of T_{EX} cells during chronic viral infection. To better understand the molecular mechansisms, SATB1-KO and Ctrl CD62L$^+$ T_{PEX}, CD62L$^-$ T_{PEX}, CX3CR1$^+$ T_{EX}, and CD101$^+$ T_{EX} cells were sorted on day 21 p.i. from infected mice (Figure 3.21A) and performed bulk RNA-Sequencing. Pairwise subset-specific analysis of the RNA-seq data identified 127 differentially expressed genes between SATB1-KO and Ctrl cells. CD62L$^+$ T_{PEX} and CD62L$^-$ T_{PEX} cells showed the showed the highest number of differentially expressed genes (Figure 3.21B). Several genes, including the metabolic enzyme *Car2* and transcription factor *Prdm1*, were upregulated in SATB1-KO T_{PEX} cells compared to Ctrl cells. In contrast, expression of genes such as *Tgfbr1* and *Lag-3* was increased in SATB1-KO T_{PEX} cells (Figure 3.21B). Further, we observed that both SATB1-KO CD62L$^+$ and CD62L$^-$ T_{PEX} cells exhibited downregulation of *Caspase3* (Figure 3.21B), critical in apoptosis, suggesting that SATB1 may affect cell death in T_{PEX} cells. Similarly, SATB1-KO CD101$^+$ T_{EX} cells but not for CX3CR1$^+$ T_{EX} cells also downregulated *Caspase3* compared to Ctrl cells. Analysis with KEEG, GO, and Hallmark revealed pathways that are related to chromatid segregation and cell cycle to be strongly enriched among the differentially expressed genes (Figure 3.21C). These results indicate that SATB1 loss has a pronounced effect on the transcriptional

landscape of T_{PEX} cells, particularly in pathways regulating cell proliferation and chromatin organization, while T_{EX} cells are less affected. Collectively, these findings suggest that SATB1 modulates T cell differentiation and survival by shaping key transcriptional programs that influence effector versus exhausted cell fates.

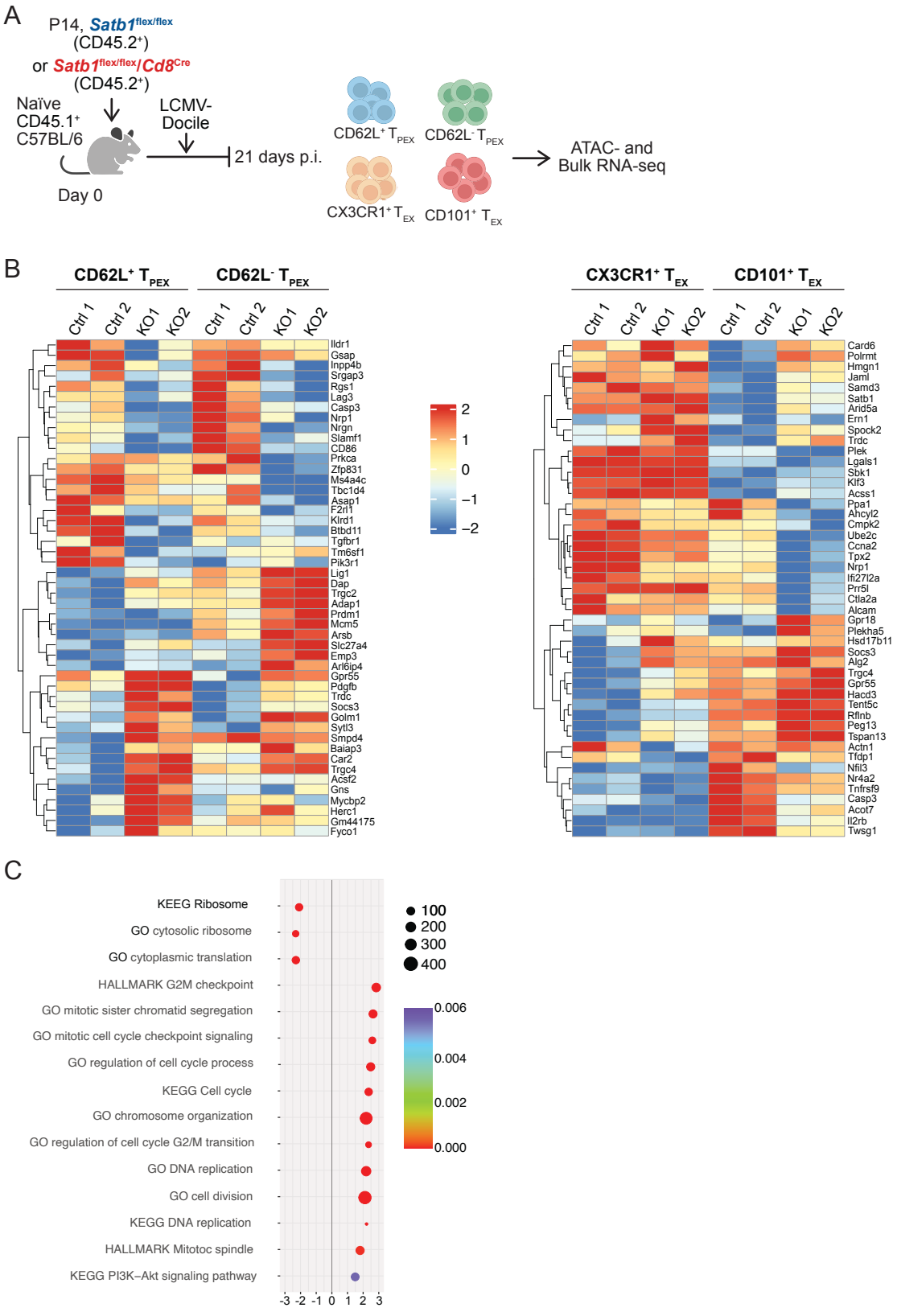

Figure 3.21: Loss of SATB1 alters gene expression in T_{PEX} and T_{EX} cells. (A-C) Naïve CD45.2$^+$ SATB1-KO P14 cells (*Satb1*$^{flex/flex}$/*Cd8*^{Cre}) or Ctrl cells (*Satb1*$^{flex/flex}$) P14 cells were adoptively transferred into naïve wildtype CD45.1$^+$

mice and subsequently infected with LCMV-Docile. On 21 p.i. CD62L^{+} and CD62L^{-} T_{PEX} and CX3CR1^{+} and CD101^{+} T_{EX} were sorted from either SATB1-KO or Ctrl spleens and used for bulk-RNA. (A) Schematic of experimental setup. (B) Heatmap showing genes differentially expressed (DEG) between indicated SATB1-KO and control T_{PEX} and T_{EX} cell subsets. (C) Bubble plot showing pathway analysis (KEEG, GO and Hallmark) for DEG genes detected in T_{PEX} cell subsets. Data is representative or pooled from two independent experiments.

SATB1 has previously been shown to act in chromatin reorganization (Cai *et al.*, 2003). We therefore performed ATAC-sequencing on all four subsets. More than 40,000 regions showed subset-specific differences in chromatin accessibility. As reported in previous studies (Jadhav *et al.*, 2019; Utzschneider *et al.*, 2020), the highest number of differentially accessible regions (DARs) was observed between T_{PEX} and T_{EX} cells (Figure 3.22A). Additionally, significant differences in chromatin accessibility were evident between CX3CR1^{+} and CD101^{+} T_{EX} cells (Figure 3.22A). In contrast, no major differences were observed between CD62L^{+} T_{PEX} and CD62L^{-} T_{PEX} (Figure 3.22A). Unexpectedly, only 1140 DARs were detected when comparing SATB1-KO and control cells (Figure 3.22A). Nevertheless, SATB1-KO cells showed a subtle but consistent reduction in accessibility across the genome (Figure 3.22A). We next paired previously published CHIP-sequencing datasets (Kitagawa *et al.*, 2017) with our RNA- and ATAC-sequencing datasets. These data revealed a total of 4230 SATB1 binding sites in chromatin regions accessible in chronically stimulated CD8^{+} T cells (Figure 3.22B). T_{PEX}-specific accessible regions were significantly enriched for SATB1 binding sites compared to T_{EX}-specific regions (Figure 3.22A). For example, the T_{PEX} specific gene *Tcf7* showed two SATB1 binding sites in accessible chromatin regions that were closed in T_{EX} cells (Figure 3.22C). Additional analysis of KO and Ctrl P14 cells revealed 26 differentially expressed genes, which showed different DARs and SATB1 binding in open regions (Figure 3.22B). This included *Prdm1* (Example ATAC Peaks for *Prdm1* in (Figure 3.22D) along with other genes involved in transcriptional regulation (*Tox2, Klf3, Maf*), protein translation (*Arid5a*), cytokine signalling (*Tgfbr1, Tgfbr2*), surface markers (*Slamf6*) (Figure 3.22E), and cell cycle regulation (*Ccna2, Mki67*). Taken

together, these findings indicate that, in chronically activated $CD8^+$ T cells, SATB1 primarily functions as a transcriptional regulator rather than a global epigenetic regulator, influencing the expression of genes that govern T cell differentiation, proliferation, and effector function.

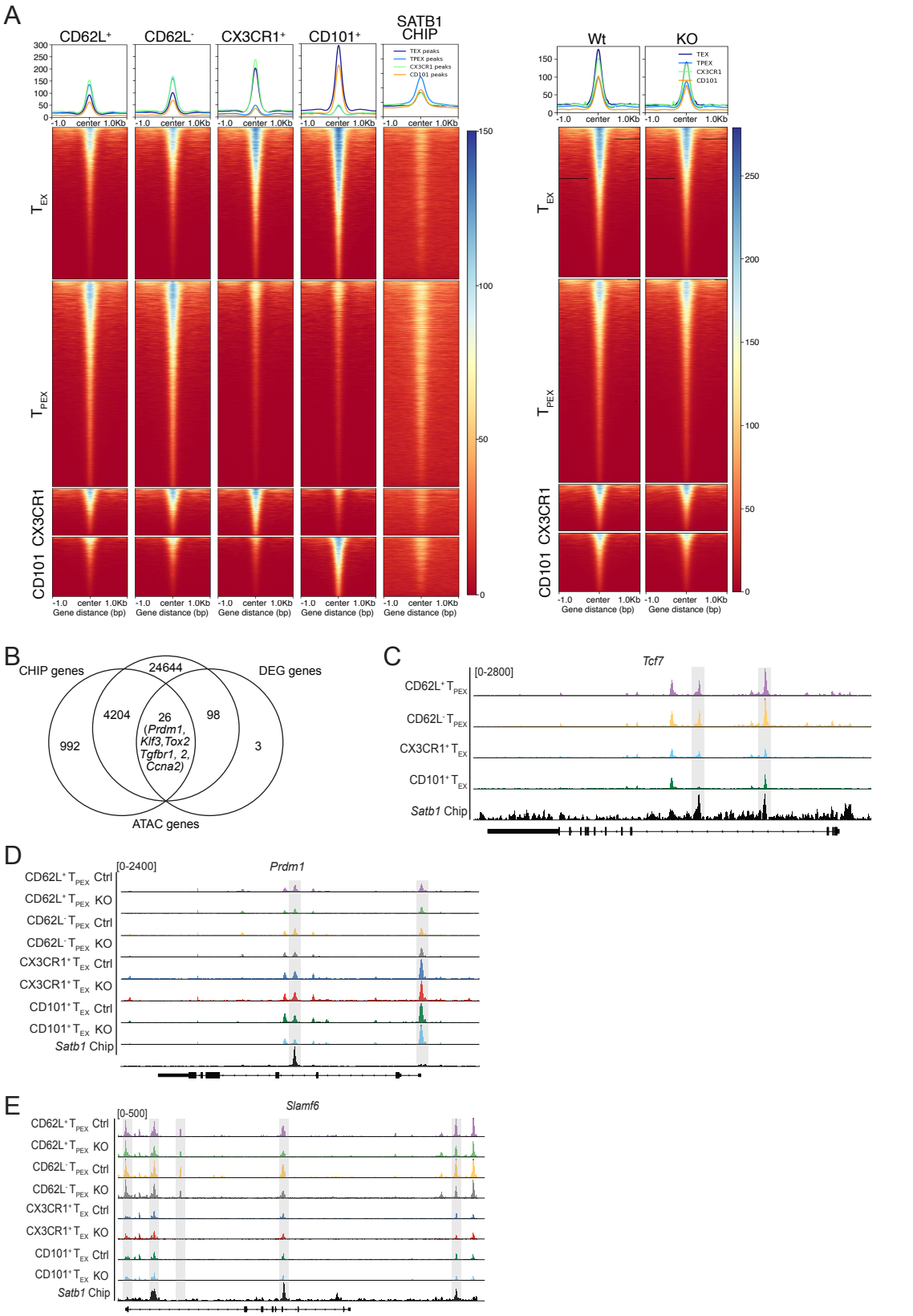

Figure 3.22: Loss of SATB1 does not substantially alter the chromatin organisation in T_{PEX} and T_{EX} cells.

(A-C) Naïve CD45.2$^+$ SATB1-KO P14 cells (*Satb1*$^{flex/flex}$/*Cd8*^{Cre}) or Ctrl cells (*Satb1*$^{flex/flex}$) P14 cells were adoptively transferred into naïve wildtype CD45.1$^+$ mice and subsequently infected with LCMV-Docile. On 21 p.i. CD62L$^+$ and CD62L$^-$ T_{PEX} and CX3CR1$^+$ and CD101$^+$ T_{EX} were sorted from either SATB1-KO or Ctrl spleens and used for bulk-RNA. (A) Heatmap showing regions differentially accessible (DAR) between the indicated exhausted T cell subsets and SATB1-Chip binding sites (Kitagawa *et al.*, 2017). (B) Venn-diagram showing overlap of DEG and genes with DAR or SATB1 binding sites with selected genes highlighted. (C) Comparison of gene accessibility in control CD62L$^+$ T_{PEX}, CD62L$^-$ T_{PEX}, CX3CR1$^+$ T_{EX} and CD101$^+$ T_{EX} cells. *TCF7* is shown as examples. (D) Comparison of gene accessibility in SATB1-KO and control CD62L$^+$ T_{PEX}, CD62L$^-$ T_{PEX}, CX3CR1$^+$ T_{EX} and CD101$^+$ T_{EX} cells. *Prdm1* is shown as examples. (E) Comparison of gene accessibility in SATB1-KO and control CD62L$^+$ T_{PEX}, CD62L$^-$ T_{PEX}, CX3CR1$^+$ T_{EX} and CD101$^+$ T_{EX} cells. *Slamf6* is shown as examples. Data is representative or pooled from two independent experiments.

SATB1 contains multiple domains, including a DNA binding site. SATB1 binds DNA through tetramerization, facilitated by its ubiquitin-like domain. (Z. Wang *et al.*, 2012; Wang *et al.*, 2014), thereby organizing chromatin (Cai *et al.*, 2003), or facilitating gene expression by recruiting remodelling enzymes (Yasui *et al.*, 2002). To further understand the mechanistic roles of SATB1, we assessed whether SATB1 binding to its target DNA is essential for its function. We created mixed bone marrow chimeras using a published mouse model (*Satb1*$^{m1Anu/m1Anu}$) (Nüssing *et al.*, 2022), in which SATB1 has a point mutation in the active DNA binding pocket. Even though SATB1 protein is expressed, its ability to bind to DNA is impaired. Chimeric mice were infected with LCMV-Docile, and splenocytes were analysed at day 21 after infection (Figure 3.23A). Similar to the SATB1-KO model, an increased accumulation of exhausted T cells was observed in the *Satb1*$^{m1Anu/m1Anu}$ cell compartment. Compared to Ctrl cells, the frequencies of antigen-specific Gp33$^+$ and polyclonal PD-1$^+$ *Satb1*$^{m1Anu/m1Anu}$ cells were increased (Figure 3.23B and C). Further, PD-1$^+$ *Satb1*$^{m1Anu/m1Anu}$ cells displayed increased expression levels of PD-1 compared to Ctrl cells (Figure 3.23D). Similar to the SATB1-KO model, the frequencies of *Satb1*$^{m1Anu/m1Anu}$ T_{EX} cells were increased compared to Ctrl T_{EX}, whereas *Satb1*$^{m1Anu/m1Anu}$ T_{PEX} cell frequencies were reduced (Figure 3.23E). *Satb1*$^{m1Anu/m1Anu}$ T_{PEX} cells also displayed increased expression of Ly108, but no differences in TCF1 expression

levels compared to Ctrl cells (Figure 3.23F). No differences were observed in frequencies of CD62L$^+$ T_{PEX} cells between *Satb1*$^{m1Anu/m1Anu}$ and Ctrl cells (Figure 3.23G). Moreover, we observed increased proportions of CD101$^+$ and reduced frequencies of CX3CR1$^+$ *Satb1*$^{m1Anu/m1Anu}$ T_{EX} cells compared with Ctrl T_{EX} cells (Figure 3.23H). Lastly, *Satb1*$^{m1Anu/m1Anu}$ cells exhibited a reduced ability to produce IFN-γ and TNF compared to Ctrl cells (Figure 3.23I). Overall, the phenotype of *Satb1*$^{m1Anu/m1Anu}$ cells was similar to that of SATB1-KO cells compared to Ctrl cells, indicating that DNA binding is required for of SATB1-mediated functions.

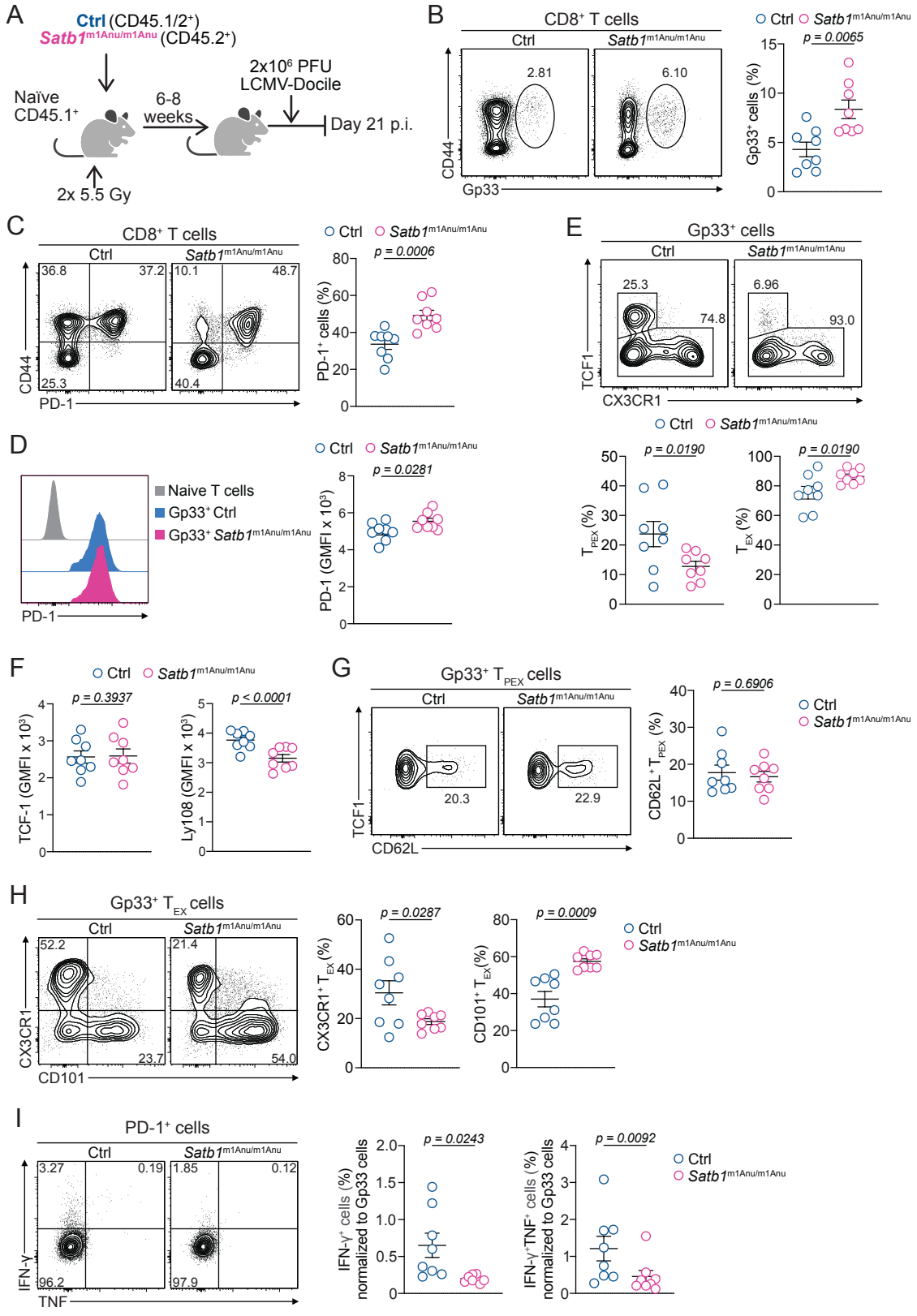

Figure 3.23: DNA-binding is required for SATB1 function in T cell exhaustion.

(A-I) Mixed bone marrow chimeric mice containing *Satb1*$^{m1Anu/m1Anu}$ (CD45.2$^+$) and Ctrl T cells (CD45.1/2$^+$) were infected with LCMV-Docile. On day 21 p.i. spleens were analysed using flow cytometry. (A) Schematic of experimental setup. (B) Representative flow cytometry plots and quantification showing frequencies of activated Gp33$^+$ *Satb1*$^{m1Anu/m1Anu}$ or Ctrl cells. (C) Representative flow cytometry plots and quantification showing frequencies of polyclonal exhausted PD-1$^+$ *Satb1*$^{m1Anu/m1Anu}$ or Ctrl cells. (D) Representative histogram and quantification showing the expression of PD-1 in Gp33$^+$ *Satb1*$^{m1Anu/m1Anu}$ or Ctrl cells. (E) Representative flow cytometry plots and quantification showing frequencies of *Satb1*$^{m1Anu/m1Anu}$ or Ctrl T_{PEX} and T_{EX} cells. (F) Quantification showing the expression of TCF1 and Ly108 in Gp33$^+$ *Satb1*$^{m1Anu/m1Anu}$ or Ctrl cells. (G) Representative flow cytometry plots and quantification showing frequencies of *Satb1*$^{m1Anu/m1Anu}$ or Ctrl CD62L$^+$ T_{PEX} cells. (H) Representative flow cytometry plots and quantification showing frequencies of *Satb1*$^{m1Anu/m1Anu}$ or Ctrl CX3CR1$^+$ and CD101$^+$ T_{EX} cells. (I) Representative flow cytometry plots and quantification showing frequencies of IFN-γ and TNF producing *Satb1*$^{m1Anu/m1Anu}$ or Ctrl cells after stimulation with Gp33 peptide *ex vivo*. Dots in graphs represent individual mice; horizontal lines and error bars of bar graphs indicate means ± SEM, respectively. Data is pooled from two independent experiments. P values are from paired student's t test.

3.2.8 Deregulated Blimp1 expression contributes to SATB1-KO phenotype in exhausted T cells

Our data indicate a role for SATB1 in the exhaustion trajectories of CD8$^+$ T cells. However, the precise molecular mechanisms by which SATB1 constrains T_{EX} and effector differentiation remain unclear, necessitating further investigation into its downstream targets and transcriptional network interactions. Our sequencing analysis revealed that *Prdm1* (encoding Blimp1) was significantly elevated in SATB1-KO T_{PEX} cells, with the *Prdm1* locus displaying differential chromatin accessibility and a SATB1 binding site, suggesting direct transcriptional regulation. Given its well-established role in T cell fate decisions, we sought to explore a potential role for Blimp1 in the SATB1-KO phenotype. Blimp1 is a transcriptional regulator known to drive terminal differentiation of effector CD8$^+$ T cells in acute antigen settings (Rutishauser *et al.*, 2009; Kallies *et al.*, 2009). In chronic infection, Blimp1 expression is significantly upregulated in the PD-1^{high} T_{EX} population, whereas its expression is lower in the PD-1^{intermediate} T_{PEX} subset (Shin *et al.*, 2009). Furthermore, conditional deletion of the *Prdm1* gene in CD8$^+$

T cells enhances the differentiation of T_{PEX} cells while concurrently suppressing T_{EX} differentiation (Shin *et al.*, 2009), a pattern opposite to the effects observed upon SATB1 overexpression. Based on these observations, we hypothesized that the increased T_{EX} differentiation observed upon SATB1 deletion, might be reversible through simultaneous depletion of Blimp1. To this end, we used the CRISPR-Cas9 system to deplete Blimp1 in SATB1-KO P14 cells (termed dKO). Ctrl, SATB1-KO, Blimp1-KO and dKO P14 cells were transferred into recipient mice, that were subsequently infected with LCMV-Docile and analysed using flow cytometry on day 28 of infection (Figure 3.24A). Consistent with our results, the frequencies of SATB1-KO P14 cells were increased compared to Ctrl cells (Figure 3.24B and C). Blimp1-KO P14 cells demonstrated frequencies comparable to those of Ctrl P14 cells (Figure 3.24B and C). The dKO P14 cells were increased in frequencies compared to both Ctrl and Blimp1-KO P14 cells, while they were similar compared to SATB1-KO P14 cells (Figure 3.24B and C). Both SATB1-KO and dKO P14 cells also showed increased numbers of P14 cells compared to Ctrl and Blimp1-KO P14 cells (Figure 3.24C). dKO P14 cells were reduced in numbers compared to SATB1-KO P14 cells (Figure 3.24C). Blimp1-KO and dKO P14 cells expressed similar levels of PD-1; however, compared to expression levels in Ctrl and SATB1-KO P14 cells, PD-1 expression was elevated (Figure 3.24D and E). The expression of TOX remained unaltered by the depletion of SATB1 or Blimp1, with all P14 cell groups expressing similar levels (Figure 3.24D and E).

In summary, Blimp1 deletion in SATB1-KO $CD8^+$ T cells (dKO) partially reversed the increased cell numbers seen in SATB1-KO, while PD-1 remained elevated and TOX unchanged. Collectively, these data indicate that Blimp1 contributes to the accumulation of SATB1-KO P14 cells and shows that Blimp1 and Satb1 collaboratively regulate PD-1 expression in exhausted T cells.

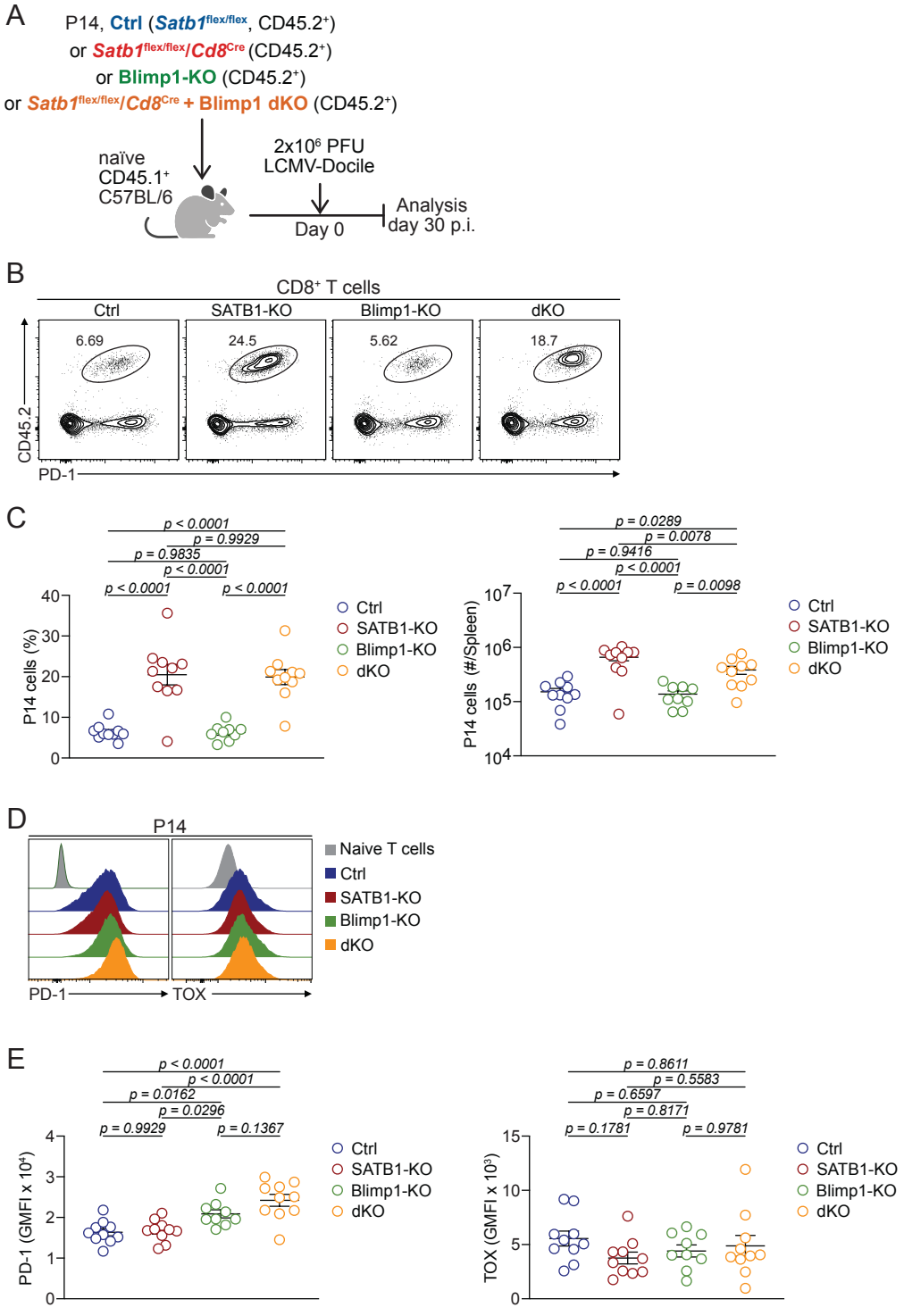

Figure 3.24: Blimp depletion in SATB1-KO P14 cells increases expression. Of PD-1 and decreases P14 cell numbers.

(A-E) Naïve CD45.2+ SATB1-KO P14 cells (*Satb1*$^{flex/flex}$/*Cd8*^{Cre}), Ctrl cells (*Satb1*$^{flex/flex}$) P14 cells, Blimp1-KO P14 cells and SATB1-Blimp1-dKO P14 cells were adoptively transferred into naïve wildtype CD45.1+ mice and subsequently infected with LCMV-Docile. On 28 p.i. spleens were analysed using flow cytometry. (A) Schematic of experimental setup. (B) Representative flow

cytometry plots showing frequencies of SATB1-KO, Blimp1-KO, dKO and Ctrl P14 cells within the CD8 T cells. (C) Quantification showing frequencies and numbers of SATB1-KO, Blimp1-KO, dKO and Ctrl P14 cells in the spleen. (D) Representative histograms showing expression of PD-1 and TOX in SATB1-KO, Blimp1-KO, dKO and Ctrl P14 cells compared to naïve CD8 T cells. (E) Quantification of PD-1 and TOX expression levels in SATB1-KO, Blimp1-KO, dKO and Ctrl P14 cells. Dots in graphs represent individual mice; horizontal lines and error bars of bar graphs indicate means ± SEM, respectively. Data is pooled from two independent experiments. P values are from unpaired student's t test.

To further assess the impact of Blimp1 depletion on the maintenance and differentiation of SATB1-KO P14 cells, we compared the frequencies of T_{PEX} and T_{EX} subsets between Ctrl, SATB1-KO, Blimp-KO and dKO cells in the spleen on day 28 post infection, using flow-cytometry. Unexpectedly, compared to our observation on day 21 p.i., no major changes were observed in the frequencies of SATB1-KO and Ctrl T_{PEX} or T_{EX} cells; however, a numerical increase in SATB1-KO T_{PEX} and T_{EX} cells was noted compared to Ctrl cells (Figure 3.25A-C). Consistent with existing literature (Shin et al., 2009), Blimp1-KO T_{PEX} cell frequencies were increased, while T_{EX} cell frequencies were reduced compared to Ctrl cells (Figure 3.25A and B). Numerically, Blimp-KO T_{PEX} cells were similar to SATB1-KO T_{PEX} cells, while increased compared to Ctrl cell (Figure 3.25C). Blimp1-KO T_{EX} cell numbers were decreased compared to SATB1-KO T_{EX} cells but comparable to Ctrl cells (Figure 3.25C). Additionally, the proportions of dKO T_{PEX} cells were increased relative to Ctrl and SATB1-KO T_{PEX} cells but reduced compared to Blimp-KO T_{PEX} cells (Figure 3.25A and B). Correspondingly, dKO T_{EX} cell frequencies were reduced compared to Ctrl and SATB1-KO T_{EX} cells but increased compared to Blimp-KO T_{EX} cells (Figure 3.25A and B). The numbers of dKO T_{PEX} cells were similar to SATB1-KO T_{PEX} cell numbers, thus increased compared to Blimp1-KO and Ctrl T_{PEX} cell numbers (Figure 3.25C). The numbers of dKO T_{EX} cells on the other hand were similar to the numbers of Ctrl T_{EX} cells, reduced compared to SATB1-KO T_{EX} cells and increased compared to Blimp1-KO T_{EX} cell numbers (Figure 3.25C). Similar to T_{PEX} cells, we observed an unexpected increase in frequencies and numbers of SATB1-KO CD62L^{+} T_{PEX} cells was observed compared to Ctrl cells on day 28 p.i. (Figure 3.25D and E),

further suggesting that SATB1 depletion enhances TPEX maintenance at later stages of infection. The frequencies of Blimp1-KO CD62L$^+$ T_{PEX} cells were reduced compared to Ctr cells, while both exhibited similar numbers of CD62L$^+$ T_{PEX} cells per spleen (Figure 3.25D and E). This indicates that the CD62L$^+$ T_{PEX} cells are not impacted by depletion of Blimp1. Despite the dKO CD62L$^+$ T_{PEX} cell frequencies being similar to those of Blimp1-KO, their numbers were increased, showing levels comparable to SATB1-KO CD62L$^+$ T_{PEX} cells (Figure 3.25D and E). Furthermore, no significant differences were observed between CD101$^+$ or CX3CR1$^+$ T_{EX} cell frequencies between the T_{EX} groups (Figure 3.25F and G). Numerically, both SATB1-KO CX3CR1$^+$ and CD101$^+$ T_{EX} cells were increased compared to Ctrl cells, while Blimp1-KO CX3CR1$^+$ and CD101$^+$ T_{EX} cells were reduced compared to Ctrl and SATB1-KO cells (Figure 3.25G). The depletion of Blimp1 in SATB1-KO cells resulted in similar cell numbers of CX3CR1$^+$ and CD101$^+$ T_{EX} cells compared to Ctrl cells. While the dKO CX3CR1$^+$ and CD101$^+$ T_{EX} cells were reduced compared to SATB1-KO cells, they were increased compared to Blimp1-KO cells CX3CR1$^+$ and CD101$^+$ T_{EX} cells (Figure 3.25G). Taken together, these data indicate that the increased SATB1-KO T_{EX} cell expansion is in part regulated by Blimp1. In summary Blimp1 deletion in SATB1-KO cells reduced T_{EX} expansion while T_{PEX} maintenance remained high, indicating Blimp1 drives SATB1-KO–induced T_{EX} differentiation but does not affect T_{PEX} persistence.

Collectively in this sub-chapter, we observed that Blimp1 impairs accumulation of SATB1-KO P14 cells. In particular, the differentiation of T_{EX} cells but not T_{PEX} cells was impaired, suggesting a model in which the downregulation of SATB1 may lead to the upregulation of Blimp1, thereby promoting T_{EX} differentiation. Additionally, depletion of Blimp1 enhanced PD-1 expression in SATB1-KO P14 cells. Moreover, this data enhances our findings on SATB1 in T cell exhaustion, suggesting, that in the late stage of infection, the maintenance of T_{PEX} is enhanced upon SATB1 depletion.

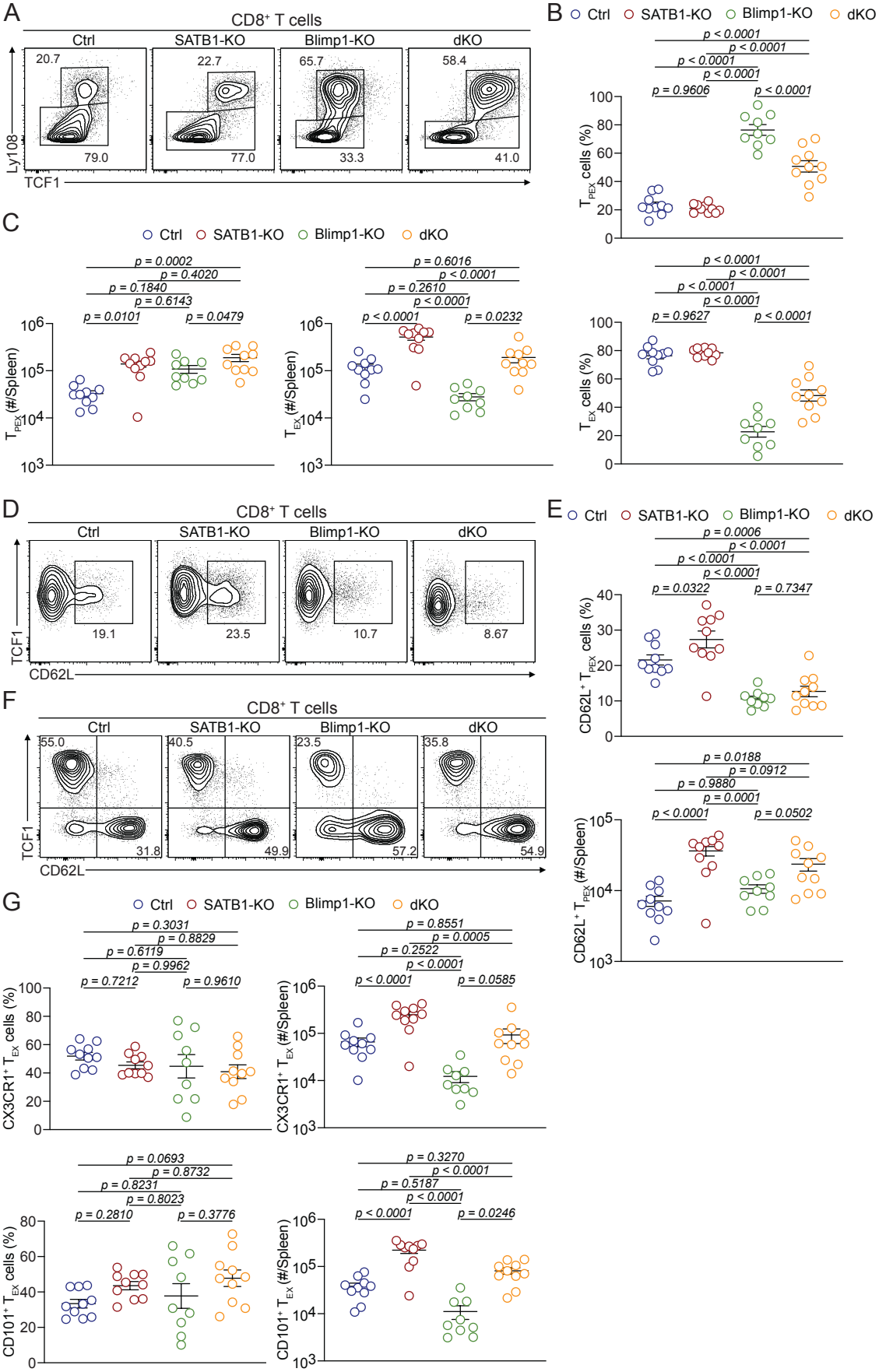
A
CD8⁺ T cells
Ctrl
SATB1-KO
Blimp1-KO
dKO
20.7
79.0
22.7
77.0
65.7
33.3
58.4
41.0
Ly108
TCF1
B
Ctrl
SATB1-KO
Blimp1-KO
dKO
p < 0.0001
p < 0.0001
p < 0.0001
p < 0.0001
p = 0.9606
p < 0.0001
T_PEX cells (%)
C
Ctrl
SATB1-KO
Blimp1-KO
dKO
p = 0.0002
p = 0.4020
p = 0.1840
p = 0.6143
p = 0.0101
p = 0.0479
T_PEX (#/Spleen)
p = 0.6016
p < 0.0001
p = 0.2610
p < 0.0001
p < 0.0001
p = 0.0232
T_EX (#/Spleen)
p < 0.0001
p < 0.0001
p < 0.0001
p < 0.0001
p = 0.9627
p < 0.0001
T_EX cells (%)
D
CD8⁺ T cells
Ctrl
SATB1-KO
Blimp1-KO
dKO
19.1
23.5
10.7
8.67
TCF1
CD62L
E
Ctrl
SATB1-KO
Blimp1-KO
dKO
p = 0.0006
p < 0.0001
p < 0.0001
p < 0.0001
p = 0.0322
p = 0.7347
CD62L⁺ T_PEX cells (%)
p = 0.0188
p = 0.0912
p = 0.9880
p = 0.0001
p < 0.0001
p = 0.0502
CD62L⁺ T_PEX (#/Spleen)
F
CD8⁺ T cells
Ctrl
SATB1-KO
Blimp1-KO
dKO
55.0
31.8
40.5
49.9
23.5
57.2
35.8
54.9
TCF1
CD62L
G
Ctrl
SATB1-KO
Blimp1-KO
dKO
p = 0.3031
p = 0.8829
p = 0.6119
p = 0.9962
p = 0.7212
p = 0.9610
CX3CR1⁺ T_EX cells (%)
p = 0.8551
p = 0.0005
p = 0.2522
p < 0.0001
p < 0.0001
p = 0.0585
CX3CR1⁺ T_EX (#/Spleen)
p = 0.0693
p = 0.8732
p = 0.8231
p = 0.8023
p = 0.2810
p = 0.3776
CD101⁺ T_EX cells (%)
p = 0.3270
p < 0.0001
p = 0.5187
p < 0.0001
p < 0.0001
p = 0.0246
CD101⁺ T_EX (#/Spleen)

Figure 3.25: SATB1-KO T_{EX} differentiation but not T_{PEX} differentiation is impaired upon Blimp1 depletion.
(A-G) Naïve CD45.2$^+$ SATB1-KO P14 cells (*Satb1*$^{flex/flex}$/*Cd8*^{Cre}), Ctrl cells (*Satb1*$^{flex/flex}$) P14 cells, Blimp1-KO P14 cells and SATB1-Blimp1-dKO P14 cells were adoptively transferred into naïve wildtype CD45.1$^+$ mice and subsequently infected with LCMV-Docile. On 28 p.i. spleens were analysed using flow cytometry. (A) Representative flow cytometry plots showing frequencies of SATB1-KO, Blimp1-KO, dKO and Ctrl T_{PEX} and T_{EX} cells. (B) Quantification showing frequencies of SATB1-KO, Blimp1-KO, dKO and Ctrl T_{PEX} and T_{EX} cells. (C) Quantification showing frequencies and numbers of SATB1-KO, Blimp1-KO, dKO and Ctrl T_{PEX} and T_{EX} cells in the spleen. (D) Representative flow cytometry plots showing frequencies of SATB1-KO, Blimp1-KO, dKO and Ctrl CD62L$^+$ T_{PEX} cells. (E) Quantification showing frequencies and numbers of SATB1-KO, Blimp1-KO, dKO and Ctrl CD62L$^+$ T_{PEX} cells in the spleen. (F) Representative flow cytometry plots showing frequencies of SATB1-KO, Blimp1-KO, dKO and Ctrl CX3CR1$^+$ T_{EX} and CD101$^+$ T_{EX} cells. (E) Quantification showing frequencies and numbers of SATB1-KO, Blimp1-KO, dKO and Ctrl CX3CR1$^+$ T_{EX} and CD101$^+$ T_{EX} cells in the spleen. Dots in graphs represent individual mice; horizontal lines and error bars of bar graphs indicate means ± SEM, respectively. Data is pooled from two independent experiments. P values are from unpaired student's t test.

Chapter 4 – T cells positioning in secondary lymphoid organs impacts exhausted T cell differentiation

4.1 Introduction

Precursors of exhausted T cells have been well characterized in previous years. These cells, whose differentiation is dependent on the transcription factor TCF1 (Utzschneider *et al.*, 2016) and several other transcription factors (Kallies *et al.*, 2020), retain the capacity of self-renewal and can give rise to the T_{EX} population. (Utzschneider *et al.*, 2016; Im *et al.*, 2016; Kallies *et al.*, 2020; Beltra *et al.*, 2020; Utzschneider *et al.*, 2020). T_{PEX} cells have been shown to be critical in maintaining the $CD8^+$ T cell response in chronic infection and cancer (Kallies *et al.*, 2020; Zehn *et al.*, 2022; Gago da Graça *et al.*, 2025). Furthermore, T_{PEX} cells are critical for the $CD8^+$ T cell response to ICB therapy (Miller *et al.*, 2019; Kallies *et al.*, 2020; B. Liu *et al.*, 2021).

ICB therapy, targeting CTLA-4 or PD-1/PD-L1, has greatly changed cancer therapy (Lonberg and Korman, 2017). Indeed, anti-PD-L1 and anti-CTLA4 have become prominent drugs for various types of cancer (Wei *et al.*, 2018). T_{PEX} cells respond to therapeutic ICB by undergoing enhanced proliferation and production of $CX3CR1^+$ effector-like T_{EX} cells (Siddiqui *et al.*, 2019; Miller *et al.*, 2019; Hudson *et al.*, 2019; Fang *et al.*, 2022), that have high expression of cytotoxic molecules such as GzmB (Zander *et al.*, 2019; Ishigaki *et al.*, 2024). Further increased levels of CX3CR1+ T_{EX} cells in the blood of ICB treated patients, have been correlated with clinical response of the therapy and improved long term survival rates (Yamauchi *et al.*, 2021). T_{PEX} cells express high levels of molecules such as CXCR5, CXCR3, CCR7, and CD62L compare to T_{EX} cells (Im *et al.*, 2016; He *et al.*, 2016; Leong *et al.*, 2016), indicating that T_{PEX} and T_{EX} cells are attracted to different locations in lymphoid organs that could influence their differentiation. Indeed CXCR5 allows T_{PEX} cells to migrate to the B cell zone where they have been shown to interact with B cells (Im *et al.*, 2016; He *et al.*, 2016; Leong *et al.*, 2016). This implies that environmental factors may direct T_{PEX} and T_{EX} differentiation.

Recently our group has identified two populations of transcriptionally and functionally distinct T_{PEX} cells that can be distinguished by the expression of

CD62L. CD62L$^+$ T_{PEX} cells have the highest efficacy to repones to ICB therapy like PD-L1 blockage (Tsui *et al.*, 2022). The molecular mechanisms and environmental influences that drive the differentiation of T_{PEX} cells, are yet to be explored further. CD62L$^+$ T_{PEX} have a higher expression of genes, which encode molecules that are associated with lymphocyte trafficking, such as CCR7, CD62L, S1PR1 and KLF2, compared to CD62L$^-$ T_{PEX} cells (Tsui *et al.*, 2022). This indicates that migratory behaviour of both subsets could be differentially regulated. In line with this notion, our group has discovered that the LN microenvironment favours the development of the CD62L$^+$ T_{PEX} and CX3CR1$^+$ T_{EX} cells (unpublished, Kallies Lab), suggesting that these two types of T_{PEX} cells may be exposed to different combination of environmental cues during chronic infection.

The spleen and LN exhibit differences in their architecture and cell composition. For example, LN are structured around a network of lymphatic vessels, whereas the spleen lacks these vessels (Ruddle and Akirav, 2009). Consequently, while immune cells enter the LN through specialized HEVs (Ruddle and Akirav, 2009), they have to enter the spleen through the blood (Lewis *et al.*, 2019). In general the spleen serves as a peripheral circulatory organ that contains two distinct compartments, including the red pulp (RP) and white pulp (WP) (Bronte and Pittet, 2013). Furthermore, LN and spleen harbour different myeloid and stromal cells (Haan *et al.*, 2012) suggesting that different niches for the maintenance and development of lymphocytes exist in both organs (Haan *et al.*, 2012).

In the context of LCMV infection, it was shown that the RP is the main site of infection in the spleen (Jung *et al.*, 2010; Im *et al.*, 2016). For example, during chronic LCMV infection, the RP contains high amounts of virus-infected macrophages, whereas a smaller number of infected cells (dendritic cells and fibroblastic reticular cells) were found in the splenic white pulp (Mueller *et al.*, 2007; Im *et al.*, 2016). As the RP does not occur in LN, this would suggest that T cells recognize their cognate antigen differently in the two organs.

These differences between the two organs support our hypothesis that CD62L$^+$ and CD62L$^-$ T_{PEX} cells are exposed to different signalling cues, which are coupled

to their intrinsically different migratory behaviour. In line with this hypothesis, previous studies have shown that during acute LCMV infection, most effector and central memory cells reside in the white pulp and terminally differentiated effector cells are exclusively localised in the red pulp (Jung *et al.*, 2010). Similar to the localisation of $CD8^+$ T cells in acute LCMV infection, a distinct localisation during chronic LCMV infection was found. T_{PEX} cells mainly reside in the splenic white pulp and LN, whereas T_{EX} cells are found in both the spleen and LN, but mainly in the red pulp, as well as in the blood and non-lymphoid organs such as the liver, brain, and intestines (Im *et al.*, 2016). Overall, these findings suggest an important role of tissue localisation in differentiation of exhausted T cells.

To understand whether and how differences in migratory behaviour and subsequent exposure to different microenvironments might influence exhausted T cells differentiation, we tested the role of three molecules that play an important role in trafficking of lymphocytes and that are expressed at high levels in $CD62L^+$ T_{PEX} cells, CD62L, CCR7 and S1PR1. By deleting these molecules separately, we aimed to further understand the function of the contribution of each molecule to trafficking and localisation of T_{PEX} cells and how this impacts the differentiation and function of exhausted T cell.

4.2 Results

4.2.1 Exhausted T cell accumulation and development of CX3CR1^{+} T_{EX} cell are dependent on CD62L mediated functions

CD62L (L-selectin) is an adhesion molecule known to be important for entry to the lymph nodes (Girard *et al.*, 2012). It is expressed on the surface of naïve, circulating memory T cells and a fraction of T_{PEX} cells . Mechanistically, CD62L enables the tethering of lymphocytes to its specific ligands CD34 (Puri *et al.*, 1995; Bai *et al.*, 2007; Martin and Badovinac, 2018; Tsui *et al.*, 2022) and glycosylation-dependent cell adhesion molecule-1 (GlyCAM-1) (Nicholson *et al.*, 1998). GlyCAM-1 is highly expressed on HEVs within lymph nodes (Diacovo *et al.*, 1998). Tethering of lymphocytes allows them to be slowed down, which facilitates their crossing of the endothelium to enter into the paracortex of the LN (Von Andrian and Mempel, 2003).

Whether the expression of CD62L on T_{PEX} cells is required for their development, maintenance and function has not been addressed. To investigate this, we deleted CD62L expression on P14 T cells using the CRISPR-Cas9 system (CD62L-KO). We confirmed the efficacy of our CRISPR-Cas9 gene targeting approach by flow cytometry (Figure 4.1). To this end, CD62L-KO and Ctrl cells were plated *in vitro* and left unstimulated or stimulated with Gp33. After 24 hrs, we measured the surface expression of CD62L in Ctrl and CD62L-KO P14 cells. The majority of stimulated and unstimulated CD62L-KO cells had lost CD62L expression (Figure 4.1A). CD62L-KO cells that still maintained some level of CD62L expression had lower expression of the protein compared to Ctrl cells (Figure 4.1A). These data showed an efficient deletion strategy using our targeting approach.

To test the effect of the loss of CD62L expression *in vivo*, naïve CD62L-KO cells or Ctrl P14 cells were transferred to recipient mice, which were then infected with LCMV-Clone13 (Figure 4.1B). On day 21 post infection, we analysed T_{PEX} and T_{EX} cells by flow cytometry. Compared to Ctrl P14 cells, CD62L-KO P14 cells exhibited a significant decrease in frequencies in both organs (Figure 4.1C and

D). A numerical reduction of CD62L-KO P14 cells was also observed in the LN, but not in the spleens, likely due to the small sample size used in this experiment (Figure 4.1D). Additionally, the loss of CD62L also resulted in increased expression of PD-1 in the spleen but not the LN (Figure 4.1E).

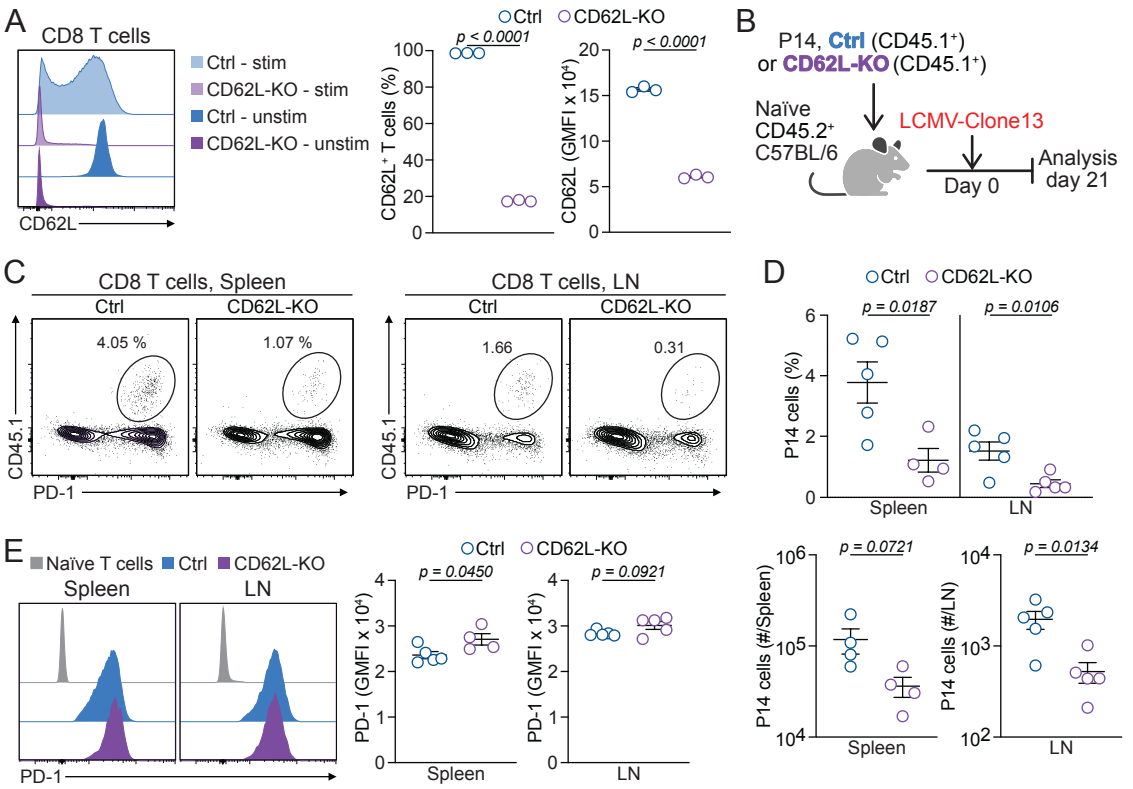

Figure 4.1: Loss of CD62L impairs the accumulation of P14 CD8⁺ T cells in the LN.

(A) Naïve CD62L-KO (CD45.1⁺) or Ctrl (CD45.1⁺) P14 cells were incubated in vitro for 24 hrs with or without Gp33 peptide. CD62L expression was quantified using flow cytometry. Representative histogram and quantification of frequencies and expression of CD62L in CD62L-KO or Ctrl P14 cells. (B-E) Naïve CD62L-KO (CD45.1⁺) or Ctrl (CD45.1⁺) P14 cells were adoptively transferred into naïve wildtype CD45.2⁺ mice and subsequently infected with LCMV-Clone13. On day 21 p.i. spleens and LN were analysed using flow cytometry. (B) Schematic of experimental setup. (C) Representative flow cytometry plots showing frequencies of CD62L-KO or Ctrl P14 cells. (D) Quantification of frequencies and numbers of CD62L-KO or Ctrl P14 cells. (E) Representative histogram and quantification of PD-1 expression in CD62L-KO or Ctrl P14 cells. Dots in graphs represent individual mice; horizontal lines and error bars of bar graphs indicate means ± SEM, respectively. Data is representative of one experiment. P values are from unpaired student's t test.

To evaluate how CD62L-KO P14 cells impacted exhausted T cell differentiation, we compared the frequencies of both T_{PEX} and T_{EX} cells between Ctrl and CD62L-KO cell in the spleens and LN. CD62L-KO T_{PEX} cell frequencies were reduced in the LN but not the spleens, compared with Ctrl T_{PEX} cells (Figure 4.2A-C). Overall, no differences were observed in the expression of TCF1 and Ly108 between CD62L-KO and Ctrl cells in the spleens and LN (Figure 4.2D). As expected, CD62L-KO T_{PEX} cells exhibited reduced CD62L expression compared to Ctrl T_{PEX} cells (Figure 4.2E and F). In the LN, the frequencies of KO T_{PEX} cells expressing CD62L was reduced by approximately 50 % compared Ctrl T_{PEX} cells (Figure 4.2E and F) suggesting inefficient targeting and selection of cells that had not deleted CD62L efficiently or have undergone double-stranded DNA break repairments (Xue and Greene, 2021). These data strongly suggest a role of CD62L in the development of T_{PEX} cells. Within the T_{EX} compartment in both the spleens and LN, we observed a consistent reduction of $CX3CR1^+$ T_{EX} cells but not $CD101^+$ T_{EX} cells in the CD62L-KO cells (Figure 4.2G and H). We did not observe changes in the expression of the inhibitory receptors, including Lag-3, 2B4, and Tim-3, among Ctrl and CD62L-KO T_{EX} cells (Figure 4.2I). Taken together the loss of CD62L impairs the maintenance of T_{PEX} cells and differentiation of $CX3CR1^+$ T_{EX} cells.

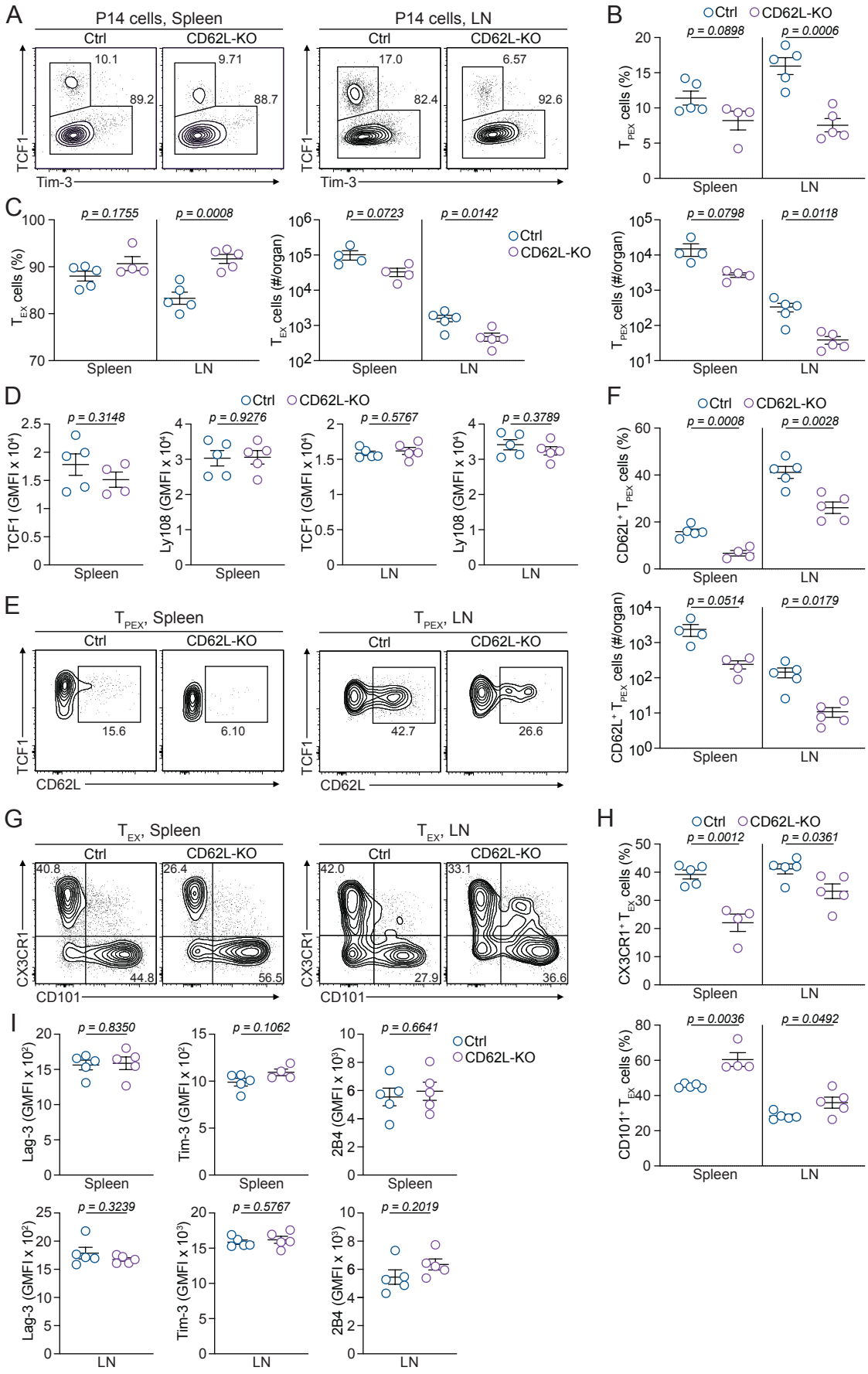
A
P14 cells, Spleen
Ctrl
CD62L-KO
10.1
89.2
9.71
88.7
TCF1
Tim-3
P14 cells, LN
17.0
82.4
6.57
92.6
B
Ctrl
CD62L-KO
p = 0.0898
p = 0.0006
T_PEX cells (%)
Spleen
LN
p = 0.0798
p = 0.0118
T_PEX cells (#/organ)
C
p = 0.1755
p = 0.0008
T_EX cells (%)
p = 0.0723
p = 0.0142
T_EX cells (#/organ)
D
p = 0.3148
p = 0.9276
p = 0.5767
p = 0.3789
TCF1 (GMFI x 10⁴)
Ly108 (GMFI x 10⁴)
F
p = 0.0008
p = 0.0028
CD62L⁺ T_PEX cells (%)
p = 0.0514
p = 0.0179
CD62L⁺ T_PEX cells (#/organ)
E
T_PEX, Spleen
15.6
6.10
CD62L
T_PEX, LN
42.7
26.6
G
T_EX, Spleen
40.8
44.8
26.4
56.5
CX3CR1
CD101
T_EX, LN
42.0
27.9
33.1
36.6
H
p = 0.0012
p = 0.0361
CX3CR1⁺ T_EX cells (%)
p = 0.0036
p = 0.0492
CD101⁺ T_EX cells (%)
I
p = 0.8350
p = 0.1062
p = 0.6641
Lag-3 (GMFI x 10²)
Tim-3 (GMFI x 10²)
2B4 (GMFI x 10³)
p = 0.3239
p = 0.5767
p = 0.2019
Tim-3 (GMFI x 10³)

Figure 4.2: Loss of CD62L impairs maintenance of T_{PEX} cells and differentiation CX3CR1$^+$ T_{EX} cells.
(A-I) Naïve CD62L-KO (CD45.1$^+$) or Ctrl (CD45.1$^+$) P14 cells were adoptively transferred into naïve wildtype CD45.2$^+$ mice and subsequently infected with LCMV-Clone13. On day 21 p.i. spleens and LN were analysed using flow cytometry. (A) Representative flow cytometry plots showing of CD62L-KO or Ctrl T_{PEX} (TCF1$^+$Tim-3$^-$) and T_{EX} (TCF1$^-$Tim-3$^+$) cells. (B) Quantification of CD62L-KO or Ctrl T_{PEX} (TCF1$^+$Tim-3$^-$) frequencies and numbers. (C) Quantification of CD62L-KO or Ctrl T_{EX} (TCF1$^-$Tim-3$^+$) frequencies and numbers. (D) Quantification of TCF1 and Ly108 expression in CD62L-KO or Ctrl T_{PEX} cells. (E) Representative flow cytometry plots showing of CD62L-KO or Ctrl CD62L$^+$ T_{PEX} cells. (F) Quantification of CD62L-KO or Ctrl CD62L$^+$ T_{PEX} cells frequencies and numbers. (G) Representative flow cytometry plots showing of CD62L-KO or Ctrl CX3CR1$^+$ and CD101$^+$ T_{EX} cells. (H) Quantification of CD62L-KO or Ctrl CX3CR1$^+$ and CD101$^+$ T_{EX} cells frequencies and numbers. (I) Quantification of Lag3, 2B4, and Tim-3 expression in CD62L-KO or Ctrl T_{EX} cells. Dots in graphs represent individual mice; horizontal lines and error bars of bar graphs indicate means ± SEM, respectively. Data is representative of one experiment. P values are from unpaired student's t test.

We next explored whether the loss of CD62L-KO P14 cells was associated with changes in the proliferative capacity of the cells (Figure 4.3). We found that similar frequencies of Ctrl and CD62L-KO P14 cells, including T_{PEX} and T_{EX} cells, expressed Ki-67 in both organs (Figure 4.3A). Furthermore, expression levels of Ki-67 between CD62L-KO and Ctrl P14 cells were not altered (Figure 4.3B). To test whether the changes in T_{PEX} and T_{EX} cell development in the absence of CD62L were accompanied by changes in functionality, we measured their capacity to produce effector cytokines upon restimulation and GzmB in the spleens. In general, no major differences were observed for IFN-γ^+ cells between CD62L-KO and Ctrl P14 cells (Figure 4.3D). We did observe, however, a mild increase of polyfunctional IFN-γ^+TNF$^+$ CD62L-KO P14 cells compared to Ctrl P14 cells (Figure 4.3D). However, analysis on T_{PEX} and T_{EX} population separately revealed no significant differences in the frequency of IFN-γ cells that could express TNF (Figure 4.3E and F). Expression of IFN-γ and TNF on a per cell basis in CD62L-KO and Ctrl P14 cells was not different (Figure 4.3D). Notably, however, CD62L-KO T_{EX} cells produced reduced levels of GrzmB compared with

Ctrl cells (Figure 4.3G). Taken together these data suggest that the loss of CD62L has a modest impact on effector capacity of T_{PEX} and T_{EX} cells in chronic infection.

In summary this section has characterised the effect of CD62L deletion on the differentiation, maintenance and functionality of T_{PEX} and T_{EX} cells. We found that CD62L expression is required for the accumulation of T_{PEX} cells particularly in the LN. We also observed that CX3CR1^{+} T_{EX} cell differentiation was impacted by the loss of CD62L. Given that CD62L is not expressed in T_{EX} cells, these findings supported a model by which the expression of CD62L in T_{PEX} cells affects the downstream generation of CX3CR1^{+} T_{EX} cells. However, these experiments were done only once, and the data needs to be confirmed.

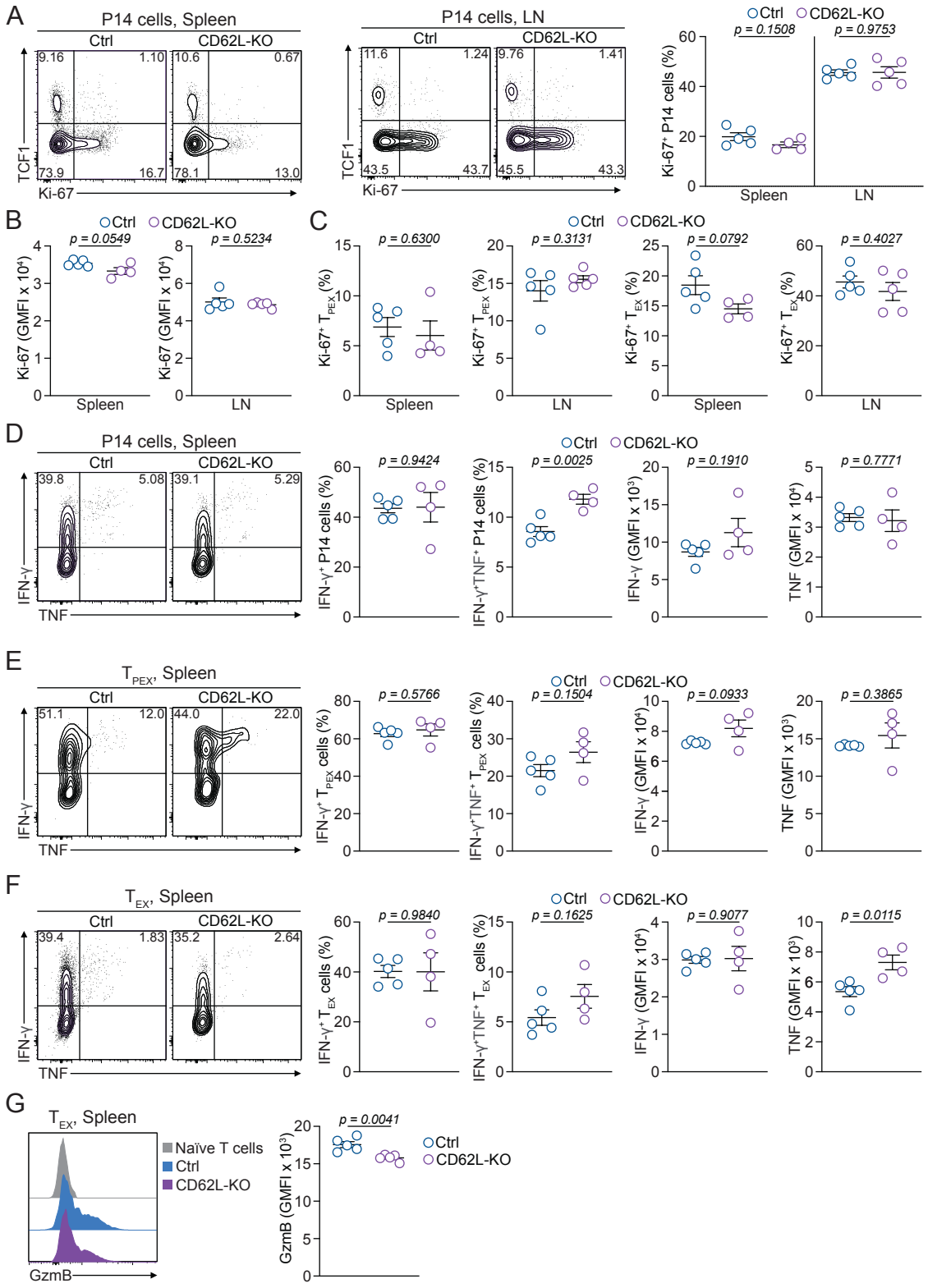

Figure 4.3: No or modest impact of CD62L on Ki-67 expression and production of effector cytokines IFN-γ and TNF and GzmB.
(A-G) Naïve CD62L-KO (CD45.1⁺) or Ctrl (CD45.1⁺) P14 cells were adoptively transferred into naïve wildtype CD45.2⁺ mice and subsequently infected with LCMV-Clone13. On day 21 p.i. spleens and LN were analysed using flow

cytometry. For (D-G) splenocytes were stimulated with Gp33 ex vivo. (A) Representative flow cytometry plots and quantification showing frequencies of Ki-67$^+$ CD62L-KO and Ctrl P14 cells. (B) Quantification of Ki-67 expression in CD62L-KO and Ctrl P14 cells. (C) Quantification of Ki-67 expression in CD62L-KO and Ctrl T_{PEX} and T_{EX} cells. (D) Representative flow cytometry plots and quantification showing frequencies of IFN-γ and TNF producing CD62L-KO and Ctrl P14 cells and expression levels of IFN-γ and TNF. (E) Representative flow cytometry plots and quantification showing frequencies of IFN-γ and TNF producing CD62L-KO and Ctrl T_{PEX} cells and expression levels of IFN-γ and TNF. (F) Representative flow cytometry plots and quantification showing frequencies of IFN-γ and TNF producing CD62L-KO and Ctrl T_{EX} cells and expression levels of IFN-γ and TNF. (G) Representative histogram and quantification showing production of GzmB in CD62L-KO and Ctrl T_{EX} cells. Dots in graphs represent individual mice; horizontal lines and error bars of bar graphs indicate means ± SEM, respectively. Data is representative of one experiment. P values are from unpaired student's t test.

4.2.2 Differentiation of CD62L$^+$ T_{PEX} and CX3CR1$^+$ T_{EX} cells is dependent on CCR7

We next tested the function of CCR7 in maintenance and function of exhausted T cell. CCR7 is a chemokine receptor necessary for the migration and localization of CD8$^+$ T cells to and within the secondary lymphoid organs, including spleen and LN (Bjorkdahl *et al.*, 2003; Höpken *et al.*, 2004; Masopust and Schenkel, 2013). More specifically CCR7 enables the migration of CD8$^+$ T cells to the T cells zone, where they are primed by APC cells and undergo rapid clonal expansion (Hickman *et al.*, 2008; Zhang and Bevan, 2011; Hickman *et al.*, 2011).

Whether CCR7 expression in T_{PEX} cells contributes to development, maintenance or function has to be further investigated. To this end, we used the CRISPR-Cas9 system to delete CCR7 (CCR7-KO). Naïve CCR7-KO and Ctrl P14 cells were adoptively transferred into recipient mice, that were later infected with LCMV-Clone13 (Figure 4.4A). At day 21 post infection, CCR7-KO and Ctrl P14 cells in the spleens and LN were analysed using flow cytometry. We validated the effectiveness of our CRISPR-Cas9 gene targeting method, by flow analysis of CCR7 expression in T_{PEX} cells. We observed reduction of CCR7 expression level on a single cell level in CCR7-KO T_{PEX} cells, compared to Ctrl T_{PEX} cells in both

the spleens and the LN (Figure 4.4B) demonstrating the effectiveness of our targeting approach. Frequencies of CCR7-KO P14 cells were severely reduced in the spleens and LN compared to Ctrl P14 cells (Figure 4.4C and D). Further CCR7-KO P14 cells expressed elevated levels of PD-1 in the spleens compared to Ctrl P14 cells, but not in the LN, while expression levels of TOX were similar in both organs (Figure 4.4E and F).

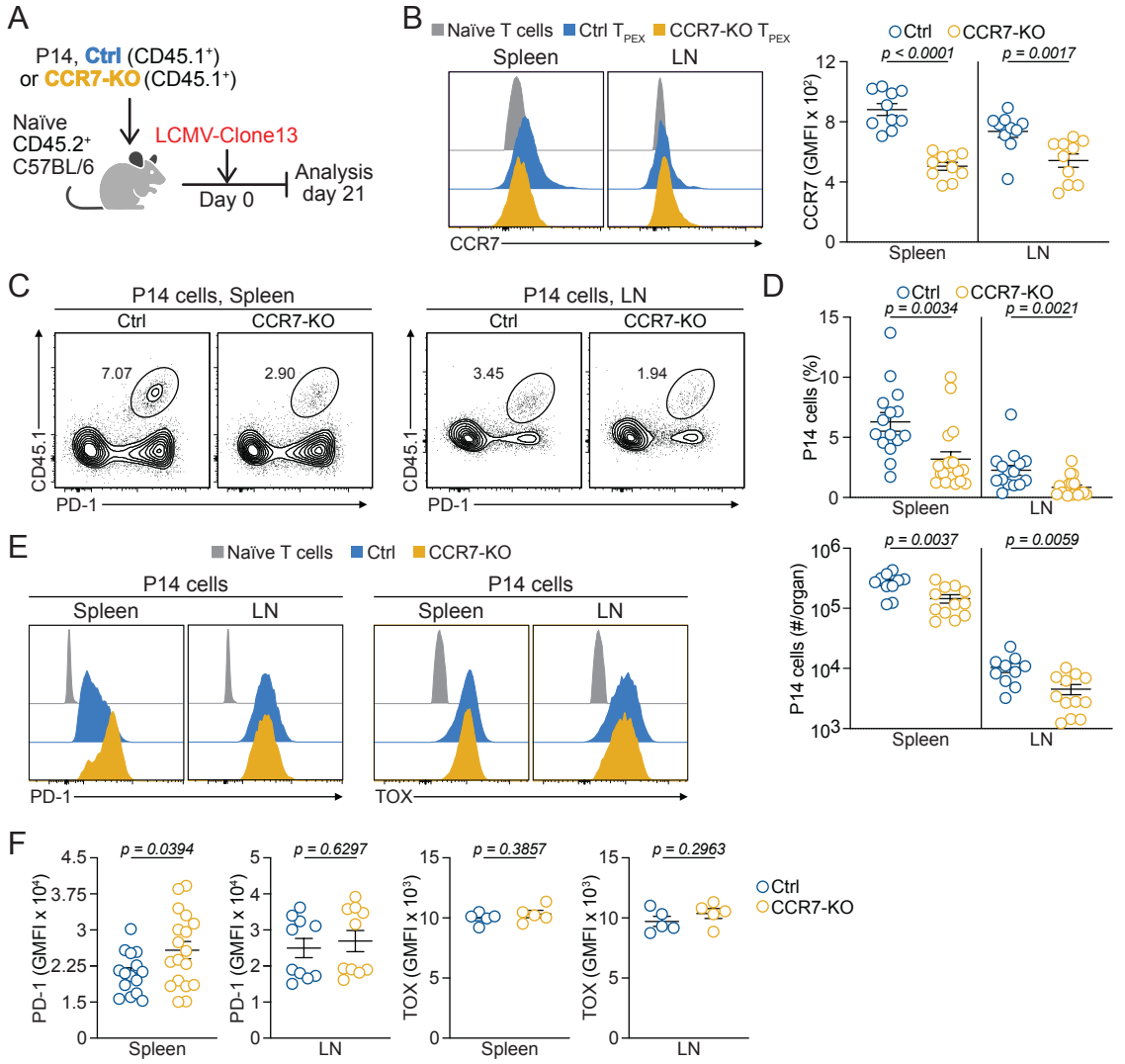

Figure 4.4: CCR7 is required for CD8⁺ T cell expansion in lymphoid organs spleen and LN.
(A-F) Naïve CCR7-KO (CD45.1⁺) or Ctrl (CD45.1⁺) P14 cells were adoptively transferred into naïve wildtype CD45.2⁺ mice and subsequently infected with LCMV-Clone13. On day 21 p.i. spleens and LN were analysed using flow cytometry. (A) Schematic of experimental setup. (B) Representative histograms and quantification of CCR7 expression in CCR7-KO and Ctrl T_{PEX} cells. (C) Representative flow cytometry plots showing frequencies of CCR7-KO or Ctrl

P14 cells. (D) Quantification of frequencies and numbers of CCR7-KO or Ctrl P14 cells. (E) Representative histogram showing PD-1 and TOX expression in CCR7-KO or Ctrl P14 cells. (F) Quantification of PD-1 and TOX expression in CCR7-KO or Ctrl P14 cells. Dots in graphs represent individual mice; horizontal lines and error bars of bar graphs indicate means ± SEM, respectively. Data is pooled from two (B-F) independent experiments or representative of one (F). P values are from unpaired student's t test.

We next compared the frequencies of T_{PEX} and T_{EX} cells between Ctrl and CCR7-KO cells in the spleens and LN. CCR7-KO cells were showed decreased frequencies in both organs; conversely, there were increased frequencies of CCR7-KO T_{EX} cells compared to Ctrl cells (Figure 4.5A and B). Numerically, compared to Ctrl T_{PEX} cells, CCR7-KO T_{PEX} cells were reduced in both organs. Similar numbers of CCR7-KO T_{EX} cells and Ctrl T_{EX} cells were in the spleens, while decreased CCR7-KO T_{EX} cells were found in the LN (Figure 4.5C). In the spleens, levels of TCF1, but not Ly108, were reduced in CCR7-KO T_{PEX} cells compared to Ctrl T_{PEX} cells (Figure 4.5D). In the LN, the expression of Ly108, but not TCF1, was reduced upon CCR7 depletion (Figure 4.5D). Furthermore CCR7-KO T_{EX} cells in the LN but not the spleens expressed reduced levels of inhibitory receptor Tim-3 compared to Ctrl T_{EX} cells (Figure 4.5D), overall indicating that CCR7 affects exhausted T cells differently in the spleen and LN. The frequencies and numbers of CCR7-KO CD62L$^+$ T_{PEX} cells were reduced compared to Ctrl CD62L$^+$ T_{PEX} cells in both the spleen and LN (Figure 4.5E and F). Finally, CCR7-KO T_{EX} cells exhibited reduced frequencies and numbers of effector-like CX3CR1$^+$ T_{EX} population compared to Ctrl T_{EX} cells in the spleens and LN (Figure 4.5G and H). In contrast, the frequencies of CCR7-KO CD101$^+$ T_{EX} cells were increased in both organs compared to Ctrl CD101$^+$ T_{EX} cells, although the numbers were not different (Figure 4.5G and H).

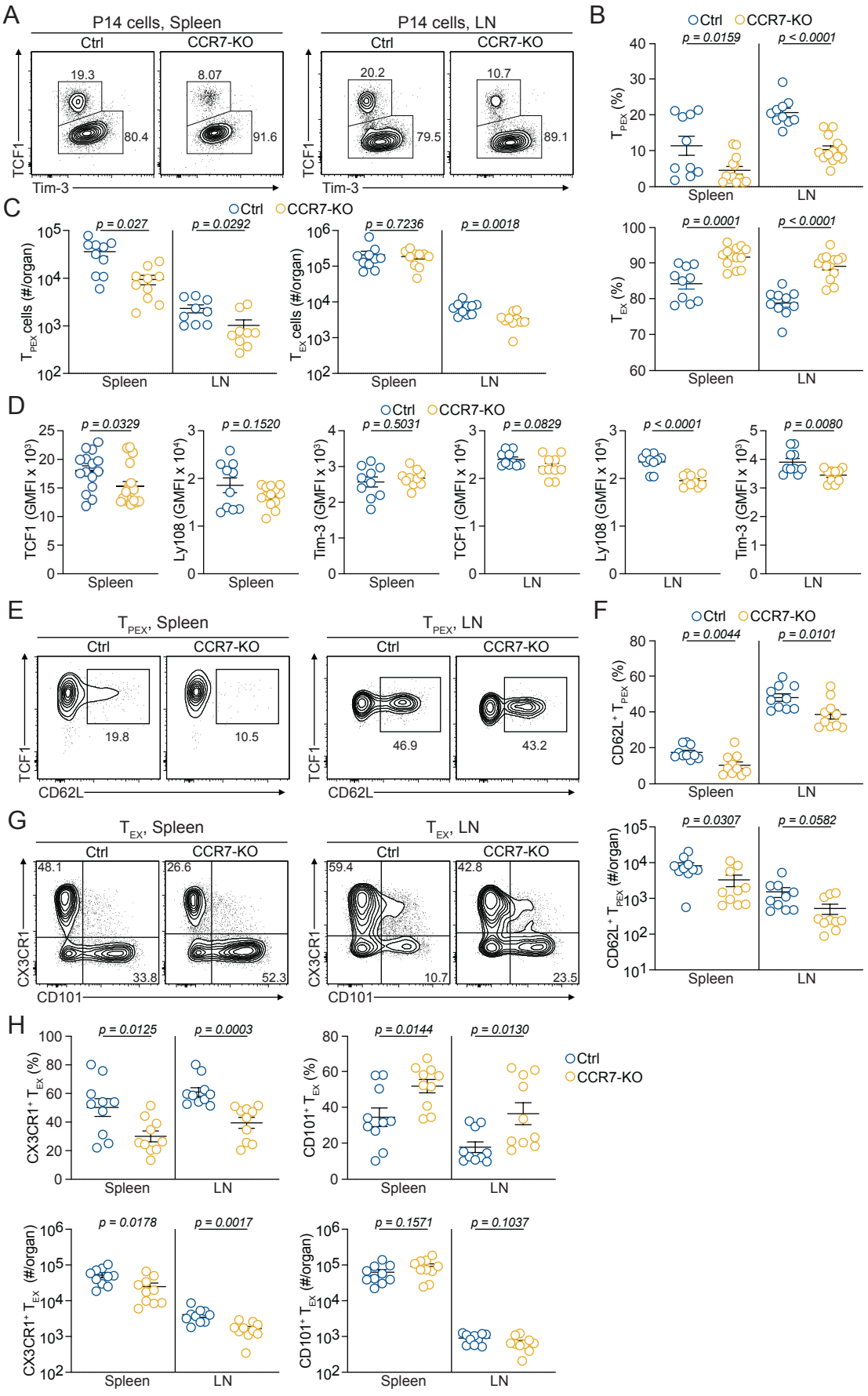
A
P14 cells, Spleen
P14 cells, LN
Ctrl
CCR7-KO
TCF1
Tim-3
19.3
80.4
8.07
91.6
20.2
79.5
10.7
89.1
B
Ctrl
CCR7-KO
p = 0.0159
p < 0.0001
T_PEX (%)
Spleen
LN
C
p = 0.027
p = 0.0292
p = 0.7236
p = 0.0018
T_PEX cells (#/organ)
T_EX cells (#/organ)
p = 0.0001
p < 0.0001
T_EX (%)
D
p = 0.0329
p = 0.1520
p = 0.5031
p = 0.0829
p < 0.0001
p = 0.0080
TCF1 (GMFI x 10³)
Ly108 (GMFI x 10⁴)
Tim-3 (GMFI x 10³)
TCF1 (GMFI x 10⁴)
Ly108 (GMFI x 10⁴)
Tim-3 (GMFI x 10³)
E
T_PEX, Spleen
T_PEX, LN
19.8
10.5
46.9
43.2
CD62L
F
p = 0.0044
p = 0.0101
CD62L⁺ T_PEX (%)
G
T_EX, Spleen
T_EX, LN
48.1
33.8
26.6
52.3
59.4
10.7
42.8
23.5
CX3CR1
CD101
p = 0.0307
p = 0.0582
CD62L⁺ T_PEX (#/organ)
H
p = 0.0125
p = 0.0003
p = 0.0144
p = 0.0130
CX3CR1⁺ T_EX (%)
CD101⁺ T_EX (%)
p = 0.0178
p = 0.0017
p = 0.1571
p = 0.1037
CX3CR1⁺ T_EX (#/organ)
CD101⁺ T_EX (#/organ)

Figure 4.5: CCR7 deletion impairs the development and quality of T_{PEX} cells and the differentiation of CX3CR1$^+$ T_{EX} cells.
(A-H) Naïve CCR7-KO (CD45.1$^+$) or Ctrl (CD45.1$^+$) P14 cells were adoptively transferred into naïve wildtype CD45.2$^+$ mice and subsequently infected with LCMV-Clone13. On day 21 p.i. spleens and LN were analysed using flow cytometry. (A) Representative flow cytometry plots showing CCR7-KO and Ctrl T_{PEX} (TCF1$^+$Tim-3$^-$) and T_{EX} (TCF1$^-$Tim-3$^+$) cells. (B) Quantification of CCR7-KO and Ctrl T_{PEX} and T_{EX} frequencies. (C) Quantification of CCR7-KO and Ctrl T_{PEX} and T_{EX} numbers per organ. (D) Quantification of TCF1 and Ly108 expression in CCR7-KO and Ctrl T_{PEX} cells and Tim-3 expression in CCR7-KO and Ctrl T_{EX} cells. (E) Representative flow cytometry plots showing CCR7-KO and Ctrl CD62L$^+$ T_{PEX} cells. (F) Quantification of CCR7-KO and Ctrl CD62L$^+$ T_{PEX} frequencies and numbers per organ. (G) Representative flow cytometry plots showing CCR7-KO and Ctrl CX3CR1$^+$ and CD101$^+$ T_{EX} cells. (H) Quantification of CCR7-KO and Ctrl CX3CR1$^+$ and CD101$^+$ T_{EX} frequencies and numbers per organ. Dots in graphs represent individual mice; horizontal lines and error bars of bar graphs indicate means ± SEM, respectively. Data is pooled from two independent experiments. P values are from unpaired student's t test.

Next, we tested if the loss of CCR7 impairs effector functions of exhausted T cells. Overall, we observed no major differences between CCR7-KO and Ctrl P14 cells in the ability to produce IFN-γ and TNF$^+$ (Figure 4.6A-C). On a single cell level, however, the amount of IFN-γ in CCR7-KO T_{PEX} cells was higher than in Ctrl cells, although only modest, while expression levels of TNF were similar in both CCR7-KO cells and Ctrl cells (Figure 4.6A-C). Finally, CCR7-KO T_{EX} cells produced reduced levels of GzmB compared with Ctrl cells (Figure 4.6D), which was likely due to reduced numbers of CCR7-KO CX3CR1$^+$ T_{EX} cells.

Overall, our data suggest that the loss of CCR7 impairs the maintenance and quality of T_{PEX} cells particularly the CD62L$^+$ T_{PEX} cells. Moreover, CX3CR1$^+$ T_{EX} cell differentiation was also severely impaired by the loss of CCR7. In contrast the development of CD101$^+$ T_{EX} cells was independent of the function of CCR7. Similar to our previous chapter, these finding support a model by which the expression and function of CCR7 in T_{PEX} cells affects the generation of CX3CR1$^+$ T_{EX} cells.

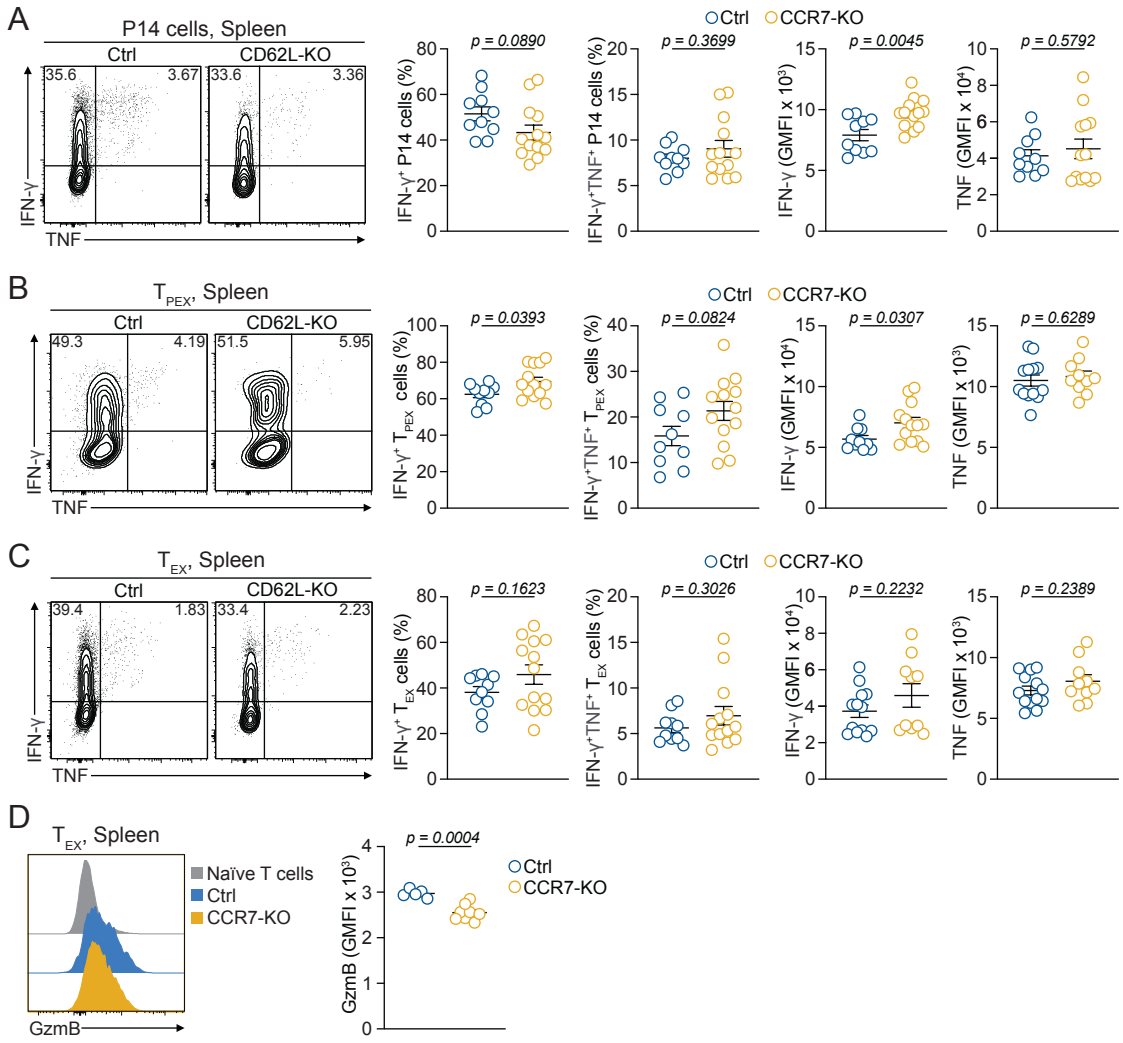

Figure 4.6: Effector cytokine production in T_{PEX} and T_{EX} cells is largely independent of CCR7-mediated functions.
(A-G) Naïve CCR7-KO (CD45.1$^+$) or Ctrl (CD45.1$^+$) P14 cells were adoptively transferred into naïve wildtype CD45.2$^+$ mice and subsequently infected with LCMV-Clone13. On day 21 p.i. spleens were analysed using flow cytometry. Splenocytes were stimulated with Gp33 *ex vivo*. (A) Representative flow cytometry plots and quantification showing frequencies of IFN-γ and TNF producing CCR7-KO and Ctrl P14 cells and expression levels of IFN-γ and TNF. (B) Representative flow cytometry plots and quantification showing frequencies of IFN-γ and TNF producing CCR7-KO and Ctrl T_{PEX} cells and expression levels of IFN-γ and TNF. (C) Representative flow cytometry plots and quantification showing frequencies of IFN-γ and TNF producing CCR7-KO and Ctrl T_{EX} cells and expression levels of IFN-γ and TNF. (D) Representative histogram and quantification showing production of GzmB in CCR7-KO and Ctrl T_{EX} cells. Dots in graphs represent individual mice; horizontal lines and error bars of bar graphs indicate means ± SEM, respectively. Data is pooled from two independent experiments. P values are from unpaired student's t test.

4.2.3 CX3CR1$^+$ T_{EX} cells egress from the LN to other secondary lymphoid organs using S1PR1

We next investigated how changes in migratory behaviour influences the differentiation of exhausted T cells by targeting S1PR1. S1PR1 is a G-coupled protein receptor which is expressed on T cells and regulates the egress of T cells from the thymus (Allende *et al.*, 2004). It also affects the systemic trafficking of peripheral CD8$^+$ T cells (Chi and Flavell, 2005). Specifically, egress of CD8$^+$ T cells from the LN requires S1PR1 (Cyster and Schwab, 2012; Benechet *et al.*, 2016). In chronic infection S1PR1 has been shown to be expressed by T_{PEX} cells and CX3CR1$^+$ T_{EX} cells but not CD101$^+$ T_{EX} cells (unpublished data, Kallies lab).

To investigate how the deletion of S1PR1 affect maintenance, differentiation and functionality of T_{PEX} and T_{EX} cells, we used the CRISPR-Cas9 system to deplete S1PR1 (S1PR1-KO). S1PR1-KO and Ctrl P14 cells were adoptively co-transferred into recipients at a ratio of 1:1. Mice were then infected with chronic LCMV-Clone13 and spleen and LN analysed on day 21 post infection using flow cytometry (Figure 4.7A). We observed no differences in the ratio of S1PR1-KO to Ctrl P14 in the spleen or LN (Figure 4.7B and C) with a mild decrease of S1PR1-KO in the spleen (Figure 4.7C). S1PR1-KO P14 cells expressed higher levels of PD-1 in the spleen than Ctrl P14 cells (Figure 4.7D). However, in the LN decreased expression levels of PD-1 was observed in S1PR1-KO cells compared to Ctrl P14 cells (Figure 4.7D). Expression of TOX was not altered by the deletion of S1PR1 in P14 cells residing in the spleen but mildly decreased in S1PR1-KO P14 cells in the LN compared to Ctrl P14 cells (Figure 4.7E).

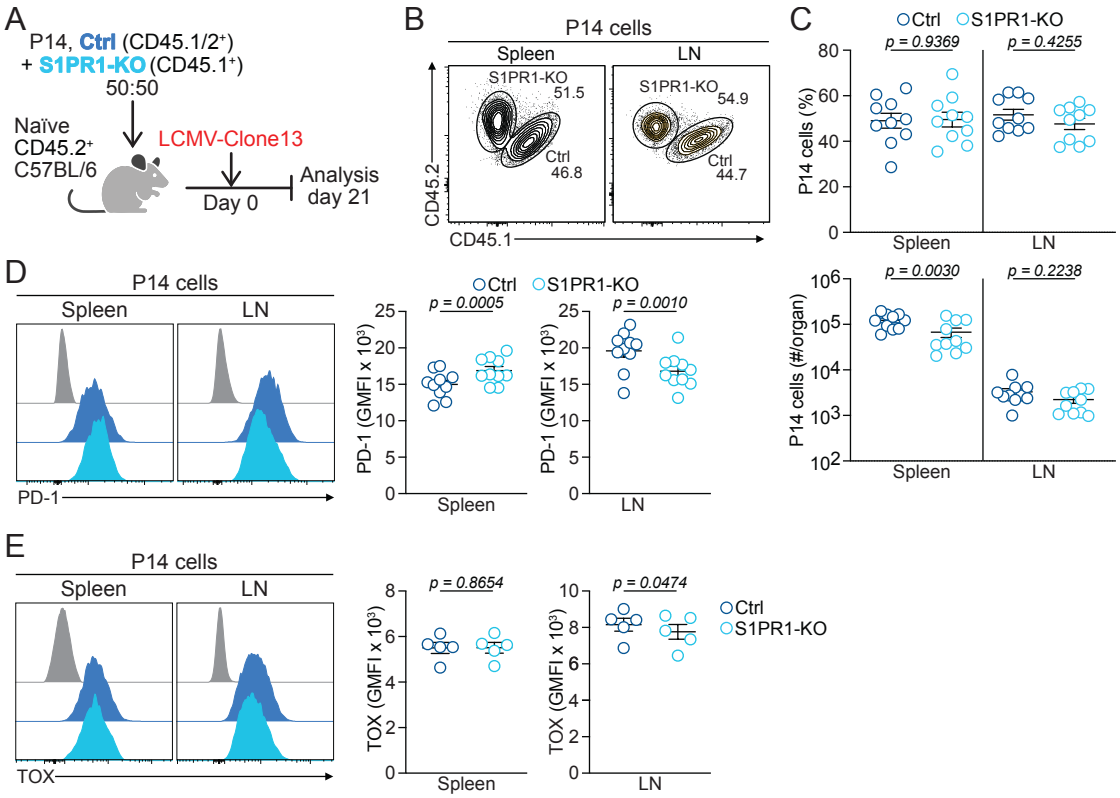

Figure 4.7: S1PR1 deletion does not impact P14 accumulation in the spleen and LN but affects PD-1 and TOX expression.
(A-F) Naïve S1PR1-KO (CD45.1+) or Ctrl (CD45.1/2+) P14 cells were adoptively co-transferred into naïve wildtype CD45.2+ mice and subsequently infected with LCMV-Clone13. On day 21 p.i. spleens and LN were analysed using flow cytometry. (A) Schematic of experimental setup. (B) Representative flow cytometry plots showing ratios of S1PR1-KO or Ctrl P14 cells. (C) Quantification of frequencies and numbers of S1PR1-KO or Ctrl P14 cells. (D) Representative histogram and quantification showing PD-1 expression in S1PR1-KO or Ctrl P14 cells. (E) Representative histogram and quantification showing TOX expression in S1PR1-KO or Ctrl P14 cells. Dots in graphs represent individual mice; horizontal lines and error bars of bar graphs indicate means ± SEM, respectively. Data is pooled from two independent experiments. P values are from paired student's t test.

Previous studies have shown that the activation marker CD69 can physically interact with S1PR1. This binding initiates the degradation of S1PR1 (Bankovich *et al.*, 2010), decreasing expression levels, and blocking egress from the LN (Shiow *et al.*, 2006). In line with this notion, we could observe that the majority of S1PR1-KO P14 cells in the spleens were CD69+, whereas only half of the Ctrl P14 cells expressed CD69 (Figure 4.8A). In the LN, this increase was less strong, with approximately 75 % of S1PR1-KO P14 cells and 55 % of Ctrl P14 cells

expressing CD69 (Figure 4.8A). Further CD69 expression levels were significantly increased in S1PR1-KO P14 cells in the spleens but not in the LN (Figure 4.8B).

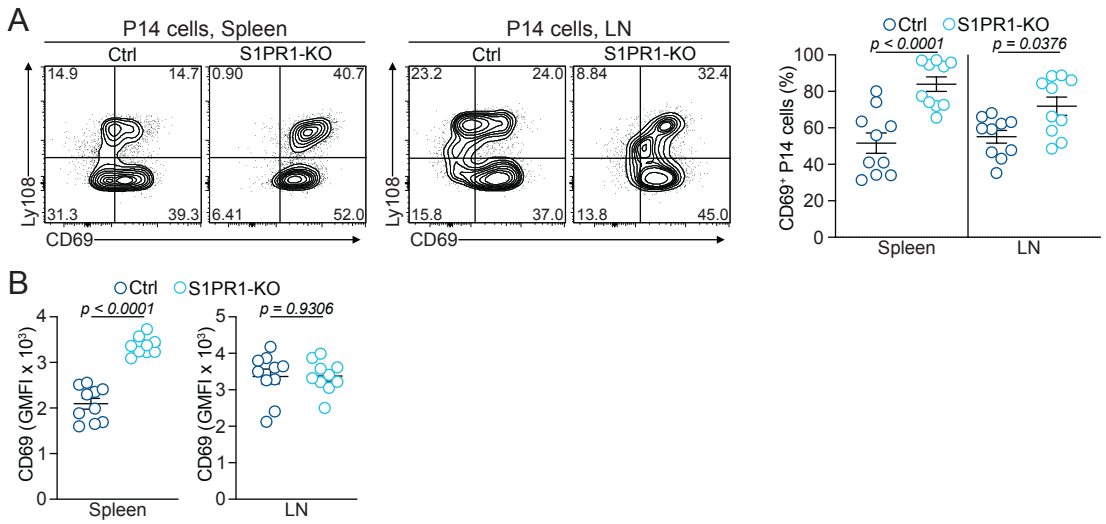

Figure 4.8 S1PR1-KO P14 cells upregulate CD69.
(A-H) Naïve S1PR1-KO (CD45.1$^+$) or Ctrl (CD45.1/2$^+$) P14 cells were adoptively co-transferred into naïve wildtype CD45.2$^+$ mice and subsequently infected with LCMV-Clone13. On day 21 p.i. spleens and LN were analysed using flow cytometry. (A) Representative flow cytometry plots and quantification showing CD69$^+$ T_{PEX} and T_{EX} cells in S1PR1-KO and Ctrl P14. (B) Quantification of CD69 expression in S1PR1-KO and Ctrl P14 cells. Dots in graphs represent individual mice; horizontal lines and error bars of bar graphs indicate means ± SEM, respectively. Data is pooled from two independent experiments. P values are from paired student's t test.

Next, we evaluated if S1PR1 deletion affect the maintenance and differentiation of T_{PEX} and T_{EX} subset populations. We observed increased frequencies and numbers of T_{PEX} cells and decreased frequencies and numbers of T_{EX} cells in the spleens upon depletion of S1PR1 compared to Ctrl T_{PEX} cells (Figure 4.9A and B). The opposite was seen in the LN, where frequencies and numbers of S1PR1-KO T_{PEX} cells were reduced and S1PR1-KO T_{EX} cells increased compared to Ctrl cells (Figure 4.9A - C). In the LN, numbers of S1PR1-KO T_{EX} cells were reduced compared to Ctrl T_{EX} cells, while no obvious changes were seen between the number S1PR1-KO and Ctrl T_{PEX} cells (Figure 4.9C). Expression levels of TCF1

and Ly108 in the spleens were similar between S1PR1-KO and Ctrl T_{PEX} cells and S1PR1-KO T_{EX} displayed similar expression of Tim-3 as Ctrl T_{EX} cells (Figure 4.9D). S1PR1-KO T_{PEX} cells in the LN expressed decreased amounts of both TCF1 and Ly108 compared to Ctrl T_{PEX} cells (Figure 4.9D). Additionally, Tim-3 expression was reduced in S1PR1-KO T_{EX} cells compared to Ctrl cells. The frequencies of S1PR1-KO and Ctrl CD62L$^+$ T_{PEX} were similar in both organs (Figure 4.9E and F), while the number of S1PR1-KO CD62L$^+$ T_{PEX} cells was mildly decreased in the LN but similar to Ctrl cells in the spleens (Figure 4.9F). Importantly, S1PR1 impacted accumulation of CX3CR1$^+$ T_{EX} and CD101$^+$ T_{EX} cells in both organs. Indeed, frequencies and numbers of S1PR1-KO CX3CR1$^+$ T_{EX} cells were reduced in the spleens compared to Ctrl CX3CR1$^+$ T_{EX} cells (Figure 4.9G and H). Correspondingly, frequencies but not numbers of S1PR1-KO CD101$^+$ T_{EX} cells were increased in the spleens (Figure 4.9G and H). In contrast, there were increased proportions of CX3CR1$^+$ T_{EX} cells and decreased frequencies of CD101$^+$ T_{EX} cells among S1PR1-KO compared to Ctrl in the LN (Figure 4.9G and H). LN, however, harboured similar numbers of S1PR1-KO and Ctrl CX3CR1$^+$ T_{EX} cells but decreased amounts of S1PR1-KO CD101$^+$ T_{EX} cells (Figure 4.9G and H). Overall, our data suggest that the loss of S1PR1 impairs T_{PEX} and T_{EX} cells. Further, development of CX3CR1$^+$ T_{EX} cells was specifically impaired by the loss of S1PR1 in particular in the LN.

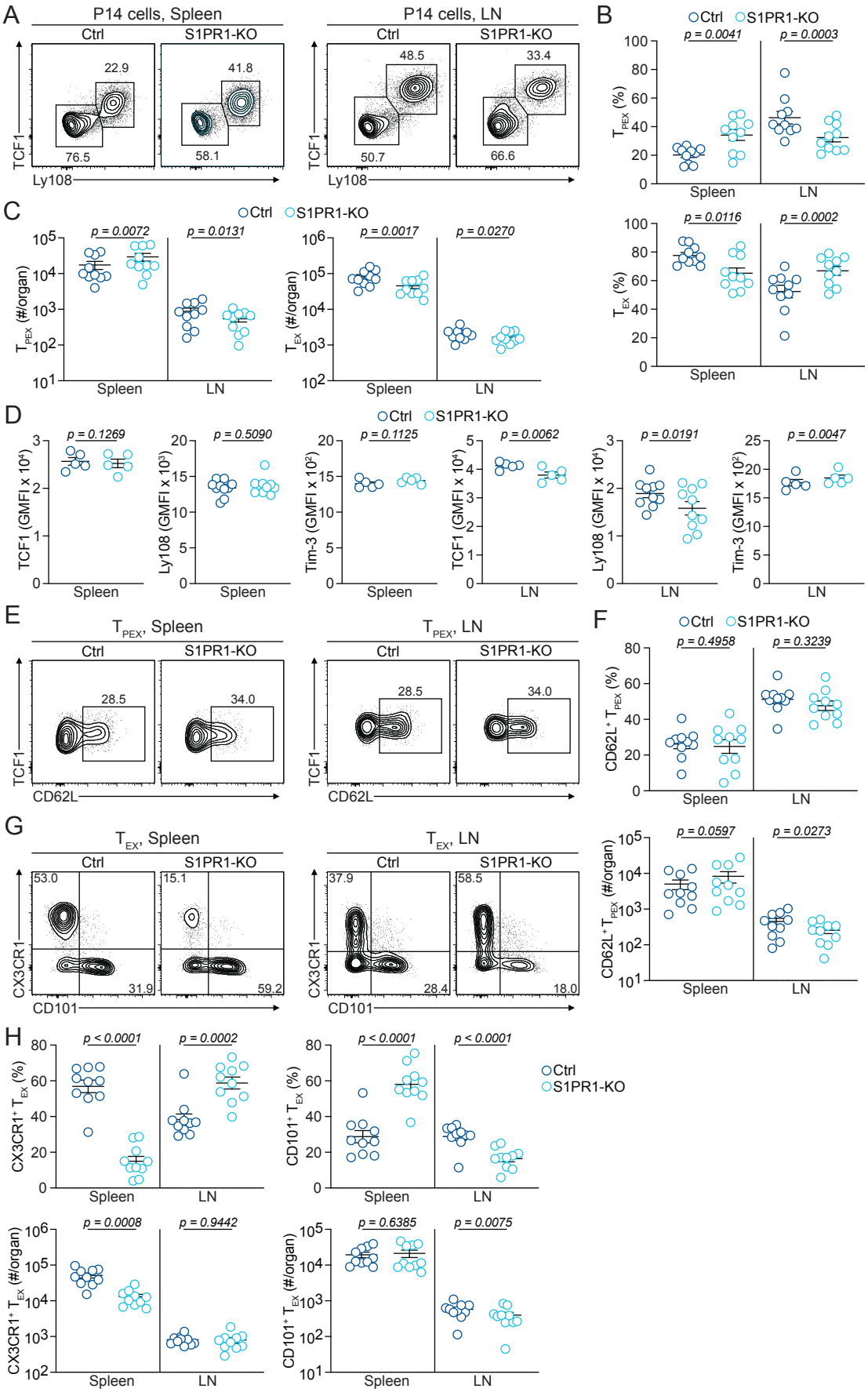
A
P14 cells, Spleen
P14 cells, LN
Ctrl
S1PR1-KO
TCF1
Ly108
22.9
76.5
41.8
58.1
48.5
50.7
33.4
66.6
B
Ctrl
S1PR1-KO
p = 0.0041
p = 0.0003
p = 0.0116
p = 0.0002
T_PEX (%)
T_EX (%)
Spleen
LN
C
p = 0.0072
p = 0.0131
p = 0.0017
p = 0.0270
T_PEX (#/organ)
T_EX (#/organ)
D
p = 0.1269
p = 0.5090
p = 0.1125
p = 0.0062
p = 0.0191
p = 0.0047
TCF1 (GMFI x 10^4)
Ly108 (GMFI x 10^3)
Tim-3 (GMFI x 10^2)
TCF1 (GMFI x 10^4)
Ly108 (GMFI x 10^4)
Tim-3 (GMFI x 10^2)
E
T_PEX, Spleen
T_PEX, LN
28.5
34.0
CD62L
F
p = 0.4958
p = 0.3239
CD62L+ T_PEX (%)
G
T_EX, Spleen
T_EX, LN
53.0
31.9
15.1
59.2
37.9
28.4
58.5
18.0
CX3CR1
CD101
p = 0.0597
p = 0.0273
CD62L+ T_PEX (#/organ)
H
p < 0.0001
p = 0.0002
p < 0.0001
p < 0.0001
CX3CR1+ T_EX (%)
CD101+ T_EX (%)
p = 0.0008
p = 0.9442
p = 0.6385
p = 0.0075
CX3CR1+ T_EX (#/organ)
CD101+ T_EX (#/organ)

Figure 4.9: T_{PEX} and CX3CR1$^+$ T_{EX} cells are impacted by the loss of S1PR1. (A-H) Naïve S1PR1-KO (CD45.1$^+$) or Ctrl (CD45.1/2$^+$) P14 cells were adoptively co-transferred into naïve wildtype CD45.2$^+$ mice and subsequently infected with LCMV-Clone13. On day 21 p.i. spleens and LN were analysed using flow cytometry. (A) Representative flow cytometry plots showing S1PR1-KO and Ctrl T_{PEX} (TCF1$^+$Tim-3$^-$) and T_{EX} (TCF1$^-$Tim-3$^+$) cells. (B) Quantification of S1PR1-KO and Ctrl T_{PEX} and T_{EX} frequencies. (C) Quantification of S1PR1-KO and Ctrl T_{PEX} and T_{EX} numbers per organ. (D) Quantification of TCF1 and Ly108 expression in S1PR1-KO and Ctrl T_{PEX} cells and Tim-3 expression in S1PR1-KO and Ctrl T_{EX} cells. (E) Representative flow cytometry plots showing S1PR1-KO and Ctrl CD62L$^+$ T_{PEX} cells. (F) Quantification of S1PR1-KO and Ctrl CD62L$^+$ T_{PEX} frequencies and numbers per organ. (G) Representative flow cytometry plots showing S1PR1-KO and Ctrl CX3CR1$^+$ and CD101$^+$ T_{EX} cells. (H) Quantification of S1PR1-KO and Ctrl CX3CR1$^+$ and CD101$^+$ T_{EX} frequencies and numbers per organ. Dots in graphs represent individual mice; horizontal lines and error bars of bar graphs indicate means ± SEM, respectively. Data is pooled (A-H) or representative (D) from two independent experiments. P values are from paired student's t test.

Next, we investigated if the loss of S1PR1 impacts the proliferative capacity of T_{PEX} and T_{EX} cells by examining the expression of proliferation protein Ki-67. In the spleens we observed reduced proportions of Ki-67$^+$ S1PR1-KO P14 cells compared to Ctrl P14 cells, while in the LN no obvious differences were seen (Figure 4.10A and B). This was consistent in T_{PEX} and T_{EX} cells. Compared to Ctrl cells the expression of Ki-67 was reduced in S1PR1-KO P14, T_{PEX}, and T_{EX} cells in the spleens, but not in the LN (Figure 4.10C).

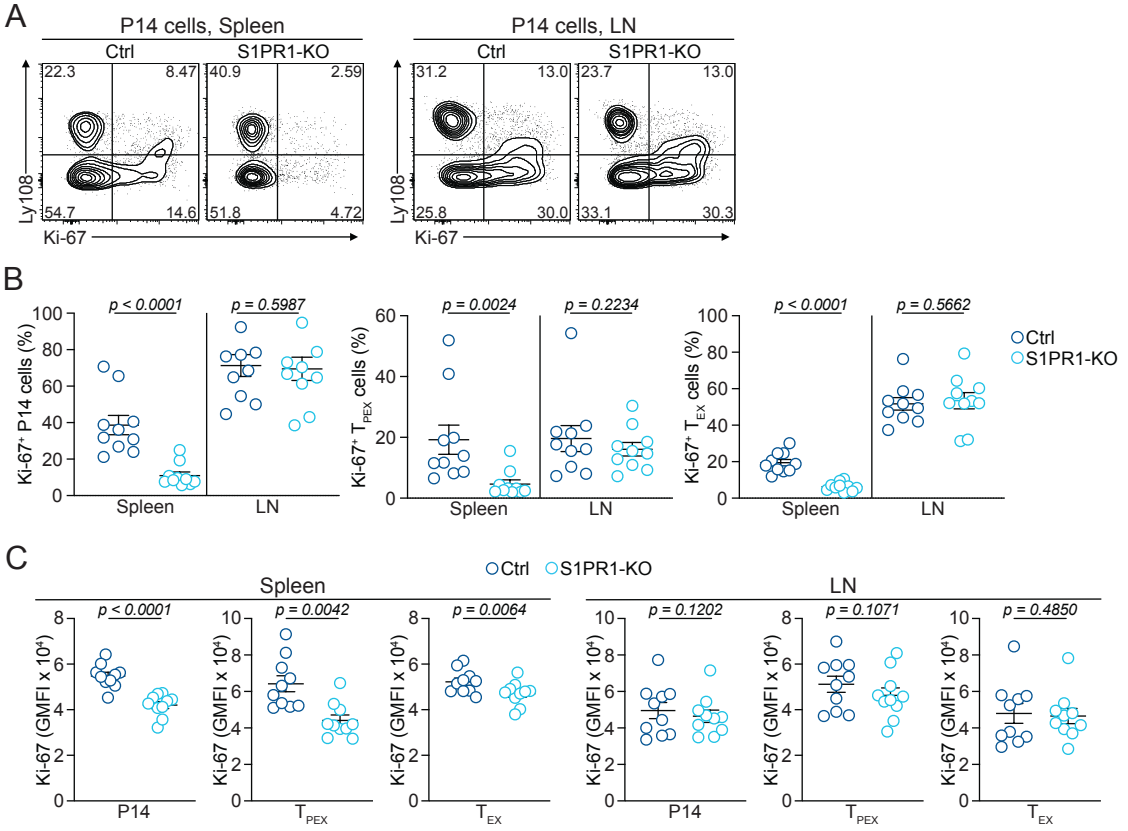

Figure 4.10: The proliferative capacity of T_{PEX} and T_{EX} cells in the spleens, but not in the LN are dependent on S1PR1-mediated functions.
(A-H) Naïve S1PR1-KO (CD45.1$^+$) or Ctrl (CD45.1/2$^+$) P14 cells were adoptively co-transferred into naïve wildtype CD45.2$^+$ mice and subsequently infected with LCMV-Clone13. On day 21 p.i. spleens and LN were analysed using flow cytometry. (A) Representative flow cytometry plots showing Ki-67$^+$ T_{PEX} and T_{EX} cells in S1PR1-KO and Ctrl P14. (B) Quantification of S1PR1-KO and Ctrl Ki-67$^+$ P14, T_{PEX} and T_{EX} cells. (C) Quantification of Ki-67 expression levels in S1PR1-KO and Ctrl Ki-67$^+$ P14, T_{PEX} and T_{EX} cells. Dots in graphs represent individual mice; horizontal lines and error bars of bar graphs indicate means ± SEM, respectively. Data is pooled from two independent experiments. P values are from paired student's t test.

Lastly, we evaluated if the effector functions of T_{PEX} and T_{EX} in the spleens are impaired upon depletion of S1PR1. Overall, S1PR1-KO P14 cells exhibited increased IFN-γ and IFN-γ/TNF double-producing cells, which was accompanied by increased expression levels of IFN-γ and TNF compared to Ctrl cells (Figure 4.11A), which was also observed in T_{PEX} and T_{EX} cells (Figure 4.11B and C). Compared to Ctrl T_{PEX} cells, S1PR1-KO T_{PEX} cells, however, expressed reduced levels of TNF on a single cell level (Figure 4.11B). IFN-γ expression levels in S1PR1-KO T_{EX} cells were increased while TNF expression was similar to that in Ctrl cells (Figure 4.11C). Finally, S1PR1-KO T_{EX} cells produced lower amounts of GzmB than Ctrl T_{EX} cells (Figure 4.11D).

In summary, the accumulation of CX3CR1$^+$ but not CD101$^+$ T_{EX} cells in the spleens was impaired, while increased in the LN, suggesting that S1PR1 is required for LN exit of CX3CR1$^+$ T_{EX} cells. Further, both the quantity and quality of T_{PEX} cells, including the proliferative capacity and effector capacity in the spleens is dependent on S1PR1-mediated function. T_{PEX} and T_{EX} cells in LN also exhibited dependency on S1PR1-mediated functions, however to a lesser degree.

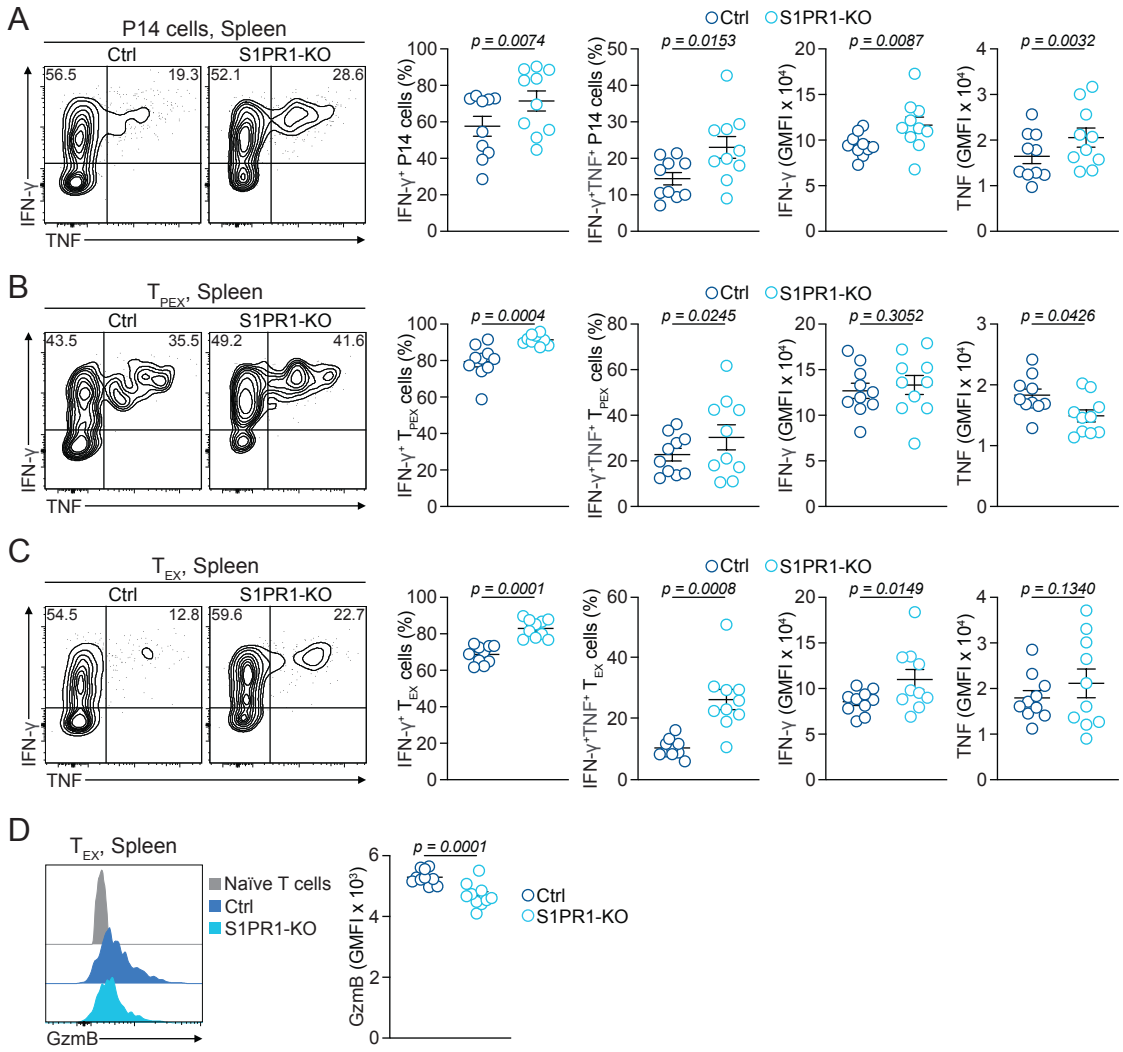

Figure 4.11: Loss of S1PR1 impacts the effector capacity of T_{PEX} and T_{EX} cells in the spleens.

(A-D) Naïve CCR7-KO (CD45.1⁺) or Ctrl (CD45.1⁺) P14 cells were adoptively transferred into naïve wildtype CD45.2⁺ mice and subsequently infected with LCMV-Clone13. On day 21 p.i. spleens were analysed using flow cytometry. Splenocytes were stimulated with Gp33 *ex vivo*. (A) Representative flow cytometry plots and quantification showing frequencies of IFN-γ and TNF producing S1PR1-KO and Ctrl P14 cells and expression levels of IFN-γ and TNF. (B) Representative flow cytometry plots and quantification showing frequencies of IFN-γ and TNF producing S1PR1-KO and Ctrl T_{PEX} cells and expression levels of IFN-γ and TNF. (C) Representative flow cytometry plots and quantification showing frequencies of IFN-γ and TNF producing S1PR1-KO and Ctrl T_{EX} cells and expression levels of IFN-γ and TNF. (D) Representative histogram and quantification showing production of GzmB in S1PR1-KO and Ctrl T_{EX} cells. Dots in graphs represent individual mice; horizontal lines and error bars of bar graphs indicate means ± SEM, respectively. Data is representative of one experiment. P values are from paired student's t test.

Chapter 5 – Molecular regulation of CD62L$^+$ T_{PEX}/CX3CR1$^+$ T_{EX} lineage differentiation is regulated by the transcription factor KLF2

5.1 Introduction

In the previous chapter, we investigated how the disruption of migratory genes CD62L, CCR7 and S1PR1 influenced exhausted T cell differentiation, maintenance and functionality in chronic viral infection. Our findings provided crucial insights suggesting that CX3CR1$^+$ T_{EX} cells and CD101$^+$ T_{EX} cells exhibit distinct regulation of differentiation. Furthermore, based on our data, we propose a model wherein CD62L$^+$ T_{PEX} cells give rise to the CX3CR1$^+$ T_{EX} cell population. A common regulator of all three genes is the Krüppel-like factor 2 (Carlson *et al.*, 2006; Bai *et al.*, 2007). KLF2 is a member of the Krüppel-like factor family of transcription factors that contains a zinc-finger-containing DNA binding domain (Preiss *et al.*, 1985; Anderson *et al.*, 1995). KLF2 is expressed in several different immune and non-immune cell types, including endothelial cells, subsets of the B and T cell lineages, NK cells, monocytes, macrophages, and neutrophils (Hart *et al.*, 2012). In T cells, KLF2 regulates not only adhesion and migration but is also crucial for quiescence of naïve and memory T cells (Hart *et al.*, 2012). Migration is regulated through upregulation of CD62L (Rosen, 2004) and CCR7 that recognize chemokines, such as CCL21, CCL19, CXCL13, CXCR4, and CXCR5 (Anderson *et al.*, 2014). Moreover, KLF2 controls exit from tissues through the upregulation of S1PR1 (Matloubian *et al.*, 2004) by directly binding to the S1PR1 promoter (Carlson *et al.*, 2006). The transcription factors Hobit and Blimp1 directly bind the *Klf2* gene, downregulating KLF2. They also bind to and downregulate *Ccr7* and *S1pr1*, which itself are target genes of KLF2. Thereby, Hobit and Blimp1 through direct and indirect mechanisms lock T_{RM} cells in the tissues and preventing them from re-entering circulation (Mackay *et al.*, 2016).

Klf2 expression in exhausted T cell subsets has previously been analysed by RNA sequencing datasets, including our own (Tsui *et al.*, 2022; Unpublished data, Kallies). *Klf2* was elevated in T_{PEX}, particularly in CD62L$^+$ T_{PEX} cells compared to CD62L$^-$ T_{PEX} cells. Furthermore, CX3CR1$^+$ T_{EX} cells expressed *Klf2*,

while terminally exhausted CD101$^+$ T_{EX} cells did not. Based on the expression data and the function of KLF2 target genes, we hypothesised that KLF2 might have important functions in exhausted T cells, determining the fate of differentiation in T_{PEX} and T_{EX} populations. In particular, we postulated that KLF2 regulates the differentiation of CD62L$^+$ T_{PEX} and their subsequent differentiation into CX3CR1$^+$ T_{EX} cells. Although exhausted T cell subsets have been studied extensively (Zander *et al.*, 2019; Beltra *et al.*, 2020; Utzschneider *et al.*, 2020; Tsui *et al.*, 2022), their differentiation trajectories remain incompletely understood. Two competing models have been proposed: a bifurcation model where T_{PEX} cells become either CX3CR1$^+$ effector-like T_{EX} cells or CD101$^+$ T_{EX} cells (Zander *et al.*, 2019; Tsui *et al.*, 2022; Giles *et al.*, 2022; Daniel *et al.*, 2022; Kasmani *et al.*, 2023), and a linear progression model (Hudson *et al.*, 2019; Beltra *et al.*, 2020).

In this chapter, we investigate the role of KLF2 in T_{PEX} and T_{EX} differentiation, focusing on its function and how its regulation influences fate commitment and functional divergence within the exhausted T cell compartment. To this end, we used the CRISPR/Cas9 system to delete KLF2 and examined its impact on exhausted T cell differentiation and function. By refining our understanding of KLF2 function, we seek to establish a framework for how transcriptional and migratory programs intersect to shape T cell fate in chronic infection.

5.2 Results

5.2.1 Characterisation of KLF2 expression *in vitro*.

To investigate its role, we depleted KLF2 expression in P14 cells using the CRISPR/Cas-9 system (KLF2-KO). Before examining the the impact of KLF2 depletion *in vitro*, we confirmed sufficient depletion of KLF2 by FACS. In both Spleen and LN KLF-KO cells showed no protein expression compared to Ctrl cells (Figure 5.1A and B). To this end, CTV labelled KLF2-KO and Ctrl cells were plated *in vitro* and stimulated using the Gp33 peptide. After 72 hours the proliferation and surface expression of CD25, PD-1, CD44 and CD62L was analysed using flow cytometry (Figure 5.1C). After 72 hrs 50% of all KLF2-P14 cells exhibited 10 divisions, compared to only 35% of Ctrl P14 cells (Figure 5.1D and E), indicating, that KLF2-KO cells undergo faster proliferation. KLF2-KO cells also exhibited increased frequencies of $CD25^+$ and $PD\text{-}1^+$ cells, compared to Ctrl P14 cells (Figure 5.1F and G). However, frequencies of $CD44^+$ cells were similar in KLF2-KO and Ctrl P14 cells (Figure 5.1F and G). Further the expression levels of CD25 and PD-1, but not CD44 was increased in the KLF2-KO P14 cells compared to Ctrl cells on a single cell level (Figure 5.1F and G). To test the efficacy of our CRISPR-Cas9 system gene targeting, we analysed the expression of CD62L. As KLF2 is known to induce and maintain the expression of CD62L (Rosen, 2004), depletion of KLF2 should also reduce CD62L expression. Indeed, even though KLF2-KO P14 cells still maintained CD62L expression on a single cell level the protein expression was reduced compared to Ctrl cells (Figure 5.1H), suggesting efficient depletion of KLF2 by our approach.

Collectively, these experiments indicate that KLF2 plays a role in regulating proliferation and activation in $CD8^+$ T cells *in vitro*. However, this experiment was done only once, and the data needs to be confirmed.

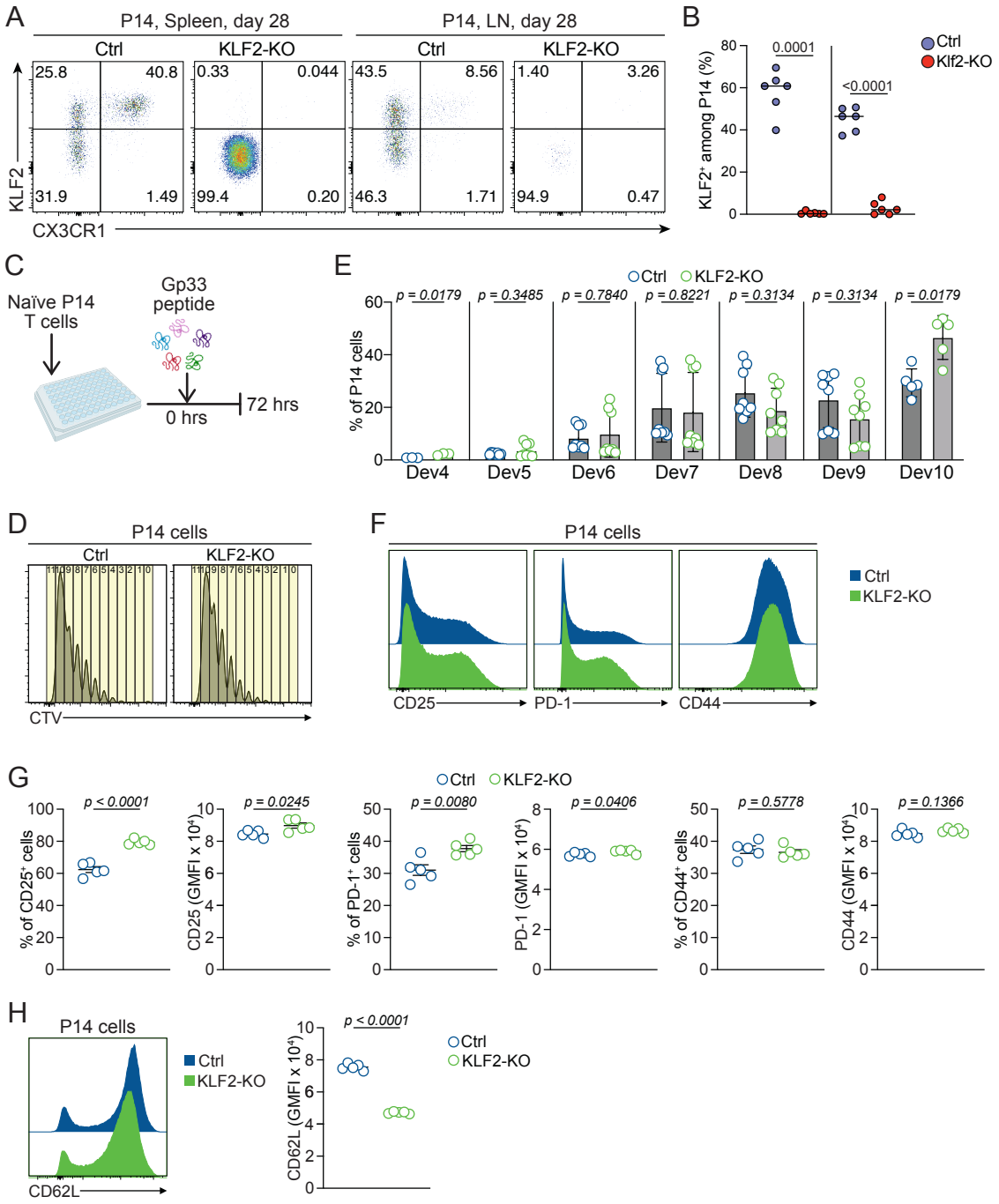

Figure 5.1: KLF2-KO cells proliferate more and show increased activation than Ctrl cells *in vitro*.

(A-B) Naïve KLF2-KO (CD45.2$^+$) and Ctrl (CD45.1/2$^+$) P14 cells were adoptively co-transferred into naïve wildtype CD45.2$^+$ mice at a ratio of 50:50 and subsequently infected with LCMV-Clone13. Spleens and LN were harvested at day 28 of infection and analysed using flow cytometry. Representative FACS plot (A) and quantification (B) showing KLF2 expression in Ctrl and KLF2-KO P14 cells in the spleen and LN. (Unpublished data, Kallies/Carlson Tsui) (C-H) Naïve KLF2-KO or Ctrl P14 cells were activated *in vitro* with Gp33-peptide for 72hrs. Cells were analysed using FACS cytometry. (C) Schematic of experimental

setup. (D) Representative FACS plots showing CTV staining of dividing KLF2-KO and Ctrl cells. (E) Quantification KLF2-KO and Ctrl cell division. (F) Representative histogram showing CD25, PD-1 and CD44 expression in KLF2-KO and Ctrl cells. (G) Quantification of frequencies and expression levels of CD25, PD-1 and CD44 in KLF2-KO and Ctrl P14 cells. (H) Representative histogram and quantification showing CD62L expression in KLF2-KO and Ctrl P14 cells. Dots in graphs represent individual samples or mice; horizontal lines and error bars of bar graphs indicate means ± SEM, respectively. Data is representative of one experiment. P values are from unpaired student's t test.

5.2.2 KLF2 is required for CD8$^+$ T cell accumulation in the lymph node during chronic viral infection.

To test the effect of the loss of KLF2 expression *in vivo*, naïve KLF2-KO cells or Ctrl P14 cells were adoptively co-transferred into recipient mice, which were then infected with LCMV-Clone13 (Figure 5.2A). Before the transfer, the ratio of cells was confirmed to be approximately 1:1 (Figure 5.2B). The expansion of P14 cells in the spleen and LN was analysed over a period of 34 days by flow cytometry. On day 5 p.i. percentages and numbers of KLF2-KO and Ctrl P14 cells changed to approximately 35 % KLF2-KO cells and 65 % Ctrl P14 cells in the spleen, indicating that KLF2-KO cells expanded less at the beginning of infection (Figure 5.2C and D). By day 8 post-infection, the percentages and numbers changed in the opposite direction, with approximately 75 % of P14 cells being KLF2-KO and 25 % being Ctrl cells (Figure 5.2C and D). At later time points (on days 12, 28 and 34 post-infections), even larger numbers of KLF2-KO were present, with 90% of all P14 being KLF2-KO cells and only 10 % Ctrl P14 cells (Figure 5.2C and D). Numerically, KLF2-KO P14 cells exhibited a 10-fold increase compared to Ctrl P14 cells in the spleen (Figure 5.2C and D). In the LN we observed the opposite results. KLF2-KO P14 cells exhibited a significant reduction, with a frequency of approximately 10 %, compared to 90 % of Ctrl P14 cells at days 5, 12 and 28 post-infection, and approximately 30 % KLF2-KO P14 cells on day 34, compared to 70 % Ctrl P14 cells (Figure 5.2E and F). This was also observed numerically, with KLF2-KO P14 cells demonstrating almost approximately a 10-fold reduction in numbers within the LN compared to Ctrl P14 cells (Figure 5.2F). Taken

together, our data indicate that the loss of KLF2 impairs the accumulation of P14 in the LN and promotes their accumulation in the spleen.

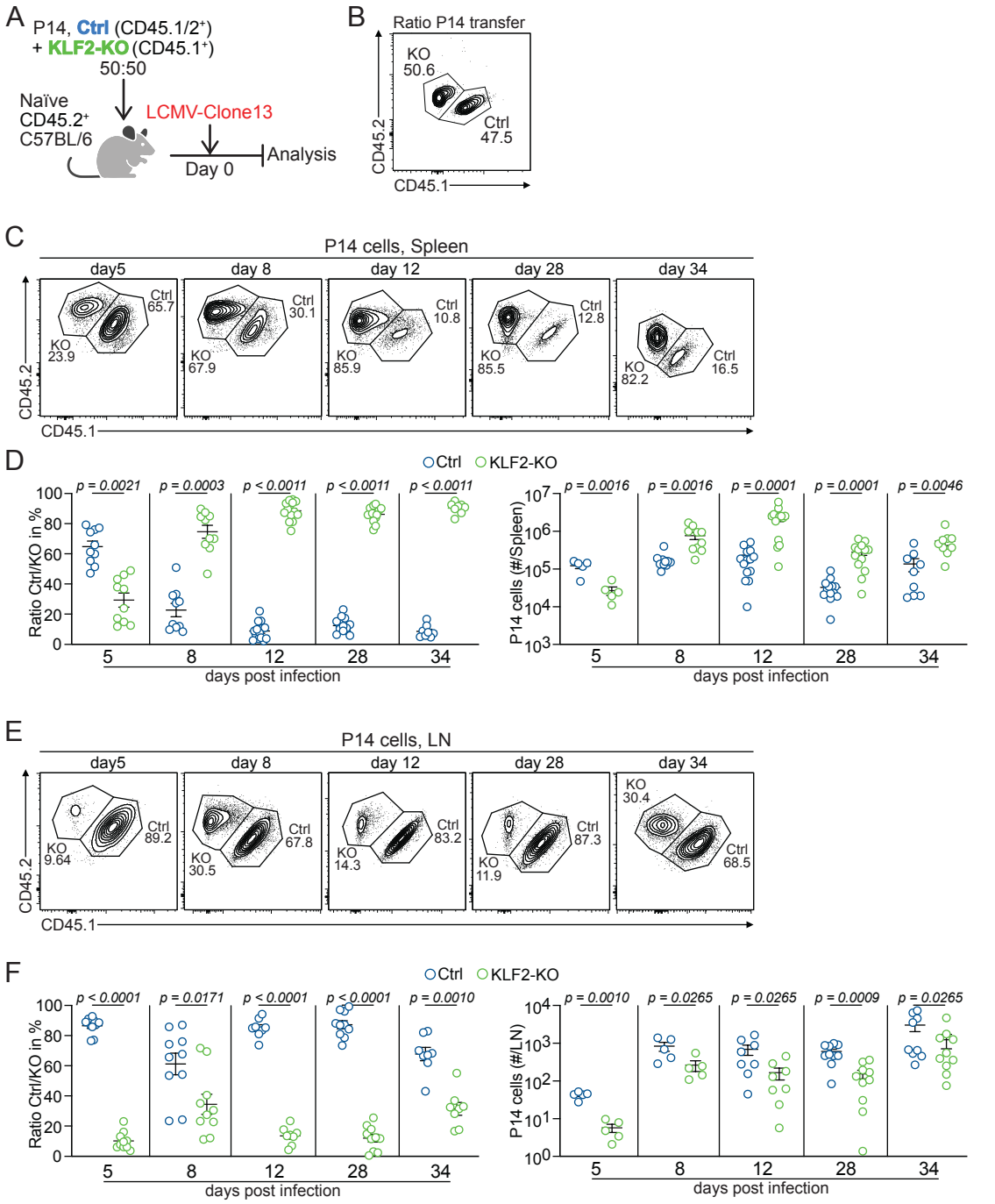

Figure 5.2: Loss of KLF2 impairs the accumulation of P14 in the LN and promotes their accumulation in the spleen.
(A-D) Naïve KLF2-KO (CD45.2$^+$) and Ctrl (CD45.1/2$^+$) P14 cells were adoptively co-transferred into naïve wildtype CD45.2$^+$ mice *at a ratio of approximately 50:50* and subsequently infected with LCMV-Clone13. On days 5, 8, 12, 28 and 34 p.i. spleens and LN were analysed using flow cytometry. (A) Schematic of experimental setup. (B) Representative FACS plots showing ratio of KLF2-KO

and Ctrl cells before adoptive transfer. (B) Representative flow cytometry plots showing ratio of KLF2-KO and Ctrl P14 cells in the spleen. (C) Quantification of frequencies and numbers of KLF2-KO and Ctrl P14 cells in the spleen. (D) Representative flow cytometry plots showing frequencies of KLF2-KO and Ctrl P14 cells in the LN. (E) Quantification of frequencies and numbers of KLF2-KO and Ctrl P14 cells in the LN. Dots in graphs represent individual mice; horizontal lines and error bars of bar graphs indicate means ± SEM, respectively. Data is pooled or representative of two independent experiments. P values are from multiple student's t test.

To further evaluate whether the impaired accumulation of KLF2-KO P14 cells in the LN was a result of the infection, or if KLF2-KO P14 cells were generally incapable of accumulating in the LN, we compared the frequency of Ctrl and KLF2-KO P14 cells in the spleen and LN prior to infection. To this end, we co-transferred KLF2-KO and Ctrl P14 cells into naïve recipient mice and analysed the spleen, and the axillary, brachial, cervical, and inguinal LNs 18 hours later using flow cytometry. (Figure 5.3A and B). The transfer mix included 42 % KLF2-KO and 58 % Ctrl P14 cells prior to transfer. In the spleen, we observed no significant differences in the KLF2-KO and Ctrl P14 cells ratio following transfer (Figure 5.3C). However, the frequencies of KLF2-KO P14 cells in the LN were reduced, leading to a change in the ratio by approximately 7-fold (Figure 5.3C and D). These findings were further corroborated numerically, with no substantial changes in KLF2-KO and Ctrl P14 cell numbers in the spleen, while the number of KLF2-KO P14 cells in the LNs was reduced by approximately 10-fold (Figure 5.3E). Furthermore, KLF2-KO cells exhibited alterations in the expression of CD62L and CD69, which are controlled by KLF2 directly (CD62L) or indirectly (CD69, controlled by expression of S1PR1). In both the spleen and LN, KLF2-KO P14 cells maintained CD62L expression, albeit significantly lower than that of Ctrl cells on a single cell level (Figure 5.3F). Moreover, KLF2-KO P14 cells in the spleen and LN demonstrated upregulation of CD69, with up to approximately 50 % $CD69^+$ $CD8^+$ T cells compared to merely 10 % of Ctrl P14 cells, and elevated expression levels at the single-cell level (Figure 5.3G). Collectively, the data demonstrate that KLF2 controls accumulation in the LN of both naïve and exhausted $CD8^+$ T cell.

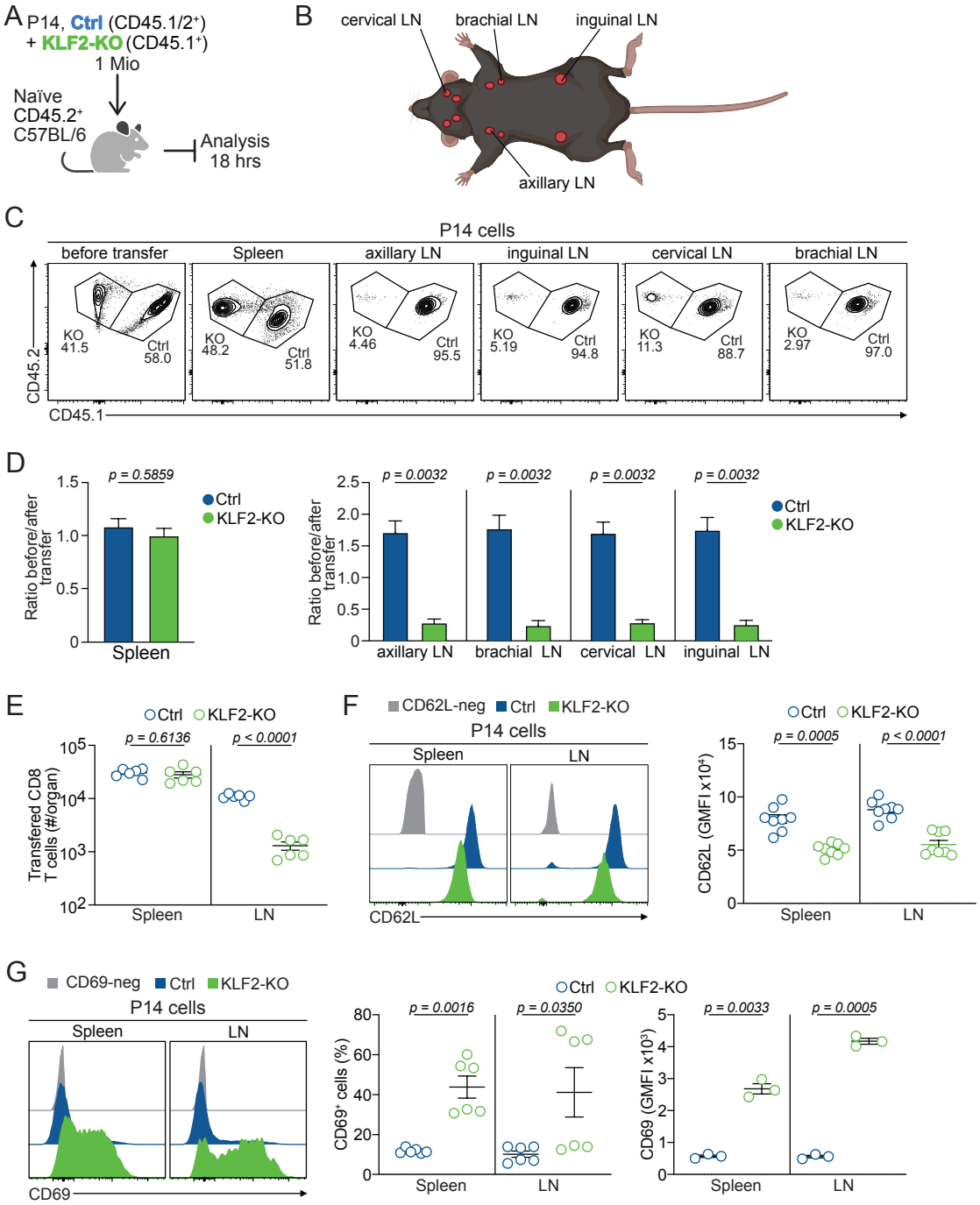

Figure 5.3: Naïve KLF2-KO P14 cells do not accumulate in the LN.
(A-G) Naïve KLF2-KO (CD45.2⁺) and Ctrl (CD45.1/2⁺) P14 cells were adoptively co-transferred into naïve wildtype CD45.2⁺ mice at a ratio of approximately 42:58. After 18 hrs the spleens, axillary, brachial, cervical and inguinal LN were analysed using flow cytometry. For C-D, the LN were analysed separately. For E-G, all LN were pooled for analysis. (A) Schematic of experimental setup. (B) Schematic illustration of different LN harvested from mice. (C) Representative FACS plots showing the ratio of KLF2-KO and Ctrl cells before and after the transfer in the organs. (D) Quantification of the change in ratio of KLF2-KO and Ctrl P14 cells in the organs. (E) Quantification of KLF2-KO and Ctrl P14 cells numbers per spleen

and LN. (F) Representative FACS plots and quantification of CD62L expression in KLF2-KO and Ctrl P14 cells in the spleen and LN. (G) Representative FACS plots and quantification of CD69^{+} KLF2-KO and Ctrl P14 cells and CD69 expression in the spleen and LN. Dots in graphs represent individual mice or n=6 in bar graphs; horizontal lines and error bars of bar graphs indicate means ± SEM, respectively. Data is pooled from two independent experiments (D-G) or representative of two independent experiment (GMFI in G). P values are from paired student's t test.

To test how KLF2 depletion impacted P14 cell accumulation in other organs, we analysed the blood, salivary glands, lungs, and liver at day 34 post infection (Figure 5.4). We did not observe major differences in the representation of KLF2-KO and Ctrl P14 cells in the lungs (Figure 5.4A-C). In the salivary gland, the frequencies of KLF2-KO comparted to Ctrl P14 cells were reduced (Figure 5.4A-C). In contrast, in both the liver and blood, the representation of KLF2-KO P14 cells was substantially increased (Figure 5.4A-C). Taken together these data suggest that the loss of KLF2 does not impact the accumulation of exhausted T cells in non-lymphoid organs during chronic infection. The increase of KLF2-KO P14 cells in the liver, is likely due to increased P14 cells in the blood. However, this experiment was done only once, and the data needs to be confirmed.

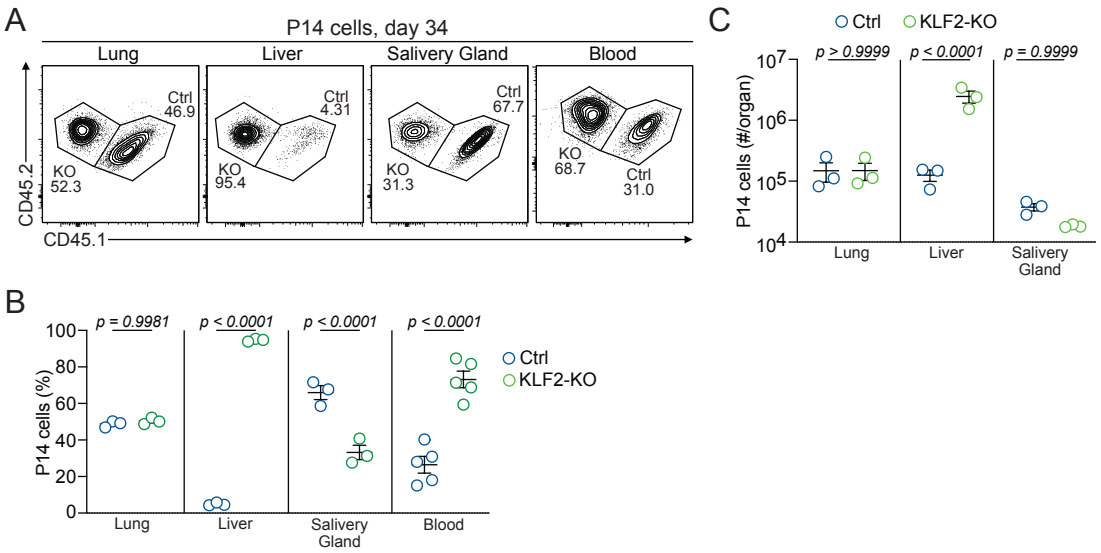

Figure 5.4: KLF2-KO P14 cells accumulate in other non-lymphoid tissues. (A-C) Naïve KLF2-KO (CD45.2$^+$) and Ctrl (CD45.1/2$^+$) P14 cells were adoptively co-transferred into naïve wildtype CD45.2$^+$ mice at a ratio of 50:50 and subsequently infected with LCMV-Clone13. On day 34 p.i. the spleens, lungs, liver and blood were analysed using flow cytometry. (A) Representative FACS plots showing ratio of KLF2-KO and Ctrl cells in organs. (B) Quantification of KLF2-KO and Ctrl P14 cells ratios in organs. Dots in graphs represent individual mice; horizontal lines and error bars of bar graphs indicate means ± SEM, respectively. Data is representative of one independent experiment. P values are from multiple paired student's t test.

5.2.3 KLF2 impacts expression of PD-1, CD69 and CXCR3

To evaluate the impact of KLF2 on P14 cells in chronic infection, we analysed expression of key exhaustion molecules PD-1 and TOX. Further we evaluated CD69 expression (as an indirect measure for the loss of S1PR1 and expression of the chemokine receptor CXCR3, which has been reported to be upregulated in KLF2-KO cells (Sebzda *et al.*, 2008). KLF2-KO P14 cells in the spleen exhibited increased expression of the inhibitory receptor PD-1 on day 12 p.i., whereas expression levels in the LN were similar between KLF2-KO and Ctrl P14 cells (Figure 5.5A and B). On day 28 p.i., KLF2-KO P14 cells in both the spleen and LN expressed elevated levels of PD-1 (Figure 5.5A and B). We observed no major changes in the expression of TOX between KLF2-KO and Ctrl P14 cells in the spleen and LN on both days (Figure 5.5C and D). In both the spleen and LN, the majority of KLF2-KO P14 cells expressed CD69 on day 12 p.i., compared to approximately 20-40 % of Ctrl cells (Figure 5.5E), while expression on a single-cell level was similar (Figure 5.5F). Finally, the proportion of cells expressing the migration marker CXCR3 was elevated on KLF2-KO P14 cells compared to Ctrl P14 cells in the spleen, but not in the LN, where almost all KLF2-KO and Ctrl P14 cells expressed CXCR3 (Figure 5.5G).

In summary, KLF2 influences the expression of PD-1 but not TOX in exhausted CD8 T cells. Furthermore, we validated that *in vivo* KLF2 depletion results in upregulation of CD69, likely due to loss of S1PR1 expression. Additionally,

chemokine receptor CXCR3 is upregulated, further supporting the efficacy of our *Klf2* targeting approach as a depletion strategy.

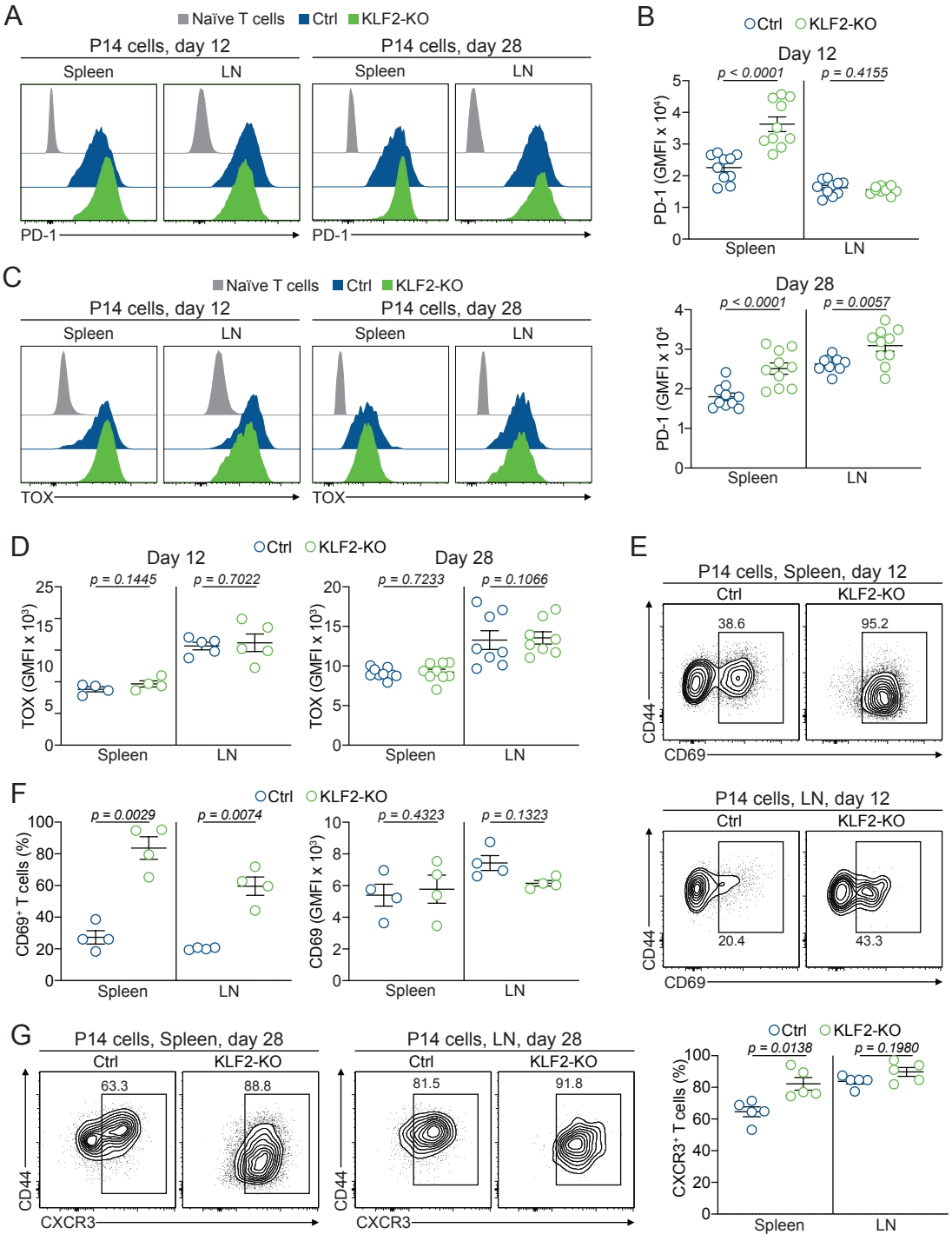

Figure 5.5 KLF2 impacts the expression of PD-1, CD69 and CXCR3.
(A-G) Naïve KLF2-KO (CD45.2⁺) and Ctrl (CD45.1/2⁺) P14 cells were adoptively co-transferred into naïve wildtype CD45.2⁺ mice at a ratio of 50:50 and subsequently infected with LCMV-Clone13. On days 12 and 28 p.i. the spleens,

and LN were analysed using flow cytometry. (A) Representative histograms showing expression of PD-1 in KLF2-KO and Ctrl P14 cells. (B) Quantification of PD-1 expression levels in KLF2-KO and Ctrl P14 cells. (C) Representative histograms showing expression of TOX in KLF2-KO and Ctrl P14 cells. (D) Quantification of TOX expression levels in KLF2-KO and Ctrl P14 cells. (E) Representative flow cytometry plots showing $CD69^+$ KLF2-KO and Ctrl T_{PEX} and T_{EX} cells. (F) Quantification of proportions of $CD69^+$ KLF2-KO and Ctrl P14 cells and expression levels of CD69. (G) Representative flow cytometry plots and quantification of $CXCR3^+$ KLF2-KO and Ctrl P14 cells. Dots in graphs represent individual mice; horizontal lines and error bars of bar graphs indicate means ± SEM, respectively. Data is pooled from two independent experiments (A-B, C-D day 12) or representative of one independent experiment (C-D day 12, E-G). P values are from paired student's t test.

5.2.4 KLF2 expression is essential for the $CD62L^+$ T_{PEX}/$CX3CR1^+$ T_{EX} lineage

We next compared the frequency of both T_{PEX} and T_{EX} subsets between Ctrl and KLF2-KO cell in the spleen and LN at day 12 and 28 p.i. by flow cytometry. In both organs the frequencies of KLF2-KO T_{PEX} cells decreased, and the frequencies of KLF2-KO T_{EX} cells increased compared to Ctrl cells on day 12 post infection (Figure 5.6A). KLF2-KO and Ctrl T_{PEX} cell numbers were similar in the spleen but reduced in the LN (Figure 5.6A). The numbers of KLF2-KO T_{EX} cells were increased compared to Ctrl T_{EX} cells in the spleen, while decreased in the LN (Figure 5.6A). This indicated that T_{PEX} cells in the LN, but not in the spleen, are affected by the loss of KLF2, whereas T_{EX} cells residing in both tissues are impacted. On day 28 post infection, the frequencies of KLF2-KO T_{PEX} cells were significantly reduced in both organs, whereas the frequency of T_{EX} cells was increased (Figure 5.6B). Furthermore, in the LN, KLF2-KO T_{PEX} and T_{EX} cells were reduced compared to Ctrl cells. However, in contrast to day 12 p.i., on day 28 p.i. KLF2-KO T_{PEX} and T_{EX} cells exhibited a numerical increase in the spleen (Figure 5.6B).

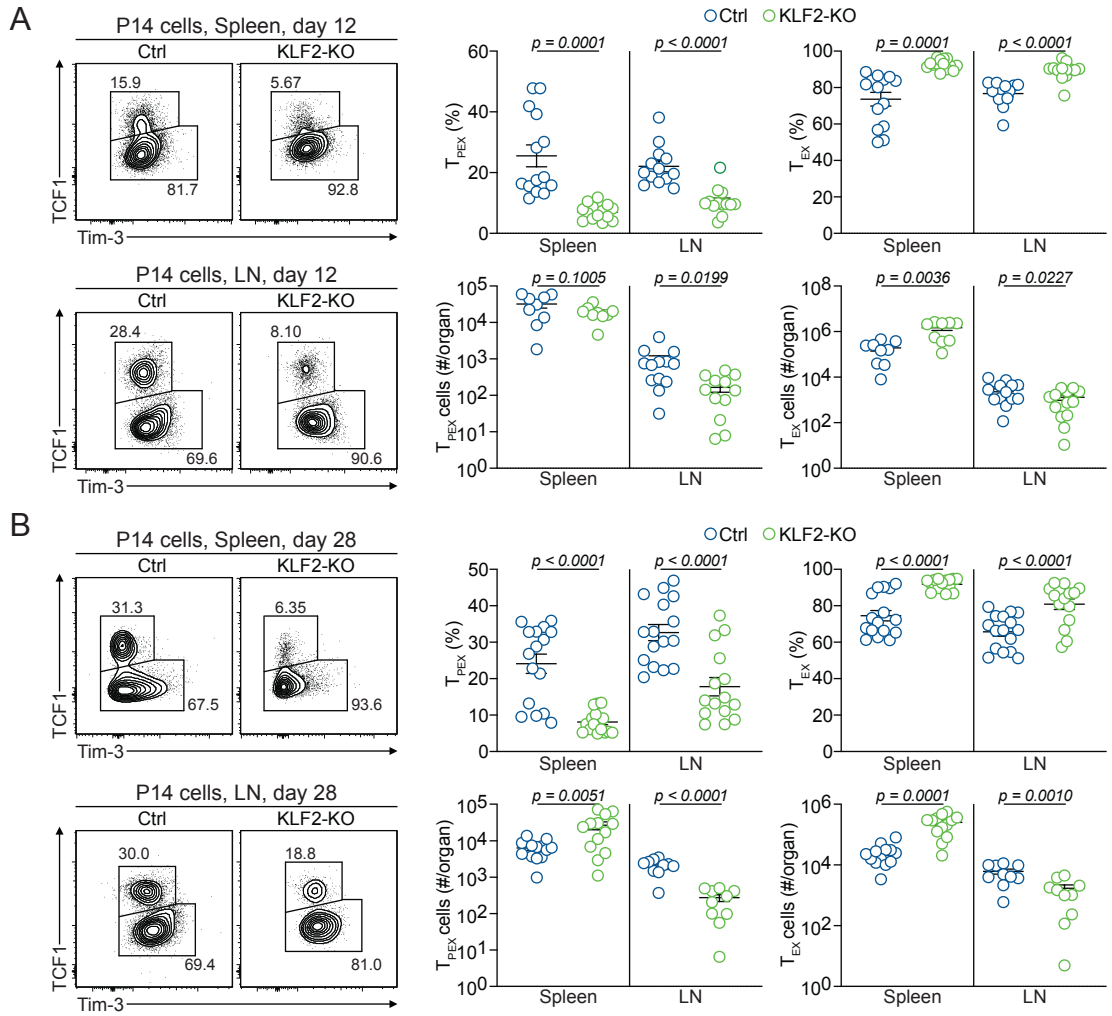

Figure 5.6: Loss of KLF2 impairs T_{PEX} and T_{EX} cells in the LN but not in the spleen.

(A-B) Naïve KLF2-KO (CD45.2$^+$) and Ctrl (CD45.1/2$^+$) P14 cells were adoptively co-transferred into naïve wildtype CD45.2$^+$ mice at a ratio of 50:50 and subsequently infected with LCMV-Clone13. On days 12 and 28 p.i. the spleens, and LN were analysed using flow cytometry. (A) Representative flow cytometry plots and quantification showing frequencies and numbers of KLF2-KO and Ctrl T_{PEX} (TCF1$^+$) and T_{EX} (TCF1$^-$) cells on day 12 post infection. (B) Representative flow cytometry plots and quantification showing frequencies and numbers of KLF2-KO and Ctrl T_{PEX} (TCF1$^+$) and T_{EX} (TCF1$^-$) cells on day 28 post infection. Dots in graphs represent individual mice; horizontal lines and error bars of bar graphs indicate means ± SEM, respectively. Data is pooled from three independent experiments. P values are from paired student's t test.

We next analysed the expression of TCF1 and Ly108 in T_{PEX} and Tim-3 in T_{EX} cells and compared the expression levels on a single cell level to Ctrl cells in the spleen and LN. We could observed reduced expression of Ly108, but not TCF1 in KLF2-KO T_{PEX} cells compared to Ctrl T_{PEX} cells of day 12 p.i. (Figure 5.7A). In the LN, the expression of TCF1 but not Ly108 was increased upon KLF2 deletion (Figure 5.7A). Further, expression of Tim-3 in KLF2-KO T_{EX} cells was increased in the spleen, while it remained unaltered in the LN compared to Ctrl T_{EX} cells (Figure 5.7A). On day 28 p.i. we observed reduced expression of Ly108, but not TCF1 in KLF2-KO T_{PEX} cells compared to Ctrl T_{PEX} cells (Figure 5.7C). Additionally, in the LN, the expression of Ly108, but not TCF1, was reduced upon KLF2 deletion (Figure 5.7C). Compared to Ctrl T_{EX} cells, the expression of Tim-3 in KLF2-KO T_{EX} cells was decreased in the spleen, while it was elevated in the LN (Figure 5.7A).

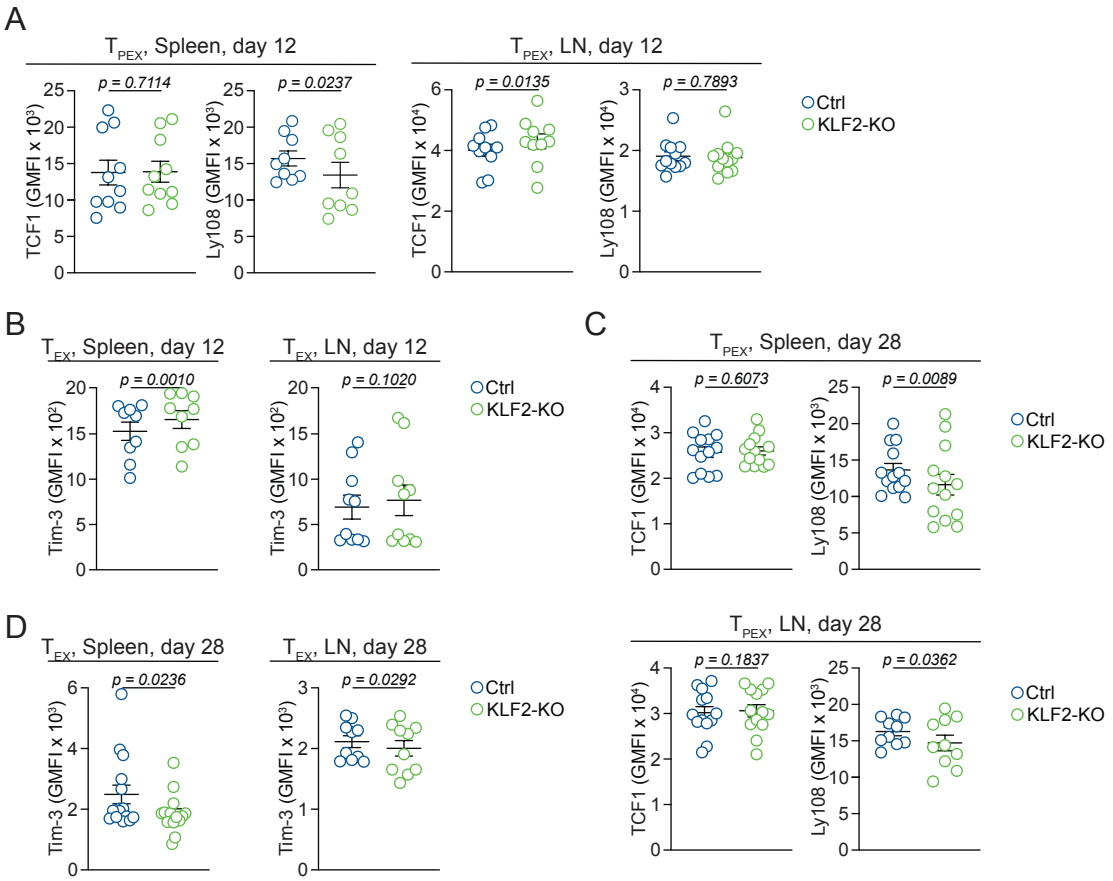

Figure 5.7 KLF2 deletion affects expression of TCF1, Ly108 and Tim-3 in T_{PEX} and T_{EX} cells across tissues.

(A-D) Naïve KLF2-KO (CD45.2$^+$) and Ctrl (CD45.1/2$^+$) P14 cells were adoptively co-transferred into naïve wildtype CD45.2$^+$ mice at a ratio of 50:50 and mice subsequently infected with LCMV-Clone13. On days 12 and 28 p.i. the spleens, and LN were analysed using flow cytometry. (A) Quantification of TCF1 and Ly108 expression levels in KLF2-KO and Ctrl T_{PEX} cells on day 12 post infection. (B) Quantification of Tim-3 expression levels in KLF2-KO and Ctrl T_{EX} cells on day 12 post infection. (C) Quantification of TCF1 and Ly108 expression levels in KLF2-KO and Ctrl T_{PEX} cells on day 28 post infection. (D) Quantification of Tim-3 expression levels in KLF2-KO and Ctrl T_{EX} cells on day 28 post infection. Dots in graphs represent individual mice; horizontal lines and error bars of bar graphs indicate means ± SEM, respectively. Data is pooled from two (day 12) or three (day 28) independent experiments. P values are from paired student's t test.

We next compared the frequencies of both CD62L$^+$ T_{PEX} and CX3CR1$^+$ and CD101$^+$ T_{EX} subsets between Ctrl and KLF2-KO cell in the spleen and LN. On days 12 and 28 post-infection, the frequencies of KLF2-KO CD62L$^+$ T_{PEX} cells were significantly reduced compared to Ctrl in the spleen and LN (Figure 5.8A-D). This impact was also observed numerically, with decreased numbers of KLF2-KO CD62L$^+$ T_{PEX} cells in the spleen and LN by approximately 10-fold (Figure 5.8A-D), indicating that that CD62L$^+$ T_{PEX} cells are more substantially affected by the loss of KLF2 than CD62L$^-$ T_{PEX} cells. Further, KLF2-KO T_{EX} cells on days 12 and 28 post infection demonstrated drastically reduced frequencies of effector-like CX3CR1$^+$ T_{EX} cell compared to Ctrl in both spleen and LN (Figure 5.8E-G). Additionally, they were numerically reduced in both organs on both days (Figure 5.8F and H). Conversely, on day 28 post infection, the frequencies and numbers of KLF2-KO CD101$^+$ T_{EX} cells were elevated compared to Ctrl in the spleen (Figure 5.8E-G). In the LN, the frequencies of KLF2-KO CD101$^+$ T_{EX} cells were increased compared to Ctrl CD101$^+$ T_{EX} cells; however, numerically they did not differ (Figure 5.8E-G).

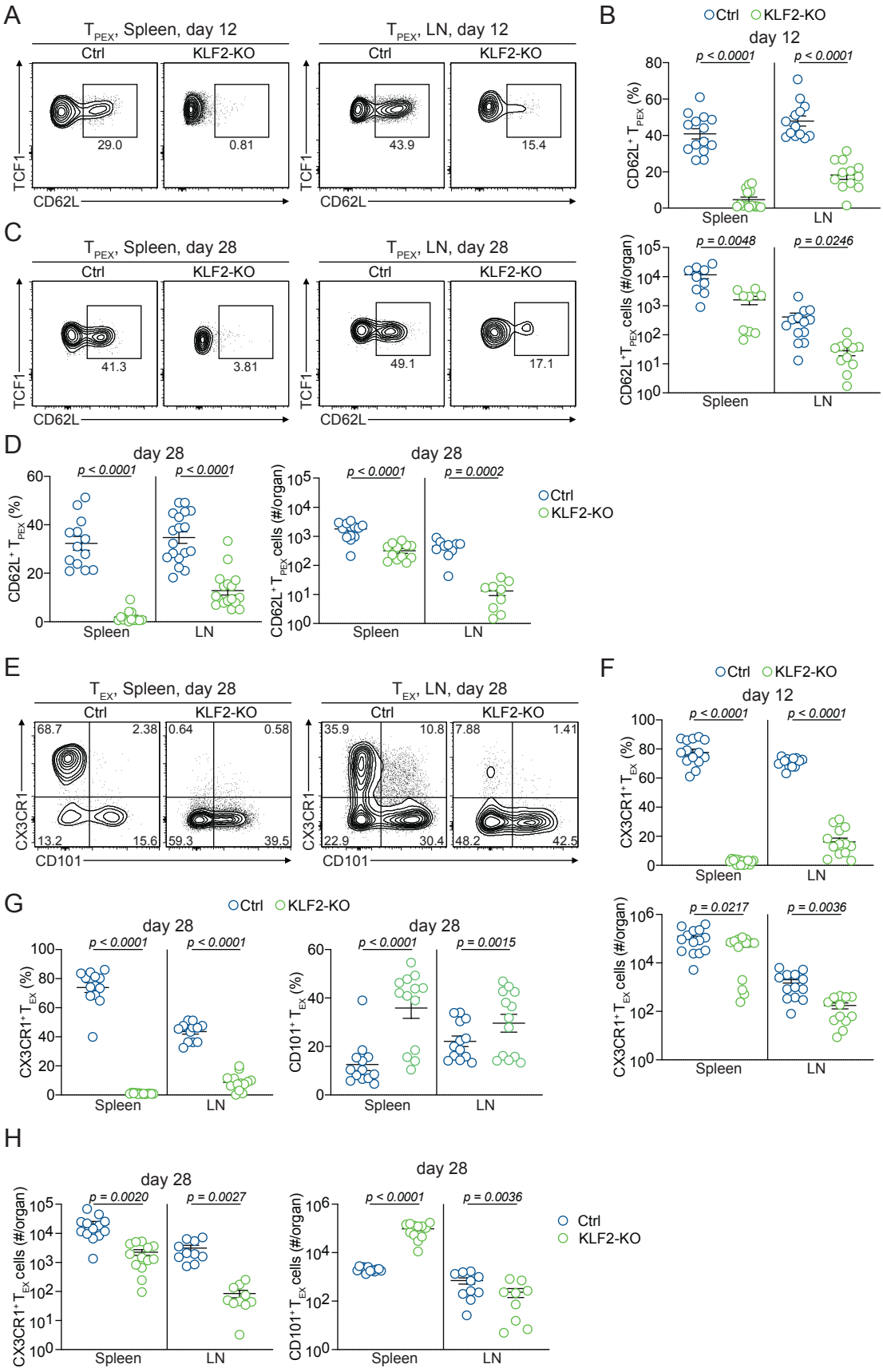

Figure 5.8: KLF2 is required for the CD62L$^+$ T_{PEX}/CX3CR1$^+$ T_{EX} lineage.

(A-H) Naïve KLF2-KO (CD45.2$^+$) and Ctrl (CD45.1/2$^+$) P14 cells were adoptively co-transferred into naïve wildtype CD45.2$^+$ mice at a ratio of 50:50 and subsequently infected with LCMV-Clone13. On days 12 and 28 p.i. the spleens, and LN were analysed using flow cytometry. (A) Representative flow cytometry plots of KLF2-KO and Ctrl CD62L$^+$ T_{PEX} cells on day 12 post infection. (B) Quantification of frequencies and numbers on day 12 post-infection of KLF2-KO and Ctrl CD62L$^+$ T_{PEX} cells. (C) Representative flow cytometry plots of KLF2-KO and Ctrl CD62L$^+$ T_{PEX} cells on day 28 post infection. (D) Quantification of frequencies and numbers on day 28 post-infection of KLF2-KO and Ctrl CD62L$^+$ T_{PEX} cells. (E) Representative flow cytometry plots of KLF2-KO and Ctrl CX3CR1$^+$ and CD101$^+$ T_{EX} cells on day 28 post infection. (F) Quantification of frequencies and numbers of KLF2-KO and Ctrl CX3CR1$^+$ T_{EX} cells on day 12 post-infection. (G) Quantification of frequencies of KLF2-KO and Ctrl CX3CR1$^+$ and CD101$^+$ T_{EX} cells on day 28 post-infection. (H) Quantification of numbers of KLF2-KO and Ctrl CX3CR1$^+$ and CD101$^+$ T_{EX} cells per organ on day 28 post-infection. Dots in graphs represent individual mice; horizontal lines and error bars of bar graphs indicate means ± SEM, respectively. Data is pooled from three independent experiments. P values are from paired student's t test.

Our cytometry data thus far indicate that the differentiation of CD62L$^+$ T_{PEX} and CX3CR1$^+$ T_{EX} cells is significantly impaired upon deletion of KLF2. However, to determine whether the absence of these populations in our flow cytometry results was due to a loss of the respective populations or merely a loss of Sell (CD62L) and Cx3cr1 gene expression, we conducted single-cell RNA sequencing (scRNA-seq) on Ctrl and KLF2-KO P14 cells from the spleens of LCMV cl13 infected mice on day 28 post infection (Figure 5.9A). UMAP analysis identified six different cell clusters (Figure 5.9B and C). T_{PEX} are represented in clusters 1 and 2, expressing the transcription factor Tcf7, with cluster 1 representing CD62L$^+$ T_{PEX} cells (Figure 5.9B and C). Clusters 3-6 represented different T_{EX} cell populations (Figure 5.9B and C). CX3CR1$^+$ T_{EX} could be identified as cluster 3, whereas the more differentiated T_{EX} cells, including CD101$^+$ T_{EX} cells, comprised cluster 4-6 (Figure 5.9B and C). *Klf2* expression was predominantly observed in both T_{PEX} clusters, although it was higher in CD62L$^+$ T_{PEX} cells, and in Cx3cr1$^+$ T_{EX} cells (Figure 5.9B and C). *S1pr1*, a target of KLF2, was exclusively expressed in CD62L$^+$ T_{PEX} and CX3CR1$^+$ T_{EX} cells (Figure 5.9B and C). In line with our flow cytometry data, KLF2-KO P14 cells lacked CD62L$^+$ T_{PEX} cells (cluster 1) but not CD62L$^-$ T_{PEX} cells (cluster 2), whereas Ctrl P14 cells contained both CD62L$^-$ and CD62L$^+$ cell

clusters 1 and 2 (Figure 5.9D). Additionally, CX3CR1$^+$ T_{EX} cell cluster 3 was absent in KLF2-KO P14 cells while CD101$^+$ T_{EX} cells were unimpaired (Figure 5.9D). Ctrl P14 cells were found in both the CX3CR1$^+$ T_{EX} and CD101$^+$ T_{EX} clusters (Figure 5.9D). Gene set enrichment analysis confirmed depletion of the stem-like CD62L$^+$ T_{PEX} cell signature in KLF2-KO P14 cells (Figure 5.9E), overall confirming that loss of KLF2 resulted in abrogated CD62L$^+$ T_{PEX} and CX3CR1$^+$ T_{EX} cell differentiation.

Dimension reduction and Slingshot trajectory analysis of P14 cell scRNAseq data (unpublished, Kallies lab) had identified two major lineages starting from *Tcf7*$^+$ T_{PEX} cells and progressing into either *Cx3cr1*$^+$ or *Cd101*$^+$ T_{EX} cells and trajectory-defining genes (Figure 5.10A and B). We thus analysed the expression of genes associated with the *Cx3cr1*$^+$ or *Cd101*$^+$ T_{EX} cells differentiation trajectory in KLF2-KO and Ctrl P14 cells. KLF2-KO cells uniformly expressed low levels of genes associated with the CX3CR1$^+$ T_{EX} differentiation trajectory but exhibited high levels of transcripts associated with the CD101$^+$ T_{EX} differentiation trajectory (Figure 5.9F). Finally, we explored differentially expressed genes. In total, 658 differentially expressed (DE, adjusted $p<0.05$) genes were identified between Ctrl and KLF2-KO P14 cells (Figure 5.9G). These genes include transcription factors that are known to be involved in exhausted T cell biology, such as *Nfatc1*, *Eomes*, *Id2*, *Ikzf2*, and *Maf*, cell cycle regulation, such as *Ccnd3* and *Cdk6,* and cell survival molecule *Bcl2*. Additionally, genes involved in TCR signalling, such as *Ptpn1* and *Ptpn2*, as well as cell migration molecules such as *Sell*, *Itgb1*, *S1pr1*, *Ccr7*, *Ly6c2*, and *Itgb7*, and inhibitory receptors *Tigit* and *Lag3* were differentially expressed. Analysis of a published KLF2 Chip-sequencing data (Yeo *et al.*, 2014) showed that KLF2 binds to 420 DE genes, suggesting they are directly regulated by KLF2.

Taken together, these results indicate that KLF2 is critical for the development of the CD62L$^+$ T_{PEX}/CX3CR1$^+$ T_{EX} cell lineage but is not required for the development of the CD62L$^-$ T_{PEX}/CD101$^+$ T_{EX} cell lineage. Furthermore, our results strongly support the notion of two independent differentiation lineages,

with CX3CR1^{+} T_{EX} cells developing from CD62L^{+} T_{PEX} cells, while CD101^{+} T_{EX} cells differentiate downstream of CD62L^{-} T_{PEX} cells.

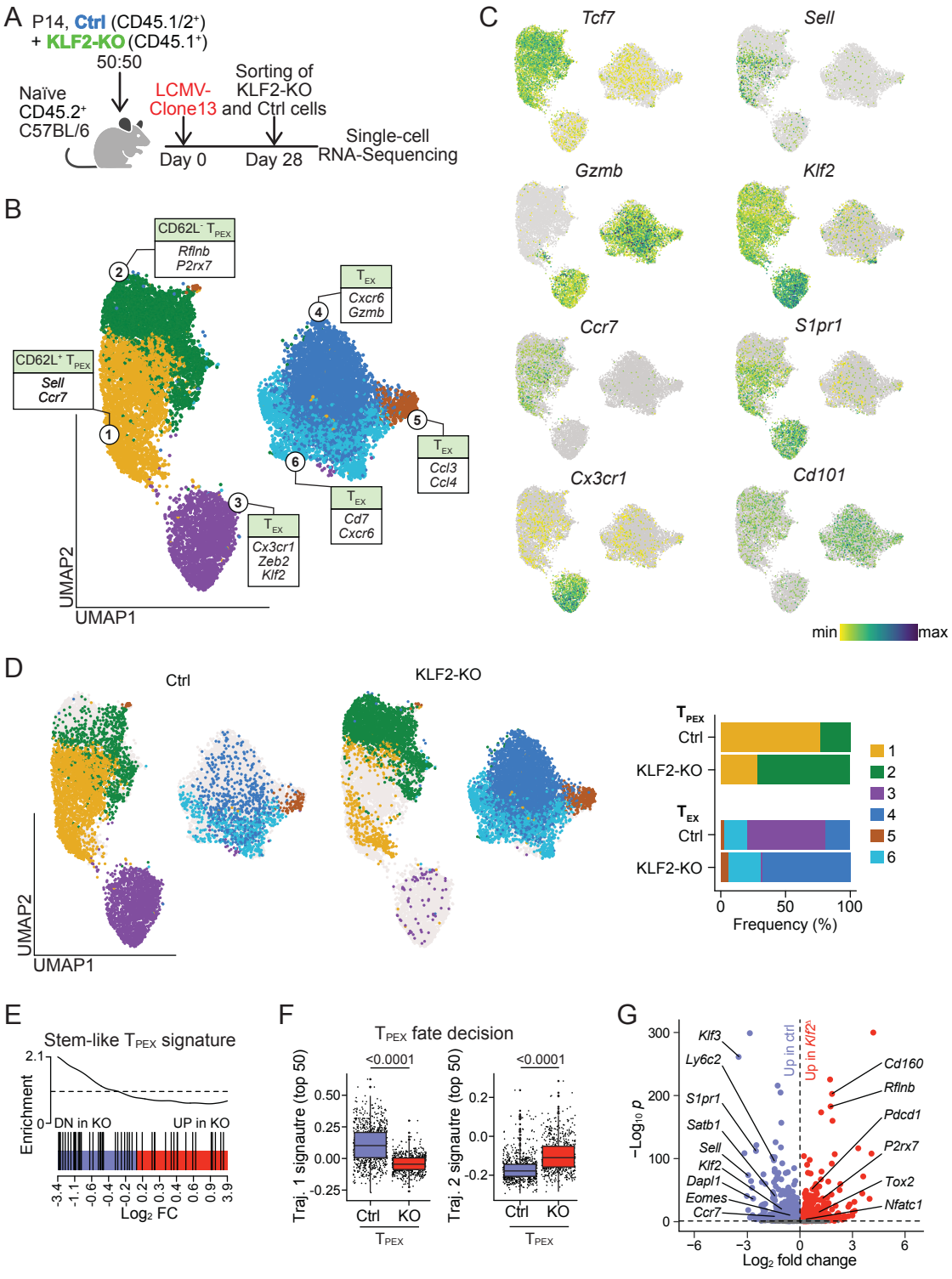

Figure 5.9: KLF2 is critical for the development of the CD62L$^+$ T_{PEX}/CX3CR1$^+$ T_{EX} cell lineage but dispensable for the development of the CD62L$^-$ T_{PEX}/CD101$^+$ T_{EX} cell lineage.
(A-G) Naïve KLF2-KO (CD45.2$^+$) and Ctrl (CD45.1/2$^+$) P14 cells were adoptively co-transferred into naïve wildtype CD45.2$^+$ mice at a ratio of 50:50 and subsequently infected with LCMV-Clone13. On day 28 post-infection P14 cells from the spleen were subjected to scRNA-seq. (A) Schematic of the experimental setup. (B) Uniform manifold approximation and projection (UMAP) plot with signature annotation of single P14 T cells coloured according to cluster classification. (C) UMAPs exhibiting expression of different genes. (D) UMAP plots and quantification showing the proportions of the transcriptomic distribution of identified T_{PEX} and T_{EX} clusters in KLF2-KO and Ctrl cells. (E) Enrichment plot displaying the expression of the transcriptional CD62L$^+$ T_{PEX} cell signature (Tsui *et al.*, 2022) in KLF2-KO and Ctrl T_{PEX} cells. (F) Quantification of enriched gene expression associated with either the CX3CR1$^+$ or the CD101$^+$ T_{EX} differentiation trajectory in KLF2-KO and Ctrl P14 cells.

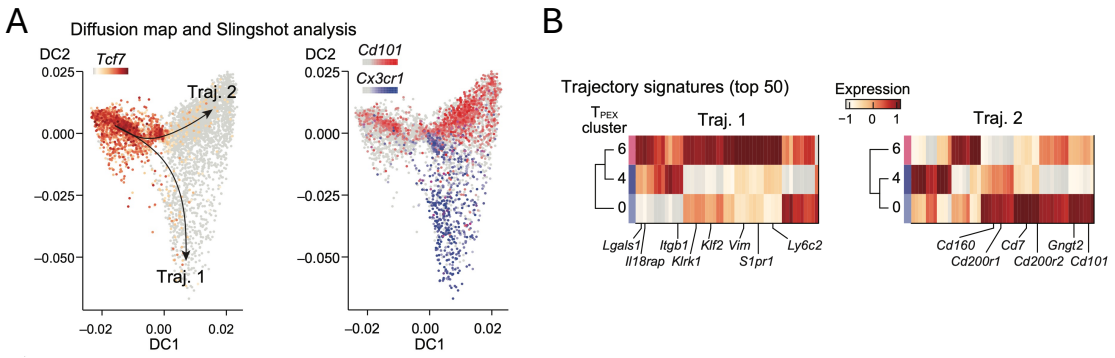

Figure 5.10: CX3CR1$^+$ and CD101$^+$ T_{EX} cells have two distinct trajectories.
(A-B) Naïve congenically marked (CD45.1$^+$) P14 CD8$^+$ T cells were adoptively transferred into naïve wildtype (CD45.2$^+$) mice, which were subsequently infected with LCMV Docile. P14 cells were harvested from the spleen and pooled LNs on day 30 p.i. and subjected to scRNA-seq. (A) Dimension reduction and Slingshot trajectory analysis of P14 cell transcriptomes showing two major lineages starting from *Tcf7*$^+$ T_{PEX} cells and progressing into either *Cx3cr1*$^+$ or *Cd101*$^+$ T_{EX} cells. (B) Enrichment analyses using the top 50 characteristic genes of Trajectories 1 and 2 were performed in the T_{PEX} cell clusters. (Unpublished data, Kallies/Carlson Tsui)

5.2.5 KLF2 negatively regulates cytokine production in exhausted T cells

Next, we investigated whether the loss of KLF2 impacted effector functions of P14 cells. KLF2-KO P14 cells demonstrated superior abilities to produce effector cytokines IFN-γ compared to Ctrl P14 cells (Figure 5.11A). Further, the frequencies of polyfunctional double producing IFN-γ/TNF$^+$ KLF2-KO cells were elevated compared to Ctrl cells (Figure 5.11A). At the single-cell level, the expression of IFN-γ and TNF in KLF2-KO T_{PEX} cells was higher than in Ctrl P14 cells (Figure 5.11B). To determine whether this superiority in cytokine production was specific to T_{PEX} or T_{EX} cell populations, we restimulated T_{PEX} and T_{EX} to analyse their individual cytokine levels. Both KLF2-KO T_{PEX} and T_{EX} cells exhibited increased frequencies of IFN-γ producing cells, and higher proportions of IFN-γ/TNF double-producing cells compared to Ctrl T_{PEX} and T_{EX} cells (Figure 5.11C and D). Notably, KLF2-KO T_{EX} cells were highly polyfunctional, with more than three times higher proportions of IFN-γ$^+$/TNF$^+$ T_{EX} cells. KLF2-KO T_{PEX} and T_{EX} cells demonstrated increased IFN-γ and TNF levels (Figure 5.11E), and KLF2-KO T_{EX} cells produced similar levels of GrzmB compared with Ctrl T_{EX} cells (Figure 5.11F).

In summary, loss of KLF2 enhances the effector capacity of T_{PEX} and T_{EX} cells in chronic infection, indicating that KLF2 negatively regulates cytokines production.

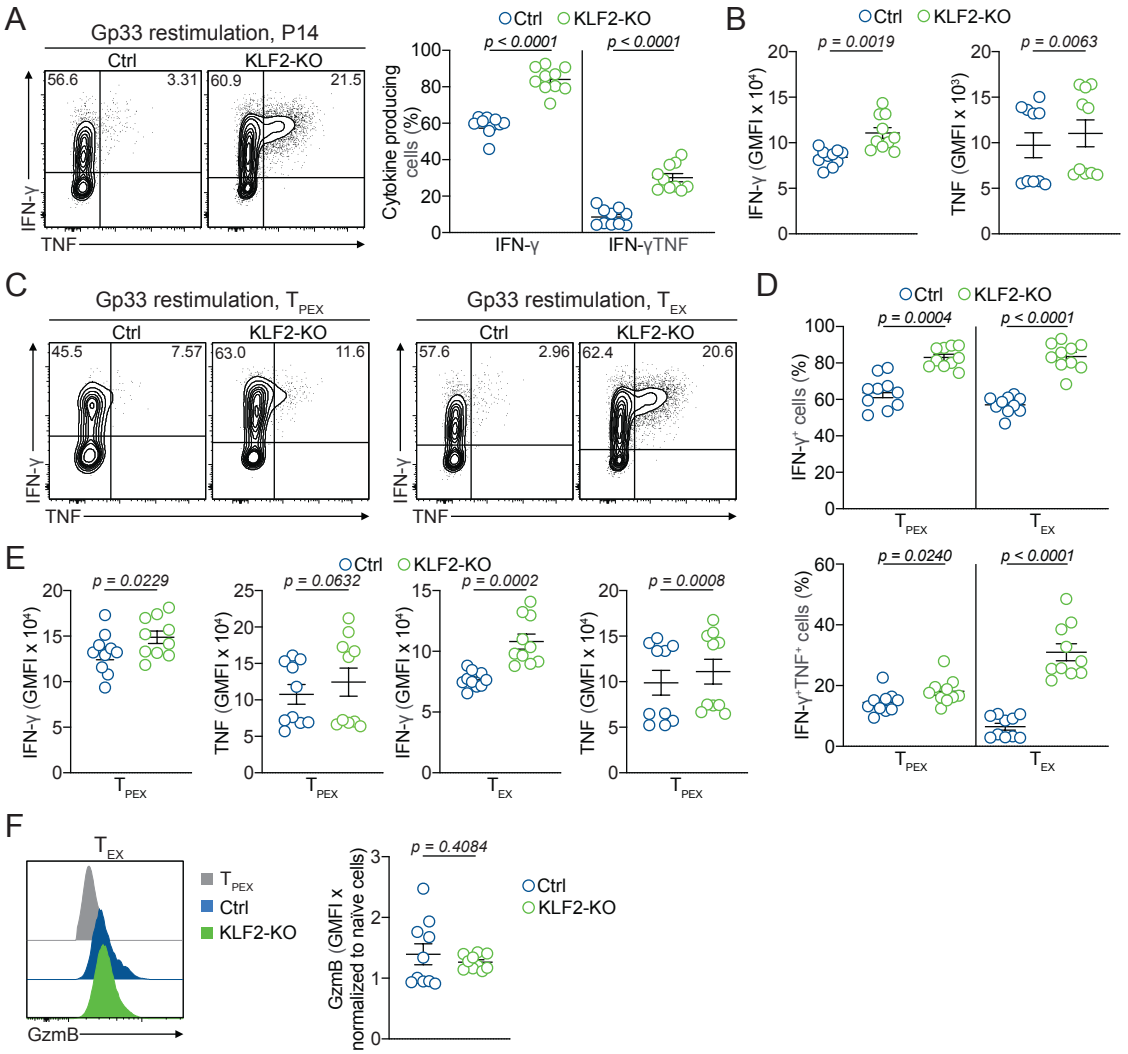

Figure 5.11: KLF2 deletion enhances cytokine production in T_{PEX} and T_{EX} in chronic infection.

(A-F) Naïve KLF2-KO (CD45.2⁺) and Ctrl (CD45.1/2⁺) P14 cells were adoptively co-transferred into naïve wildtype CD45.2⁺ mice at a ratio of 50:50 and subsequently infected with LCMV-Clone13. On days 28 p.i. the spleens were isolated and splenocytes restimulated with *ex vivo* with Gp33, for 5 hrs before analysation using flow cytometry. (A) Representative flow cytometry plots and quantification showing frequencies of IFN-γ and TNF producing KLF2-KO and Ctrl P14 cells and (B) expression levels of IFN- γ and TNF. (C) Representative flow cytometry plots and (D) quantification showing frequencies of IFN- γ and TNF producing KLF2-KO and Ctrl T_{PEX} and T_{EX} cells. (E) Quantification of IFN- γ and TNF expression levels in KLF2-KO and Ctrl T_{PEX} and T_{EX} cells. (F) Representative histogram and quantification showing production of GzmB in KLF2-KO and Ctrl T_{EX} cells. Dots in graphs represent individual mice; horizontal lines and error bars of bar graphs indicate means ± SEM, respectively. Data is pooled from two individual experiment. P values are from paired student's t test.

5.2.6 Regulation of KLF2 by cytokines and chemical compounds

Our data demonstrated the significance of KLF2 function for the differentiation of CD62L$^+$ T_{PEX} and CX3CR1$^+$ T_{EX} cells. However, the environmental cues driving the expression of KLF2 remain to be elucidated. To start our investigation, we aimed to determine whether qPCR is an appropriate method to examine the effect of cytokines on the expression of KLF2 in CD8$^+$ T cells. As KLF2 is downregulated upon TCR engagement (Hart *et al.*, 2012), we conducted an experiment in which we stimulated naïve P14 cells with the Gp33 peptide and measured the expression levels of *Klf2* mRNA by qPCR in a time-dependent manner (Figure 5.12A). As anticipated, cells stimulated with their cognate antigen demonstrated downregulation of *Klf2* mRNA in comparison to unstimulated cells after 24 hrs (Figure 5.12B). After 3 hours of stimulation, cells exhibited approximately half the *Klf2* mRNA level observed in unstimulated cells (Figure 5.12C). This decreased further after 6 hours, which was maintained for up to 24 hours. The reduction in *Klf2* mRNA coincided with an increase in *Cd69* mRNA at 3 hours of stimulation, followed by a decrease in *Cd69* mRNA levels after 6 and 24 hours (Figure 5.12D). Thus, qPCR is an efficient strategy to measure changes in KLF2 expression.

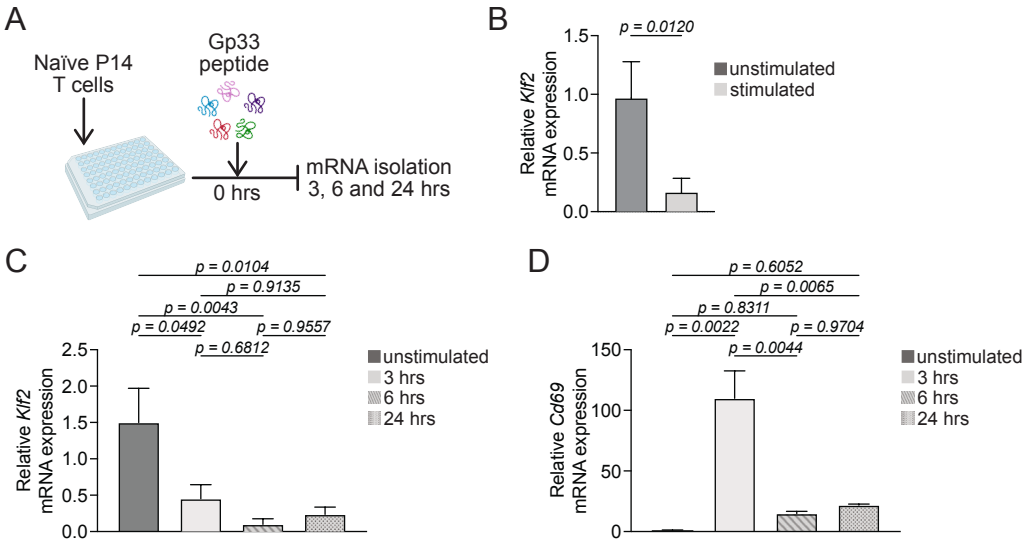

Figure 5.12: KLF2 is downregulated upon TCR-mediated activation.
(A-D) Naïve P14 cells were activated *in vitro* with Gp33-peptide for indicated times. The mRNA of the cells was isolated, and gene specific mRNA determined by qPCR. (A) Schematic of experimental setup. (B) Quantification of relative *Klf2*-mRNA in naïve (unstimulated) and stimulated T cells. (C) Quantification of relative *Klf2*-mRNA in naïve (unstimulated) and T cells stimulated for 3, 6 and 24

hrs. (D) Quantification of relative *Cd69*-mRNA in naïve (unstimulated) and stimulated T cells. Horizontal lines and error bars of bar graphs indicate means ± SEM, respectively. Data is pooled from two independent experiment with n>3. P values are from unpaired student's t test.

KLF2 is tightly downregulated in T_{RM} cells (Skon *et al.*, 2013). We therefore sought to investigate the potential impact on *Klf2* mRNA levels of TGFβ and IL-15, two cytokines that play important roles in the differentiation T_{RM} cells (Laura K. Mackay *et al.*, 2015). Additionally, we aimed to examine whether 3-hydroxy-3-methylglutaryl coenzyme A inhibitors (HMG-CoA reductase inhibitors, statins) exert a positive effect on *Klf2* mRNA levels. Statins, a class of drugs that have been utilised as cardiovascular medication for over two decades, effectively inhibit HMG-CoA, targeting cholesterol biosynthesis to reduce cholesterol levels in patients (Satish Ramkumar *et al.*, 2016). Moreover, statins have been demonstrated to upregulate KLF2 in diverse cell types. For instance, simvastatin upregulates KLF2 in macrophages, resulting in anti-inflammatory effects (Tuomisto *et al.* 2008). To address the roles of these cytokines and statins in KLF2 expression, we stimulated naïve P14 cells with Gp33 peptide *in vitro*. After 72 hrs, IL-15, TGFβ or Simvastatin was added to the cells and incubated for an additional 24 hrs. mRNA was subsequently isolated and *Klf2* mRNA quantified by qPCR (Figure 5.13A). Following IL-15 treatment, the level of *Klf2* mRNA was reduced compared to Ctrl cells (Figure 5.13B). Similarly, TGFβ treatment also reduced the levels of *Klf2* mRNA compared to Ctrl cells (Figure 5.13C). In contrast, Simvastatin resulted in increased levels of *Klf2* mRNA compared to Ctrl cells by approximately 18-fold (Figure 5.13D). This upregulation of KLF2 occurred in a concentration dependent manner, with increasing Simvastatin concentration correlating with an increased *Klf2* mRNA level (Figure 5.13E).

Overall, IL-15 and TGFβ may be negative regulators of KLF2, while Simvastatin upregulates KLF2 expression, indicating a possible therapeutic approach to target KLF2 expression *in vivo*. However, the experiment in (Figure 5.13E) was done only once, and the data needs to be confirmed.

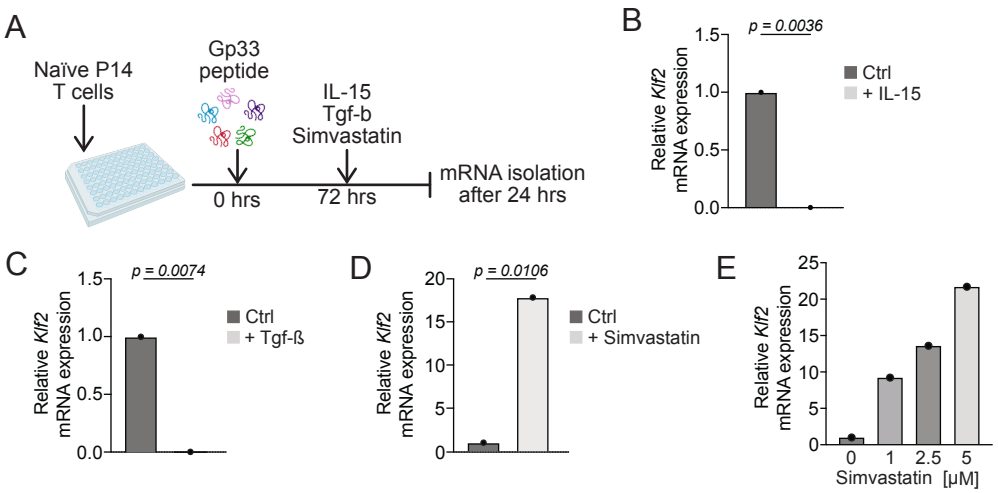

Figure 5.13: KLF2 expression is downregulated by IL-15 and TGFβ and upregulated by Simvastatin in a concentration dependent manner.
(A-D) Naïve P14 cells were activated *in vitro* with Gp33-peptide for 72 hrs. IL-15, TGFβ and Simvastatin were added to the culture for another 24 hrs. The mRNA of the cells was isolated, and the *Klf2* mRNA determined by qPCR. (A) Schematic of experimental setup. (B) Quantification of relative *Klf2*-mRNA in untreated and IL-15 treated P14 cells. (C) Quantification of relative *Klf2*-mRNA in untreated and TGFβ treated P14 cells. (D) Quantification of relative *Klf2*-mRNA in untreated and Simvastatin treated P14 cells. (E) Quantification of relative *Klf2*-mRNA in untreated and treated P14 cells with Simvastatin in a concentration dependent manner. Data is pooled from two independent experiments with n>3 for B-D and representative of 1 experiment with n>3 for E. P values are from unpaired student's t test.

5.2.7 KLF2 is required for the anti-PD-1 checkpoint inhibitor response

Previous studies have demonstrated that CD62L$^+$ T_{PEX} cells respond to ICB (anti-PD-L1) treatment (Tsui *et al.*, 2022). They undergo a proliferative burst and differentiation into CX3CR1$^+$ T_{EX} cells (Siddiqui *et al.*, 2019; Fang *et al.*, 2022). We identified KLF2 as a key regulator of CD62L$^+$ T_{PEX} /CX3CR1$^+$ T_{EX} differentiation suggesting that it may be involved in the ICB response. To test the role of KLF2 in ICB response, we co-transferred KLF2-KO and Ctrl P14 cells into recipient mice and infected the mice with LCMV-Clone13. One group of mice was subjected to anti-PD-L1 treatment, whilst the other group received PBS as a control (Figure 5.14A). We observed in the blood that KLF2-KO P14 cells did not respond in the same way as Ctrl P14 cells. Prior to treatment, approximately five

times more KLF2-KO P14 cells were circulating in the blood compared to Ctrl P14 cells. Following anti-PD-L1 treatment, this number decreased to three times more KLF2-KO P14 cells, indicating that Ctrl P14 cells in the blood expanded to a greater extent (Figure 5.14B). This increase was attributable to a proliferative burst and differentiation of CX3CR1$^+$ T_{EX} cells, which significantly increased in Ctrl cells following treatment in the blood, suggesting a burst and egress from lymphoid organs (Figure 5.14C and D). As observed in previous experiments, KLF2-KO P14 cells did not efficiently differentiate into CX3CR1$^+$ T_{EX} cells. The proportion of KLF2-KO CD101$^+$ T_{EX} cells decreased in the blood upon treatment (Figure 5.14C and D). Similar results were observed in the spleen. Prior to treatment, spleens harboured seven times more KLF2-KO cells than Ctrl cells (Figure 5.14E and F). After the treatment Ctrl cells expanded to a greater extent than KLF2-KO cells, reducing this number to four times more KO cells than Ctrl P14 cells (Figure 5.14E and F). This was accompanied by an increase in Ctrl P14 numbers in the spleen after treatment, while numbers of KLF2-KO P14 numbers did not change significantly (Figure 5.14G).

In the LN, the representation of KLF2-KO and Ctrl cells did not change significantly upon treatment (Figure 5.14F). However, numerically, the number of Ctrl P14 cells increased in the LN after treatment, while no changes in the number of KLF2-KO P14 cells were observed (Figure 5.14G), indicating that KLF2-KO P14 did not proliferate upon treatment. Upon anti-PD-L1 treatment there was a significant increase in numbers for Ctrl T_{PEX}, particularly numbers of Ctrl CD62L$^+$ T_{PEX} levels increased significantly (Figure 5.14H-K). KLF2-KO T_{PEX} and CD62L$^+$ T_{PEX} cells, however, did not expand (Figure 5.14H-K). No significant differences were observed between the treated and untreated Ctrl or KLF2-KO T_{PEX} and CD62L$^+$ T_{PEX} cells in the LN (Figure 5.14H-K). In the spleen, the numbers of Ctrl T_{EX} cells increased after treatment, but not for KLF2-KO T_{EX} cells. No differences were observed in LN (Figure 5.14H-K).

Collectively, these data demonstrate that CD62L$^+$ T_{PEX} cells are the main responding cell population to anti-PD-L1 treatment, and that deletion of KLF2 leads to an overall impairment of the CD8$^+$ T cell mediated ICB response.

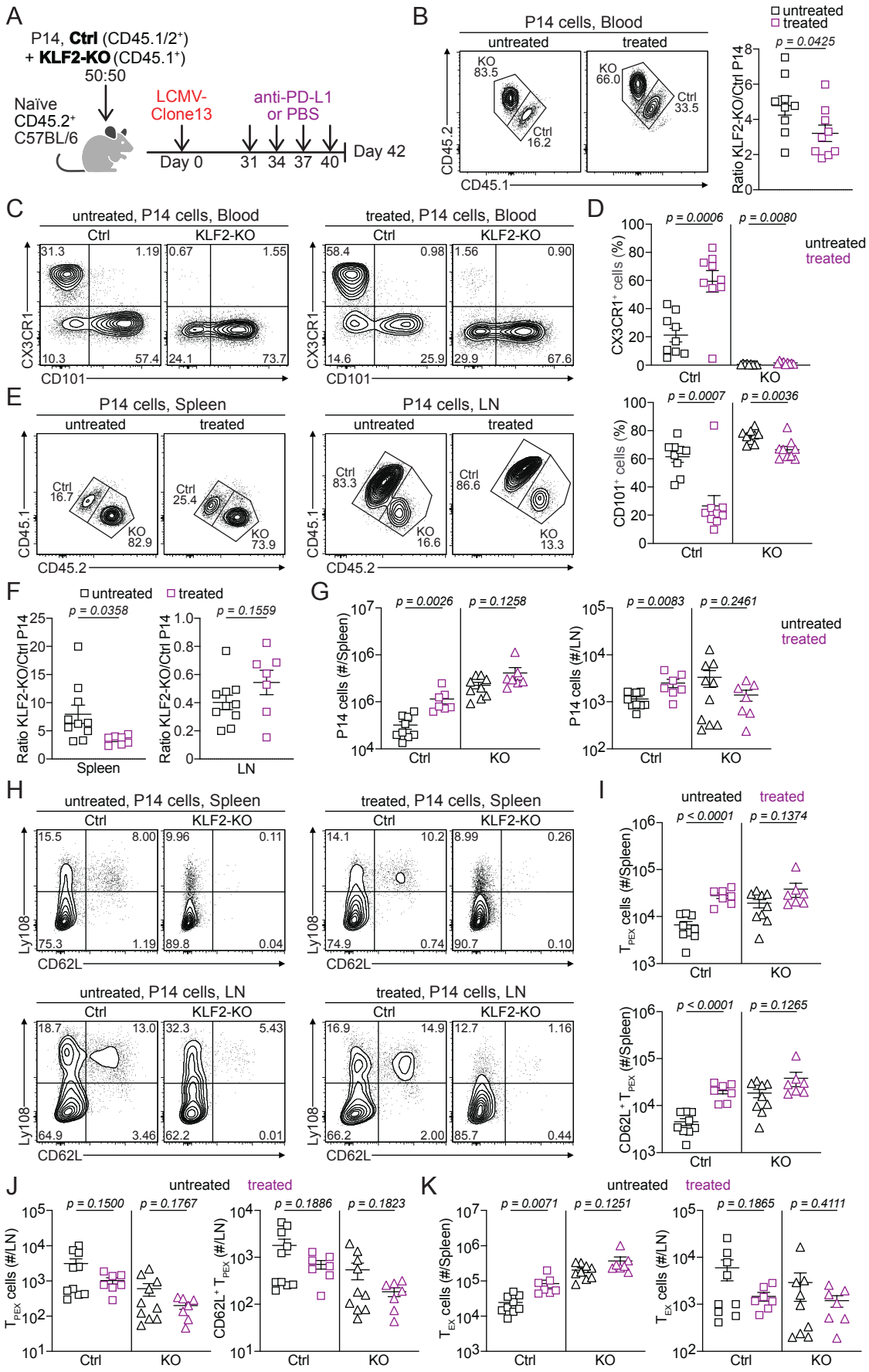
A
P14, Ctrl (CD45.1/2+)
+ KLF2-KO (CD45.1+)
50:50
Naïve
CD45.2+
C57BL/6
LCMV-
Clone13
anti-PD-L1
or PBS
Day 0
31 34 37 40
Day 42
B
P14 cells, Blood
untreated
treated
KO
83.5
Ctrl
16.2
KO
66.0
Ctrl
33.5
CD45.2
CD45.1
untreated
treated
p = 0.0425
Ratio KLF2-KO/Ctrl P14
C
untreated, P14 cells, Blood
treated, P14 cells, Blood
Ctrl
KLF2-KO
CX3CR1
CD101
31.3
1.19
10.3
57.4
0.67
1.55
24.1
73.7
58.4
0.98
14.6
25.9
1.56
0.90
29.9
67.6
D
p = 0.0006
p = 0.0080
untreated
treated
CX3CR1+ cells (%)
Ctrl
KO
p = 0.0007
p = 0.0036
CD101+ cells (%)
E
P14 cells, Spleen
P14 cells, LN
untreated
treated
Ctrl
16.7
KO
82.9
Ctrl
25.4
KO
73.9
Ctrl
83.3
KO
16.6
Ctrl
86.6
KO
13.3
CD45.1
CD45.2
F
untreated
treated
p = 0.0358
p = 0.1559
Ratio KLF2-KO/Ctrl P14
Spleen
LN
G
p = 0.0026
p = 0.1258
p = 0.0083
p = 0.2461
P14 cells (#/Spleen)
P14 cells (#/LN)
H
untreated, P14 cells, Spleen
treated, P14 cells, Spleen
untreated, P14 cells, LN
treated, P14 cells, LN
Ly108
CD62L
15.5
8.00
75.3
1.19
9.96
0.11
89.8
0.04
14.1
10.2
74.9
0.74
8.99
0.26
90.7
0.10
18.7
13.0
64.9
3.46
32.3
5.43
62.2
0.01
16.9
14.9
66.2
2.00
12.7
1.16
85.7
0.44
I
untreated
treated
p < 0.0001
p = 0.1374
TPEX cells (#/Spleen)
p < 0.0001
p = 0.1265
CD62L+ TPEX (#/Spleen)
J
untreated
treated
p = 0.1500
p = 0.1767
TPEX cells (#/LN)
p = 0.1886
p = 0.1823
CD62L+ TPEX (#/LN)
K
untreated
treated
p = 0.0071
p = 0.1251
TEX cells (#/Spleen)
p = 0.1865
p = 0.4111
TEX cells (#/LN)

Figure 5.14: KLF2 plays a major role in regulating the CD8$^+$ T cell response to ICB.
(A-J) Naïve KLF2-KO (CD45.2$^+$) and Ctrl (CD45.1/2$^+$) P14 cells were adoptively co-transferred into naïve wildtype CD45.2$^+$ mice at a ratio of 50:50 and subsequently infected with LCMV-Clone13. On days 31, 34 37 and 40 p.i. mice were treated with 200 µg anti-PD-L1 (purple) or PBS (black). spleens, blood and LN were analysed using flow cytometry on day 42 post infection. (A) Schematic of the experimental setup. (B) Representative flow cytometry plots and quantification of KLF2-KO and Ctrl P14 cells ratios in the blood before and after treatment. (C) Representative flow cytometry plots of KLF2-KO and Ctrl CX3CR1$^+$ and CD101$^+$ T_{EX} cell in the blood before and after treatment. (D) Quantification of KLF2-KO and Ctrl CX3CR1$^+$ and CD101$^+$ T_{EX} cell in the blood before and after treatment. (E) Representative flow cytometry plots of KLF2-KO and Ctrl P14 cells in the spleen and LN before and after treatment. (F) Quantification of change in ratio of KLF2-KO and Ctrl P14 cells in the spleen and LN. (G) Quantification of KLF2-KO and Ctrl P14 cells numbers in the spleen and LN. (H) Representative flow cytometry plots showing KLF2-KO and Ctrl CD62L$^+$ and CD62L$^-$ T_{PEX} cells and T_{EX} cells in the spleen and LN before and after treatment. (I) Quantification of KLF2-KO and Ctrl CD62L$^-$ and CD62L$^+$ T_{PEX} cells numbers per spleen. (J) Quantification of KLF2-KO and Ctrl CD62L$^-$ and CD62L$^+$ T_{PEX} cells numbers per LN. (J) Quantification of KLF2-KO and Ctrl T_{EX} cells numbers per spleen and LN. Dots in graphs represent individual mice; horizontal lines and error bars of bar graphs indicate means ± SEM, respectively. Data is pooled from two independent experiments. P values are from unpaired student's t test.

5.2.8 Statins impact exhausted CD8$^+$ T cell differentiation in a KLF2 dependent manner

Next, we aimed to test the potential effects of statins, which can effectively upregulate KLF2 as our data (Chapter 5.2.6) and published data (Bu et al., 2010) show. As Simvastatin is highly hydrophobic and challenging to administer to mice due to its poor solubility, we utilised another statin, Fluvastatin, for the administration *in vivo*. To this end, we administered Fluvastatin or PBS three times to chronically LCMV-infected mice that had previously received KLF2-KO and Ctrl P14 cells at a ratio of 1:1 (Figure 5.15A). Fluvastatin treatment did not alter the ratio of KLF2-KO and Ctrl P14 cells in the spleen and LN, suggesting that Fluvastatin does not affect CD8$^+$ T cell proliferation (Figure 5.15B and C). However, Fluvastatin treatment significantly reduced the proportion of P14 cells

expressing the activation marker CD69 in Ctrl P14 cells of both the spleen and LN (Figure 5.15D). In contrast, the expression of CD69 in KLF2-KO P14 cells was not affected by Fluvastatin treatment (Figure 5.15E). These findings suggest that the reduction of CD69 in Ctrl P14 cells upon treatment is KLF2-mediated.

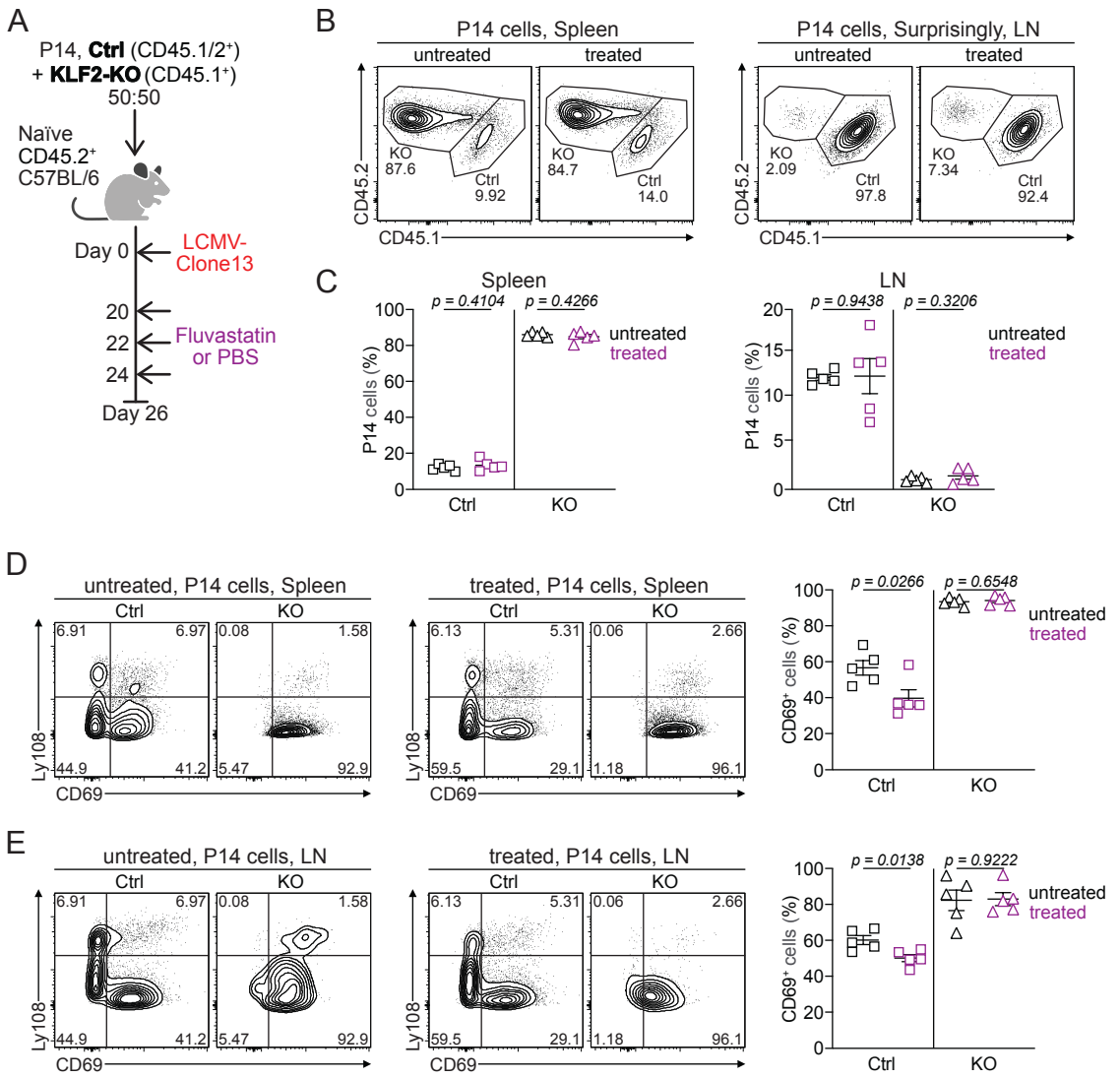

Figure 5.15: Fluvastatin impacts KLF2-mediated regulation of CD69 expression.
(A-E) Naïve KLF2-KO (CD45.2+) and Ctrl (CD45.1/2+) P14 cells were adoptively co-transferred into naïve wildtype CD45.2+ mice at a ratio of 50:50 and subsequently infected with LCMV-Clone13. On days 20, 22 and 24 p.i. mice were treated with 10 µg/mg mouse weight Fluvastatin (purple) or PBS (black). spleens and LN were analysed using flow cytometry on day 26 post infection. (A) Schematic of the experimental setup. (B) Representative flow cytometry plots and quantification of KLF2-KO and Ctrl P14 cells ratios before and after treatment. (C) Quantification of KLF2-KO and Ctrl P14 cells ratios before and

after treatment. (D) Representative flow cytometry plots showing CD69$^+$ T_{PEX} and T_{EX} cells in KLF2-KO and Ctrl cells and quantification of CD69$^+$ KLF2-KO and Ctrl P14 cells in the spleen before and after treatment. (E) Representative flow cytometry plots showing CD69$^+$ T_{PEX} and T_{EX} cells in KLF2-KO and Ctrl cells and quantification of CD69$^+$ KLF2-KO and Ctrl P14 cells in the LN before and after treatment. Dots in graphs represent individual mice; horizontal lines and error bars of bar graphs indicate means ± SEM, respectively. Data is representative of two independent experiments. P values are from unpaired student's t test.

Next, we evaluated exhausted T cell differentiation following Fluvastatin treatment. In the spleen, no significant differences were observed in the frequencies of T_{PEX} cells and CD62L$^+$ T_{PEX} cells between Ctrl and KLF2-KO P14 cells in treated and untreated mice (Figure 5.16A and B). However, in the LN, we observed a notable increase in Ctrl T_{PEX} cells and CD62L$^+$ T_{PEX} cells frequencies in treated mice in comparison to untreated mice (Figure 5.16C and D). KLF2-KO cells in the LN did not exhibit an increase in CD62L$^+$ T_{PEX}, indicating that the increase in Ctrl CD62L$^+$ T_{PEX} is mediated by KLF2 (Figure 5.16C and D). Further we observed increased frequencies of CX3CR1$^+$ T_{EX} cells and reduced frequencies of CD101$^+$ T_{EX} cells in the spleen and LN (Figure 5.16E-G). KLF2-KO cells did not show an increase in either CX3CR1$^+$ or CD101$^+$ T_{EX} cells or after treatment with Fluvastatin (Figure 5.16E-G), indicating that this increase in the Ctrl cells is regulated through KLF2-mediated function.

In summary, we observed that the differentiation of CD62L$^+$ T_{PEX} and CX3CR1$^+$ T_{EX} cells could be enhanced by statins in a KLF2 dependent manner. Further, Fluvastatin altered regulation of CD69 expression, but does not affect the expansion of CD8$^+$ T cells in the timeframe of our experiments. However, the experiment was done only once, and the data needs to be confirmed.

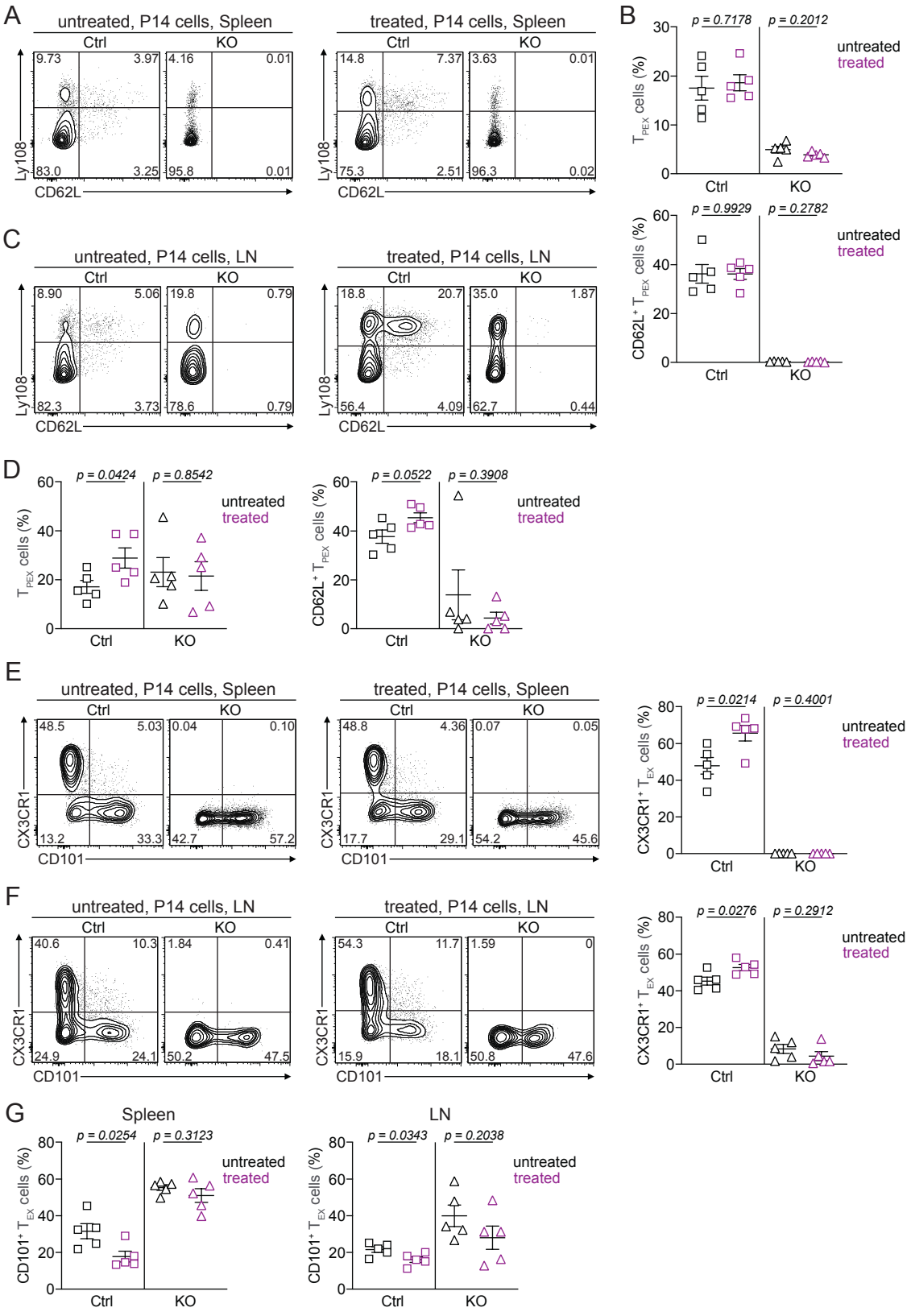

Figure 5.16: Fluvastatin treatment enhances the differentiation of CD62L$^+$ T_{PEX} and CX3CR1$^+$ T_{EX} cells through KLF2.

(A-E) Naïve KLF2-KO (CD45.2$^+$) and Ctrl (CD45.1/2$^+$) P14 cells were adoptively co-transferred into naïve wildtype CD45.2$^+$ mice at a ratio of 50:50 and subsequently infected with LCMV-Clone13. On days 20, 22 and 24 p.i. mice were treated with 10 µg/mg mouse weight Fluvastatin (purple) or PBS (black). spleens and LN were analysed using flow cytometry on day 26 post infection. (A) Representative flow cytometry plots showing KLF2-KO and Ctrl CD62L$^+$ and CD62L$^-$ T_{PEX} cells and T_{EX} cells. (B) Quantification of KLF2-KO and Ctrl T_{PEX} and CD62L$^+$ T_{PEX} cells in the spleen before and after treatment. (C) Representative flow cytometry plots showing KLF2-KO and Ctrl CD62L$^+$ and CD62L$^-$ T_{PEX} cells and T_{EX} cells. (D) Quantification of KLF2-KO and Ctrl T_{PEX} and CD62L$^+$ T_{PEX} cells in the LN before and after treatment. (E) Representative flow cytometry plots showing KLF2-KO and Ctrl CX3CR1$^+$ and CD101$^+$ T_{EX} cells and quantification of KLF2-KO and Ctrl CX3CR1$^+$ T_{EX} cells in the spleen before and after treatment. (F) Representative flow cytometry plots showing KLF2-KO and Ctrl CX3CR1$^+$ and CD101$^+$ T_{EX} cells and quantification of KLF2-KO and Ctrl CX3CR1$^+$ T_{EX} cells in the LN before and after treatment. (G) Quantification of KLF2-KO and Ctrl CD101$^+$ T_{EX} cells in the spleen and LN before and after treatment. Dots in graphs represent individual mice; horizontal lines and error bars of bar graphs indicate means ± SEM, respectively. Data is representative of one independent experiments. P values are from unpaired student's t test.

Chapter 6 – Discussion and outlook

6.1 Molecular regulation of T cell differentiation by the transcription regulator SATB1

Exhausted $CD8^+$ T cell differentiation proceeds along defined developmental trajectories from cells with high self-renewal capacity and developmental potential but limited effector function to cells that are terminally differentiated with different degrees of effector function. This process needs to balance relative quiescence and stemness on the one side and proliferation and differentiation on the other side. Thus, precursors of exhausted T (T_{PEX}) cells, which have high self-renewal capacity and developmental potential, require mechanisms that maintain expression of regulators linked of stemness such as TCF1, a transcription factor usually downregulated when cells get activated by their cognate antigen. Our data show that SATB1 is part of the group of regulators that balances stemness and differentiation. Similar to TCF1, it is expressed in naïve T cells, maintaining the naïve transcriptional status and blocking ectopic expression of effector genes (Nüssing *et al.*, 2022).

We found that SATB1 is specifically expressed in T_{PEX} cells that play a central role in maintaining $CD8^+$ T cell responses to persistent stimulation. We show that SATB1 was critical in maintaining the balance between stemness and effector differentiation of exhausted T cells by limiting the expansion and differentiation of exhausted effector and terminally differentiated cells. In addition, tight regulation of SATB1 expression levels was critical for the appropriate expression of multiple inhibitory receptors, including PD-1, Lag-3, and Tim-3 and the cytokine producing capacity of $CD8^+$ T cells.

Our data show that in acute infection, $CD8^+$ T cells maintain a certain level of SATB1 expression, whereas in chronic infection, T_{PEX} cells retain SATB1 expression, while it is lost in both $CX3CR1^+$ and $CD101^+$ T_{EX} cells. This suggests that exposure to persistent antigen stimulation necessitates a more stringent regulation of SATB1 expression compared to acute antigen exposure. Notably, SATB1 expression in T_{PEX} cells is significantly lower than in naïve $CD8^+$ T cells

or $CD8^+$ T cells during acute infections, suggesting that downregulation of SATB1 is critical for T cell differentiation under chronic antigen exposure. Previous studies by Khare *et al.*, 2019, have demonstrated that SATB1 expression can be regulated by three alternative promoters for the *Satb1* gene: proximal P1, middle P2, and distal P3, which regulate the expression of different SATB1 isoforms. Furthermore, during the peripheral differentiation of $CD4^+$ T cells, differential promoter activation leads to the preferential development of different $CD4^+$ T cell subsets. The P2 and P3 promoters promote Tfh differentiation, whereas activated T cells and Treg preferentially utilize the P1 promoter for gene expression regulation. TCR and IL-4 signalling activate NF-kB and STAT6, leading to the use of the P2 and P3 promoters. This promoter switching in $CD4^+$ T cells is hypothesized to regulate SATB1 in a context- and cell-type-specific manner (Khare *et al.*, 2019). A similar switching mechanism may occur in $CD8^+$ T cells during chronic infection, potentially resulting in varying levels of SATB1 expression. However, this has to be further investigated. For example, promoter activity could be examined using qPCR with promoter-specific primers or Cap Analysis of Gene Expression sequencing (CAGE-Seq) to determine transcription start site usage in T_{PEX} versus T_{EX} cells. In addition, chromatin accessibility and histone modification profiling (ATAC-Seq and ChIP-Seq for promoter-associated marks such as H3K4me3) could be used to identify regulatory elements that drive differential promoter activation in acute and chronic infection.

The context-specific regulation of SATB1 was further observed in experiments where SATB1 was deleted or overexpressed. While the depletion or overexpression of SATB1 had significant impacts on $CD8^+$ T cells during chronic infection, the effects during acute infection were comparatively less pronounced. In the context of acute antigen stimulation, the depletion of SATB1 promoted the differentiation of SLEC, whereas the overexpression of SATB1 facilitated the differentiation of memory precursor cells (MPC). This may occur by repressing effector genes such as *Bhlhe40, Gata3, Hic1, Irf4, Prdm1, Runx3, Stat5a, Stat5b, Tox, Zeb1,* and *Zeb2*, and promoting the expression of genes associated with a naïve state, including *Bcl6, Bcl11b, Foxo1, Lef1,* and *Tcf7* that have been shown

to be regulated by SATB1 (Nüssing *et al.*, 2022). This shift in differentiation was also evident at later stages in the memory CD8$^+$ T cell populations. Specifically, the depletion of SATB1 promoted the development of T_{EM} cells and impaired the development of T_{CM} and T_{RM} cells, whereas the overexpression of SATB1 had the opposite effect, enhancing the formation of T_{CM} and T_{RM} cells. Overall, the data suggest that in acute antigen infection, the level of SATB1 expression can influence the differentiation towards either effector or memory transcriptional differentiation programs (Figure 6.2). During chronic infection high levels of SATB1 limit a critical feature of T_{PEX} cells, specifically their ability to produce effector progeny. Downregulation of SATB1 was essential for T_{EX} cell differentiation, as neither CX3CR1$^+$ nor CD101$^+$ T_{EX} cells developed in cells that constitutively overexpressed SATB1, indicating that SATB1 maintains the identity of T_{PEX} cells. In contrast, the depletion of SATB1 resulted in increased differentiation of T_{EX} cells, while the differentiation of T_{PEX} cells was not visibly affected. Notably, while the proportion of T_{PEX} cells within the antigen-specific CD8$^+$ T cell population decreased in the absence of SATB1, their absolute numbers remained largely unchanged. This suggests that the apparent drop in T_{PEX} frequency is driven by a relative expansion of T_{EX} subsets, particularly CX3CR1$^+$ and CD101$^+$ cells, rather than by a loss of T_{PEX} themselves. Together, these observations suggest that T_{PEX} formation may be established independently of SATB1-regulated pathways, with SATB1 playing a more prominent role in controlling the transition from T_{PEX} to downstream T_{EX} states. This transition may be orchestrated by preventing the expression of effector genes necessary for T_{EX} cell differentiation or by enforcing the expression of genes associated with stemness and the naïve transcriptional program to maintain T_{PEX}, such as *Tcf7* similar as it has been shown in acute infection (Nüssing *et al.*, 2022). Alternatively, compensatory transcriptional regulators may sustain the T_{PEX} pool in the absence of SATB1, thereby buffering its impact on their maintenance.

In the absence of SATB1, antigen-specific CD8$^+$ T cells were significantly more abundant compared to control cells in chronic infection settings, but not in acute

infection indicating that SATB1 restricts population expansion in a context-specific manner. The mechanisms by which SATB1 limits population expansion require further investigation. Two potential mechanisms may be involved: SATB1 could inhibit the proliferation of exhausted T cells, or it may upregulate pro-apoptotic genes, leading to enhanced survival of exhausted T cells upon SATB1 depletion. Indeed, transcriptomic and epigenetic analyses revealed altered expression of *Mki67* and *Casp3* (encoding Caspase3), suggesting that SATB1 depletion affects both the proliferation and apoptotic characteristics of $CD8^+$ T cells. However, this requires more exploration. I*n vivo* BRDU/EDU staining could assess cell proliferation upon SATB1 depletion. Additionally, apoptotic assays and staining of pro- and anti-apoptotic proteins such as Bim and Bcl2 could provide insights into whether SATB1 constrains cell death in chronic infection. A related important question is whether these alterations in $CD8^+$ T cell expansion influence viral control. Future studies should assess viral titers to determine if SATB1-mediated modulation of exhausted T cell subsets impacts pathogen clearance or viral persistence.

Despite previous findings indicating increased PD-1 expression in the absence of SATB1 (Stephen *et al.*, 2017), we did not observe altered PD-1 expression in SATB1-KO compared to control $CD8^+$ cells during chronic infection. However, SATB1 overexpression significantly reduced PD-1 expression. Conversely, in the context of acute infection, SATB1-KO $CD8^+$ T cells exhibited elevated PD-1 levels, whereas cells overexpressing SATB1 demonstrated reduced PD-1 expression. These observations suggest that SATB1 plays a context-specific role in regulating PD-1 expression. This may be attributed to alternative mechanisms governing PD-1 expression during chronic infection, while SATB1 is crucial in restraining PD-1 expression during acute infection. For instance, T-Bet and EOMES have been implicated in regulating PD-1 expression in exhausted T cells (Kao *et al.*, 2011; Li *et al.*, 2018), indicating potential SATB1-independent regulatory pathways. This hypothesis aligns with the expression profile of SATB1, which is highly expressed in effector cells during acute infection but is downregulated or not expressed in mature exhausted T cells.

Independent of the infection, loss of SATB1 impaired effector cytokine production IFN-γ and TNF. On the other hand, high expression of SATB1 in chronic infection enhanced the capacity of T_{PEX} and T_{EX} cells to produce effector cytokines, while the overexpression in acute antigen settings, did not alter cytokine production. Thus, SATB1 expression in $CD8^+$ T cells promotes cytokine production. These findings are in line with earlier observations, which demonstrated that ectopic expression of SATB1 in Treg cells resulted in inappropriate production of proinflammatory cytokines (Beyer *et al.*, 2011). Given that SATB1 is only expressed in T_{PEX} cells, this may indicate that SATB1 expression is required for establishing an epigenetic or transcriptional program in T_{PEX} cells that persists as they differentiate into T_{EX} cells. In this scenario, loss of SATB1 could impair the proper programming of downstream T_{EX} cells, reducing their functionality and cytokine production.

The precise mechanism by which SATB1 regulates transcription in T_{PEX} and T_{EX} cells remains unclear. While SATB1 is predominantly recognized as a chromatin organizer (Cai *et al.*, 2006), evidence also suggests its direct involvement in gene expression regulation (Ahlfors *et al.*, 2010). In the context of Treg cell development, SATB1 has been identified as a pioneering factor that binds to closed chromatin, initiating the Treg differentiation pathway through the induction of repressed chromatin in an IL-2-dependent manner (Kitagawa *et al.*, 2017; Chorro *et al.*, 2018). Consistent with its expression, SATB1 binding was found to be enriched in chromatin regions that were accessible specifically in T_{PEX} cells. Contrary to expectations, however, the data indicate that SATB1 is not essential for defining the chromatin accessibility landscape specific to exhausted T cells. Instead, the findings using the $Satb1^{m1Anu/m1Anu}$ suggest that direct SATB1 binding to DNA is essential for its transcriptional activity. Despite SATB1 being expressed, impaired binding resulted in changes in exhausted $CD8^+$ T cells, similar to those observed in SATB1-KO experiments. This is implying SATB1s role as a conventional transcriptional regulator in $CD8^+$ T cells. Additionally, SATB1 may facilitate the recruitment of other molecules to DNA binding sites and

regulatory elements, such as the NuRD repressive complex, β-catenin, or p300 (Notani *et al.*, 2010; Stephen *et al.*, 2017). Notably, pathway analyses of RNA sequencing data revealed that SATB1 regulates genes associated with cell cycle regulation and chromatid segregation, suggesting a potential higher-order function in chromatin organization linked to cell cycle progression. Supporting this notion, SATB1 in T cells has been shown to contribute to 3D genome architecture, partly through its interaction with CTCF, thereby influencing the transcription of critical regulators of T cell activation (Wang *et al.*, 2023). However, recent data indicate that in naïve $CD8^+$ T cells, SATB1 plays only a minor role in remodelling chromatin architecture (Russ *et al.*, 2023).

In our study, we also investigated a potential involvement of Blimp1, a transcriptional regulator critical in T cell differentiation (Rutishauser *et al.*, 2009; Kallies *et al.*, 2009), in SATB1 mediated processes. Blimp1 expression is high in T_{EX} cells during chronic infection, and its deletion enhances T_{PEX} differentiation while suppressing T_{EX} differentiation (McLane *et al.*, 2019; Kallies *et al.*, 2020; Baessler and Vignali, 2024). Sequencing analysis of SATB1-KO cells revealed increased *Prdm1* expression in T_{PEX} cells, with our ATAC- and Chip sequencing suggesting direct transcriptional regulation by SATB1. We hypothesized that the effects of SATB1 depletion on T_{EX} differentiation might be reversible through simultaneous Blimp1 depletion. To test this, we therefore depleted *Prdm1* in SATB1-KO P14 cells. Collectively, it was observed that the depletion of Blimp1 in SATB1-KO P14 cells resulted in impaired expansion of P14 cells, particularly of the T_{EX}, suggesting that upregulation of Blimp1 in SATB1-deficient T cells contributes to T_{EX} differentiation. To substantiate this model, future experiments could combine SATB1 and Blimp1 perturbations with lineage-tracing approaches to track T_{PEX}-to-T_{EX} transitions *in vivo*. In addition, single-cell RNA sequencing coupled with ATAC-Seq could reveal whether Blimp1 deletion rescues the transcriptional and epigenetic programs altered by SATB1 loss.

The molecular mechanism responsible for initiating the downregulation of SATB1 expression in T_{PEX}, which may subsequently lead to T_{EX} differentiation requires

more investigations. SATB1 may be regulated through intrinsic or extrinsic signalling pathways. One plausible signalling mechanism involves cytokines. A notable molecule identified in the literature as being involved in the regulation of SATB1 expression is TGFβ. Previous studies have demonstrated that TGFβ silences SATB1 expression in $CD4^+$ T cells, thereby permitting their differentiation into T_{FH} cells . Another potential mechanism is the Wnt signalling pathway. In T_{H2} cells, SATB1 regulates the expression of GATA3 in a Wnt/β-catenin signalling-dependent manner. Upon Wnt signalling, β-catenin translocates to the nucleus and binds to SATB1, leading to the de-repression of a cascade of genes essential for differentiation (Notani *et al.*, 2010; Stephen *et al.*, 2017). Furthermore, in colorectal cancer, SATB1 has been suggested to share a feedback regulatory network with TCF7L2/β-catenin signalling and is required for Wnt signalling-dependent regulation of β-catenin (Mir *et al.*, 2016). However, further research is necessary to test such relationships in T cells. For example, SATB1 expression could be assessed in T_{PEX} and T_{EX} cells following *in vitro* and *in vivo* blockade of TGFβ or Wnt signalling, using neutralising antibodies, receptor antagonists, or small-molecule inhibitors. Complementary experiments employing β-catenin or Smad transcriptional reporters could identify downstream pathway activation in SATB1-high versus SATB1-low populations.

Based on our findings on SATB1 in exhausted T cells, SATB1 emerges as a promising target for adoptive T cell therapy and cancer treatments. Chimeric antigen receptor (CAR) T cell therapy has revolutionized the treatment of some haematological malignancies; however, its effectiveness in solid tumours remains constrained (Chen *et al.*, 2024). This limitation is attributed to factors such as inadequate tumor trafficking and the terminal differentiation of CAR T cells, which diminish their effector function (Chen *et al.*, 2024). Depleting SATB1 could potentially enhance the differentiation of the T_{EX} population, thereby increasing tumor infiltration. Another promising therapeutic strategy involves utilizing microRNAs to target cancer cells, either by using microRNAs that suppress oncogenic tumor genes or restore tumor-suppressive genes, an approach already explored in multiple cancer types (Fu *et al.*, 2021). SATB1 has been

linked to several microRNAs in different disease models. For instance, miR-376a has been shown to directly target and inhibits SATB1 in osteosarcomas (Zhou *et al.*, 2018), while SATB1 is targeted by miR-409 in various breast cancer lines (Chen *et al.*, 2022). Conversely, in primary T cells, overexpression of miR-641 results in the downregulation of SATB1 (H. Zhu *et al.*, 2024). These findings not only suggest a mechanism by which SATB1 expression is regulated but also present a potential avenue for targeted therapy.

Overall, our data identifies SATB1 as a novel regulator that governs effector differentiation and function of $CD8^+$ T cells during chronic infection. In particular, SATB1 emerges as a negative regulator of the transition from T_{PEX} to T_{EX} cells (Figure 6.1), thereby emerging as a viable target for therapeutic interventions.

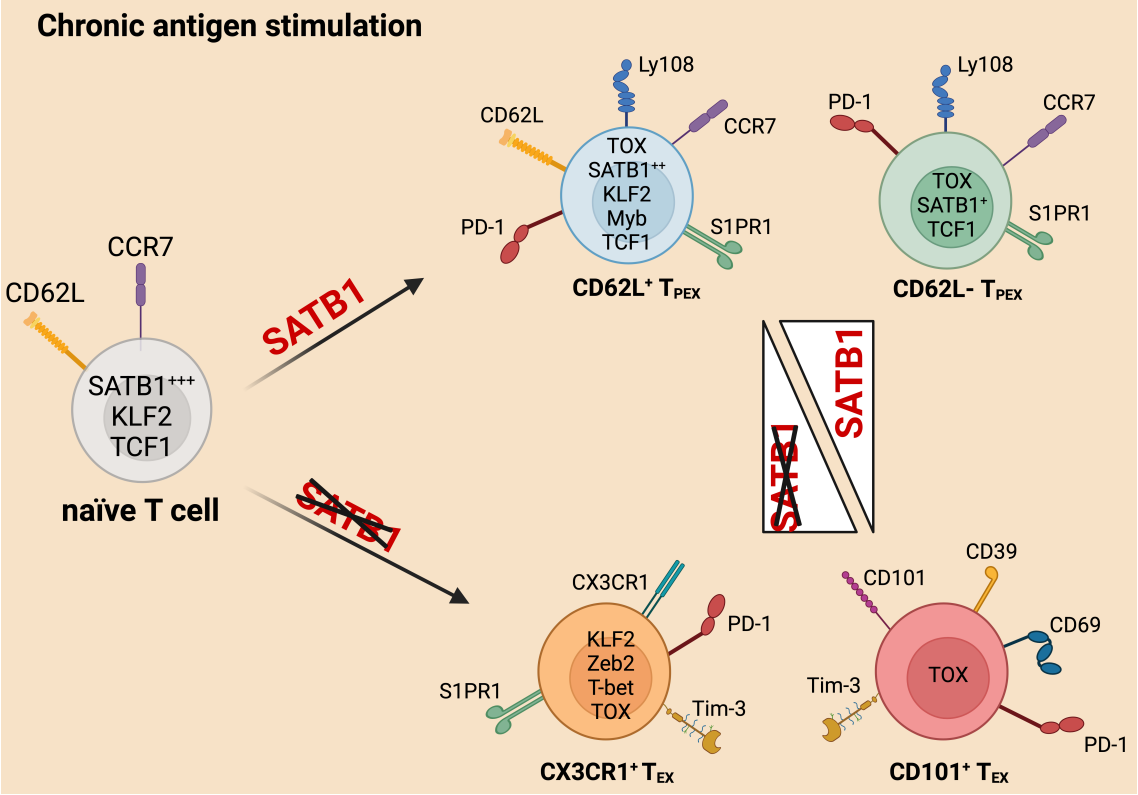

Figure 6.1: Proposed model of the functional role of SATB1 in chronic infection.
In chronic antigen stimulation SATB1 act like a balance between T_{PEX} and T_{EX}. High expression prevents T_{EX} differentiation, while loss of SATB1 facilitates T_{EX} differentiation.

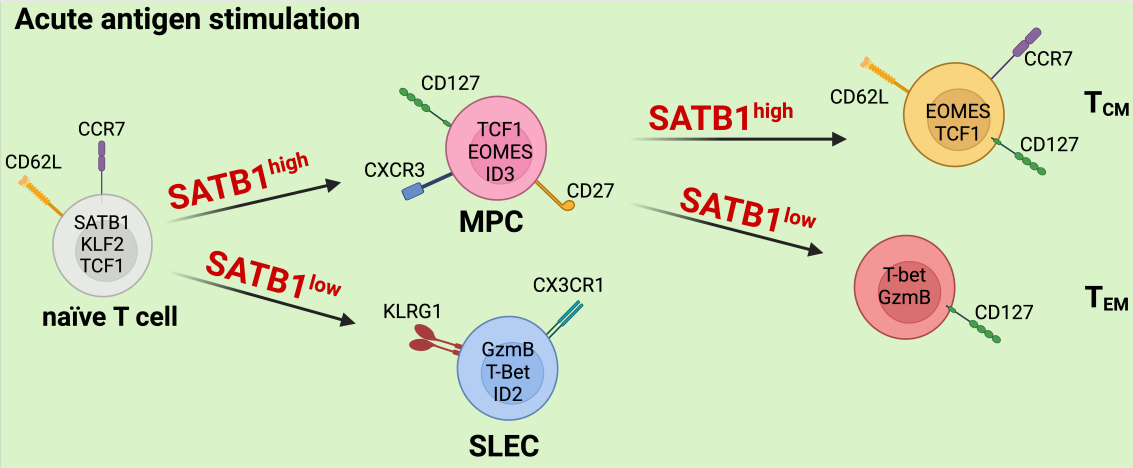

Figure 6.2 Proposed model of the functional role of SATB1 in acute infection.
In acute antigen stimulation, high levels of SATB1 promote differentiation of MPC and TCM while lower levels support differentiation of SLEC and TEM.

6.2 T cells markers associated with positioning in secondary lymphoid organs impact exhausted T cell differentiation

The differentiation of exhausted T cells is a dynamic process influenced by various intrinsic and extrinsic factors. Emerging evidence (Im *et al.*, 2016; He *et al.*, 2016; Leong *et al.*, 2016) suggests that environmental cues play a crucial role in directing the differentiation of T_{PEX} and T_{EX} cell subsets. However, the molecular mechanisms governing T_{PEX} and T_{EX} differentiation remain incompletely understood. T_{PEX} and T_{EX} cells exhibit distinct transcriptional profiles. For example T_{PEX} cells, particularly CD62L$^+$ T_{PEX} cells, express high levels of genes involved in lymphocyte trafficking, including CXCR5, CCR7, CD62L, S1PR1, and KLF2 (Tsui *et al.*, 2022). This suggests that migratory behaviour may be differentially regulated between T_{PEX} and T_{EX} cell subsets. Furthermore, our data indicates that the lymph node microenvironment preferentially supports the development of CD62L$^+$ T_{PEX} and CX3CR1$^+$ T_{EX} cells (unpublished data, Kallies), reinforcing the idea that distinct niches contribute to their fate. We therefore hypothesized that T_{PEX} and T_{EX} cells due to their differential migratory behaviour encounter different signalling cues that shape their differentiation and function. Accordingly, we explored the function of trafficking molecules expressed on T_{PEX} cells including CD62L, CCR7, and S1PR1 in the differentiation, maintenance and functionality of exhausted T cells in chronic viral infection. Our data show different roles of these trafficking molecules in shaping the tissue distribution of T_{PEX} and T_{EX} cells and provide critical insights on the spatial regulation of exhausted T cell differentiation. Indeed, we showed that CD62L, CCR7 and S1PR1 not only impacted the differentiation of T_{PEX} and T_{EX} cells but did so in an organ specific manner.

Deletion of the homing molecule CD62L resulted in decreased accumulation of CD8$^+$ T cells to secondary lymphoid organs such as the LN. In the absence of CD62L, we observed a more severe reduction of T_{PEX} cells in the LN compared to T_{EX} cells. Consistent with the idea, that T_{PEX} cells are required for the maintenance of T_{EX} cell output (Kallies *et al.*, 2020; Baessler and Vignali, 2024), we also observed reduced T_{EX} cell accumulation in the absence of CD62L.

Additionally, we found that the depletion of CD62L inhibited the formation of CX3CR1$^+$ T_{EX} cells more than the formation of CD101$^+$ T_{EX} cells. This implies, that differentiation of CX3CR1$^+$ T_{EX} cells is differentially regulated compared to CD101$^+$ T_{EX} cells and may exhibit differences in their dependency on CD62L-mediated function. Our results suggest that trafficking to the LN is an important factor for maintenance of T_{PEX} cells in chronic infection. We did not observe any changes in effector cytokine production or in expression of Ki-67 in CD62L-KO cells; however, GzmB production was decrease in CD62L-KO T_{EX} cells. This suggest that the intrinsic effector function and the proliferative capacity of exhausted T cells are largely independent to CD62L mediated LN entry. However, our study has limitations. Using this depletion of CD62L model, we were not able to fully characterize the effect that CD62L depletion had on the development of CD62L$^+$ T_{PEX} cells. We were unable to determine whether the depletion of CD62L expression in T_{PEX} cells induced the actual depletion of CD62L$^+$ T_{PEX} cells or merely the downregulation of CD62L itself. Further experiments are needed to fully assess the role of CD62L in exhausted T cells. Notably, in the LN, residual CD62L$^+$ T_{PEX} cells were observed, potentially representing CRISPR escapees. These cells may sustain TCF1 expression in the LN, which could explain why overall TCF1 levels were not reduced in this organ, in contrast to the spleen, where CD62L$^+$ T_{PEX} are less abundant

CCR7 is a critical mediator of T cell migration to and within secondary lymphoid organs to specific microenvironments, facilitating optimal cell priming and immune responses (Bjorkdahl *et al.*, 2003; Höpken *et al.*, 2004; Bromley *et al.*, 2005; Sharma *et al.*, 2015; Jung *et al.*, 2016). We therefore studied the role of CCR7 in T_{PEX} cell biology. Similar to CD62L, we observed that depletion of CCR7 reduced the accumulation of P14 cells in the spleen and LNs, suggesting that CCR7-mediated migration plays an important role in the expansion of exhausted T cells in chronic infection, similar to its role in acute infection, as previously published (Junt *et al.*, 2004). We observed that depletion of CCR7 resulted in fewer T_{PEX} including CD62L$^+$ T_{PEX} cells in the spleen and LNs, suggesting that cell migration to the T cell zone is particularly important for T_{PEX} differentiation.

This observation is in line with previous results showing that T_{PEX} cells preferentially reside in the T cell zone (Im *et al.*, 2016). In our data, LN CCR7-KO T_{PEX} cells but not spleen CCR7-KO T_{PEX} cells exhibited reduced expression of proteins expressed in T_{PEX}, such as TCF1 and Ly108, suggesting that the quality of T_{PEX} cells in the LN is dependent on CCR7. Thus, our work points to an essential role of entry to and migration towards the T cell area in maintaining the identity of T_{PEX}. Further, our data show that CX3CR1$^+$ T_{EX} cells were reduced in the spleen and LN upon CCR7 depletion, whereas CD101$^+$ T_{EX} cells were not affected. These data demonstrate a specific dependency of CX3CR1$^+$ T_{EX} cells on CCR7-mediated tissue migration. Our data further shows that production of GzmB and effector cytokines IFN-γ and TNF in T_{PEX} and T_{EX} cells in the spleen is not impacted by CCR7 depletion. This is in agreement with previous studies showing that CCR7-deficient effector CTLs (Unsoeld *et al.*, 2002) and memory T cells (Jung *et al.*, 2016) produce similar IFN-γ levels to Ctrl cells during acute viral infection. In line with our CD62L data, this indicates effector functions are not dependent on the ability of exhausted T cells to migrate to the T cell zone.

Our study, however, has not fully elucidated the mechanism by which CCR7 mediates exhausted T cell accumulation. A possible mechanism could be attributed to CCR7-mediated migration, resulting in exposure to specific environmental cues. Indeed, previous studies demonstrated that CCR7-deficient CD8$^+$ T cells alter their migration to and within different tissues, resulting in altered survival and maintenance of CCR7-deficient memory CD8$^+$ T cells (Jung *et al.*, 2016). More significantly, these studies suggested that this altered migration led to a cytokine dependency switch from IL-7 to IL-15 for homeostasis, indicating the possibility of separate niches that provide environmental cues to T cell (Jung *et al.*, 2016). Similarly, CCR7-directed migration could direct T_{PEX} subsets to specific localizations within tissues, exposing them to distinct microenvironmental signals, thus shaping their differentiation and survival. However, thus far, our data does not provide sufficient evidence to conclude that the mechanism is migration. This aspect requires further investigation through additional experiments using microscopy to study the localization and migration of T_{PEX} and T_{EX} cells.

The experiments with CD62L-KO and CCR7-KO P14 cells revealed a differential regulation of CX3CR1$^+$ T_{EX} cells and CD101$^+$ T_{EX} cells differentiation. Specifically, CX3CR1$^+$ T_{EX} cells were much more sensitive to the deletion of either CD62L or CCR7. This suggested that the formation of these cells was more reliant on cell migration to the LNs. This pointed to a possible origin of CX3CR1$^+$ T_{EX} cells in the LNs from where the cells might be exported into the periphery. To test this idea, we explored how deletion of the egress-mediating receptor S1PR1 affected the differentiation, maintenance and functionality of P14 cells during chronic viral infection. S1PR1 is well-known for its role in T cell egress from lymphoid organs and the thymus (Thangada *et al.*, 2010) but has also been implicated in homing to lymphoid organs (Bai *et al.*, 2007). The balance between the signals that encourage T cells to leave (via the S1PR1/S1P axis) and those that make them stay (via the CCR7/CCL21 axis) is critical (Pham *et al.*, 2008).

Deletion of S1PR1 showed that the accumulation of P14 cells in the spleen and LN per se was not dependent on S1PR1-mediated functions. We observed, however, that deletion of S1PR1 altered the distribution of T_{PEX} and T_{EX} cells. Indeed, we detected increased numbers of T_{PEX} cells in the spleen, while fewer resided in the LN. Conversely, fewer T_{EX} cells were found in the spleen and, unexpectedly, also in the LN. Notably, CX3CR1$^+$ T_{EX} cells in the spleen were most affected by depletion of S1PR1, with substantially decreased numbers per organ. This supports the idea that egress from the LN is required to seed the spleen, supporting our model, wherein CX3CR1$^+$ T_{EX} cells preferentially develop in the LN. A similar phenomenon was reported in a previous study which employed acute infection with vesicular stomatitis virus (VSV). Using a S1PR1-KO model, the authors demonstrated that the egress of effector CD8$^+$ T cells from the LN into the blood, and consequently migration to other tissues, was dependent on the function of S1PR1 (Benechet *et al.*, 2016). Although S1PR1-deficient cells could localise to the paracortex of the LN, followed by intranodal migration to positions adjacent to both cortical and medullary lymphatic sinuses, they failed to enter the sinuses to actually exit the LN (Benechet *et al.*, 2016).

Similar to the deletion of CCR7 and CD62L, depletion of S1PR1 did not impair the development of CD101$^+$ T_{EX} cells. This observation further supports the hypothesis that CX3CR1$^+$ T_{EX} cells and CD101$^+$ T_{EX} cells require distinct regulatory pathways for their differentiation.

In addition to the different distribution, we observed decreased expression of TCF1 and Ly108 in T_{PEX} cells and reduced expression of Tim-3 in T_{EX} cells in the absence of S1PR1 in the LN but not spleen. This indicates that S1PR1-mediated migration maintains the quality of T_{PEX} and T_{EX} cells in the LN. Our data also showed that the production of GzmB and effector cytokines IFN-γ and TNF in T_{PEX} and T_{EX} cells in the spleen was reduced in the S1PR1-KO cells. Additionally, their proliferation, as measured by Ki-67, in the spleen but not the LN was impaired by depletion of S1PR1. This indicates that effector function and proliferative capacity of exhausted T cells are partially dependent on S1PR1-mediated positioning. Mechanistically, S1PR1 dysfunction may disrupt positioning of T_{PEX} and T_{EX} cells within the spleen, resulting in different environmental signals, that influences their capacity to produce effector cytokines and to proliferate. In line with this idea, our data demonstrates that T_{EX} cells in the LN exhibit enhanced effector functions and higher cellular proliferation compared to those in the spleen (unpublished data, Kallies lab). S1PR1-mediated egress could be disrupted, resulting in an accumulation of functionally superior T_{EX} cells. To further elucidate these observations and gain a more comprehensive understanding, *in vivo* imaging and lineage-tracing experiments, combined with adoptive transfer studies, could provide valuable insights.

In agreement with the known interaction between CD69 and S1PR1, we found that CD69 was highly expressed on S1PR1-deficient compared to control CD8$^+$ T cells. Interestingly, the increase on a single cell level was particularly pronounced in the spleen, whereas in the LN CD69 levels remained largely unchanged, suggesting an additional organ-specific regulation of CD69 in response to S1PR1 depletion. Previous studies have shown that CD69 physically interacts with S1PR1, leading to S1PR1 degradation (Bankovich *et al.*, 2010; Laura K. Mackay *et al.*, 2015). Specific studies, however, directly demonstrating

that CD69 expression is upregulated in the absence of S1PR1 are limited. Indeed, existing literature primarily focuses on how CD69 regulates S1PR1 expression and function. Our data indicates, that CD69 expression is induced upon S1PR1 depletion. Notably, CD69 itself can induce changes in other cells. For instance, binding of CD69 on T cells to one of its ligands, galactolectin-1 (Gal-1) (Li *et al.*, 2024), which is expressed on DCs and macrophages (Cibrián and Sánchez-Madrid, 2017; Li *et al.*, 2024), triggers an anti-inflammatory mechanism promoting the production of cytokines, such as TGF-β and IL-35 (Adamson *et al.*, 2009; Li *et al.*, 2024), thus potentially altering the environmental signals that may impact $CD8^+$ T cells. The inability to distinguish between effects due to S1PR1 depletion and those due to increased CD69 expression presents a challenge. To investigate the impact of increased CD69 expression on exhausted T cells, further experiments should be conducted using CD69 knockout models generated with CRISPR-Cas9 as well as CD69 overexpression systems.

While our data show that deletion of CD62L, CCR7, or S1PR1 alters T_{PEX} and T_{EX} populations, it is important to acknowledge that some effects may reflect earlier roles of these molecules on naïve $CD8^+$ T cells. Impaired homing of naïve cells to the LN or altered initial priming could contribute to the observed reductions in T_{PEX} cells, which in turn may impact T_{EX} cell output. Dissecting naïve- versus T_{PEX}-intrinsic effects will require approaches that specifically target T_{PEX} cells after differentiation, such as inducible or conditional knockout models, or adoptive transfer of WT naïve cells into KO recipients. Incorporating such strategies would clarify the precise contribution of migratory molecules at different stages and strengthen our understanding of how T_{PEX} positioning influences T_{EX} cell differentiation.

Overall, our study provides evidence that disruption of migration and positioning alter T_{PEX} and T_{EX} populations, likely due to changes in their subsequent exposure to different signalling cues. These environmental cues may include variations in antigen exposure, cytokines, or co-stimulatory interactions. Given

that CD62L, CCR7 and S1PR1 are typically not expressed in T_{EX} cells, our findings support a model wherein the expression and function of migratory genes in T_{PEX} cells affect the generation of T_{EX} cells. Notably, CX3CR1$^+$ T cell formation appears to be more reliant on origin in the lymph nodes overall suggesting that CX3CR1$^+$ T_{EX} cells and CD101$^+$ T_{EX} cells exhibit distinct regulation of differentiation. As CD62L$^+$ T_{PEX} cells express higher levels of genes involved in lymph node trafficking, including CCR7, CD62L and S1PR1 (Tsui et al., 2022), and disruption of these genes primarily affected the CX3CR1$^+$ T_{EX} cells, we hypothesize that CD62L$^+$ T_{PEX} cells, residing in LNs, are the progenitors of CX3CR1$^+$ T_{EX} cells. To further enhance our study, the localization and migration of T_{PEX} and T_{EX} cells should be assessed. A possible approach would be to examine CCR7-mediated distribution of T_{PEX} and T_{EX} within the spleen and LN utilising microscopy techniques.

6.3 Molecular regulation of CD62L$^+$ T_{PEX}/CX3CR1$^+$ T_{EX} lineage differentiation is regulated by the transcription factor KLF2

Immunotherapy has demonstrated significant success in the treatment of cancer, often presenting fewer side effects compared to conventional treatments such as chemotherapy (Ling *et al.*, 2022). Nevertheless, its efficacy varies based on the type of cancer and individual patient factors (Li *et al.*, 2025). Recent advancements in the field have shown that central role of T_{PEX} cells in the response to immune checkpoint blockade. T_{PEX} cells, particularly CD62L$^+$ T_{PEX} cells respond with a proliferative burst upon checkpoint inhibition, resulting in the differentiation of CX3CR1$^+$ effector-like T_{EX} cells that contribute anti-tumor immunity (Siddiqui *et al.*, 2019; Miller *et al.*, 2019; Hudson *et al.*, 2019; Fang *et al.*, 2022). Despite these advances, the precise mechanisms governing T_{PEX} differentiation and the cellular trajectories leading to distinct T_{EX} subsets remain incompletely understood. Current research has proposed two competing models: a bifurcation model and a linear progression model. The bifurcation model suggests that T_{PEX} cells give rise to either CX3CR1$^+$ effector-like T_{EX} cells or CD101$^+$ terminally exhausted T_{EX} cells (Zander *et al.*, 2019; Tsui *et al.*, 2022; Giles *et al.*, 2022; Daniel *et al.*, 2022; Kasmani *et al.*, 2023). In contrast, the linear progression model proposes that T_{EX} cells differentiate through a series of intermediate states in a stepwise manner (Hudson *et al.*, 2019; Beltra *et al.*, 2020). Our recent single-cell RNA sequencing data have indicated two distinct lineages originating from TCF1$^+$ T_{PEX} cells and progressing into either CX3CR1$^+$ or CD101$^+$ T_{EX} subsets (Unpublished data, Kallies lab). This finding prompted us to search for molecular regulators driving these differentiation trajectories and better understand T_{PEX} and T_{EX} fate decisions. Understanding these mechanisms could potentially inform novel strategies to modulate T cell exhaustion in various disease settings, ultimately contributing to the development of more effective immunotherapies. Among potential regulators, the transcription factor KLF2 emerged as a promising candidate. KLF2 is expressed in T_{PEX} cells, with higher expression observed in CD62L$^+$ T_{PEX} cells and CX3CR1$^+$ T_{EX} cells (Unpublished data, Kallies). We thus hypothesized that KLF2 plays a defining role in directing the differentiation of the CX3CR1$^+$ T_{EX} lineage. Indeed, the data presented in this

chapter reveal KLF2 to be a critical regulator of fate decision in exhausted T cells. KLF2 was required for the CD62L$^+$ T_{PEX}/CX3CR1$^+$ T_{EX} lineage, strongly supporting the bifurcation model.

By using the CRISPR-Cas9 approach, we depleted KLF2 in P14 cells. Our data provide significant insights into the role of KLF2 in T cell fate decisions within exhausted T cells during chronic viral infection. The depletion of KLF2 resulted in reduced differentiation of CD62L$^+$ T_{PEX} and CX3CR1$^+$ T_{EX} cells. The CD62L$^-$ T_{PEX} and CD101$^+$ T_{EX} populations were less affected by the absence of KLF2, supporting and extending the bifurcated model. This is similar to previous findings, that have shown that KLF2 depletion resulted in reduced differentiation of CD62L$^+$CX3CR1$^-$ CAR-T cells and CD62L$^-$CX3CR1$^+$ CAR-T cells (Z. Zhu *et al.*, 2024). Indeed, based on this data we propose a model wherein CD62L$^+$ T_{PEX} cells give rise to CX3CR1$^+$ T_{EX} cells in a KLF2 dependent manner. In contrast, CD62L$^-$ T_{PEX} cells differentiate into CD101$^+$ T_{EX} cells in a KLF2 independent manner. Previous studies have demonstrated that KLF2 controls differentiation processes and CD4$^+$ T cell fate decisions in the thymus. Low expression levels of KLF2 are associated with differentiation into regulatory T cells or CD8$^+$ T cells, whereas T cells expressing high levels of KLF2 typically differentiate into classical CD4$^+$ T helper cells (Pabbisetty *et al.*, 2014). Similar differentiation decisions may occur in T_{PEX} cells, which may differentiate into CX3CR1$^+$ T_{EX} cells due to high KLF2 expression or into CD101$^+$ T_{EX} cells due to low KLF2 expression levels. Our data indicate that KLF2-dependent T cells exhibit a circulating expression profile characterized by high levels of migratory genes such as *Ccr7*, *Sell*, *S1pr1*, and *Ly6c2*. Conversely, KLF2-independent T cells display a tissue-resident profile associated with markers such as *Cd101* and *Itga1* (CD49a). This pattern is similar to that observed in acute infections, where KLF2 controls whether memory T cells will circulate or remain in the tissue (Skon *et al.*, 2013). Overall, this suggests that the same genetic program may be operative in exhausted T cells during chronic infection.

Further, the depletion of KLF2 led to the upregulation of key exhaustion proteins, including PD-1 and TOX. This observation aligns with previously published data indicating increased expression of TOX and PD-1 in KLF2-deficient CAR T cells (Z. Zhu *et al.*, 2024), suggesting that KLF2 negatively regulates the expression of TOX and PD-1. This is further validated by recent findings that identified KLF2 as a suppressor of $CD8^+$ T cell exhaustion during acute LCMV infection, with KLF2-deficient cells exhibiting elevated levels of PD-1 and TOX in the context of acute LCMV infection (Fagerberg *et al.*, 2025). Additionally, the depletion of KLF2 resulted in the upregulation of the activation protein CD69. As discussed in the previous chapter, this is likely attributable to the downregulation of S1PR1, as KLF2 upregulates expression of S1PR1 (Matloubian *et al.*, 2004). Furthermore, an upregulation of CXCR3 was observed. This finding is consistent with previous data demonstrating that KLF2 expression inhibits CXCR3 in immune-activated $CD8^+$ T cells via a cell-non-autonomous pathway (Weinreich et al., 2009; Preston et al., 2013). Interestingly, some of these alterations are present even before infection. This suggests that KLF2 influences baseline T cell phenotypes, not just infection-induced responses.

Upon the depletion of KLF2, P14 cells were observed to accumulate in the spleen while being nearly absent in the LN. This observation is likely a result of the well-described role of KLF2 in $CD8^+$ T cell migration. KLF2 positively regulates expression of CD62L (Rosen, 2004), CCR7 (Anderson *et al.*, 2014) and S1PR1 (Matloubian *et al.*, 2004), and all three migratory molecules that have been shown to facilitate the entering of $CD8^+$ T cells in the LN (Masopust and Schenkel, 2013). The depletion of KLF2 in P14 cells thus leads to impaired migration to the LN. However, since migration to the spleen has been shown to be independent of these migration molecules, KLF2-deficient cells accumulate in the spleen. Furthermore, our data show high frequencies of KLF2-deficient cells in the blood and liver, indicating that egress from the spleen is KLF2-independent. This further suggests that the depletion of KLF2 may enhance the proliferative capacity of exhausted T cells, as indicated by our *in vitro* proliferation assay. Indeed, *in vitro* studies of IL-2-dependent human T cell lymphoma cells (Kit225) have shown that

KLF2 restricts T cell proliferation by suppressing the c-myc protein and the cell cycle regulator human telomerase reverse transcriptase (hTERT), while activating the cell cycle inhibitor p21 (Mizuguchi *et al.*, 2021). However, whether the accumulation of P14 cells is due to insufficient migration to the LN or an acceleration of proliferation requires further investigation. Additionally, the possibility that KLF2-deficient cells may undergo increased cell death following division, which could also contribute to the reduced prevalence of these cells at certain time points it cannot be excluded. Proper *in vivo* assessment of proliferation and cell survival, such as via CTV or BrdU/EdU incorporation, will be required to clarify this.

Notably, we observed increased capacity to produce the cytokines IFN-γ and TNF in KLF2-KO cells. This is in line with recently published data on KLF2 depletion in acute LCMV infection, which demonstrated that KLF2 depletion in P14 cells enhanced the effector capacity and increased generation of polyfunctional IFN-γ/TNF co-producing cells (Fagerberg *et al.*, 2025). Other studies have reported spontaneous of IL-4 production in KLF2 deficient naïve $CD8^+$ T cells, leading to upregulation of CXCR3 (Weinreich *et al.*, 2009). This indicates that effector function and cytokine production of $CD8^+$ T cells is negatively regulated by KLF2.

Furthermore, our study explored the potential impact of environmental factors on KLF2 expression and the differentiation fate of $CD62L^+$ T_{PEX}/$CX3CR1^+$ T_{EX} cells. Our data, in conjunction with those of other researchers, indicate that TCR signalling downregulates KLF2 (Preston *et al.*, 2013). Strong TCR signalling may thus downregulate KLF2, leading to the differentiation of KLF2-independent lineages, whereas weak signalling may result in the opposite effect. This would align with the notion that TCR signalling is a primary driver of T cell exhaustion (Baessler and Vignali, 2024). However, whether differential TCR engagement controls KLF2 expression in exhausted T cells needs to be tested. In addition to TCR signalling, cytokines may influence KLF2 expression. Indeed, it was demonstrated before that specific cytokines plus continuous TCR signalling promote KLF2 degradation (Takada *et al.*, 2011). Low levels of cytokines,

including IL-2, IL-7, and IL-15, allow for reactivation of KLF2 expression. Conversely, IL-4, IL-12, and low levels of IL-2 maintain effector T cells by inhibiting KLF2 re-expression (Takada *et al.*, 2011). Other research has shown that type I IFN and Tgfβ, alone or in combination with IL-33, can disrupt KLF2 expression in $CD8^+$ T cells (Skon *et al.*, 2013). Although these studies were conducted in vitro, they strongly suggest that precise cytokine regulation influences KLF2 expression. Our *in vitro* studies indicate that both IL-15 and Tgfβ can promote downregulation of KLF2 expression. Notably, Tgfβ has been associated with T cell exhaustion (Gabriel *et al.*, 2021; Xie *et al.*, 2022; Hu *et al.*, 2022; Saadey *et al.*, 2023) and other cytokines such as IL-2 have also been linked to the induction of exhaustion (Y. Liu *et al.*, 2021). These environmental cues could be dependent on both the tissue and the type of infection. For example, APCs have been shown to be different in chronic and acute infections. For instance, comparisons of dendritic cells from chronic and acute infections suggest a distinct immunogenic phenotype, with chronic infection characterized by decreased CD8 expression and increased expression of PD-L1, B7-H4, Tgfβ, and IL-10 (Yoo *et al.*, 2023). This could result in distinct environmental cues influencing KLF2 expression. Further we have found that in the lymph node environment, migratory dendritic cells enhanced the fitness of exhausted T cells, further suggesting that tissue-specific environments can influence KLF2-dependent T cell differentiation (Unpublished data, Kallies lab). To comprehensively understand which cytokines in specific tissues promote or inhibit the expression of KLF2 requires further work.

Finally, we explored potential therapeutic strategies to target the $CD62L^+$ T_{PEX}/$CX3CR1^+$ T_{EX} differentiation axis. In line with previous studies from the Kallies lab (Tsui *et al.*, 2022), the loss of the $CD62L^+$ T_{PEX} cells led to reduced responses to anti-PD-L1 treatments. We also investigated ways to boost the differentiation of $CD62L^+$ T_{PEX}/$CX3CR1^+$ T_{EX} using statins, which are known to upregulate KLF2 expression (Tuomisto *et al.*, 2008; Bu *et al.*, 2010). Indeed, our *in vitro* data demonstrates, that KLF2 expression is upregulated by the statin Simvastatin. Our experiments showed that Fluvastatin treatment reduced CD69

expression, suggesting increased KLF2 levels. Furthermore, $CD8^+$ T cells in Fluvastatin treated mice exhibited increased differentiation of $CD62L^+$ T_{PEX} population and an increase in $CX3CR1^+$ T_{EX} cells highlighting the therapeutic potential of statins in enhancing T cell function during chronic infection and cancer. Notably, statins have been considered as potential anticancer agents since 1990 (Matusewicz *et al.*, 2015), and studies have shown improved survival rates in patients taking statins before cancer diagnosis in pancreatic (Hamada *et al.*, 2018), breast (Wu *et al.*, 2015), prostate (Tan *et al.*, 2016), endometrial (Feng *et al.*, 2016), gastric (Spence *et al.*, 2019), lung (Xing *et al.*, 2015), cervical (Song *et al.*, 2017), and kidney (Nayan *et al.*, 2017) cancers, as well as in myeloma (Sanfilippo *et al.*, 2016). Lee *et al.*, 2018 showed enhanced pro-apoptotic activity of Venetoclax in combination with simvastatin. Similarly, statins in combination with EGFR-TKIs and chemotherapy in non-small cell lung cancer enhanced the therapeutic effect and increased patient survival (Hung *et al.*, 2017). The potential use in CAR-T cell therapy was demonstrated in a study of patients suffering from aggressive B-cell Lymphoma. Patients exposed to statins while receiving CD19-CAR-T cell therapy exhibited improved progression-free survival and median overall survival with similar toxicity rates (Adroja *et al.*, 2024). Our data, which demonstrate that statins can induce upregulation of KLF2 in $CD8^+$ T cells and result increase in $CD62L^+$ T_{PEX}/$CX3CR1^+$ T_{EX}, indicate a potential mechanism for these observations and suggest that statins have promising therapeutic potential in cancer treatment. However, their low bioavailability and potential toxicity at high doses remain a challenge (Matusewicz *et al.*, 2020). Nonetheless, combining statins with other therapies, such as immune checkpoint blockade (ICB) or CAR-T cell therapy, could enhance their efficacy. Further research, however, is necessary to determine the optimal timing and methodology for statin use.

To further enhance our understanding whether the accumulation of P14 cells is due to insufficient migration to the LN or an acceleration of proliferation *in vivo* proliferation assays with CTV or BRDU/EDU could be conducted, to provide additional insights into the role of KLF2 in regulating proliferative capacity. Further the understanding, whether differential TCR engagement controls KLF2

expression in exhausted T cells needs to be tested. For instance, the expression of KLF2 in T_{PEX} cells following TCR engagement could be analysed *ex vivo*. Additionally, employing inducible inhibition of TCR signalling could be a viable approach. Small molecule inhibitors or inducible genetic knockdown of key TCR signalling proteins, such as ZAP-70 or LAT, could be utilized to better understand the relationship between TCR engagement and KLF2 downregulation in exhausted T cells. To comprehensively understand which cytokines in specific tissues promote or inhibit the expression of KLF2, profiling cytokines in the LN vs spleen using Luminex or ELISA approaches, and subsequently assessing their impact on KLF2 expression, would provide additional insights. Lastly, the optimal timing and methodology for statin use has to be determined. One potential strategy involves combining statins with commonly employed ICB treatments, such as anti-PD-L1/CTLA4, across cancer models. Another intriguing approach is the ex vivo treatment of CAR-T cells prior to transfusion.

In summary, we identify KLF2 as a pivotal regulator of T cell exhaustion, with significant implications for enhancing immunotherapy in cancer and chronic infections. Our findings support a bifurcation model wherein CD62L$^+$ T_{PEX} cells differentiate into CX3CR1$^+$ T_{EX} in KLF2 dependent manner, while CD62L$^-$ T_{PEX} cells give rise to CD101$^+$ T_{EX} in a KLF2 independent pathway (Figure 6.3). Furthermore, statins have been identified as potential therapeutic agents to anti-tumour therapy by inducing the upregulation of KLF2.

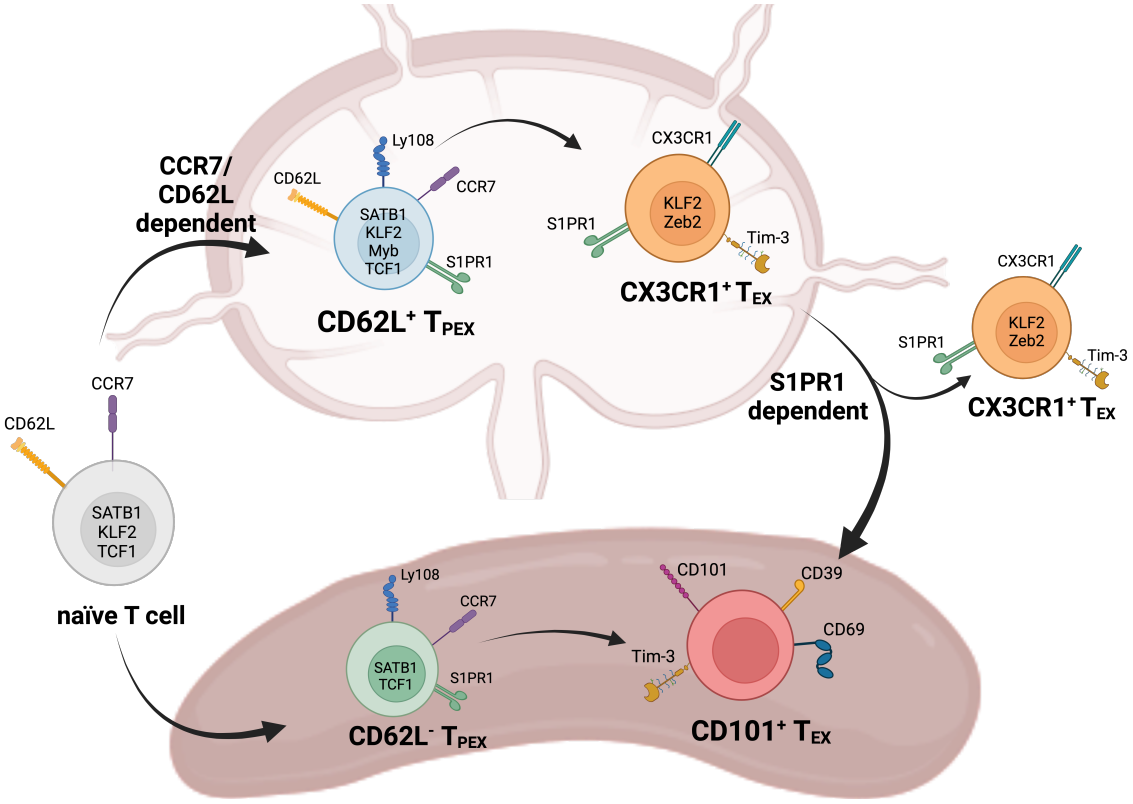

Figure 6.3: Proposed model of KLF2-mediated differentiation of CD62L⁺ T_{PEX}/CX3CR1⁺ T_{EX} cells in the LN and spleen.
Proposed bifurcation model wherein CD62L⁺ T_{PEX} cells differentiate into CX3CR1⁺ T_{EX} while CD62L⁻ T_{PEX} cells give rise to CD101⁺ T_{EX}. KLF2 is a crucial regulator of the CD62L⁺ T_{PEX}/CX3CR1⁺ T_{EX} lineage. The LN environment promotes the differentiation of the CD62L⁺ T_{PEX}/CX3CR1⁺ T_{EX} lineage, while the pleen promotes development of CD62L⁻ T_{PEX}/CD101⁺ T_{EX} cells. Migration proteins CCR7 and CD62L mediate the entry of T cell in the LN while CX3CR1⁺ T_{EX} cells utilize S1PR1to egress from the LN.

6.4 Concluding remarks

$CD8^+$ T cells play a crucial role in the immune response to chronic infection, forming a precursor-progeny relationship that enables the differentiation of effector cells while maintaining the self-renewal capacity of antigen-specific T cells. This balance is essential for sustaining long-term immune protection. However, the molecular pathways that govern precursor cell development, maintenance, and differentiation toward effector fate remain incompletely understood. Elucidating these regulatory mechanisms is critical for advancing immunotherapeutic strategies that can enhance T cell function and durability.

In this thesis, we investigated key molecular regulators that shape the differentiation and functionality of $CD8^+$ T cells in chronic infection. Through a combination of genetic perturbation models, transcriptomic and epigenetic profiling, and functional assays, we identified pivotal factors that dictate the quality of precursor cells and their transition into effector and terminally exhausted states. Our findings provide novel insights into the mechanisms underlying T cell exhaustion and offer potential avenues for therapeutic intervention.

We identified SATB1 as a key regulator of $CD8^+$ T cell differentiation, influencing the balance between T_{PEX} and T_{EX} cells. SATB1 deficiency in chronic infection led to an increased differentiation of T_{EX} cells, while in acute infection, it skewed $CD8^+$ T cells toward a T_{EM} rather than a T_{CM} phenotype. Furthermore, STAB1 was required for maintaining cytokine expression and regulated expression of PD-1 in a context specific manner, suggesting a role in exhaustion dynamics. These findings indicate that modulating SATB1 expression could be leveraged to improve the efficacy of CAR-T therapies.

Furthermore, we examined the role of migratory molecules, namely CD62L, CCR7 and S1PR1, in shaping the differentiation and fate of T_{PEX} and T_{EX} cells during chronic infection. Our results suggest that T_{PEX} cells rely on lymph node homing and specific microenvironmental cues to sustain their identity and efficiently generate T_{EX} cells. Disruption of these molecules primarily affected

CX3CR1$^+$ T_{EX} cells, suggesting differential regulatory mechanisms compared to CD101$^+$ T_{EX} cells. These findings underscore the importance of spatial organization in the regulation of exhausted T cell differentiation and provide a foundation for future studies on optimizing T cell localization for enhanced immunotherapy.

Finally, our study establishes KLF2 as a central regulator of T cell exhaustion, controlling the development of CD62L$^+$ T_{PEX} cells and their differentiation into CX3CR1$^+$ T_{EX} cells. These findings lend strong support for the bifurcation model of T_{PEX} differentiation, with KLF2 playing a critical role in fate decisions. Loss of KLF2 was associated with enhanced effector function but also an upregulation of exhaustion markers such as PD-1 and TOX, highlighting its dual role in balancing functionality and exhaustion. Importantly, we demonstrated that statins could upregulate KLF2 expression, suggesting a novel strategy for enhancing immunotherapies by modulating the T_{PEX}/T_{EX} lineage dynamics.

Together, the findings of this thesis contribute to a more comprehensive understanding of the molecular determinants governing CD8$^+$ T cell differentiation and exhaustion. By identifying SATB1, migratory molecules, and KLF2 as key regulators, we provide mechanistic insights into the pathways that sustain precursor cells and drive effector fate. These insights have significant implications for the development of targeted immunotherapies aimed at reinvigorating exhausted T cells in chronic infections and cancer. Future studies should explore the translational potential of these findings, with a focus on developing pharmacological and genetic interventions to enhance CD8$^+$ T cell responses and improve patient outcomes.

References

Abbas, A.K. *et al.* (2018) 'Revisiting IL-2: Biology and Therapeutic Prospects'. *Science Immunology*, 3(25), p. eaat1482. DOI: 10.1126/sciimmunol.aat1482.

Abdel-Hakeem, M.S. *et al.* (2021) 'Epigenetic Scarring of Exhausted T Cells Hinders Memory Differentiation upon Eliminating Chronic Antigenic Stimulation'. *Nature Immunology*, 22(8), pp. 1008–1019. DOI: 10.1038/s41590-021-00975-5.

Adamson, A.S. *et al.* (2009) 'The Current STATus of Lymphocyte Signaling: New Roles for Old Players'. *Current Opinion in Immunology*, 21(2), pp. 161–166. DOI: 10.1016/j.coi.2009.03.013.

Adroja, S. *et al.* (2024) 'Statins May Improve Outcomes and Toxicities in Patients Undergoing CD19-Specific CAR T-Cell Therapy for Aggressive B-Cell Lymphomas'. *Blood*, 144(Supplement 1), pp. 5131–5131. DOI: 10.1182/blood-2024-211656.

Agata, Y. *et al.* (1996) 'Expression of the PD-1 Antigen on the Surface of Stimulated Mouse T and B Lymphocytes'. *International Immunology*, 8(5), pp. 765–772. DOI: 10.1093/intimm/8.5.765.

Agrelo, R. *et al.* (2009) 'SATB1 Defines the Developmental Context for Gene Silencing by Xist in Lymphoma and Embryonic Cells'. *Developmental Cell*, 16(4), pp. 507–516. DOI: 10.1016/j.devcel.2009.03.006.

Ahlfors, H. *et al.* (2010) 'SATB1 Dictates Expression of Multiple Genes Including IL-5 Involved in Human T Helper Cell Differentiation'. *Blood*, 116(9), pp. 1443–1453. DOI: 10.1182/blood-2009-11-252205.

Akiba, Y. *et al.* (2018) 'Special AT-Rich Sequence Binding Protein 1 Is Required for Maintenance of T Cell Receptor Responsiveness and Development of Experimental Autoimmune Encephalomyelitis: EAE Development Requires SATB1'. *Microbiology and Immunology*, 62(4), pp. 255–268. DOI: 10.1111/1348-0421.12579.

Alexopoulou, L. *et al.* (2001) 'Recognition of Double-Stranded RNA and Activation of NF-κB by Toll-like Receptor 3'. *Nature*, 413(6857), pp. 732–738. DOI: 10.1038/35099560.

Alfei, F. *et al.* (2019) 'TOX Reinforces the Phenotype and Longevity of Exhausted T Cells in Chronic Viral Infection'. *Nature*, 571(7764), pp. 265–269. DOI: 10.1038/s41586-019-1326-9.

Aliahmad, P., Seksenyan, A. and Kaye, J. (2012) 'The Many Roles of TOX in the Immune System'. *Current Opinion in Immunology*, 24(2), pp. 173–177. DOI: 10.1016/j.coi.2011.12.001.

Allende, M.L. *et al.* (2004) 'Expression of the Sphingosine 1-Phosphate Receptor, S1P1, on T-Cells Controls Thymic Emigration'. *Journal of Biological Chemistry*, 279(15), pp. 15396–15401. DOI: 10.1074/jbc.M314291200.

Alvarez, J.D. *et al.* (2000) 'The MAR-Binding Protein SATB1 Orchestrates Temporal and Spatial Expression of Multiple Genes during T-Cell Development'. *Genes & Development*, 14(5), pp. 521–535. DOI: 10.1101/gad.14.5.521.

Ammerman, N.C., Beier-Sexton, M. and Azad, A.F. (2008) 'Growth and Maintenance of Vero Cell Lines'. *Current Protocols in Microbiology*, Appendix 4, p. Appendix 4E. DOI: 10.1002/9780471729259.mca04es11.

Anaya, J.-M. *et al.* (eds.) (2013) *Autoimmunity: From Bench to Bedside*. first edition. Bogota, Colombia: Center for Autoimmune Diseases Research, School of Medicine and Health Sciences, El Rosario University.

Anderson, K.P. *et al.* (1995) 'Isolation of a Gene Encoding a Functional Zinc Finger Protein Homologous to Erythroid Krüppel-Like Factor: Identification of a New Multigene Family'. *Molecular and Cellular Biology*, 15(11), pp. 5957–5965. DOI: 10.1128/MCB.15.11.5957.

Anderson, L.R., Owens, T.W. and Naylor, M.J. (2014) 'Structural and Mechanical Functions of Integrins'. *Biophysical Reviews*, 6(2), pp. 203–213. DOI: 10.1007/s12551-013-0124-0.

Andrews, L.P., Yano, H. and Vignali, D.A.A. (2019) 'Inhibitory Receptors and Ligands beyond PD-

1, PD-L1 and CTLA-4: Breakthroughs or Backups'. *Nature Immunology*, 20(11), pp. 1425–1434. DOI: 10.1038/s41590-019-0512-0.

Ariotti, S. *et al.* (2014) 'Skin-Resident Memory CD8$^+$ T Cells Trigger a State of Tissue-Wide Pathogen Alert'. *Science*, 346(6205), pp. 101–105. DOI: 10.1126/science.1254803.

Austin, S. and St-Pierre, J. (2012) 'PGC1α and Mitochondrial Metabolism – Emerging Concepts and Relevance in Ageing and Neurodegenerative Disorders'. *Journal of Cell Science*, 125(21), pp. 4963–4971. DOI: 10.1242/jcs.113662.

Badovinac, V.P. *et al.* (2005) 'Accelerated CD8+ T-Cell Memory and Prime-Boost Response after Dendritic-Cell Vaccination'. *Nature Medicine*, 11(7), pp. 748–756. DOI: 10.1038/nm1257.

Badovinac, V.P., Porter, B.B. and Harty, J.T. (2004) 'CD8+ T Cell Contraction Is Controlled by Early Inflammation'. *Nature Immunology*, 5(8), pp. 809–817. DOI: 10.1038/ni1098.

Baessler, A. and Vignali, D.A.A. (2024) 'T Cell Exhaustion'. *Annual Review of Immunology*, 42(1), pp. 179–206. DOI: 10.1146/annurev-immunol-090222-110914.

Bai, A. *et al.* (2007) 'Krüppel-Like Factor 2 Controls T Cell Trafficking by Activating L-Selectin (CD62L) and Sphingosine-1-Phosphate Receptor 1 Transcription'. *The Journal of Immunology*, 178(12), pp. 7632–7639. DOI: 10.4049/jimmunol.178.12.7632.

Bajénoff, M., Glaichenhaus, N. and Germain, R.N. (2008) 'Fibroblastic Reticular Cells Guide T Lymphocyte Entry into and Migration within the Splenic T Cell Zone'. *The Journal of Immunology*, 181(6), pp. 3947–3954. DOI: 10.4049/jimmunol.181.6.3947.

Balamotis, M.A. *et al.* (2012) 'Satb1 Ablation Alters Temporal Expression of Immediate Early Genes and Reduces Dendritic Spine Density during Postnatal Brain Development'. *Molecular and Cellular Biology*, 32(2), pp. 333–347. DOI: 10.1128/MCB.05917-11.

Ball, A.R. and Yokomori, K. (2011) 'Damage Site Chromatin: Open or Closed?' *Current Opinion in Cell Biology*, 23(3), pp. 277–283. DOI: 10.1016/j.ceb.2011.03.012.

Banerjee, A. *et al.* (2010) 'Cutting Edge: The Transcription Factor Eomesodermin Enables CD8+ T Cells To Compete for the Memory Cell Niche'. *The Journal of Immunology*, 185(9), pp. 4988–4992. DOI: 10.4049/jimmunol.1002042.

Bankovich, A.J., Shiow, L.R. and Cyster, J.G. (2010) 'CD69 Suppresses Sphingosine 1-Phosophate Receptor-1 (S1P1) Function through Interaction with Membrane Helix 4'. *Journal of Biological Chemistry*, 285(29), pp. 22328–22337. DOI: 10.1074/jbc.M110.123299.

Barber, D.L. *et al.* (2006) 'Restoring Function in Exhausted CD8 T Cells during Chronic Viral Infection'. *Nature*, 439(7077), pp. 682–687. DOI: 10.1038/nature04444.

Beltra, J.-C. *et al.* (2020) 'Developmental Relationships of Four Exhausted CD8+ T Cell Subsets Reveals Underlying Transcriptional and Epigenetic Landscape Control Mechanisms'. *Immunity*, 52(5), pp. 825-841.e8. DOI: 10.1016/j.immuni.2020.04.014.

Benechet, A.P. *et al.* (2016) 'T Cell-Intrinsic S1PR1 Regulates Endogenous Effector T-Cell Egress Dynamics from Lymph Nodes during Infection'. *Proceedings of the National Academy of Sciences*, 113(8), pp. 2182–2187. DOI: 10.1073/pnas.1516485113.

Bengsch, B. *et al.* (2016) 'Bioenergetic Insufficiencies Due to Metabolic Alterations Regulated by the Inhibitory Receptor PD-1 Are an Early Driver of CD8 + T Cell Exhaustion'. *Immunity*, 45(2), pp. 358–373. DOI: 10.1016/j.immuni.2016.07.008.

Bergsbaken, T., Bevan, M.J. and Fink, P.J. (2017) 'Local Inflammatory Cues Regulate Differentiation and Persistence of CD8 + Tissue-Resident Memory T Cells'. *Cell Reports*, 19(1), pp. 114–124. DOI: 10.1016/j.celrep.2017.03.031.

Berns, K., Hijmans, E.M. and Bernards, R. (1997) 'Repression of C-Myc Responsive Genes in Cycling Cells Causes G1 Arrest through Reduction of Cyclin E/CDK2 Kinase Activity'. *Oncogene*, 15(11), pp. 1347–1356. DOI: 10.1038/sj.onc.1201280.

Beyer, M. *et al.* (2011) 'Repression of the Genome Organizer SATB1 in Regulatory T Cells Is

Required for Suppressive Function and Inhibition of Effector Differentiation'. *Nature Immunology*, 12(9), pp. 898–907. DOI: 10.1038/ni.2084.

Bjorkdahl, O. *et al.* (2003) 'Characterization of CC-chemokine Receptor 7 Expression on Murine T Cells in Lymphoid Tissues'. *Immunology*, 110(2), pp. 170–179. DOI: 10.1046/j.1365-2567.2003.01727.x.

Blackburn, S.D. *et al.* (2009) 'Coregulation of CD8+ T Cell Exhaustion by Multiple Inhibitory Receptors during Chronic Viral Infection'. *Nature Immunology*, 10(1), pp. 29–37. DOI: 10.1038/ni.1679.

Blackburn, S.D. *et al.* (2008) 'Selective Expansion of a Subset of Exhausted CD8 T Cells by αPD-L1 Blockade'. *Proceedings of the National Academy of Sciences*, 105(39), pp. 15016–15021. DOI: 10.1073/pnas.0801497105.

Blanchard, L. and Girard, J.-P. (2021) 'High Endothelial Venules (HEVs) in Immunity, Inflammation and Cancer'. *Angiogenesis*, 24(4), pp. 719–753. DOI: 10.1007/s10456-021-09792-8.

Blank, C.U. *et al.* (2019) 'Defining "T Cell Exhaustion"'. *Nature Reviews Immunology*, 19(11), pp. 665–674. DOI: 10.1038/s41577-019-0221-9.

Bonilla, F.A. and Oettgen, H.C. (2010) 'Adaptive Immunity'. *Journal of Allergy and Clinical Immunology*, 125(2), pp. S33–S40. DOI: 10.1016/j.jaci.2009.09.017.

Bromley, S.K., Thomas, S.Y. and Luster, A.D. (2005) 'Chemokine Receptor CCR7 Guides T Cell Exit from Peripheral Tissues and Entry into Afferent Lymphatics'. *Nature Immunology*, 6(9), pp. 895–901. DOI: 10.1038/ni1240.

Bronte, V. and Pittet, M.J. (2013) 'The Spleen in Local and Systemic Regulation of Immunity'. *Immunity*, 39(5), pp. 806–818. DOI: 10.1016/j.immuni.2013.10.010.

Brooks, D.G. *et al.* (2008) 'IL-10 and PD-L1 Operate through Distinct Pathways to Suppress T-Cell Activity during Persistent Viral Infection'. *Proceedings of the National Academy of Sciences*, 105(51), pp. 20428–20433. DOI: 10.1073/pnas.0811139106.

Brooks, D.G. *et al.* (2006) 'Interleukin-10 Determines Viral Clearance or Persistence in Vivo'. *Nature Medicine*, 12(11), pp. 1301–1309. DOI: 10.1038/nm1492.

Bu, D. *et al.* (2010) 'Statin-Induced Kruppel-like Factor 2 Expression in Human and Mouse T Cells Reduces Inflammatory and Pathogenic Responses'. *Journal of Clinical Investigation*, 120(6), pp. 1961–1970. DOI: 10.1172/JCI41384.

Buckley, A.F., Kuo, C.T. and Leiden, J.M. (2001) 'Transcription Factor LKLF Is Sufficient to Program T Cell Quiescence via a C-Myc–Dependent Pathway'. *Nature Immunology*, 2(8), pp. 698–704. DOI: 10.1038/90633.

Cai, S., Han, H.-J. and Kohwi-Shigematsu, T. (2003) 'Tissue-Specific Nuclear Architecture and Gene Expession Regulated by SATB1'. *Nature Genetics*, 34(1), pp. 42–51. DOI: 10.1038/ng1146.

Cai, S., Lee, C.C. and Kohwi-Shigematsu, T. (2006) 'SATB1 Packages Densely Looped, Transcriptionally Active Chromatin for Coordinated Expression of Cytokine Genes'. *Nature Genetics*, 38(11), pp. 1278–1288. DOI: 10.1038/ng1913.

Cairns, B.R. (2009) 'The Logic of Chromatin Architecture and Remodelling at Promoters'. *Nature*, 461(7261), pp. 193–198. DOI: 10.1038/nature08450.

Campbell, J.J., O'Connell, D.J. and Wurbel, M.-A. (2007) 'Cutting Edge: Chemokine Receptor CCR4 Is Necessary for Antigen-Driven Cutaneous Accumulation of CD4 T Cells under Physiological Conditions'. *The Journal of Immunology*, 178(6), pp. 3358–3362. DOI: 10.4049/jimmunol.178.6.3358.

Cannarile, M.A. *et al.* (2006) 'Transcriptional Regulator Id2 Mediates CD8+ T Cell Immunity'. *Nature Immunology*, 7(12), pp. 1317–1325. DOI: 10.1038/ni1403.

Carlson, C.M. *et al.* (2006) 'Kruppel-like Factor 2 Regulates Thymocyte and T-Cell Migration'.

Nature, 442(7100), pp. 299–302. DOI: 10.1038/nature04882.

Castanza, A.S. *et al.* (2023) 'Extending Support for Mouse Data in the Molecular Signatures Database (MSigDB)'. *Nature Methods*, 20(11), pp. 1619–1620. DOI: 10.1038/s41592-023-02014-7.

Chemnitz, J.M. *et al.* (2004) 'SHP-1 and SHP-2 Associate with Immunoreceptor Tyrosine-Based Switch Motif of Programmed Death 1 upon Primary Human T Cell Stimulation, but Only Receptor Ligation Prevents T Cell Activation'. *The Journal of Immunology*, 173(2), pp. 945–954. DOI: 10.4049/jimmunol.173.2.945.

Chen, L. and Flies, D.B. (2013) 'Molecular Mechanisms of T Cell Co-Stimulation and Co-Inhibition'. *Nature Reviews Immunology*, 13(4), pp. 227–242. DOI: 10.1038/nri3405.

Chen, T. *et al.* (2024) 'Current Challenges and Therapeutic Advances of CAR-T Cell Therapy for Solid Tumors'. *Cancer Cell International*, 24(1), p. 133. DOI: 10.1186/s12935-024-03315-3.

Chen, Y. *et al.* (2018) 'Transcriptional and Epigenetic Regulation of Effector and Memory CD8 T Cell Differentiation'. *Frontiers in Immunology*, 9, p. 2826. DOI: 10.3389/fimmu.2018.02826.

Chen, Z. *et al.* (2022) 'MicroRNA-409 Regulates the Proliferation and Invasion of Breast Cancer Cell Lines by Targeting Special AT-Rich Sequence-Binding Protein 1 (SATB1)'. *Bioengineered*, 13(5), pp. 13045–13054. DOI: 10.1080/21655979.2022.2073320.

Chi, H. and Flavell, R.A. (2005) 'Cutting Edge: Regulation of T Cell Trafficking and Primary Immune Responses by Sphingosine 1-Phosphate Receptor 1'. *The Journal of Immunology*, 174(5), pp. 2485–2488. DOI: 10.4049/jimmunol.174.5.2485.

Chihara, N. *et al.* (2018) 'Induction and Transcriptional Regulation of the Co-Inhibitory Gene Module in T Cells'. *Nature*, 558(7710), pp. 454–459. DOI: 10.1038/s41586-018-0206-z.

Chorro, L. *et al.* (2018) 'Interleukin 2 Modulates Thymic-Derived Regulatory T Cell Epigenetic Landscape'. *Nature Communications*, 9(1), p. 5368. DOI: 10.1038/s41467-018-07806-6.

Choudhary, S. and Satija, R. (2022) 'Comparison and Evaluation of Statistical Error Models for scRNA-Seq'. *Genome Biology*, 23(1), p. 27. DOI: 10.1186/s13059-021-02584-9.

Christo, S.N. *et al.* (2021) 'Discrete Tissue Microenvironments Instruct Diversity in Resident Memory T Cell Function and Plasticity'. *Nature Immunology*, 22(9), pp. 1140–1151. DOI: 10.1038/s41590-021-01004-1.

Cibrián, D. and Sánchez-Madrid, F. (2017) 'CD69: From Activation Marker to Metabolic Gatekeeper'. *European Journal of Immunology*, 47(6), pp. 946–953. DOI: 10.1002/eji.201646837.

Collier, J.L. *et al.* (2021) 'Not-so-Opposite Ends of the Spectrum: CD8+ T Cell Dysfunction across Chronic Infection, Cancer and Autoimmunity'. *Nature Immunology*, 22(7), pp. 809–819. DOI: 10.1038/s41590-021-00949-7.

Crawford, A. *et al.* (2014) 'Molecular and Transcriptional Basis of CD4+ T Cell Dysfunction during Chronic Infection'. *Immunity*, 40(2), pp. 289–302. DOI: 10.1016/j.immuni.2014.01.005.

Crespo, J. *et al.* (2013) 'T Cell Anergy, Exhaustion, Senescence, and Stemness in the Tumor Microenvironment'. *Current Opinion in Immunology*, 25(2), pp. 214–221. DOI: 10.1016/j.coi.2012.12.003.

Crowl, J.T. *et al.* (2022) 'Tissue-Resident Memory CD8+ T Cells Possess Unique Transcriptional, Epigenetic and Functional Adaptations to Different Tissue Environments'. *Nature Immunology*, 23(7), pp. 1121–1131. DOI: 10.1038/s41590-022-01229-8.

Cyster, J.G. and Schwab, S.R. (2012) 'Sphingosine-1-Phosphate and Lymphocyte Egress from Lymphoid Organs'. *Annual Review of Immunology*, 30(1), pp. 69–94. DOI: 10.1146/annurev-immunol-020711-075011.

Danecek, P. *et al.* (2021) 'Twelve Years of SAMtools and BCFtools'. *GigaScience*, 10(2), p. giab008. DOI: 10.1093/gigascience/giab008.

Daniel, B. *et al.* (2022) 'Divergent Clonal Differentiation Trajectories of T Cell Exhaustion'. *Nature Immunology*, 23(11), pp. 1614–1627. DOI: 10.1038/s41590-022-01337-5.

David, C.J. and Massagué, J. (2018) 'Contextual Determinants of TGFβ Action in Development, Immunity and Cancer'. *Nature Reviews Molecular Cell Biology*, 19(7), pp. 419–435. DOI: 10.1038/s41580-018-0007-0.

Day, C.L. *et al.* (2006) 'PD-1 Expression on HIV-Specific T Cells Is Associated with T-Cell Exhaustion and Disease Progression'. *Nature*, 443(7109), pp. 350–354. DOI: 10.1038/nature05115.

De Silva, N.S. and Klein, U. (2015) 'Dynamics of B Cells in Germinal Centres'. *Nature Reviews Immunology*, 15(3), pp. 137–148. DOI: 10.1038/nri3804.

Diacovo, T.G. *et al.* (1998) 'Circulating Activated Platelets Reconstitute Lymphocyte Homing and Immunity in L-Selectin–Deficient Mice'. *The Journal of Experimental Medicine*, 187(2), pp. 197–204. DOI: 10.1084/jem.187.2.197.

Dias, S. *et al.* (2017) 'Effector Regulatory T Cell Differentiation and Immune Homeostasis Depend on the Transcription Factor Myb'. *Immunity*, 46(1), pp. 78–91. DOI: 10.1016/j.immuni.2016.12.017.

Dickinson, L.A., Dickinson, C.D. and Kohwi-Shigematsu, T. (1997) 'An Atypical Homeodomain in SATB1 Promotes Specific Recognition of the Key Structural Element in a Matrix Attachment Region'. *Journal of Biological Chemistry*, 272(17), pp. 11463–11470. DOI: 10.1074/jbc.272.17.11463.

Dobin, A. *et al.* (2013) 'STAR: Ultrafast Universal RNA-Seq Aligner'. *Bioinformatics*, 29(1), pp. 15–21. DOI: 10.1093/bioinformatics/bts635.

Doering, T.A. *et al.* (2012) 'Network Analysis Reveals Centrally Connected Genes and Pathways Involved in CD8+ T Cell Exhaustion versus Memory'. *Immunity*, 37(6), pp. 1130–1144. DOI: 10.1016/j.immuni.2012.08.021.

Doherty, P.C. and Zinkernagel, R.M. (1984) 'MHC Restriction and Cytotoxic T Lymphocytes'. In Notkins, A.L. and Oldstone, M.B.A. (eds.) *Concepts in Viral Pathogenesis*. New York, NY: Springer New York, pp. 53–57. DOI: 10.1007/978-1-4612-5250-4_8.

Doi, Y. *et al.* (2018) 'Variable SATB1 Levels Regulate Hematopoietic Stem Cell Heterogeneity with Distinct Lineage Fate'. *Cell Reports*, 23(11), pp. 3223–3235. DOI: 10.1016/j.celrep.2018.05.042.

Dominguez, C.X. *et al.* (2015) 'The Transcription Factors ZEB2 and T-Bet Cooperate to Program Cytotoxic T Cell Terminal Differentiation in Response to LCMV Viral Infection'. *Journal of Experimental Medicine*, 212(12), pp. 2041–2056. DOI: 10.1084/jem.20150186.

Dong, H. *et al.* (1999) 'B7-H1, a Third Member of the B7 Family, Co-Stimulates T-Cell Proliferation and Interleukin-10 Secretion'. *Nature Medicine*, 5(12), pp. 1365–1369. DOI: 10.1038/70932.

Eisenbarth, S.C. (2019) 'Dendritic Cell Subsets in T Cell Programming: Location Dictates Function'. *Nature Reviews Immunology*, 19(2), pp. 89–103. DOI: 10.1038/s41577-018-0088-1.

Ejrnaes, M. *et al.* (2006) 'Resolution of a Chronic Viral Infection after Interleukin-10 Receptor Blockade'. *Journal of Experimental Medicine*, 203(11), pp. 2461–2472. DOI: 10.1084/jem.20061462.

El-Awady, A.R. *et al.* (2022) 'Dendritic Cells a Critical Link to Alveolar Bone Loss and Systemic Disease Risk in Periodontitis: Immunotherapeutic Implications'. *Periodontology 2000*, 89(1), pp. 41–50. DOI: 10.1111/prd.12428.

Erdmann, I. *et al.* (2002) 'Fucosyltransferase VII-Deficient Mice with Defective E-, P-, and L-Selectin Ligands Show Impaired CD4+ and CD8+ T Cell Migration into the Skin, but Normal Extravasation into Visceral Organs'. *The Journal of Immunology*, 168(5), pp. 2139–2146. DOI: 10.4049/jimmunol.168.5.2139.

Esensten, J.H. *et al.* (2016) 'CD28 Costimulation: From Mechanism to Therapy'. *Immunity*, 44(5),

pp. 973–988. DOI: 10.1016/j.immuni.2016.04.020.

Fagerberg, E. *et al.* (2025) 'KLF2 Maintains Lineage Fidelity and Suppresses CD8 T Cell Exhaustion during Acute LCMV Infection'. *Science*, 387(6735), p. eadn2337. DOI: 10.1126/science.adn2337.

Fang, X. *et al.* (2022) 'TCF-1+ PD-1+ CD8+T Cells Are Associated with the Response to PD-1 Blockade in Non-Small Cell Lung Cancer Patients'. *Journal of Cancer Research and Clinical Oncology*, 148(10), pp. 2653–2660. DOI: 10.1007/s00432-021-03845-7.

Feng, C.H. *et al.* (2016) 'Statin Use Significantly Improves Overall Survival in High-Grade Endometrial Cancer'. *International Journal of Gynecological Cancer*, 26(9), pp. 1642–1649. DOI: 10.1097/IGC.0000000000000819.

Feng, D. *et al.* (2022) 'Chromatin Organizer SATB1 Controls the Cell Identity of CD4+ CD8+ Double-Positive Thymocytes by Regulating the Activity of Super-Enhancers'. *Nature Communications*, 13(1), p. 5554. DOI: 10.1038/s41467-022-33333-6.

Fenwick, C. *et al.* (2019) 'T-cell Exhaustion in HIV Infection'. *Immunological Reviews*, 292(1), pp. 149–163. DOI: 10.1111/imr.12823.

Fessing, M.Y. *et al.* (2011) 'P63 Regulates *Satb1* to Control Tissue-Specific Chromatin Remodeling during Development of the Epidermis'. *Journal of Cell Biology*, 194(6), pp. 825–839. DOI: 10.1083/jcb.201101148.

Fredholm, S. *et al.* (2018) 'SATB1 in Malignant T Cells'. *Journal of Investigative Dermatology*, 138(8), pp. 1805–1815. DOI: 10.1016/j.jid.2018.03.1526.

Frias, A.B. *et al.* (2021) 'Epigenetic Regulation of T Cell Adaptive Immunity'. *Immunological Reviews*, 300(1), pp. 9–21. DOI: 10.1111/imr.12943.

Fu, Z. *et al.* (2021) 'MicroRNA as an Important Target for Anticancer Drug Development'. *Frontiers in Pharmacology*, 12, p. 736323. DOI: 10.3389/fphar.2021.736323.

Fukunaga, R. *et al.* (1986) 'Uudermethylation of Interferon-γ Gene in Human T Cell Lines and Normal T Lymphocytes'. *Nucleic Acids Research*, 14(11), pp. 4421–4436. DOI: 10.1093/nar/14.11.4421.

Gabriel, C.H. *et al.* (2016) 'Identification of Novel Nuclear Factor of Activated T Cell (NFAT)-Associated Proteins in T Cells'. *Journal of Biological Chemistry*, 291(46), pp. 24172–24187. DOI: 10.1074/jbc.M116.739326.

Gabriel, S.S. *et al.* (2021) 'Transforming Growth Factor-β-Regulated mTOR Activity Preserves Cellular Metabolism to Maintain Long-Term T Cell Responses in Chronic Infection'. *Immunity*, 54(8), pp. 1698-1714.e5. DOI: 10.1016/j.immuni.2021.06.007.

Gago da Graça, C. *et al.* (2025) 'Stem-like Memory and Precursors of Exhausted T Cells Share a Common Progenitor Defined by ID3 Expression'. *Science Immunology*, 10(103), p. eadn1945. DOI: 10.1126/sciimmunol.adn1945.

Galande, S. *et al.* (2001) 'SATB1 Cleavage by Caspase 6 Disrupts PDZ Domain-Mediated Dimerization, Causing Detachment from Chromatin Early in T-Cell Apoptosis'. *Molecular and Cellular Biology*, 21(16), pp. 5591–5604. DOI: 10.1128/MCB.21.16.5591-5604.2001.

Germain, R.N. *et al.* (2006) 'Dynamic Imaging of the Immune System: Progress, Pitfalls and Promise'. *Nature Reviews Immunology*, 6(7), pp. 497–507. DOI: 10.1038/nri1884.

Ghoneim, H.E. *et al.* (2017) 'De Novo Epigenetic Programs Inhibit PD-1 Blockade-Mediated T Cell Rejuvenation'. *Cell*, 170(1), pp. 142-157.e19. DOI: 10.1016/j.cell.2017.06.007.

Giles, J.R. *et al.* (2022) 'Shared and Distinct Biological Circuits in Effector, Memory and Exhausted CD8+ T Cells Revealed by Temporal Single-Cell Transcriptomics and Epigenetics'. *Nature Immunology*, 23(11), pp. 1600–1613. DOI: 10.1038/s41590-022-01338-4.

Girard, J.-P., Moussion, C. and Förster, R. (2012) 'HEVs, Lymphatics and Homeostatic Immune Cell Trafficking in Lymph Nodes'. *Nature Reviews Immunology*, 12(11), pp. 762–773. DOI:

10.1038/nri3298.

Gnanaprakasam, J.N. and Wang, R. (2017) 'MYC in Regulating Immunity: Metabolism and Beyond'. *Genes*, 8(3), p. 88. DOI: 10.3390/genes8030088.

Gong, F. *et al.* (2011) 'The BCL2 Gene Is Regulated by a Special AT-Rich Sequence Binding Protein 1-Mediated Long Range Chromosomal Interaction between the Promoter and the Distal Element Located within the 3'-UTR'. *Nucleic Acids Research*, 39(11), pp. 4640–4652. DOI: 10.1093/nar/gkr023.

Gottimukkala, K.P. *et al.* (2016) 'Regulation of SATB1 during Thymocyte Development by TCR Signaling'. *Molecular Immunology*, 77, pp. 34–43. DOI: 10.1016/j.molimm.2016.07.005.

Grandi, F.C. *et al.* (2022) 'Chromatin Accessibility Profiling by ATAC-Seq'. *Nature Protocols*, 17(6), pp. 1518–1552. DOI: 10.1038/s41596-022-00692-9.

Grebinoski, S. *et al.* (2022) 'Autoreactive CD8+ T Cells Are Restrained by an Exhaustion-like Program That Is Maintained by LAG3'. *Nature Immunology*, 23(6), pp. 868–877. DOI: 10.1038/s41590-022-01210-5.

Greenwald, R.J., Freeman, G.J. and Sharpe, A.H. (2005) 'THE B7 FAMILY REVISITED'. *Annual Review of Immunology*, 23(1), pp. 515–548. DOI: 10.1146/annurev.immunol.23.021704.115611.

Gregg, R.K. *et al.* (2010) 'Mechanisms of Spatial and Temporal Development of Autoimmune Vitiligo in Tyrosinase-Specific TCR Transgenic Mice'. *The Journal of Immunology*, 184(4), pp. 1909–1917. DOI: 10.4049/jimmunol.0902778.

Greiff, V. *et al.* (2017) 'Systems Analysis Reveals High Genetic and Antigen-Driven Predetermination of Antibody Repertoires throughout B Cell Development'. *Cell Reports*, 19(7), pp. 1467–1478. DOI: 10.1016/j.celrep.2017.04.054.

Gretz, J.E. *et al.* (2000) 'Lymph-Borne Chemokines and Other Low Molecular Weight Molecules Reach High Endothelial Venules via Specialized Conduits While a Functional Barrier Limits Access to the Lymphocyte Microenvironments in Lymph Node Cortex'. *The Journal of Experimental Medicine*, 192(10), pp. 1425–1440. DOI: 10.1084/jem.192.10.1425.

Groom, J.R. and Luster, A.D. (2011) 'CXCR3 in T Cell Function'. *Experimental Cell Research*, 317(5), pp. 620–631. DOI: 10.1016/j.yexcr.2010.12.017.

Guermonprez, P. *et al.* (2002) 'Antigen Presentation and T Cell Stimulation by Dendritic Cells'. *Annual Review of Immunology*, 20(1), pp. 621–667. DOI: 10.1146/annurev.immunol.20.100301.064828.

Gulati, G.S. *et al.* (2020) 'Single-Cell Transcriptional Diversity Is a Hallmark of Developmental Potential'. *Science*, 367(6476), pp. 405–411. DOI: 10.1126/science.aax0249.

Haan, J.M.D., Mebius, R.E. and Kraal, G. (2012) 'Stromal Cells of the Mouse Spleen'. *Frontiers in Immunology*, 03. DOI: 10.3389/fimmu.2012.00201.

Hamada, T. *et al.* (2018) 'Statin Use and Pancreatic Cancer Risk in Two Prospective Cohort Studies'. *Journal of Gastroenterology*, 53(8), pp. 959–966. DOI: 10.1007/s00535-018-1430-x.

Hamann, A. *et al.* (1994) 'Role of Alpha 4-Integrins in Lymphocyte Homing to Mucosal Tissues in Vivo.' *The Journal of Immunology*, 152(7), pp. 3282–3293. DOI: 10.4049/jimmunol.152.7.3282.

Hammarlund, E. *et al.* (2003) 'Duration of Antiviral Immunity after Smallpox Vaccination'. *Nature Medicine*, 9(9), pp. 1131–1137. DOI: 10.1038/nm917.

Hammelman, J. *et al.* (2020) 'Identification of Determinants of Differential Chromatin Accessibility through a Massively Parallel Genome-Integrated Reporter Assay'. *Genome Research*, 30(10), pp. 1468–1480. DOI: 10.1101/gr.263228.120.

Hao, B. *et al.* (2015) 'An Anti-Silencer– and SATB1-Dependent Chromatin Hub Regulates Rag1 and Rag2 Gene Expression during Thymocyte Development'. *Journal of Experimental Medicine*, 212(5), pp. 809–824. DOI: 10.1084/jem.20142207.

Hao, Y. *et al.* (2021) 'Integrated Analysis of Multimodal Single-Cell Data'. *Cell*, 184(13), pp. 3573-

3587.e29. DOI: 10.1016/j.cell.2021.04.048.

Hart, G.T., Hogquist, K.A. and Jameson, S.C. (2012) 'Krüppel-like Factors in Lymphocyte Biology'. *The Journal of Immunology*, 188(2), pp. 521–526. DOI: 10.4049/jimmunol.1101530.

Hartana, C.A. *et al.* (2018) 'Urothelial Bladder Cancer May Suppress Perforin Expression in CD8+ T Cells by an ICAM-1/TGFβ2 Mediated Pathway' Shiku, H. (ed.). *PLOS ONE*, 13(7), p. e0200079. DOI: 10.1371/journal.pone.0200079.

Harty, J.T. and Badovinac, V.P. (2008) 'Shaping and Reshaping CD8+ T-Cell Memory'. *Nature Reviews Immunology*, 8(2), pp. 107–119. DOI: 10.1038/nri2251.

Hashimoto, M. *et al.* (2018) 'CD8 T Cell Exhaustion in Chronic Infection and Cancer: Opportunities for Interventions'. *Annual Review of Medicine*, 69(1), pp. 301–318. DOI: 10.1146/annurev-med-012017-043208.

Haslam, A., Gill, J. and Prasad, V. (2020) 'Estimation of the Percentage of US Patients With Cancer Who Are Eligible for Immune Checkpoint Inhibitor Drugs'. *JAMA Network Open*, 3(3), p. e200423. DOI: 10.1001/jamanetworkopen.2020.0423.

Haslam, A. and Prasad, V. (2019) 'Estimation of the Percentage of US Patients With Cancer Who Are Eligible for and Respond to Checkpoint Inhibitor Immunotherapy Drugs'. *JAMA Network Open*, 2(5), p. e192535. DOI: 10.1001/jamanetworkopen.2019.2535.

He, R. *et al.* (2016) 'Follicular CXCR5-Expressing CD8+ T Cells Curtail Chronic Viral Infection'. *Nature*, 537(7620), pp. 412–416. DOI: 10.1038/nature19317.

Heath, W.R. and Carbone, F.R. (2001) 'Cross-Presentation, Dendritic Cells, Tolerance and Immunity'. *Annual Review of Immunology*, 19(1), pp. 47–64. DOI: 10.1146/annurev.immunol.19.1.47.

Hedrick, S.M. *et al.* (2012) 'FOXO Transcription Factors throughout T Cell Biology'. *Nature Reviews Immunology*, 12(9), pp. 649–661. DOI: 10.1038/nri3278.

Heeg, M. and Goldrath, A.W. (2023) 'Insights into Phenotypic and Functional $CD8^+$ T_{RM} Heterogeneity'. *Immunological Reviews*, 316(1), pp. 8–22. DOI: 10.1111/imr.13218.

Heesters, B.A., Myers, R.C. and Carroll, M.C. (2014) 'Follicular Dendritic Cells: Dynamic Antigen Libraries'. *Nature Reviews Immunology*, 14(7), pp. 495–504. DOI: 10.1038/nri3689.

Henrickson, Sarah E. *et al.* (2008) 'In Vivo Imaging of T Cell PrimingA Presentation from the 11th Joint Meeting of the Signal Transduction Society (STS), Signal Transduction: Receptors, Mediators and Genes, Weimar, Germany, 1 to 3 November 2007.' *Science Signaling*, 1(12). DOI: 10.1126/stke.112pt2.

Henrickson, Sarah E. *et al.* (2008) 'T Cell Sensing of Antigen Dose Governs Interactive Behavior with Dendritic Cells and Sets a Threshold for T Cell Activation'. *Nature Immunology*, 9(3), pp. 282–291. DOI: 10.1038/ni1559.

Hernandez, R. and Brown, D.T. (2010) 'Growth and Maintenance of Baby Hamster Kidney (BHK) Cells'. *Current Protocols in Microbiology*, 17(1). DOI: 10.1002/9780471729259.mca04hs17.

Hickman, H.D. *et al.* (2011) 'Chemokines Control Naive CD8+ T Cell Selection of Optimal Lymph Node Antigen Presenting Cells'. *Journal of Experimental Medicine*, 208(12), pp. 2511–2524. DOI: 10.1084/jem.20102545.

Hickman, H.D. *et al.* (2008) 'Direct Priming of Antiviral CD8+ T Cells in the Peripheral Interfollicular Region of Lymph Nodes'. *Nature Immunology*, 9(2), pp. 155–165. DOI: 10.1038/ni1557.

Hidmark, A., Von Saint Paul, A. and Dalpke, A.H. (2012) 'Cutting Edge: TLR13 Is a Receptor for Bacterial RNA'. *The Journal of Immunology*, 189(6), pp. 2717–2721. DOI: 10.4049/jimmunol.1200898.

Hildeman, D.A. *et al.* (2002) 'Activated T Cell Death In Vivo Mediated by Proapoptotic Bcl-2 Family Member Bim'. *Immunity*, 16(6), pp. 759–767. DOI: 10.1016/S1074-7613(02)00322-9.

Hirahara, K. *et al.* (2012) 'Interleukin-27 Priming of T Cells Controls IL-17 Production in Trans via

Induction of the Ligand PD-L1'. *Immunity*, 36(6), pp. 1017–1030. DOI: 10.1016/j.immuni.2012.03.024.

Hirai, T. *et al.* (2021) 'Competition for Active TGFβ Cytokine Allows for Selective Retention of Antigen-Specific Tissue- Resident Memory T Cells in the Epidermal Niche'. *Immunity*, 54(1), pp. 84-98.e5. DOI: 10.1016/j.immuni.2020.10.022.

Hirsch, T. *et al.* (2024) 'IRF4 Impedes Human CD8 T Cell Function and Promotes Cell Proliferation and PD-1 Expression'. *Cell Reports*, 43(7), p. 114401. DOI: 10.1016/j.celrep.2024.114401.

Höpken, U.E. *et al.* (2004) 'The Chemokine Receptor CCR7 Controls Lymph Node-dependent Cytotoxic T Cell Priming in Alloimmune Responses'. *European Journal of Immunology*, 34(2), pp. 461–470. DOI: 10.1002/eji.200324690.

Howe, D.G. *et al.* (2018) 'Model Organism Data Evolving in Support of Translational Medicine'. *Lab Animal*, 47(10), pp. 277–289. DOI: 10.1038/s41684-018-0150-4.

Hu, Y. *et al.* (2022) 'TGF-β Regulates the Stem-like State of PD-1+ TCF-1+ Virus-Specific CD8 T Cells during Chronic Infection'. *Journal of Experimental Medicine*, 219(10), p. e20211574. DOI: 10.1084/jem.20211574.

Hudson, W.H. *et al.* (2019) 'Proliferating Transitory T Cells with an Effector-like Transcriptional Signature Emerge from PD-1+ Stem-like CD8+ T Cells during Chronic Infection'. *Immunity*, 51(6), pp. 1043-1058.e4. DOI: 10.1016/j.immuni.2019.11.002.

Hui, E. *et al.* (2017) 'T Cell Costimulatory Receptor CD28 Is a Primary Target for PD-1–Mediated Inhibition'. *Science*, 355(6332), pp. 1428–1433. DOI: 10.1126/science.aaf1292.

Hung, M.-S. *et al.* (2017) 'Statin Improves Survival in Patients with EGFR-TKI Lung Cancer: A Nationwide Population-Based Study' Souglakos, J. (ed.). *PLOS ONE*, 12(2), p. e0171137. DOI: 10.1371/journal.pone.0171137.

Ibegbu, C.C. *et al.* (2005) 'Expression of Killer Cell Lectin-Like Receptor G1 on Antigen-Specific Human CD8+ T Lymphocytes during Active, Latent, and Resolved Infection and Its Relation with CD57'. *The Journal of Immunology*, 174(10), pp. 6088–6094. DOI: 10.4049/jimmunol.174.10.6088.

Ichii, H. *et al.* (2004) 'Bcl6 Acts as an Amplifier for the Generation and Proliferative Capacity of Central Memory CD8+ T Cells'. *The Journal of Immunology*, 173(2), pp. 883–891. DOI: 10.4049/jimmunol.173.2.883.

Im, S.J. *et al.* (2016) 'Defining CD8+ T Cells That Provide the Proliferative Burst after PD-1 Therapy'. *Nature*, 537(7620), pp. 417–421. DOI: 10.1038/nature19330.

International Parkinson's Disease Genomics Consortium *et al.* (2017) 'A Meta-Analysis of Genome-Wide Association Studies Identifies 17 New Parkinson's Disease Risk Loci'. *Nature Genetics*, 49(10), pp. 1511–1516. DOI: 10.1038/ng.3955.

Intlekofer, A.M. *et al.* (2005) 'Effector and Memory CD8+ T Cell Fate Coupled by T-Bet and Eomesodermin'. *Nature Immunology*, 6(12), pp. 1236–1244. DOI: 10.1038/ni1268.

Ishigaki, H. *et al.* (2024) 'Generation, Transcriptomic States, and Clinical Relevance of CX3CR1+ CD8 T Cells in Melanoma'. *Cancer Research Communications*, 4(7), pp. 1802–1814. DOI: 10.1158/2767-9764.CRC-24-0199.

Jadhav, R.R. *et al.* (2019) 'Epigenetic Signature of PD-1+ TCF1+ CD8 T Cells That Act as Resource Cells during Chronic Viral Infection and Respond to PD-1 Blockade'. *Proceedings of the National Academy of Sciences*, 116(28), pp. 14113–14118. DOI: 10.1073/pnas.1903520116.

Jalkantn, S. *et al.* (1986) 'Homing Receptors and the Control of Lymphocyte Migration'. *Immunological Reviews*, 91(1), pp. 39–60. DOI: 10.1111/j.1600-065X.1986.tb01483.x.

Jargosch, M. *et al.* (2016) 'Data Integration for Identification of Important Transcription Factors of STAT6-Mediated Cell Fate Decisions'. *Genetics and Molecular Research*, 15(2). DOI: 10.4238/gmr.15028493.

Jiang, Y., Li, Y. and Zhu, B. (2015) 'T-Cell Exhaustion in the Tumor Microenvironment'. *Cell Death & Disease*, 6(6), pp. e1792–e1792. DOI: 10.1038/cddis.2015.162.

Jin, X. *et al.* (1999) 'Dramatic Rise in Plasma Viremia after CD8+ T Cell Depletion in Simian Immunodeficiency Virus–Infected Macaques'. *The Journal of Experimental Medicine*, 189(6), pp. 991–998. DOI: 10.1084/jem.189.6.991.

Johansson-Lindbom, B. *et al.* (2003) 'Selective Generation of Gut Tropic T Cells in Gut-Associated Lymphoid Tissue (GALT)'. *The Journal of Experimental Medicine*, 198(6), pp. 963–969. DOI: 10.1084/jem.20031244.

Johansson-Percival, A. and Ganss, R. (2021) 'Therapeutic Induction of Tertiary Lymphoid Structures in Cancer Through Stromal Remodeling'. *Frontiers in Immunology*, 12, p. 674375. DOI: 10.3389/fimmu.2021.674375.

Joshi, N.S. *et al.* (2007) 'Inflammation Directs Memory Precursor and Short-Lived Effector CD8+ T Cell Fates via the Graded Expression of T-Bet Transcription Factor'. *Immunity*, 27(2), pp. 281–295. DOI: 10.1016/j.immuni.2007.07.010.

Joshi, N.S. and Kaech, S.M. (2008) 'Effector CD8 T Cell Development: A Balancing Act between Memory Cell Potential and Terminal Differentiation'. *The Journal of Immunology*, 180(3), pp. 1309–1315. DOI: 10.4049/jimmunol.180.3.1309.

Jung, Y.W. *et al.* (2016) 'CCR7 Expression Alters Memory CD8 T-Cell Homeostasis by Regulating Occupancy in IL-7– and IL-15–Dependent Niches'. *Proceedings of the National Academy of Sciences*, 113(29), pp. 8278–8283. DOI: 10.1073/pnas.1602899113.

Jung, Y.W. *et al.* (2010) 'Differential Localization of Effector and Memory CD8 T Cell Subsets in Lymphoid Organs during Acute Viral Infection'. *The Journal of Immunology*, 185(9), pp. 5315–5325. DOI: 10.4049/jimmunol.1001948.

Junt, T. *et al.* (2004) 'Impact of CCR7 on Priming and Distribution of Antiviral Effector and Memory CTL'. *The Journal of Immunology*, 173(11), pp. 6684–6693. DOI: 10.4049/jimmunol.173.11.6684.

Kaech, S.M., Hemby, S., *et al.* (2002) 'Molecular and Functional Profiling of Memory CD8 T Cell Differentiation'. *Cell*, 111(6), pp. 837–851. DOI: 10.1016/S0092-8674(02)01139-X.

Kaech, S.M. and Wherry, E.J. (2007) 'Heterogeneity and Cell-Fate Decisions in Effector and Memory CD8+ T Cell Differentiation during Viral Infection'. *Immunity*, 27(3), pp. 393–405. DOI: 10.1016/j.immuni.2007.08.007.

Kaech, S.M., Wherry, E.J. and Ahmed, R. (2002) 'Effector and Memory T-Cell Differentiation: Implications for Vaccine Development'. *Nature Reviews Immunology*, 2(4), pp. 251–262. DOI: 10.1038/nri778.

Kakugawa, K. *et al.* (2017) 'Essential Roles of SATB1 in Specifying T Lymphocyte Subsets'. *Cell Reports*, 19(6), pp. 1176–1188. DOI: 10.1016/j.celrep.2017.04.038.

Kallies, A. *et al.* (2009) 'Blimp-1 Transcription Factor Is Required for the Differentiation of Effector CD8+ T Cells and Memory Responses'. *Immunity*, 31(2), pp. 283–295. DOI: 10.1016/j.immuni.2009.06.021.

Kallies, A., Zehn, D. and Utzschneider, D.T. (2020) 'Precursor Exhausted T Cells: Key to Successful Immunotherapy?' *Nature Reviews Immunology*, 20(2), pp. 128–136. DOI: 10.1038/s41577-019-0223-7.

Kamphorst, A.O. *et al.* (2017) 'Rescue of Exhausted CD8 T Cells by PD-1–Targeted Therapies Is CD28-Dependent'. *Science*, 355(6332), pp. 1423–1427. DOI: 10.1126/science.aaf0683.

Kao, C. *et al.* (2011) 'Transcription Factor T-Bet Represses Expression of the Inhibitory Receptor PD-1 and Sustains Virus-Specific CD8+ T Cell Responses during Chronic Infection'. *Nature Immunology*, 12(7), pp. 663–671. DOI: 10.1038/ni.2046.

Kasmani, M.Y. *et al.* (2023) 'Clonal Lineage Tracing Reveals Mechanisms Skewing CD8+ T Cell Fate Decisions in Chronic Infection'. *Journal of Experimental Medicine*, 220(1), p. e20220679. DOI: 10.1084/jem.20220679.

Kaur, S. *et al.* (2016) 'Special AT-Rich Sequence-Binding Protein 1 (SATB1) Functions as an Accessory Factor in Base Excision Repair'. *Journal of Biological Chemistry*, 291(43), pp. 22769–22780. DOI: 10.1074/jbc.M116.735696.

Kawamata, N. *et al.* (2009) 'Expression of Endothelia and Lymphocyte Adhesion Molecules in Bronchus-Associated Lymphoid Tissue (BALT) in Adult Human Lung'. *Respiratory Research*, 10(1), p. 97. DOI: 10.1186/1465-9921-10-97.

Kenyon, N.J. *et al.* (2009) 'An A4β1 Integrin Antagonist Decreases Airway Inflammation in Ovalbumin-Exposed Mice'. *European Journal of Pharmacology*, 603(1–3), pp. 138–146. DOI: 10.1016/j.ejphar.2008.11.063.

Khan, O. *et al.* (2019) 'TOX Transcriptionally and Epigenetically Programs CD8+ T Cell Exhaustion'. *Nature*, 571(7764), pp. 211–218. DOI: 10.1038/s41586-019-1325-x.

Khare, S.P. *et al.* (2019) 'NF-κB Signaling and IL-4 Signaling Regulate SATB1 Expression via Alternative Promoter Usage During Th2 Differentiation'. *Frontiers in Immunology*, 10, p. 667. DOI: 10.3389/fimmu.2019.00667.

Kim, C. *et al.* (2020) 'The Transcription Factor TCF1 in T Cell Differentiation and Aging'. *International Journal of Molecular Sciences*, 21(18), p. 6497. DOI: 10.3390/ijms21186497.

Kitagawa, Y. *et al.* (2017) 'Guidance of Regulatory T Cell Development by Satb1-Dependent Super-Enhancer Establishment'. *Nature Immunology*, 18(2), pp. 173–183. DOI: 10.1038/ni.3646.

Klemm, S.L., Shipony, Z. and Greenleaf, W.J. (2019) 'Chromatin Accessibility and the Regulatory Epigenome'. *Nature Reviews Genetics*, 20(4), pp. 207–220. DOI: 10.1038/s41576-018-0089-8.

Kolberg, L. *et al.* (2020) 'Gprofiler2 -- an R Package for Gene List Functional Enrichment Analysis and Namespace Conversion Toolset g:Profiler'. *F1000Research*, 9, p. 709. DOI: 10.12688/f1000research.24956.2.

Kondo, M. *et al.* (2016) 'SATB1 Plays a Critical Role in Establishment of Immune Tolerance'. *The Journal of Immunology*, 196(2), pp. 563–572. DOI: 10.4049/jimmunol.1501429.

Krutzik, S.R. *et al.* (2005) 'TLR Activation Triggers the Rapid Differentiation of Monocytes into Macrophages and Dendritic Cells'. *Nature Medicine*, 11(6), pp. 653–660. DOI: 10.1038/nm1246.

Kumar, B.V. *et al.* (2017) 'Human Tissue-Resident Memory T Cells Are Defined by Core Transcriptional and Functional Signatures in Lymphoid and Mucosal Sites'. *Cell Reports*, 20(12), pp. 2921–2934. DOI: 10.1016/j.celrep.2017.08.078.

Kumar, P.P. *et al.* (2005) 'Displacement of SATB1-Bound Histone Deacetylase 1 Corepressor by the Human Immunodeficiency Virus Type 1 Transactivator Induces Expression of Interleukin-2 and Its Receptor in T Cells'. *Molecular and Cellular Biology*, 25(5), pp. 1620–1633. DOI: 10.1128/MCB.25.5.1620-1633.2005.

Kumari, N. *et al.* (2016) 'Role of Interleukin-6 in Cancer Progression and Therapeutic Resistance'. *Tumor Biology*, 37(9), pp. 11553–11572. DOI: 10.1007/s13277-016-5098-7.

Kunkel, E.J. *et al.* (2000) 'Lymphocyte Cc Chemokine Receptor 9 and Epithelial Thymus-Expressed Chemokine (Teck) Expression Distinguish the Small Intestinal Immune Compartment'. *The Journal of Experimental Medicine*, 192(5), pp. 761–768. DOI: 10.1084/jem.192.5.761.

Kuo, C.T., Veselits, M.L. and Leiden, J.M. (1997) 'LKLF: A Transcriptional Regulator of Single-Positive T Cell Quiescence and Survival'. *Science*, 277(5334), pp. 1986–1990. DOI: 10.1126/science.277.5334.1986.

Kwon, B. (2021) 'The Two Faces of IL-2: A Key Driver of CD8+ T-Cell Exhaustion'. *Cellular & Molecular Immunology*, 18(7), pp. 1641–1643. DOI: 10.1038/s41423-021-00712-w.

Kwon, M. *et al.* (2020) 'PD-1 Blockade Reinvigorates Bone Marrow CD8+ T Cells from Patients with Multiple Myeloma in the Presence of TGFβ Inhibitors'. *Clinical Cancer Research*, 26(7), pp. 1644–1655. DOI: 10.1158/1078-0432.CCR-19-0267.

Latchman, Y. *et al.* (2001) 'PD-L2 Is a Second Ligand for PD-1 and Inhibits T Cell Activation'.

Nature Immunology, 2(3), pp. 261–268. DOI: 10.1038/85330.

Lau, Lisa.L. *et al.* (1994) 'Cytotoxic T-Cell Memory without Antigen'. *Nature*, 369(6482), pp. 648–652. DOI: 10.1038/369648a0.

Leach, D.R., Krummel, M.F. and Allison, J.P. (1996) 'Enhancement of Antitumor Immunity by CTLA-4 Blockade'. *Science*, 271(5256), pp. 1734–1736. DOI: 10.1126/science.271.5256.1734.

Lee, J.S. *et al.* (2018) 'Statins Enhance Efficacy of Venetoclax in Blood Cancers'. *Science Translational Medicine*, 10(445), p. eaaq1240. DOI: 10.1126/scitranslmed.aaq1240.

Leong, Y.A. *et al.* (2016) 'CXCR5+ Follicular Cytotoxic T Cells Control Viral Infection in B Cell Follicles'. *Nature Immunology*, 17(10), pp. 1187–1196. DOI: 10.1038/ni.3543.

Lewis, S.M., Williams, A. and Eisenbarth, S.C. (2019) 'Structure and Function of the Immune System in the Spleen'. *Science Immunology*, 4(33), p. eaau6085. DOI: 10.1126/sciimmunol.aau6085.

Ley, K. *et al.* (2007) 'Getting to the Site of Inflammation: The Leukocyte Adhesion Cascade Updated'. *Nature Reviews Immunology*, 7(9), pp. 678–689. DOI: 10.1038/nri2156.

Li, G. *et al.* (2022) 'TGF-β-Dependent Lymphoid Tissue Residency of Stem-like T Cells Limits Response to Tumor Vaccine'. *Nature Communications*, 13(1), p. 6043. DOI: 10.1038/s41467-022-33768-x.

Li, J. *et al.* (2018) 'High Levels of Eomes Promote Exhaustion of Anti-Tumor CD8+ T Cells'. *Frontiers in Immunology*, 9, p. 2981. DOI: 10.3389/fimmu.2018.02981.

Li, M.O. *et al.* (2006) 'TRANSFORMING GROWTH FACTOR-β REGULATION OF IMMUNE RESPONSES'. *Annual Review of Immunology*, 24(1), pp. 99–146. DOI: 10.1146/annurev.immunol.24.021605.090737.

Li, X. *et al.* (2025) 'Deciphering Immune Predictors of Immunotherapy Response: A Multiomics Approach at the Pan-Cancer Level'. *Cell Reports Medicine*, p. 101992. DOI: 10.1016/j.xcrm.2025.101992.

Li, X.-D. and Chen, Z.J. (2012) 'Sequence Specific Detection of Bacterial 23S Ribosomal RNA by TLR13'. *eLife*, 1, p. e00102. DOI: 10.7554/eLife.00102.

Li, Yuchen. *et al.* (2024) 'CD69 Is a Promising Immunotherapy and Prognosis Prediction Target in Cancer'. *ImmunoTargets and Therapy*, Volume 13, pp. 1–14. DOI: 10.2147/ITT.S439969.

Liao, W., Lin, J.-X. and Leonard, W.J. (2013) 'Interleukin-2 at the Crossroads of Effector Responses, Tolerance, and Immunotherapy'. *Immunity*, 38(1), pp. 13–25. DOI: 10.1016/j.immuni.2013.01.004.

Liao, Y., Smyth, G.K. and Shi, W. (2014) 'featureCounts: An Efficient General Purpose Program for Assigning Sequence Reads to Genomic Features'. *Bioinformatics*, 30(7), pp. 923–930. DOI: 10.1093/bioinformatics/btt656.

Lin, Y.H. *et al.* (2023) 'Small Intestine and Colon Tissue-Resident Memory CD8+ T Cells Exhibit Molecular Heterogeneity and Differential Dependence on Eomes'. *Immunity*, 56(1), pp. 207-223.e8. DOI: 10.1016/j.immuni.2022.12.007.

Ling, S.P. *et al.* (2022) 'Role of Immunotherapy in the Treatment of Cancer: A Systematic Review'. *Cancers*, 14(21), p. 5205. DOI: 10.3390/cancers14215205.

Linsley, P.S. *et al.* (1991) 'CTLA-4 Is a Second Receptor for the B Cell Activation Antigen B7.' *The Journal of Experimental Medicine*, 174(3), pp. 561–569. DOI: 10.1084/jem.174.3.561.

Linsley, P.S. *et al.* (1994) 'Human B7-1 (CD80) and B7-2 (CD86) Bind with Similar Avidities but Distinct Kinetics to CD28 and CTLA-4 Receptors'. *Immunity*, 1(9), pp. 793–801. DOI: 10.1016/S1074-7613(94)80021-9.

Liu, B. *et al.* (2021) 'Temporal Single-Cell Tracing Reveals Clonal Revival and Expansion of Precursor Exhausted T Cells during Anti-PD-1 Therapy in Lung Cancer'. *Nature Cancer*, 3(1), pp. 108–121. DOI: 10.1038/s43018-021-00292-8.

Liu, C. *et al.* (2019) 'An ATAC-Seq Atlas of Chromatin Accessibility in Mouse Tissues'. *Scientific Data*, 6(1), p. 65. DOI: 10.1038/s41597-019-0071-0.

Liu, Y. *et al.* (2021) 'IL-2 Regulates Tumor-Reactive CD8+ T Cell Exhaustion by Activating the Aryl Hydrocarbon Receptor'. *Nature Immunology*, 22(3), pp. 358–369. DOI: 10.1038/s41590-020-00850-9.

Lonberg, N. and Korman, A.J. (2017) 'Masterful Antibodies: Checkpoint Blockade'. *Cancer Immunology Research*, 5(4), pp. 275–281. DOI: 10.1158/2326-6066.CIR-17-0057.

Lund, J. *et al.* (2003) 'Toll-like Receptor 9–Mediated Recognition of Herpes Simplex Virus-2 by Plasmacytoid Dendritic Cells'. *The Journal of Experimental Medicine*, 198(3), pp. 513–520. DOI: 10.1084/jem.20030162.

Lund, R. *et al.* (2005) 'Identification of Genes Involved in the Initiation of Human Th1 or Th2 Cell Commitment'. *European Journal of Immunology*, 35(11), pp. 3307–3319. DOI: 10.1002/eji.200526079.

Lund, R. *et al.* (2003) 'Identification of Novel Genes Regulated by IL-12, IL-4, or TGF-β during the Early Polarization of CD4+ Lymphocytes'. *The Journal of Immunology*, 171(10), pp. 5328–5336. DOI: 10.4049/jimmunol.171.10.5328.

Ma, C. and Zhang, N. (2022) 'Lymphoid Tissue Residency: A Key to Understand Tcf-1+PD-1+ T Cells'. *Frontiers in Immunology*, 13, p. 1074698. DOI: 10.3389/fimmu.2022.1074698.

Mackay, Laura K. *et al.* (2015) 'Cutting Edge: CD69 Interference with Sphingosine-1-Phosphate Receptor Function Regulates Peripheral T Cell Retention'. *The Journal of Immunology*, 194(5), pp. 2059–2063. DOI: 10.4049/jimmunol.1402256.

Mackay, L.K. *et al.* (2016) 'Hobit and Blimp1 Instruct a Universal Transcriptional Program of Tissue Residency in Lymphocytes'. *Science*, 352(6284), pp. 459–463. DOI: 10.1126/science.aad2035.

Mackay, Laura K. *et al.* (2015) 'T-Box Transcription Factors Combine with the Cytokines TGF-β and IL-15 to Control Tissue-Resident Memory T Cell Fate'. *Immunity*, 43(6), pp. 1101–1111. DOI: 10.1016/j.immuni.2015.11.008.

Mackay, L.K. *et al.* (2013) 'The Developmental Pathway for CD103+CD8+ Tissue-Resident Memory T Cells of Skin'. *Nature Immunology*, 14(12), pp. 1294–1301. DOI: 10.1038/ni.2744.

Madisen, L. *et al.* (2010) 'A Robust and High-Throughput Cre Reporting and Characterization System for the Whole Mouse Brain'. *Nature Neuroscience*, 13(1), pp. 133–140. DOI: 10.1038/nn.2467.

Maekawa, Y. *et al.* (2008) 'Notch2 Integrates Signaling by the Transcription Factors RBP-J and CREB1 to Promote T Cell Cytotoxicity'. *Nature Immunology*, 9(10), pp. 1140–1147. DOI: 10.1038/ni.1649.

Man, K. *et al.* (2017) 'Transcription Factor IRF4 Promotes CD8+ T Cell Exhaustion and Limits the Development of Memory-like T Cells during Chronic Infection'. *Immunity*, 47(6), pp. 1129-1141.e5. DOI: 10.1016/j.immuni.2017.11.021.

Mani, V. *et al.* (2019) 'Migratory DCs Activate TGF-β to Precondition Naïve $CD8^+$ T Cells for Tissue-Resident Memory Fate'. *Science*, 366(6462), p. eaav5728. DOI: 10.1126/science.aav5728.

Marshall, D.R. *et al.* (2001) 'Measuring the Diaspora for Virus-Specific $CD8^+$ T Cells'. *Proceedings of the National Academy of Sciences*, 98(11), pp. 6313–6318. DOI: 10.1073/pnas.101132698.

Marshall, J.S. *et al.* (2018) 'An Introduction to Immunology and Immunopathology'. *Allergy, Asthma & Clinical Immunology*, 14(S2), p. 49. DOI: 10.1186/s13223-018-0278-1.

Martin, M.D. and Badovinac, V.P. (2018) 'Defining Memory CD8 T Cell'. *Frontiers in Immunology*, 9, p. 2692. DOI: 10.3389/fimmu.2018.02692.

Masopust, D. *et al.* (2001) 'Preferential Localization of Effector Memory Cells in Non-lymphoid

Tissue'. *Science*, 291(5512), pp. 2413–2417. DOI: 10.1126/science.1058867.

Masopust, D. and Schenkel, J.M. (2013) 'The Integration of T Cell Migration, Differentiation and Function'. *Nature Reviews Immunology*, 13(5), pp. 309–320. DOI: 10.1038/nri3442.

Masopust, D. and Soerens, A.G. (2019) 'Tissue-Resident T Cells and Other Resident Leukocytes'. *Annual Review of Immunology*, 37(1), pp. 521–546. DOI: 10.1146/annurev-immunol-042617-053214.

Matloubian, M. *et al.* (2004) 'Lymphocyte Egress from Thymus and Peripheral Lymphoid Organs Is Dependent on S1P Receptor 1'. *Nature*, 427(6972), pp. 355–360. DOI: 10.1038/nature02284.

Matsuzaki, J. *et al.* (2010) 'Tumor-Infiltrating NY-ESO-1–Specific $CD8^+$ T Cells Are Negatively Regulated by LAG-3 and PD-1 in Human Ovarian Cancer'. *Proceedings of the National Academy of Sciences*, 107(17), pp. 7875–7880. DOI: 10.1073/pnas.1003345107.

Matusewicz, L. *et al.* (2015) 'The Effect of Statins on Cancer Cells—Review'. *Tumor Biology*, 36(7), pp. 4889–4904. DOI: 10.1007/s13277-015-3551-7.

Matusewicz, L., Czogalla, A. and Sikorski, A.F. (2020) 'Attempts to Use Statins in Cancer Therapy: An Update'. *Tumor Biology*, 42(7), p. 101042832094176. DOI: 10.1177/1010428320941760.

McConnell, B.B. and Yang, V.W. (2010) 'Mammalian Krüppel-Like Factors in Health and Diseases'. *Physiological Reviews*, 90(4), pp. 1337–1381. DOI: 10.1152/physrev.00058.2009.

McLane, L.M., Abdel-Hakeem, M.S. and Wherry, E.J. (2019) 'CD8 T Cell Exhaustion During Chronic Viral Infection and Cancer'. *Annual Review of Immunology*, 37(1), pp. 457–495. DOI: 10.1146/annurev-immunol-041015-055318.

McMaster, S.R. *et al.* (2018) 'Pulmonary Antigen Encounter Regulates the Establishment of Tissue-Resident CD8 Memory T Cells in the Lung Airways and Parenchyma'. *Mucosal Immunology*, 11(4), pp. 1071–1078. DOI: 10.1038/s41385-018-0003-x.

Mebius, R.E. and Kraal, G. (2005) 'Structure and Function of the Spleen'. *Nature Reviews Immunology*, 5(8), pp. 606–616. DOI: 10.1038/nri1669.

Mescher, M.F. *et al.* (2006) 'Signals Required for Programming Effector and Memory Development by $CD8^+$ T Cells'. *Immunological Reviews*, 211(1), pp. 81–92. DOI: 10.1111/j.0105-2896.2006.00382.x.

Miho, E. *et al.* (2018) 'Computational Strategies for Dissecting the High-Dimensional Complexity of Adaptive Immune Repertoires'. *Frontiers in Immunology*, 9, p. 224. DOI: 10.3389/fimmu.2018.00224.

Miller, B.C. *et al.* (2019) 'Subsets of Exhausted CD8+ T Cells Differentially Mediate Tumor Control and Respond to Checkpoint Blockade'. *Nature Immunology*, 20(3), pp. 326–336. DOI: 10.1038/s41590-019-0312-6.

Milner, J.J. *et al.* (2017) 'Runx3 Programs CD8+ T Cell Residency in Non-lymphoid Tissues and Tumours'. *Nature*, 552(7684), pp. 253–257. DOI: 10.1038/nature24993.

Mir, R. *et al.* (2016) 'Wnt/β-Catenin Signaling Regulated SATB1 Promotes Colorectal Cancer Tumorigenesis and Progression'. *Oncogene*, 35(13), pp. 1679–1691. DOI: 10.1038/onc.2015.232.

Miyamoto, K. *et al.* (2018) 'Chromatin Accessibility Impacts Transcriptional Reprogramming in Oocytes'. *Cell Reports*, 24(2), pp. 304–311. DOI: 10.1016/j.celrep.2018.06.030.

Miyazaki, M. *et al.* (2011) 'The Opposing Roles of the Transcription Factor E2A and Its Antagonist Id3 That Orchestrate and Enforce the Naive Fate of T Cells'. *Nature Immunology*, 12(10), pp. 992–1001. DOI: 10.1038/ni.2086.

Mizuguchi, M. *et al.* (2021) 'Promoter CpG Methylation Inhibits Krüppel-like Factor 2 (KLF2)-Mediated Repression of hTERT Gene Expression in Human T-Cells'. *Biochemistry and Biophysics Reports*, 26, p. 100984. DOI: 10.1016/j.bbrep.2021.100984.

Mognol, G.P. *et al.* (2017) 'Exhaustion-Associated Regulatory Regions in CD8$^+$ Tumor-Infiltrating T Cells'. *Proceedings of the National Academy of Sciences*, 114(13). DOI: 10.1073/pnas.1620498114.

Mombaerts, P. *et al.* (1992) 'Mutations in T-Cell Antigen Receptor Genes α and β Block Thymocyte Development at Different Stages'. *Nature*, 360(6401), pp. 225–231. DOI: 10.1038/360225a0.

Mueller, S.N. *et al.* (2007) 'Viral Targeting of Fibroblastic Reticular Cells Contributes to Immunosuppression and Persistence during Chronic Infection'. *Proceedings of the National Academy of Sciences of the United States of America*, 104(39), pp. 15430–15435. DOI: 10.1073/pnas.0702579104.

Mueller, S.N. and Germain, R.N. (2009) 'Stromal Cell Contributions to the Homeostasis and Functionality of the Immune System'. *Nature Reviews Immunology*, 9(9), pp. 618–629. DOI: 10.1038/nri2588.

Murphy, K.M. and Weaver, C. (2017) *Janeway's Immunobiology*. 9th edition. New York London: GS, Garland Science, Taylor & Francis Group.

Naik, R. and Galande, S. (2019) 'SATB Family Chromatin Organizers as Master Regulators of Tumor Progression'. *Oncogene*, 38(12), pp. 1989–2004. DOI: 10.1038/s41388-018-0541-4.

Najibi, A.J. and Mooney, D.J. (2020) 'Cell and Tissue Engineering in Lymph Nodes for Cancer Immunotherapy'. *Advanced Drug Delivery Reviews*, 161–162, pp. 42–62. DOI: 10.1016/j.addr.2020.07.023.

Nath, A.P. *et al.* (2019) 'Comparative Analysis Reveals a Role for TGF-β in Shaping the Residency-Related Transcriptional Signature in Tissue-Resident Memory CD8+ T Cells' Gangopadhyay, N. (ed.). *PLOS ONE*, 14(2), p. e0210495. DOI: 10.1371/journal.pone.0210495.

Nayan, M. *et al.* (2017) 'Statin Use and Kidney Cancer Survival Outcomes: A Systematic Review and Meta-Analysis'. *Cancer Treatment Reviews*, 52, pp. 105–116. DOI: 10.1016/j.ctrv.2016.11.009.

Nicholson, M.W. *et al.* (1998) 'Affinity and Kinetic Analysis of L-Selectin (CD62L) Binding to Glycosylation-Dependent Cell-Adhesion Molecule-1'. *Journal of Biological Chemistry*, 273(2), pp. 763–770. DOI: 10.1074/jbc.273.2.763.

Nie, H. *et al.* (2005) 'A Role for SATB1, a Nuclear Matrix Association Region-Binding Protein, in the Development of CD8SP Thymocytes and Peripheral T Lymphocytes'. *The Journal of Immunology*, 174(8), pp. 4745–4752. DOI: 10.4049/jimmunol.174.8.4745.

Nolte, M.A. *et al.* (2003) 'A Conduit System Distributes Chemokines and Small Blood-Borne Molecules through the Splenic White Pulp'. *The Journal of Experimental Medicine*, 198(3), pp. 505–512. DOI: 10.1084/jem.20021801.

Nolte, M.A. *et al.* (2000) 'Isolation of the Intact White Pulp. Quantitative and Qualitative Analysis of the Cellular Composition of the Splenic Compartments'. *European Journal of Immunology*, 30(2), pp. 626–634. DOI: 10.1002/1521-4141(200002)30:2<626::AID-IMMU626>3.0.CO;2-H.

Notani, D. *et al.* (2010) 'Global Regulator SATB1 Recruits β-Catenin and Regulates TH2 Differentiation in Wnt-Dependent Manner' Nusse, R. (ed.). *PLoS Biology*, 8(1), p. e1000296. DOI: 10.1371/journal.pbio.1000296.

Nüssing, S. *et al.* (2019) 'Divergent SATB 1 Expression across Human Life Span and Tissue Compartments'. *Immunology & Cell Biology*, 97(5), pp. 498–511. DOI: 10.1111/imcb.12233.

Nüssing, S. *et al.* (2020) 'Efficient CRISPR/Cas9 Gene Editing in Uncultured Naive Mouse T Cells for In Vivo Studies'. *The Journal of Immunology*, 204(8), pp. 2308–2315. DOI: 10.4049/jimmunol.1901396.

Nüssing, S. *et al.* (2022) 'SATB1 Ensures Appropriate Transcriptional Programs within Naïve CD8$^+$ T Cells'. *Immunology & Cell Biology*, p. imcb.12566. DOI: 10.1111/imcb.12566.

Obar, J.J. *et al.* (2011) 'Pathogen-Induced Inflammatory Environment Controls Effector and

Memory CD8+ T Cell Differentiation'. *The Journal of Immunology*, 187(10), pp. 4967–4978. DOI: 10.4049/jimmunol.1102335.

Obers, A. *et al.* (2024) 'Retinoic Acid and TGF-β Orchestrate Organ-Specific Programs of Tissue Residency'. *Immunity*, 57(11), pp. 2615-2633.e10. DOI: 10.1016/j.immuni.2024.09.015.

Oldenburg, M. *et al.* (2012) 'TLR13 Recognizes Bacterial 23 *S* rRNA Devoid of Erythromycin Resistance–Forming Modification'. *Science*, 337(6098), pp. 1111–1115. DOI: 10.1126/science.1220363.

Olson, J.A. *et al.* (2013) 'Effector-like CD8+ T Cells in the Memory Population Mediate Potent Protective Immunity'. *Immunity*, 38(6), pp. 1250–1260. DOI: 10.1016/j.immuni.2013.05.009.

Omilusik, K.D. *et al.* (2015) 'Transcriptional Repressor ZEB2 Promotes Terminal Differentiation of CD8+ Effector and Memory T Cell Populations during Infection'. *The Journal of Experimental Medicine*, 212(12), pp. 2027–2039. DOI: 10.1084/jem.20150194.

O'Neill, L.A.J., Golenbock, D. and Bowie, A.G. (2013) 'The History of Toll-like Receptors — Redefining Innate Immunity'. *Nature Reviews Immunology*, 13(6), pp. 453–460. DOI: 10.1038/nri3446.

O'Sullivan, C. and Dev, K.K. (2013) 'The Structure and Function of the S1P1 Receptor'. *Trends in Pharmacological Sciences*, 34(7), pp. 401–412. DOI: 10.1016/j.tips.2013.05.002.

Ouyang, W. *et al.* (2010) 'Transforming Growth Factor-β Signaling Curbs Thymic Negative Selection Promoting Regulatory T Cell Development'. *Immunity*, 32(5), pp. 642–653. DOI: 10.1016/j.immuni.2010.04.012.

Pabbisetty, S.K. *et al.* (2014) 'KLF2 Is a Rate-Limiting Transcription Factor That Can Be Targeted to Enhance Regulatory T-Cell Production'. *Proceedings of the National Academy of Sciences*, 111(26), pp. 9579–9584. DOI: 10.1073/pnas.1323493111.

Paley, M.A. *et al.* (2012) 'Progenitor and Terminal Subsets of $CD8^+$ T Cells Cooperate to Contain Chronic Viral Infection'. *Science*, 338(6111), pp. 1220–1225. DOI: 10.1126/science.1229620.

Pardoll, D.M. (2012) 'The Blockade of Immune Checkpoints in Cancer Immunotherapy'. *Nature Reviews Cancer*, 12(4), pp. 252–264. DOI: 10.1038/nrc3239.

Park, J.S. *et al.* (2023) 'Targeting PD-L2–RGMb Overcomes Microbiome-Related Immunotherapy Resistance'. *Nature*, 617(7960), pp. 377–385. DOI: 10.1038/s41586-023-06026-3.

Parkin, J. and Cohen, B. (2001) 'An Overview of the Immune System'. *The Lancet*, 357(9270), pp. 1777–1789. DOI: 10.1016/S0140-6736(00)04904-7.

Parry, R.V. *et al.* (2005) 'CTLA-4 and PD-1 Receptors Inhibit T-Cell Activation by Distinct Mechanisms'. *Molecular and Cellular Biology*, 25(21), pp. 9543–9553. DOI: 10.1128/MCB.25.21.9543-9553.2005.

Pauken, K.E. *et al.* (2016) 'Epigenetic Stability of Exhausted T Cells Limits Durability of Reinvigoration by PD-1 Blockade'. *Science*, 354(6316), pp. 1160–1165. DOI: 10.1126/science.aaf2807.

Pavan Kumar, P. *et al.* (2006) 'Phosphorylation of SATB1, a Global Gene Regulator, Acts as a Molecular Switch Regulating Its Transcriptional Activity In Vivo'. *Molecular Cell*, 22(2), pp. 231–243. DOI: 10.1016/j.molcel.2006.03.010.

Pearce, E.L. *et al.* (2003) 'Control of Effector $CD8^+$ T Cell Function by the Transcription Factor *Eomesodermin*'. *Science*, 302(5647), pp. 1041–1043. DOI: 10.1126/science.1090148.

Pham, T.H.M. *et al.* (2008) 'S1P1 Receptor Signaling Overrides Retention Mediated by Gαi-Coupled Receptors to Promote T Cell Egress'. *Immunity*, 28(1), pp. 122–133. DOI: 10.1016/j.immuni.2007.11.017.

Phan, T.G. *et al.* (2007) 'Subcapsular Encounter and Complement-Dependent Transport of Immune Complexes by Lymph Node B Cells'. *Nature Immunology*, 8(9), pp. 992–1000. DOI: 10.1038/ni1494.

Pircher, H. *et al.* (1989) 'Tolerance Induction in Double Specific T-Cell Receptor Transgenic Mice Varies with Antigen'. *Nature*, 342(6249), pp. 559–561. DOI: 10.1038/342559a0.

Pol, J.G. *et al.* (2020) 'Effects of Interleukin-2 in Immunostimulation and Immunosuppression'. *Journal of Experimental Medicine*, 217(1), p. e20191247. DOI: 10.1084/jem.20191247.

Preiss, A. *et al.* (1985) 'Molecular Genetics of Krüppel, a Gene Required for Segmentation of the Drosophila Embryo'. *Nature*, 313(5997), pp. 27–32. DOI: 10.1038/313027a0.

Preston, G.C. *et al.* (2013) 'The Impact of KLF2 Modulation on the Transcriptional Program and Function of CD8 T Cells' Alberola-Ila, J. (ed.). *PLoS ONE*, 8(10), p. e77537. DOI: 10.1371/journal.pone.0077537.

Purbey, P.K. *et al.* (2009) 'Acetylation-Dependent Interaction of SATB1 and CtBP1 Mediates Transcriptional Repression by SATB1'. *Molecular and Cellular Biology*, 29(5), pp. 1321–1337. DOI: 10.1128/MCB.00822-08.

Puri, K.D. *et al.* (1995) 'Sialomucin CD34 Is the Major L-Selectin Ligand in Human Tonsil High Endothelial Venules.' *The Journal of Cell Biology*, 131(1), pp. 261–270. DOI: 10.1083/jcb.131.1.261.

Quigley, M. *et al.* (2010) 'Transcriptional Analysis of HIV-Specific CD8+ T Cells Shows That PD-1 Inhibits T Cell Function by Upregulating BATF'. *Nature Medicine*, 16(10), pp. 1147–1151. DOI: 10.1038/nm.2232.

Radziewicz, H. *et al.* (2007) 'Liver-Infiltrating Lymphocytes in Chronic Human Hepatitis C Virus Infection Display an Exhausted Phenotype with High Levels of PD-1 and Low Levels of CD127 Expression'. *Journal of Virology*, 81(6), pp. 2545–2553. DOI: 10.1128/JVI.02021-06.

Raju, S. *et al.* (2021) 'Identification of a T-Bethi Quiescent Exhausted CD8 T Cell Subpopulation That Can Differentiate into TIM3+CX3CR1+ Effectors and Memory-like Cells'. *The Journal of Immunology*, 206(12), pp. 2924–2936. DOI: 10.4049/jimmunol.2001348.

Ramírez, F. *et al.* (2016) 'deepTools2: A next Generation Web Server for Deep-Sequencing Data Analysis'. *Nucleic Acids Research*, 44(W1), pp. W160–W165. DOI: 10.1093/nar/gkw257.

Raphael, I., Joern, R.R. and Forsthuber, T.G. (2020) 'Memory CD4+ T Cells in Immunity and Autoimmune Diseases'. *Cells*, 9(3), p. 531. DOI: 10.3390/cells9030531.

Ray, S.J. *et al.* (2004) 'The Collagen Binding A1β1 Integrin VLA-1 Regulates CD8 T Cell-Mediated Immune Protection against Heterologous Influenza Infection'. *Immunity*, 20(2), pp. 167–179. DOI: 10.1016/S1074-7613(04)00021-4.

Reiss, Y. *et al.* (2001) 'CC Chemokine Receptor (CCR)4 and the CCR10 Ligand Cutaneous T Cell–Attracting Chemokine (CTACK) in Lymphocyte Trafficking to Inflamed Skin'. *The Journal of Experimental Medicine*, 194(10), pp. 1541–1547. DOI: 10.1084/jem.194.10.1541.

Riessland, M. *et al.* (2019) 'Loss of SATB1 Induces P21-Dependent Cellular Senescence in Post-Mitotic Dopaminergic Neurons'. *Cell Stem Cell*, 25(4), pp. 514-530.e8. DOI: 10.1016/j.stem.2019.08.013.

Ritchie, M.E. *et al.* (2015) 'Limma Powers Differential Expression Analyses for RNA-Sequencing and Microarray Studies'. *Nucleic Acids Research*, 43(7), pp. e47–e47. DOI: 10.1093/nar/gkv007.

Robert, C. (2020) 'A Decade of Immune-Checkpoint Inhibitors in Cancer Therapy'. *Nature Communications*, 11(1), p. 3801. DOI: 10.1038/s41467-020-17670-y.

Robert, C. *et al.* (2018) 'Durable Complete Response After Discontinuation of Pembrolizumab in Patients With Metastatic Melanoma'. *Journal of Clinical Oncology*, 36(17), pp. 1668–1674. DOI: 10.1200/JCO.2017.75.6270.

Roberts, Brolin, and Ebert (1999) 'Integrin α_1 β_1 (VLA-1) Mediates Adhesion of Activated Intraepithelial Lymphocytes to Collagen'. *Immunology*, 97(4), pp. 679–685. DOI: 10.1046/j.1365-2567.1999.00812.x.

Rodda, L.B. *et al.* (2018) 'Single-Cell RNA Sequencing of Lymph Node Stromal Cells Reveals

Niche-Associated Heterogeneity'. *Immunity*, 48(5), pp. 1014-1028.e6. DOI: 10.1016/j.immuni.2018.04.006.

Rosen, S.D. (2004) 'Ligands for L-Selectin: Homing, Inflammation, and Beyond'. *Annual Review of Immunology*, 22(1), pp. 129–156. DOI: 10.1146/annurev.immunol.21.090501.080131.

Rott, L.S. *et al.* (1996) 'A Fundamental Subdivision of Circulating Lymphocytes Defined by Adhesion to Mucosal Addressin Cell Adhesion Molecule-1. Comparison with Vascular Cell Adhesion Molecule-1 and Correlation with Beta 7 Integrins and Memory Differentiation.' *The Journal of Immunology*, 156(10), pp. 3727–3736. DOI: 10.4049/jimmunol.156.10.3727.

Ruddle, N.H. and Akirav, E.M. (2009) 'Secondary Lymphoid Organs: Responding to Genetic and Environmental Cues in Ontogeny and the Immune Response'. *The Journal of Immunology*, 183(4), pp. 2205–2212. DOI: 10.4049/jimmunol.0804324.

Russ, B.E. *et al.* (2023) 'Active Maintenance of CD8+ T Cell Naivety through Regulation of Global Genome Architecture'. *Cell Reports*, 42(10), p. 113301. DOI: 10.1016/j.celrep.2023.113301.

Russ, B.E. *et al.* (2014) 'Distinct Epigenetic Signatures Delineate Transcriptional Programs during Virus-Specific CD8+ T Cell Differentiation'. *Immunity*, 41(5), pp. 853–865. DOI: 10.1016/j.immuni.2014.11.001.

Rutishauser, R.L. *et al.* (2009) 'Transcriptional Repressor Blimp-1 Promotes CD8+ T Cell Terminal Differentiation and Represses the Acquisition of Central Memory T Cell Properties'. *Immunity*, 31(2), pp. 296–308. DOI: 10.1016/j.immuni.2009.05.014.

Saadey, A.A. *et al.* (2023) 'Rebalancing TGFβ1/BMP Signals in Exhausted T Cells Unlocks Responsiveness to Immune Checkpoint Blockade Therapy'. *Nature Immunology*, 24(2), pp. 280–294. DOI: 10.1038/s41590-022-01384-y.

Sallusto, F. *et al.* (1999) 'Two Subsets of Memory T Lymphocytes with Distinct Homing Potentials and Effector Functions'. *Nature*, 401(6754), pp. 708–712. DOI: 10.1038/44385.

Sanfilippo, K.M. *et al.* (2016) 'Statins Are Associated With Reduced Mortality in Multiple Myeloma'. *Journal of Clinical Oncology*, 34(33), pp. 4008–4014. DOI: 10.1200/JCO.2016.68.3482.

Sarkar, S. *et al.* (2008) 'Functional and Genomic Profiling of Effector CD8 T Cell Subsets with Distinct Memory Fates'. *The Journal of Experimental Medicine*, 205(3), pp. 625–640. DOI: 10.1084/jem.20071641.

Satish Ramkumar *et al.* (2016) 'Statin Therapy: Review of Safety and Potential Side Effects'. *Acta Cardiologica Sinica*, 32(6). DOI: 10.6515/ACS20160611A.

Sato, Y. *et al.* (2023) 'The Roles of Tertiary Lymphoid Structures in Chronic Diseases'. *Nature Reviews Nephrology*, 19(8), pp. 525–537. DOI: 10.1038/s41581-023-00706-z.

Satoh, Y. *et al.* (2013) 'The Satb1 Protein Directs Hematopoietic Stem Cell Differentiation toward Lymphoid Lineages'. *Immunity*, 38(6), pp. 1105–1115. DOI: 10.1016/j.immuni.2013.05.014.

Sautès-Fridman, C. *et al.* (2019) 'Tertiary Lymphoid Structures in the Era of Cancer Immunotherapy'. *Nature Reviews Cancer*, 19(6), pp. 307–325. DOI: 10.1038/s41568-019-0144-6.

Sawant, D.V. *et al.* (2019) 'Adaptive Plasticity of IL-10+ and IL-35+ Treg Cells Cooperatively Promotes Tumor T Cell Exhaustion'. *Nature Immunology*, 20(6), pp. 724–735. DOI: 10.1038/s41590-019-0346-9.

Scharping, N.E. *et al.* (2021) 'Mitochondrial Stress Induced by Continuous Stimulation under Hypoxia Rapidly Drives T Cell Exhaustion'. *Nature Immunology*, 22(2), pp. 205–215. DOI: 10.1038/s41590-020-00834-9.

Scharping, N.E. and Delgoffe, G.M. (2016) 'Tumor Microenvironment Metabolism: A New Checkpoint for Anti-Tumor Immunity'. *Vaccines*, 4(4), p. 46. DOI: 10.3390/vaccines4040046.

Schenkel, J.M. *et al.* (2014) 'Resident Memory CD8 T Cells Trigger Protective Innate and Adaptive Immune Responses'. *Science*, 346(6205), pp. 98–101. DOI: 10.1126/science.1254536.

Schenkel, J.M. *et al.* (2013) 'Sensing and Alarm Function of Resident Memory CD8+ T Cells'. *Nature Immunology*, 14(5), pp. 509–513. DOI: 10.1038/ni.2568.

Schmitz, J.E. *et al.* (1999) 'Control of Viremia in Simian Immunodeficiency Virus Infection by $CD8^+$ Lymphocytes'. *Science*, 283(5403), pp. 857–860. DOI: 10.1126/science.283.5403.857.

Schwager, S. and Detmar, M. (2019) 'Inflammation and Lymphatic Function'. *Frontiers in Immunology*, 10, p. 308. DOI: 10.3389/fimmu.2019.00308.

Scott, A.C. *et al.* (2019) 'TOX Is a Critical Regulator of Tumour-Specific T Cell Differentiation'. *Nature*, 571(7764), pp. 270–274. DOI: 10.1038/s41586-019-1324-y.

Scott-Browne, J.P. *et al.* (2016) 'Dynamic Changes in Chromatin Accessibility Occur in CD8 + T Cells Responding to Viral Infection'. *Immunity*, 45(6), pp. 1327–1340. DOI: 10.1016/j.immuni.2016.10.028.

Sebzda, E. *et al.* (2008) 'Transcription Factor KLF2 Regulates the Migration of Naive T Cells by Restricting Chemokine Receptor Expression Patterns'. *Nature Immunology*, 9(3), pp. 292–300. DOI: 10.1038/ni1565.

Sen, D.R. *et al.* (2016) 'The Epigenetic Landscape of T Cell Exhaustion'. *Science*, 354(6316), pp. 1165–1169. DOI: 10.1126/science.aae0491.

Seo, H. *et al.* (2019) 'TOX and TOX2 Transcription Factors Cooperate with NR4A Transcription Factors to Impose $CD8^+$ T Cell Exhaustion'. *Proceedings of the National Academy of Sciences*, 116(25), pp. 12410–12415. DOI: 10.1073/pnas.1905675116.

Seo, J., Lozano, M.M. and Dudley, J.P. (2005) 'Nuclear Matrix Binding Regulates SATB1-Mediated Transcriptional Repression'. *Journal of Biological Chemistry*, 280(26), pp. 24600–24609. DOI: 10.1074/jbc.M414076200.

Seo, W. *et al.* (2020) 'Runx-Mediated Regulation of CCL5 via Antagonizing Two Enhancers Influences Immune Cell Function and Anti-Tumor Immunity'. *Nature Communications*, 11(1), p. 1562. DOI: 10.1038/s41467-020-15375-w.

Shannon, M.F. (2003) 'A Nuclear Address with Influence'. *Nature Genetics*, 34(1), pp. 4–6. DOI: 10.1038/ng0503-4.

Sharma, N. *et al.* (2015) 'CD8 T Cells Enter the Splenic T Cell Zones Independently of CCR7, but the Subsequent Expansion and Trafficking Patterns of Effector T Cells after Infection Are Dysregulated in the Absence of CCR7 Migratory Cues'. *The Journal of Immunology*, 195(11), pp. 5227–5236. DOI: 10.4049/jimmunol.1500993.

Sharma, P. *et al.* (2023) 'Immune Checkpoint Therapy—Current Perspectives and Future Directions'. *Cell*, 186(8), pp. 1652–1669. DOI: 10.1016/j.cell.2023.03.006.

Sharpe, A.H. and Pauken, K.E. (2018) 'The Diverse Functions of the PD1 Inhibitory Pathway'. *Nature Reviews Immunology*, 18(3), pp. 153–167. DOI: 10.1038/nri.2017.108.

Sherwood, R.I. *et al.* (2014) 'Discovery of Directional and Nondirectional Pioneer Transcription Factors by Modeling DNase Profile Magnitude and Shape'. *Nature Biotechnology*, 32(2), pp. 171–178. DOI: 10.1038/nbt.2798.

Shin, H. *et al.* (2009) 'A Role for the Transcriptional Repressor Blimp-1 in CD8+ T Cell Exhaustion during Chronic Viral Infection'. *Immunity*, 31(2), pp. 309–320. DOI: 10.1016/j.immuni.2009.06.019.

Shin, H. *et al.* (2007) 'Viral Antigen and Extensive Division Maintain Virus-Specific CD8 T Cells during Chronic Infection'. *The Journal of Experimental Medicine*, 204(4), pp. 941–949. DOI: 10.1084/jem.20061937.

Shiow, L.R. *et al.* (2006) 'CD69 Acts Downstream of Interferon-α/β to Inhibit S1P1 and Lymphocyte Egress from Lymphoid Organs'. *Nature*, 440(7083), pp. 540–544. DOI: 10.1038/nature04606.

Siddiqui, I. *et al.* (2019) 'Intratumoral Tcf1+PD-1+CD8+ T Cells with Stem-like Properties Promote

Tumor Control in Response to Vaccination and Checkpoint Blockade Immunotherapy'. *Immunity*, 50(1), pp. 195-211.e10. DOI: 10.1016/j.immuni.2018.12.021.

Sinclair, L.V. *et al.* (2008) 'Phosphatidylinositol-3-OH Kinase and Nutrient-Sensing mTOR Pathways Control T Lymphocyte Trafficking'. *Nature Immunology*, 9(5), pp. 513–521. DOI: 10.1038/ni.1603.

Skon, C.N. *et al.* (2013) 'Transcriptional Downregulation of S1pr1 Is Required for the Establishment of Resident Memory CD8+ T Cells'. *Nature Immunology*, 14(12), pp. 1285–1293. DOI: 10.1038/ni.2745.

Smita, S. *et al.* (2022) 'Heterogeneity and Clonality of Kidney-Infiltrating T Cells in Murine Lupus Nephritis'. *JCI Insight*, 7(8), p. e156048. DOI: 10.1172/jci.insight.156048.

Smith-Garvin, J.E. *et al.* (2010) 'T-Cell Receptor Signals Direct the Composition and Function of the Memory CD8+ T-Cell Pool'. *Blood*, 116(25), pp. 5548–5559. DOI: 10.1182/blood-2010-06-292748.

Somasundaram, A. *et al.* (2022) 'Systemic Immune Dysfunction in Cancer Patients Driven by IL6 Induction of LAG3 in Peripheral CD8+ T Cells'. *Cancer Immunology Research*, 10(7), pp. 885–899. DOI: 10.1158/2326-6066.CIR-20-0736.

Sommer, D. *et al.* (2014) 'Efficient Genome Engineering by Targeted Homologous Recombination in Mouse Embryos Using Transcription Activator-like Effector Nucleases'. *Nature Communications*, 5(1), p. 3045. DOI: 10.1038/ncomms4045.

Song, M.-K. *et al.* (2017) 'Would Lipophilic Statin Therapy as a PrognosticFactor Improve Survival in Patients With Uterine Cervical Cancer?' *International Journal of Gynecological Cancer*, 27(7), pp. 1431–1437. DOI: 10.1097/IGC.0000000000001046.

Soufi, A. *et al.* (2015) 'Pioneer Transcription Factors Target Partial DNA Motifs on Nucleosomes to Initiate Reprogramming'. *Cell*, 161(3), pp. 555–568. DOI: 10.1016/j.cell.2015.03.017.

Spence, A.D. *et al.* (2019) 'Statin Use and Survival in Patients with Gastric Cancer in Two Independent Population-based Cohorts'. *Pharmacoepidemiology and Drug Safety*, 28(4), pp. 460–470. DOI: 10.1002/pds.4688.

Steinman, R.M., Hawiger, D. and Nussenzweig, M.C. (2003) 'Tolerogenic Dendritic Cells'. *Annual Review of Immunology*, 21(1), pp. 685–711. DOI: 10.1146/annurev.immunol.21.120601.141040.

Stenstad, H. *et al.* (2006) 'Gut-Associated Lymphoid Tissue–Primed CD4+ T Cells Display CCR9-Dependent and -Independent Homing to the Small Intestine'. *Blood*, 107(9), pp. 3447–3454. DOI: 10.1182/blood-2005-07-2860.

Stephen, T.L. *et al.* (2017) 'SATB1 Expression Governs Epigenetic Repression of PD-1 in Tumor-Reactive T Cells'. *Immunity*, 46(1), pp. 51–64. DOI: 10.1016/j.immuni.2016.12.015.

Sun, Q. *et al.* (2023) 'STAT3 Regulates CD8+ T Cell Differentiation and Functions in Cancer and Acute Infection'. *Journal of Experimental Medicine*, 220(4), p. e20220686. DOI: 10.1084/jem.20220686.

Takada, K. *et al.* (2011) 'Kruppel-Like Factor 2 Is Required for Trafficking but Not Quiescence in Postactivated T Cells'. *The Journal of Immunology*, 186(2), pp. 775–783. DOI: 10.4049/jimmunol.1000094.

Tan, J.-A.T. *et al.* (2010) 'Phosphorylation-Dependent Interaction of SATB1 and PIAS1 Directs SUMO-Regulated Caspase Cleavage of SATB1'. *Molecular and Cellular Biology*, 30(11), pp. 2823–2836. DOI: 10.1128/MCB.01603-09.

Tan, J.-A.T. *et al.* (2008) 'SUMO Conjugation to the Matrix Attachment Region-Binding Protein, Special AT-Rich Sequence-Binding Protein-1 (SATB1), Targets SATB1 to Promyelocytic Nuclear Bodies Where It Undergoes Caspase Cleavage'. *Journal of Biological Chemistry*, 283(26), pp. 18124–18134. DOI: 10.1074/jbc.M800512200.

Tan, J.T. *et al.* (2001) 'IL-7 Is Critical for Homeostatic Proliferation and Survival of Naive T Cells'. *Proceedings of the National Academy of Sciences of the United States of America*, 98(15), pp.

8732–8737. DOI: 10.1073/pnas.161126098.

Tan, P. *et al.* (2016) 'The Effect of Statins on Prostate Cancer Recurrence and Mortality after Definitive Therapy: A Systematic Review and Meta-Analysis'. *Scientific Reports*, 6(1), p. 29106. DOI: 10.1038/srep29106.

Tanaka, Y. *et al.* (2017) 'SATB1 Conditional Knockout Results in Sjögren's Syndrome in Mice'. *The Journal of Immunology*, 199(12), pp. 4016–4022. DOI: 10.4049/jimmunol.1700550.

Taniuchi, I. (2009) 'Transcriptional Regulation in Helper versus Cytotoxic-Lineage Decision'. *Current Opinion in Immunology*, 21(2), pp. 127–132. DOI: 10.1016/j.coi.2009.03.012.

Thangada, S. *et al.* (2010) 'Cell-Surface Residence of Sphingosine 1-Phosphate Receptor 1 on Lymphocytes Determines Lymphocyte Egress Kinetics'. *Journal of Experimental Medicine*, 207(7), pp. 1475–1483. DOI: 10.1084/jem.20091343.

Thommen, D.S. and Schumacher, T.N. (2018) 'T Cell Dysfunction in Cancer'. *Cancer Cell*, 33(4), pp. 547–562. DOI: 10.1016/j.ccell.2018.03.012.

Tilstra, J.S. *et al.* (2018) 'Kidney-Infiltrating T Cells in Murine Lupus Nephritis Are Metabolically and Functionally Exhausted'. *Journal of Clinical Investigation*, 128(11), pp. 4884–4897. DOI: 10.1172/JCI120859.

Tsui, C. *et al.* (2022) 'MYB Orchestrates T Cell Exhaustion and Response to Checkpoint Inhibition'. *Nature*, 609(7926), pp. 354–360. DOI: 10.1038/s41586-022-05105-1.

Tuomisto, T.T. *et al.* (2008) 'Simvastatin Has an Anti-Inflammatory Effect on Macrophages via Upregulation of an Atheroprotective Transcription Factor, Kruppel-like Factor 2'. *Cardiovascular Research*, 78(1), pp. 175–184. DOI: 10.1093/cvr/cvn007.

Turnis, M.E. *et al.* (2016) 'Interleukin-35 Limits Anti-Tumor Immunity'. *Immunity*, 44(2), pp. 316–329. DOI: 10.1016/j.immuni.2016.01.013.

Unsoeld, H. *et al.* (2002) 'Cutting Edge: CCR7+ and CCR7− Memory T Cells Do Not Differ in Immediate Effector Cell Function'. *The Journal of Immunology*, 169(2), pp. 638–641. DOI: 10.4049/jimmunol.169.2.638.

Urbani, S. *et al.* (2006) 'PD-1 Expression in Acute Hepatitis C Virus (HCV) Infection Is Associated with HCV-Specific CD8 Exhaustion'. *Journal of Virology*, 80(22), pp. 11398–11403. DOI: 10.1128/JVI.01177-06.

Utzschneider, D.T. *et al.* (2018) 'Active Maintenance of T Cell Memory in Acute and Chronic Viral Infection Depends on Continuous Expression of FOXO1'. *Cell Reports*, 22(13), pp. 3454–3467. DOI: 10.1016/j.celrep.2018.03.020.

Utzschneider, D.T. *et al.* (2020) 'Early Precursor T Cells Establish and Propagate T Cell Exhaustion in Chronic Infection'. *Nature Immunology*, 21(10), pp. 1256–1266. DOI: 10.1038/s41590-020-0760-z.

Utzschneider, D.T. *et al.* (2016) 'T Cell Factor 1-Expressing Memory-like CD8+ T Cells Sustain the Immune Response to Chronic Viral Infections'. *Immunity*, 45(2), pp. 415–427. DOI: 10.1016/j.immuni.2016.07.021.

Van Not, O.J. *et al.* (2024) 'Long-Term Survival in Patients With Advanced Melanoma'. *JAMA Network Open*, 7(8), p. e2426641. DOI: 10.1001/jamanetworkopen.2024.26641.

Verdon, D.J., Mulazzani, M. and Jenkins, M.R. (2020) 'Cellular and Molecular Mechanisms of CD8+ T Cell Differentiation, Dysfunction and Exhaustion'. *International Journal of Molecular Sciences*, 21(19), p. 7357. DOI: 10.3390/ijms21197357.

Vignali, D.A.A. and Kuchroo, V.K. (2012) 'IL-12 Family Cytokines: Immunological Playmakers'. *Nature Immunology*, 13(8), pp. 722–728. DOI: 10.1038/ni.2366.

Vignali, P.D.A. *et al.* (2023) 'Hypoxia Drives CD39-Dependent Suppressor Function in Exhausted T Cells to Limit Antitumor Immunity'. *Nature Immunology*, 24(2), pp. 267–279. DOI: 10.1038/s41590-022-01379-9.

Von Andrian, U.H. and Mempel, T.R. (2003) 'Homing and Cellular Traffic in Lymph Nodes'. *Nature Reviews Immunology*, 3(11), pp. 867–878. DOI: 10.1038/nri1222.

Wakim, L.M. *et al.* (2012) 'The Molecular Signature of Tissue Resident Memory CD8 T Cells Isolated from the Brain'. *The Journal of Immunology*, 189(7), pp. 3462–3471. DOI: 10.4049/jimmunol.1201305.

Walunas, T.L. *et al.* (1994) 'CTLA-4 Can Function as a Negative Regulator of T Cell Activation'. *Immunity*, 1(5), pp. 405–413. DOI: 10.1016/1074-7613(94)90071-X.

Wang, B., Ji, L. and Bian, Q. (2023) 'SATB1 Regulates 3D Genome Architecture in T Cells by Constraining Chromatin Interactions Surrounding CTCF-Binding Sites'. *Cell Reports*, 42(4), p. 112323. DOI: 10.1016/j.celrep.2023.112323.

Wang, J. *et al.* (2012) 'Sequence Features and Chromatin Structure around the Genomic Regions Bound by 119 Human Transcription Factors'. *Genome Research*, 22(9), pp. 1798–1812. DOI: 10.1101/gr.139105.112.

Wang, S. *et al.* (2024) 'Tertiary Lymphoid Structures in Cancer: Immune Mechanisms and Clinical Implications'. *MedComm*, 5(3), p. e489. DOI: 10.1002/mco2.489.

Wang, Y. *et al.* (2017) 'Overexpression of SATB1 Gene Inhibits the Immunosuppressive Function of Regulatory T Cells in Chronic Hepatitis B'. *Annals of Clinical and Laboratory Science*, 47(4), pp. 403–408.

Wang, Z. *et al.* (2014) 'Crystal Structure of the Ubiquitin-like Domain-CUT Repeat-like Tandem of Special AT-Rich Sequence Binding Protein 1 (SATB1) Reveals a Coordinating DNA-Binding Mechanism'. *Journal of Biological Chemistry*, 289(40), pp. 27376–27385. DOI: 10.1074/jbc.M114.562314.

Wang, Z. *et al.* (2012) 'The Structural Basis for the Oligomerization of the N-Terminal Domain of SATB1'. *Nucleic Acids Research*, 40(9), pp. 4193–4202. DOI: 10.1093/nar/gkr1284.

Watts, T.H. (2005) 'TNF/TNFR FAMILY MEMBERS IN COSTIMULATION OF T CELL RESPONSES'. *Annual Review of Immunology*, 23(1), pp. 23–68. DOI: 10.1146/annurev.immunol.23.021704.115839.

Weber, J.P. *et al.* (2015) 'ICOS Maintains the T Follicular Helper Cell Phenotype by Down-Regulating Krüppel-like Factor 2'. *Journal of Experimental Medicine*, 212(2), pp. 217–233. DOI: 10.1084/jem.20141432.

Wei, S.C., Duffy, C.R. and Allison, J.P. (2018) 'Fundamental Mechanisms of Immune Checkpoint Blockade Therapy'. *Cancer Discovery*, 8(9), pp. 1069–1086. DOI: 10.1158/2159-8290.CD-18-0367.

Weinreich, M.A. *et al.* (2009) 'KLF2 Transcription-Factor Deficiency in T Cells Results in Unrestrained Cytokine Production and Upregulation of Bystander Chemokine Receptors'. *Immunity*, 31(1), pp. 122–130. DOI: 10.1016/j.immuni.2009.05.011.

Wen, J. *et al.* (2005) 'SATB1 Family Protein Expressed during Early Erythroid Differentiation Modifies Globin Gene Expression'. *Blood*, 105(8), pp. 3330–3339. DOI: 10.1182/blood-2004-08-2988.

Wherry, E.J., Teichgräber, V., *et al.* (2003) 'Lineage Relationship and Protective Immunity of Memory CD8 T Cell Subsets'. *Nature Immunology*, 4(3), pp. 225–234. DOI: 10.1038/ni889.

Wherry, E.J. *et al.* (2007) 'Molecular Signature of CD8+ T Cell Exhaustion during Chronic Viral Infection'. *Immunity*, 27(4), pp. 670–684. DOI: 10.1016/j.immuni.2007.09.006.

Wherry, E.J., Blattman, J.N., *et al.* (2003) 'Viral Persistence Alters CD8 T-Cell Immunodominance and Tissue Distribution and Results in Distinct Stages of Functional Impairment'. *Journal of Virology*, 77(8), pp. 4911–4927. DOI: 10.1128/JVI.77.8.4911-4927.2003.

Williams, M.A. and Bevan, M.J. (2007) 'Effector and Memory CTL Differentiation'. *Annual Review of Immunology*, 25(1), pp. 171–192. DOI: 10.1146/annurev.immunol.25.022106.141548.

Wittner, J. and Schuh, W. (2021) 'Krüppel-like Factor 2 (KLF2) in Immune Cell Migration'. *Vaccines*, 9(10), p. 1171. DOI: 10.3390/vaccines9101171.

Wu, J. and Lingrel, J.B. (2004) 'KLF2 Inhibits Jurkat T Leukemia Cell Growth via Upregulation of Cyclin-Dependent Kinase Inhibitor p21WAF1/CIP1'. *Oncogene*, 23(49), pp. 8088–8096. DOI: 10.1038/sj.onc.1207996.

Wu, Q.-J. *et al.* (2015) 'Statin Use and Breast Cancer Survival and Risk: A Systematic Review and Meta-Analysis'. *Oncotarget*, 6(40), pp. 42988–43004. DOI: 10.18632/oncotarget.5557.

Wu, T. *et al.* (2016) 'The TCF1-Bcl6 Axis Counteracts Type I Interferon to Repress Exhaustion and Maintain T Cell Stemness'. *Science Immunology*, 1(6), p. eaai8593. DOI: 10.1126/sciimmunol.aai8593.

Xie, F. *et al.* (2022) 'Breast Cancer Cell-Derived Extracellular Vesicles Promote CD8+ T Cell Exhaustion via TGF-β Type II Receptor Signaling'. *Nature Communications*, 13(1), p. 4461. DOI: 10.1038/s41467-022-31250-2.

Xing, B. *et al.* (2015) 'Effect of 3-Hydroxy-3-Methylglutaryl-Coenzyme A Reductase Inhibitor on Disease Activity in Patients With Rheumatoid Arthritis: A Meta-Analysis'. *Medicine*, 94(8), p. e572. DOI: 10.1097/MD.0000000000000572.

Xue, C. and Greene, E.C. (2021) 'DNA Repair Pathway Choices in CRISPR-Cas9-Mediated Genome Editing'. *Trends in Genetics*, 37(7), pp. 639–656. DOI: 10.1016/j.tig.2021.02.008.

Yamasaki, K. *et al.* (2007) 'Structural Basis for Recognition of the Matrix Attachment Region of DNA by Transcription Factor SATB1'. *Nucleic Acids Research*, 35(15), pp. 5073–5084. DOI: 10.1093/nar/gkm504.

Yamauchi, T. *et al.* (2021) 'T-Cell CX3CR1 Expression as a Dynamic Blood-Based Biomarker of Response to Immune Checkpoint Inhibitors'. *Nature Communications*, 12(1), p. 1402. DOI: 10.1038/s41467-021-21619-0.

Yang, K. and Kallies, A. (2021) 'Tissue-Specific Differentiation of CD8+ Resident Memory T Cells'. *Trends in Immunology*, 42(10), pp. 876–890. DOI: 10.1016/j.it.2021.08.002.

Yang, Y. *et al.* (2015) 'SATB1 Mediates Long-Range Chromatin Interactions: A Dual Regulator of Anti-Apoptotic BCL2 and Pro-Apoptotic NOXA Genes' Wang, Zhengqi (ed.). *PLOS ONE*, 10(9), p. e0139170. DOI: 10.1371/journal.pone.0139170.

Yao, C. *et al.* (2019) 'Single-Cell RNA-Seq Reveals TOX as a Key Regulator of CD8+ T Cell Persistence in Chronic Infection'. *Nature Immunology*, 20(7), pp. 890–901. DOI: 10.1038/s41590-019-0403-4.

Yasuda, K. *et al.* (2019) 'Satb1 Regulates the Effector Program of Encephalitogenic Tissue Th17 Cells in Chronic Inflammation'. *Nature Communications*, 10(1), p. 549. DOI: 10.1038/s41467-019-08404-w.

Yasui, D. *et al.* (2002) 'SATB1 Targets Chromatin Remodelling to Regulate Genes over Long Distances'. *Nature*, 419(6907), pp. 641–645. DOI: 10.1038/nature01084.

Yates, K.B. *et al.* (2021) 'Epigenetic Scars of CD8+ T Cell Exhaustion Persist after Cure of Chronic Infection in Humans'. *Nature Immunology*, 22(8), pp. 1020–1029. DOI: 10.1038/s41590-021-00979-1.

Yeo, J.-C. *et al.* (2014) 'Klf2 Is an Essential Factor That Sustains Ground State Pluripotency'. *Cell Stem Cell*, 14(6), pp. 864–872. DOI: 10.1016/j.stem.2014.04.015.

Yokosuka, T. *et al.* (2012) 'Programmed Cell Death 1 Forms Negative Costimulatory Microclusters That Directly Inhibit T Cell Receptor Signaling by Recruiting Phosphatase SHP2'. *Journal of Experimental Medicine*, 209(6), pp. 1201–1217. DOI: 10.1084/jem.20112741.

Yoo, S. *et al.* (2023) 'Chronic LCMV Infection Regulates the Effector T Cell Response by Inducing the Generation of Less Immunogenic Dendritic Cells'. *Experimental & Molecular Medicine*, 55(5), pp. 999–1012. DOI: 10.1038/s12276-023-00991-5.

Yu, G. *et al.* (2012) 'clusterProfiler: An R Package for Comparing Biological Themes Among Gene Clusters'. *OMICS: A Journal of Integrative Biology*, 16(5), pp. 284–287. DOI: 10.1089/omi.2011.0118.

Zajac, A.J. *et al.* (1998) 'Viral Immune Evasion Due to Persistence of Activated T Cells Without Effector Function'. *The Journal of Experimental Medicine*, 188(12), pp. 2205–2213. DOI: 10.1084/jem.188.12.2205.

Zander, R. *et al.* (2019) 'CD4+ T Cell Help Is Required for the Formation of a Cytolytic CD8+ T Cell Subset That Protects against Chronic Infection and Cancer'. *Immunity*, 51(6), pp. 1028-1042.e4. DOI: 10.1016/j.immuni.2019.10.009.

Zehn, D. *et al.* (2022) '"Stem-like" Precursors Are the Fount to Sustain Persistent CD8+ T Cell Responses'. *Nature Immunology*, 23(6), pp. 836–847. DOI: 10.1038/s41590-022-01219-w.

Zhang, N. and Bevan, M.J. (2011) 'CD8+ T Cells: Foot Soldiers of the Immune System'. *Immunity*, 35(2), pp. 161–168. DOI: 10.1016/j.immuni.2011.07.010.

Zhang, N. and Bevan, M.J. (2013) 'Transforming Growth Factor-β Signaling Controls the Formation and Maintenance of Gut-Resident Memory T Cells by Regulating Migration and Retention'. *Immunity*, 39(4), pp. 687–696. DOI: 10.1016/j.immuni.2013.08.019.

Zhang, Y. *et al.* (2008) 'Model-Based Analysis of ChIP-Seq (MACS)'. *Genome Biology*, 9(9), p. R137. DOI: 10.1186/gb-2008-9-9-r137.

Zhou, G., Jiang, H. and Ma, L. (2018) 'MicroRNA-376a Inhibits Cell Proliferation and Invasion in Osteosarcoma via Directly Targeting SATB1'. *Molecular Medicine Reports*. DOI: 10.3892/mmr.2018.9344.

Zhu, H. *et al.* (2024) 'The miR-641-STIM1 and SATB1 Axes Play Important Roles in the Regulation of the Th17/Treg Balance in ITP'. *Scientific Reports*, 14(1), p. 11243. DOI: 10.1038/s41598-024-61660-9.

Zhu, Z. *et al.* (2024) 'FOXP1 and KLF2 Reciprocally Regulate Checkpoints of Stem-like to Effector Transition in CAR T Cells'. *Nature Immunology*, 25(1), pp. 117–128. DOI: 10.1038/s41590-023-01685-w.